NOVA SCHOOL OF SCIENCE & TECHNOLOGY

TASK-SPECIFIC IONIC LIQUIDS AND DEEP EUTECTIC SOLVENTS FOR LUBRICATION TECHNOLOGY

MARIANA TRINDADE DE DONATO

Master in Chemistry

DOCTORATE IN SUSTAINABLE CHEMISTRY

NOVA University Lisbon
May 2023

NOVA SCHOOL OF SCIENCE & TECHNOLOGY

DEPARTAMENT OF CHEMISTRY

TASK-SPECIFIC IONIC LIQUIDS AND DEEP EUTECTIC SOLVENTS FOR LUBRICATION TECHNOLOGY

MARIANA TRINDADE DE DONATO

Master in Chemistry

Adviser: Luís Alexandre Almeida Fernandes Cobra Branco
Associate Professor, NOVA University Lisbon

Co-advisers: Benilde de Jesus Vieira Saramago
Associate Professor, Instituto Superior Técnico University of Lisbon

Rogério Anacleto Cordeiro Colaço
Full Professor, Instituto Superior Técnico University of Lisbon

Examination Committee:

Chair: Ana Isabel Nobre Martins Aguiar de Oliveira Ricardo,
Full Professor, FCT-NOVA

Rapporteurs: Isabel Maria Delgado Jana Marrucho Ferreira,
Full Professor, Instituto Superior Técnico

Fábio Emanuel de Sousa Ferreira,
Investigator, University of Coimbra

Adviser: Luís Alexandre Almeida Fernandes Cobra Branco,
Associate Professor, NOVA University Lisbon

Members: Diana Cristina Morais da Silva Pereira,
Junior Investigator, Instituto Superior Técnico

Ana Isabel Nobre Martins Aguiar de Oliveira Ricardo,
Full Professor, FCT-NOVA

José Manuel da Silva Simões Esperança,
Investigator, FCT-NOVA

DOCTORATE IN SUSTAINABLE CHEMISTRY

NOVA University Lisbon
May 2023

Task-Specific Ionic Liquids and Deep Eutectic Solvents for Lubrication Technology

Aos meus pais.

ACKNOWLEDGMENTS

Em primeiro lugar, gostaria de agradecer ao meu orientador, professor Luís Branco da FCT-NOVA e co-orientadores, professora Benilde Saramago e professor Rogério Colaço do IST-UL, por toda a orientação, apoio profissional e todas as ideias científicas partilhadas ao longo do meu doutoramento. Gostaria também de agradecer por todas as oportunidades de colaborações científicas que me proporcionaram.

À Fundação para a Ciência e Tecnologia pelo financiamento através da bolsa de doutoramento SFRH/BD/140079/2018 e da bolsa excecional COVID/BD/153274/2023. Agradeço também ao IDMEC, e em especial ao professor Rogério Colaço, pela bolsa BI 11.CPM.2023.IDMEC que me apoiou financeiramente na parte final do doutoramento.

Ao LAQV-REQUIMTE do Departamento de Química da FCT-NOVA e ao CQE do Departamento de Química e também ao Departamento de Mecânica do IST-UL por me darem as condições necessárias em termos de instalações, equipamentos e contactos científicos para desenvolver o trabalho experimental do doutoramento.

Gostaria também de agradecer ao professor José Mata por todas as «engenhocas» fora da caixa que arranjou para me ajudar em diversas situações e aos professores Hermínio Diogo, Fernando Caetano, Isabel Marrucho e Helena Pinheiro por disponibilizarem vários equipamentos que precisei ao longo do doutoramento e por toda a ajuda na interpretação e discussão de resultados. Nesse sentido, gostaria de agradecer também ao Dr. Jonas Deuermeier pela análise das minhas amostras por XPS e por toda a ajuda na complexa interpretação dos resultados. Foi um desafio interessante e a sua ajuda foi fundamental!

Gostaria também de agradecer ao professor Robert Carpick da Universidade da Pensilvânia, nos Estados Unidos, pela incrível oportunidade de integrar o seu grupo de investigação em Filadélfia por um período de três meses. Esta colaboração permitiu alargar muito os conhecimentos de Tribologia e terminar a caminhada do estudo de Líquidos Iónicos e Solventes Eutéticos como lubrificantes «em grande», numa vertente de aplicação mais real. Gostaria também de agradecer a todos os colegas do laboratório de Filadélfia que me ajudaram

durante o tempo que lá estive, principalmente ao Pós Doc Pranjal Nautiyal pela enorme partilha de ideias de Tribologia, pelo seu bom humor e positivismo com os meus resultados e por toda a ajuda no trabalho de laboratório.

À Karina Shimizu pelas simulações de Dinâmica Molecular.

Aos meus colegas de laboratório da NOVA e do IST, Carolina Costa, Diana Silva, Nadia Toffoletto, Noémi Jordão e, em particular, à Andreia Santos, Catarina Branco e Mónica Antunes por toda a ajuda e todos os bons momentos que passámos ao longo do doutoramento!

Aos meus amigos por todo o apoio e todas as longas conversas de desabafo e partilha de bons momentos!

Finalmente, gostaria de agradecer à minha família, em particular à minha mãe, ao meu pai e às minhas irmãs Bia e Lau por todo o apoio e por me ouvirem quando as coisas não estavam a correr tão bem e também quando partilhava os meus resultados, mesmo sem entenderem quase nada. Gostaria também de agradecer ao meu namorado Luis por todo o apoio, todas as chamadas à terra e por dizer que sim incondicionalmente; por me apoiar e me ouvir a falar do trabalho de laboratório e por, mesmo sem entender nada do que eu dizia, ter decorado (ainda nem sei bem como) dois nomes inteiros de líquidos iónicos que eu fiz. ☺

Obrigada a todos!! ☺

"You can do whatever you set your mind to." – Benjamin Franklin

ABSTRACT

It is estimated that around 23% of the world's total energy consumption comes from tribological contacts, namely due to energy losses during the mechanical movements, which accentuated the need for more efficient lubrication. Lubricants have been used to lower friction and wear by separating the surfaces sliding in relative motion, increasing the energy efficiency and lifetime of mechanical components. It is of extreme importance that the used lubricants comply with the need for higher sustainability and, with that in mind, researchers all over the world are continuously in the search for new and improved ways of reducing friction and wear.

Ionic Liquids (ILs) are organic salts with low melting point (generally lower than 100 °C) that have attracted the research community due to their very interesting properties such as high chemical and thermal stability, high ionic conductivity, non-flammability, ease in dissolving organic, inorganic and polymeric materials and their tunability towards several applications through the combination of different cations and anions. Besides that, they have very low vapor pressures which makes them environmentally friendly materials. Ionic Liquids often have good performance in friction and wear reduction, by enhancing the tribofilm formation between different tribopairs, making them very promising alternative lubricants. However, they are very expensive to be used as pure lubricants. Viable alternatives are the use of ionic liquids as additives to a base oil or the use of Deep Eutectic Solvents (DESs), which are mixtures possessing a significant decrease on the melting temperature comparing to the original individual components. DESs have similar properties to ILs but can be less toxic, cheaper and easier to prepare, which makes them very interesting and promising lubricant candidates.

In this thesis, the use of different ionic liquids as additives and deep eutectic solvents as lubricants is proposed, with the goal of reducing friction and wear between moving parts, towards a more sustainable world. The most promising fluids can be applied in Nano and Micro electromechanical devices (NEMS/MEMS) which are made of silicon, and also in bearings of steel, which is one of the main materials used in industry.

Keywords: Ionic Liquids, Deep Eutectic Solvents, Friction, Wear, MEMS/NEMS.

RESUMO

Estima-se que ~23% da energia total consumida no mundo provem de contactos tribológicos, nomeadamente devido a perdas de energia durante movimentos mecânicos, o que acentua a necessidade de uma lubrificação mais eficiente. Os lubrificantes têm vindo a ser utilizados para reduzir o atrito e desgaste através da separação das superfícies deslizantes em movimento relativo, aumentando a eficiência energética e o tempo de vida dos componentes mecânicos. É de extrema importância que o uso de lubrificantes cumpra os critérios de uma maior sustentabilidade e, com isso em mente, os investigadores estão continuamente à procura de formas novas e melhoradas de reduzir o atrito e desgaste.

Os Líquidos Iónicos são sais orgânicos com baixo ponto de fusão (geralmente abaixo de 100 °C) que têm vindo a atrair a atenção da comunidade científica devido às suas propriedades interessantes tais como elevada estabilidade química e térmica, elevada condutividade iónica, não inflamabilidade, facilidade em dissolver materiais orgânicos, inorgânicos e poliméricos e a sua capacidade de adequação para diferentes aplicações através da combinação de catiões e aniões diferentes. Além disso, apresentam uma pressão de vapor muito baixa, o que os torna materiais amigos do ambiente. Os líquidos iónicos têm frequentemente bom desempenho em termos de redução de atrito e desgaste, originando a formação de tribofilmes entre diferentes tribopares, o que os torna lubrificantes alternativos muito promissores. No entanto, o seu preço é demasiado alto para serem utilizados como lubrificantes puros. Algumas alternativas viáveis são o uso de líquidos iónicos como aditivos a um óleo base ou o uso de Solventes Eutéticos Profundos (em inglês Deep Eutectic Solvents, DESs), que são misturas cuja temperatura de fusão é muito menor do que as dos componentes individuais que lhes deram origem. Os DESs apresentam propriedades semelhantes às dos líquidos iónicos mas são menos tóxicos, mais baratos e mais fáceis de preparar, o que os torna muito interessantes como lubrificantes.

Nesta tese, propõe-se a utilização de diferentes líquidos iónicos como aditivos e solventes eutéticos profundos como lubrificantes, com o objetivo de diminuir o atrito e desgaste entre superfícies com partes móveis, tendo em vista um mundo mais sustentável. Os fluídos mais promissores poderão ser utilizados em dispositivos Nano e Micro

eletromecânicos (NEMS/MEMS) que são constituídos por silício, e também em rolamentos de aço, que é um dos principais materiais utilizados na indústria.

Palavras chave: Líquidos Iónicos, Solventes Eutéticos Profundos, Atrito, Desgaste, MEMS/NEMS.

LIST OF PUBLICATIONS

THESIS PUBLICATIONS

- **M. T. Donato**, J. Deuermeier, R. Colaço, L. C. Branco, B. Saramago, New Protic Ionic Liquids as Potential Additives to Lubricate Si-based MEMS/NEMS, *Molecules* **2023**, *28* (6), 2678.
- **M. T. Donato**, L. Santos, H. P. Diogo, R. Colaço, L. C. Branco, B. Saramago, Eutectic Systems Containing an Ionic Liquid and PEG200 as Lubricants for Silicon Surfaces: Effect of the Mixture's Molar Ratio, *Journal of Molecular Liquids* **2022**, *350*, 118572.
- **M. T. Donato**, R. Colaço, L. C. Branco, B. Saramago, A Review on Alternative Lubricants: Ionic Liquids as Additives and Deep Eutectic Solvents, *Journal of Molecular Liquids* **2021**, *333*, 116004.
- **M. T. Donato**, F. Caetano, R. Colaço, L. C. Branco, B. Saramago, Picolinium-Based Hydrophobic Ionic Liquids as Additives to PEG200 to Lubricate Steel-Silicon Contacts, *Chemistry Select* **2020**, *5* (20), 5864-5872.

OTHER RELEVANT PUBLICATIONS

- M. Antunes, **M. T. Donato**, V. Paz, F. Caetano, L. Santos, R. Colaço, L. C. Branco, B. Saramago, Improving the Lubrication of Silicon Surfaces Using Ionic Liquids as Oil Additives: The Efect of Sulfur-Based Functional Group, *Tribology Letters* **2020**, *68* (70).

CONTENTS

LIST OF FIGURES

LIST OF TABLES

LIST OF SYMBOLS AND ABBREVIATIONS

δ	Chemical shift of an NMR signal
λ	Specific Film thickness
η	Viscosity
θ	Contac angle
r	Radius of the counter-body or sphere
v	Sliding speed or velocity
Z	Sommerfeld parameter
[4-picH]	4-picolinium cation
[Aliquat]Cl	Tri-octylmethylammonium chloride
[AMIM]	Allyl methylimidazolium cation
[BMIM]	1-butyl-3-methylimidazolium cation
[C_2OHMIM]	1-(2-hydroxyethyl)-3-methylimidazolium cation
[C_6-x-pic]	1-hexyl-x-picolinium cation
[C_6MIM]	1-hexyl-3-methylimidazolium cation
[C_6pyr]	1-hexylpyridinium cation
[DBUH]	1,8-diazabicyclo[5.4.0]-undec-7-ene-8-ium cation
[EMIM]	1-ethyl-3-methylimidazolium cation
[$EtSO_4$]	Ethyl sulfate anion
[HSO_4]	Hydrogen sulfate anion
[$MeSO_3$]	Methanesulfonate or mesylate anion
[$MeSO_4$]	Methylsulfate anion
[MIMH]	Methylimidazolium cation
[N_{4444}]	Tetrabutylammonium cation

$[N_{888H}]$	Trioctylammonium cation
$[NTf_2]$	Bis(trifluoromethylsulfonyl)imide anion
[PyrH]	Pyridinium cation
[TfO]	Trifluoromethanesulfonate or triflate anion
[TMGH]	Tetramethylguanidinium cation
AFM	Atomic Force Microscopy
CoF	Coefficient of Friction
DES	Deep Eutectic Solvents
DSC	Differential Scanning Calorimetry
ES	Eutectic Systems
EHL	Elastohydrodynamic lubrication
F	Applied load
FTIR	Fourier Transform Infrared Spectroscopy
HBA	Hydrogen Bond Acceptor
HBD	Hydrogen Bond Donor
HSPM	Hot Stage Polarized Microscopy
IL	Ionic Liquid
MEMS	Microelectromechanical Systems
NEMS	Nanoelectromechanical Systems
NMR	Nuclear Magnetic Resonance
NOESY	Nuclear Overhauser Effect Spectroscopy
PAO	Polyalphaolefin
PEG 200	Polyethylene Glycol MW 200
PIL	Protic Ionic Liquid
RMS	Root Mean Square roughness
SEM	Scanning Electron Microscopy
Si	Silicon
SRR	Slide to roll ratio
SS	Stainless Steel
$T_{cold\ cristalization}$	Temperature of cold crystallization
T_g	Glass transition temperature
T_{max}	Maximum temperature of a DSC peak

$T_{melting}$	Temperature of the melting peak
T_{Onset}	Temperature of the beginning of a melting peak
XPS	X-ray Photoelectron Spectroscopy

THESIS GUIDELINES

I decided to present my thesis in an article-based format, dividing it into four chapters: Chapter 1, where a state-of-the-art is presented, focusing on the use of ionic liquids and deep eutectic solvents as alternative lubricants; Chapters 2 and 3 with focus on the application of ionic liquids as additives and eutectic systems as neat lubricants for nano and microelectromechanical devices (MEMS/NEMS); and finally Chapter 4 which focuses on the application of ionic liquids and eutetic systems to the lubrication of steel bearings.

Chapter 1 introduces the general context of lubrication and the recent developments on the use of ionic liquids and deep eutectic solvents as lubricants, as well as the main objectives and motivation for the thesis.

Chapters 2 and 3 are divided into several sub-chapters containing the published or submitted/ ready to submit peer reviewed scientific articles, although they are not in chronological order of publication. They are, instead, presented in a way that a comprehensive progress of the field is built. These chapters comprise the synthesis of the ILs and preparation of DESs, as well as their physico-chemical characterization and tribological application for MEMS/NEMS. In these chapters it is also possible to find a brief review on the state of the art, the materials and methods, the results and discussion as well as conclusion for each work.

Finally, Chapter 4 is based on the application of the most promising ionic liquids and deep eutectic solvents in the lubrication of steel bearings. This final part was performed in the University of Pennsylvania, Philadelphia, USA, under the supervision of Professor Robert Carpick and post doctoral researcher Dr. Pranjal Nautiyal.

1

INTRODUCTION

This chapter presents a state of the art on the use of Ionic Liquids and Deep Eutectic Solvents as lubricants. It is based on the published paper: **M. T. Donato**, R. Colaço, L. C. Branco, B. Saramago, A review on alternative lubricants: ionic liquids as additives and deep eutectic solvents, *Journal of Molecular Liquids* **2021**, *333*, 116004.

1.1 General context

It is estimated that around 23% of the world's total energy consumption comes from tribological contacts, namely due to energy losses during mechanical movements.[1] From those, ~20% are related with friction and~3% with wear. Efficient lubrication could eventually decrease these energy losses by 40% in the long term and by 18% in the short term. This would correspond to savings of 1.4% of the gross domestic product in the USA and of 8.7% of the worldwide energy consumption in the long term. With that in mind and moving towards a more sustainable world, it is of extreme importance to have good lubrication between moving parts, aiming at improving global energy efficiency.

Lubricants are substances used to ensure the adequate performance of equipment and machinery involving moving parts through the reduction of friction and wear.[2,3] Lubricants can be liquids (e.g. oil or water), solids (graphite, graphene, Teflon®, molybdenum and tungsten disulfide) or semi-solids (e.g. grease), depending on the application. Fluid lubrication is used when the operating conditions are mild because it is easy to apply, has long term service life, leads to low mechanical noise and promotes thermal conductance.[4] The conventional commercial fluid lubricants are pure mineral oils or mixtures with additives (between 5 and 30%). Besides reducing friction and wear, additives are used to provide better viscosity, viscosity index and resistance to processes of oxidation and corrosion. The demand for new and more efficient lubricants has grown due to technological development and ecological issues, and ionic liquids (ILs) have demonstrated great potential in lubrication. However, they are very expensive to be used as pure lubricants, so the use of ILs as additives became a much more adopted approach. Deep Eutectic Solvents (DES) share some of the unique properties of ILs but with the advantages of being cheaper, easier to prepare and less toxic, which makes them very sustainable lubricant alternatives. The objective of the Ph.D. was to develop and characterize new ionic liquids and deep eutectic solvents with potentially good tribological properties, namely in silicon contacts, which mimic NEMS/MEMS devices, and steel surfaces, since steel is yet one of the most widely used materials due to its hardness and resistance.

1.2 Tribology: friction, wear and lubrication

Tribology is the science of interaction of solid surfaces in motion and includes the study of friction, wear, and lubrication.[5] Lubrication aims at minimizing friction and wear, and can be classified in three regimes, according to the Stribeck curve defined as the plot of coefficient of friction (CoF) *vs*. Sommerfeld parameter (Figure 1.1). The Sommerfeld parameter, Z, is defined by the following equation:

$$Z = \frac{\eta v r}{N} \qquad \text{Eq. 1.1}$$

where η is the fluid viscosity, v is the sliding speed, r is the radius of the sphere used as counter-body and N is the applied load. Depending on the distance that separates the two surfaces, lubrication can be (i) hydrodynamic, (ii) elasto-hydrodynamic (EHL), (iii) mixed lubrication and (iv) boundary lubrication.

In boundary lubrication, also called limit lubrication, the sliding surfaces are separated by a very thin molecular film of lubricant so the chemical and physical natures of the surfaces and lubricant are of extreme importance. In this regime the asperities of the two lubricated surfaces in relative motion with each other may come into physical contact and the potential for abrasion and/or adhesion occurs. Under heavily load conditions or low speeds (lower Z) the surfaces may actually come into severe contact with each other because the oil film is not thick enough to overcome the surface roughness of the substrate, resulting in a specific film thickness, $\lambda<1$, in which λ is the ratio between the lubricant film thickness and the composite surface roughness of the two contacting surfaces. Improving boundary lubrication and thus avoiding higher friction can be obtained by tuning the lubricant's viscosity: a lubricant with too low viscosity cannot prevent contact between the sliding surfaces; on the other hand, a lubricant with too high viscosity will result in an increased internal friction, which in turn leads to energy loss. Another way of overcoming boundary lubrication challenges is to use anti-wear or extreme pressure additives. The additives react with the surface asperities that have come into contact by responding to the high pressure and high temperature of contact and forming a protective sacrificial film that is worn away, instead of the metal surface, as the surfaces slide or roll over each other.

As sliding speeds increase, a thicker lubricant film is formed between the sliding surfaces, reducing asperities' contact and coefficient of friction. This is known as the mixed regime, in which the load is supported by both the asperities in contact and the lubricant. As the film thickness of the lubricant increases ($1<\lambda<3$), the system moves into full film lubrication, going towards the right part of the Stribeck curve.

In elasto-hydrodynamic lubrication regime (EHL), a rolling motion exists between the moving surfaces and the contact zone has a low degree of conformity. This rolling motion causes an increase in pressure on the point of contact. This in turn causes the lubricant's pressure to rise sharply, increasing its viscosity and load-holding capability, which leads to slight deformation of the surface, called plastic deformation.

In hydrodynamic regime, the load is fully supported by the formed film, which means that the lubricant lifts the contacting surface so there is little risk of asperity contact ($\lambda>3$). For this lubrication regime to occur, the contacting pressure must be low. Also the lubricant's viscosity must be such that this regime will be maintained under every operating conditions such as high speed and high load, low speed and high load, low speed and low load, etc. However, if the lubricant's viscosity is too high, the internal resistance of the oil's molecules will reduce

operating efficiency and temperature will increase. This lubrication regime is desirable to avoid friction and wear and any remaining friction is found on the lubricant itself.

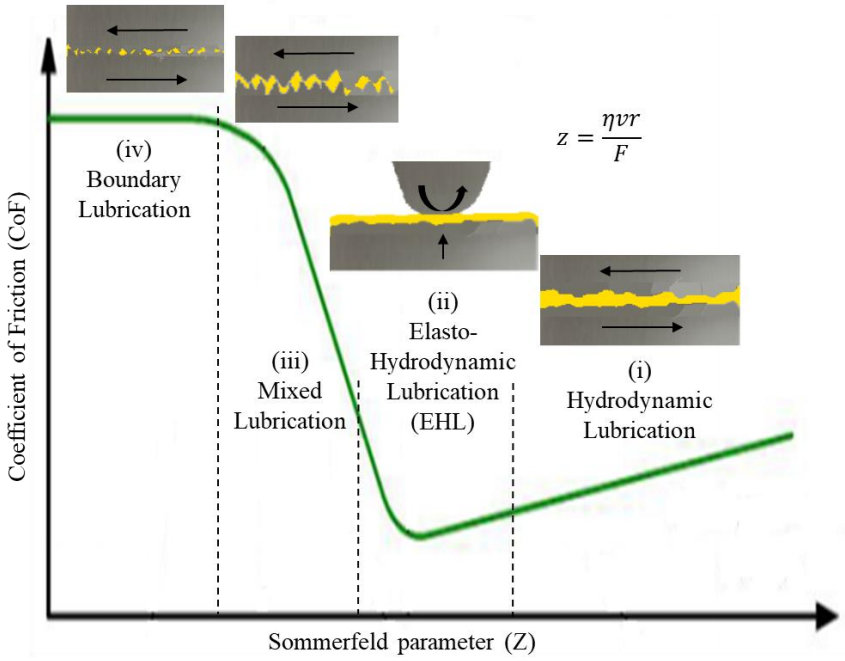

Figure 1.1. Different lubrication regimes: (i) hydrodynamic, (ii) elasto-hydrodynamic (EHL), (iii) mixed lubrication and (iv) boundary lubrication.

1.3 Ionic Liquids as lubricants

Ionic Liquids (ILs) are defined as organic salts comprised entirely of ions, which exhibit melting points below 100 °C.[6] They were first reported in the literature in the beginning of the last century, but with higher impact in the 1980's.[7] ILs have unique properties such as high chemical and thermal stability, almost negligible vapor pressure, non-flammability, high ionic conductivity and ease in dissolving organic, inorganic and polymeric materials.[8] Besides, it is important to stress the possibility of tuning the IL's physico-chemical properties such as melting point, viscosity, density, polarity and solubility through the combination of different cations and anions, making them suitable for many applications.[9] The range of applications of ILs is very wide including the use as electrolytes in batteries or for metal electrodeposition[10,11] and as alternative solvents for organic synthesis and catalysis, instead of the commonly used organic ones that are toxic and harmful to the environment.[7,12–15] In general, ILs have been applied in several research topics including Chemical Engineering, Tribology, Analytical Chemistry, Materials, Biology, Biotechnology, Physical Chemistry and Pharmacy,[16] among others.

In the Tribology field, ILs have emerged as a greener alternative for the commonly used oils. They were first proposed as lubricants in 2001 by Ye *et al*.[17] in a pioneer study using the imidazolium-based ILs 1-methyl-3-hexylimidazolium tetrafluoroborate [C_6MIM][BF_4] and 1-ethyl-3-hexylimidazolium tetrafluoroborate [C_6C_2im][BF_4]. The ILs were investigated as neat lubricants in several types of contacts and, when compared to traditional lubricants, such as perfluoropolyether and phosphazene, they exhibited superior tribological performance, namely friction and wear reduction. Since then, many papers, including some extensive reviews,[2,18–21] have been published reporting the tribological application of ILs. In contrast, the use of ILs as lubricant additives has been addressed in a much smaller number of papers and reviews [8,21,22] and thus it will be one of the focus points of this work.

1.3.1 Ionic Liquids as lubricant additives

ILs have demonstrated an excellent performance as lubricants, but they are still too expensive to be applied in industry as neat lubricants. A viable solution to overcome this disadvantage is to use ILs as additives to common lubricant base oils. ILs were firstly proposed as room temperature lubricant additives in studies performed by Iglesias *et al*.[23] and Jiménez *et al*.[24,25] in 2004-2006 but, only in 2012, with the synthesis of ILs soluble in nonpolar lubricant oils,[26] the investigation of lubrication with IL additives became a trending research topic. Since then, many articles were published, but, to our knowledge, the developments of the research in this field were addressed only in three review articles, the first one published in 2017[8] and the other two, in 2020.[21,22] The correlations of the chemical structure and other physicochemical properties of the IL additives with their tribological performance and the role of the tribofilms were discussed in the first two references,[8,21] while the use of ILs as additives in bio-lubricants was addressed in the latter one.[22]

In this chapter, the data are organized by IL families and the most relevant results are presented in chronological order. The division in families was done according to the chemical nature of their organic cations, since many studies concentrate on a particular cation combined with several anions and the number of homologous cation-based series is much larger than the one based on anions. In this context, the following organic cations were chosen: imidazolium, phosphonium, ammonium, pyrrolidinium, pyridinium and guanidinium. A final section is dedicated to miscellaneous ILs. The structures of the cations and the anions involved are presented in Figure 1.2. An overview of the studied systems, according to the cation, is given in Table 1.1 which includes the amount of IL used, the base stock, the type of system/contact and the respective paper where the results are published.

Cations

Imidazolium
[R^1R^2im]

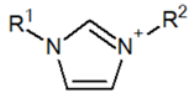

Phosphonium
[$PR^1R^2R^3R^4$]

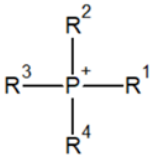

Ammonium
[$NR^1R^2R^3R^4$]

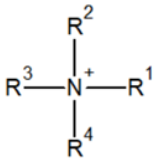

Pyridinium
[$R^1R^2R^3R^4pyr$]

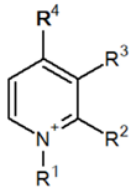

Pyrrolidinium
[R^1R^2pyrr]

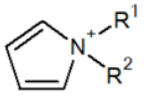

Guanidinium
[TMG]

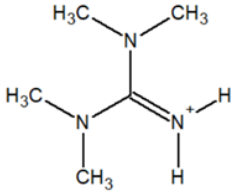

Anions

Hexafluorophosphate
[PF_6]

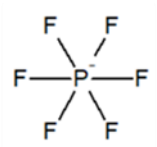

Tetrafluoroborate
[BF_4]

Triflate
[TfO]

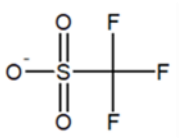

Dicyanamide
[DCA]

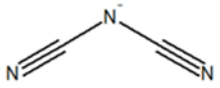

Methyl sulfate
[$MeSO_4$]

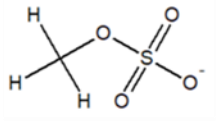

Ethyl sulfate
[$EtSO_4$]

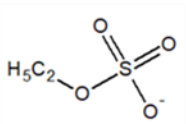

Butyl sulfate
[$BuSO_4$]

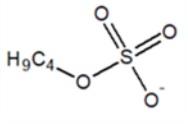

Octyl sulfate
[$OcSO_4$]

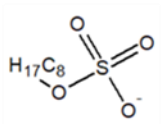

Bistrifluoromethyl sulfonyl)imide, [NTf_2]

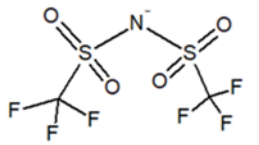

Chloride
[Cl]

Mesylate
[$MeSO_3$]

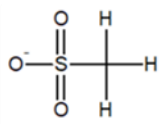

Bis(2,4,4-trimethylpentyl) phosphinate, [BTMPP]

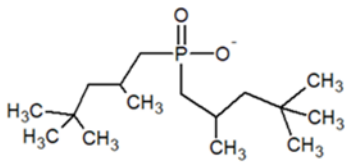

Bis(2-ethyl-hexyl) phosphate
[BEHP]

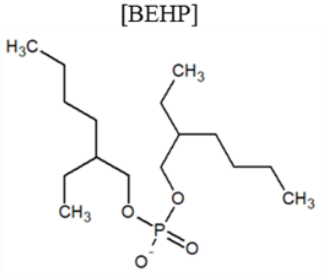

Dimethyl phosphate
[DMP]

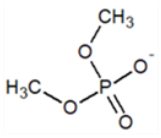

Dibutyl phosphate
[DBP]

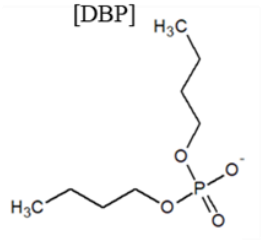

Bis(2,4,4-trimethylpentyl)
dithiophosphinate, [BTMPDTP]

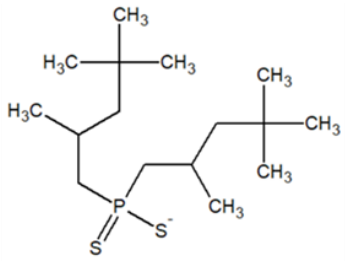

Carboxylate anions

R = [C_7H_{15}], Caprylate, [CA]

R = [C_9H_{19}], Decanoate, [DC]

R = [$C_{11}H_{23}$], Laureate, [LATS]

R = [$C_{13}H_{27}$], Myristate, [MA]

R = [$C_{15}H_{31}$], Palmitate, [PAL]

R = [$C_{17}H_{35}$], Stearate, [ST]

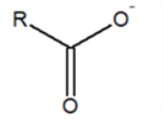

Diphenyl phosphate
[DPP]

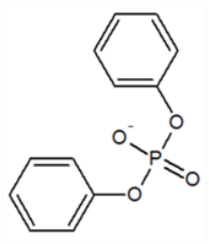

Tris(pentafluoroethyl)
trifluorophosphate, [FAP]

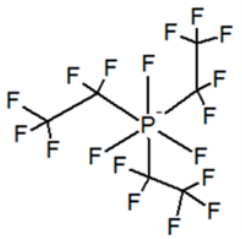

O,O-diethyl-dithiophosphate
[DEDTP]

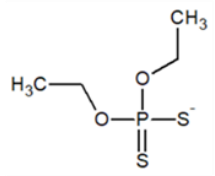

Dibutyl-dithiophosphate
[DBDTP]

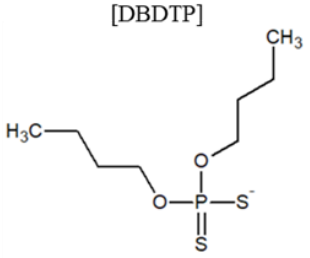

O-ethyl phosphinate
[EP]

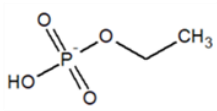

O-butyl phosphinate
[BP]

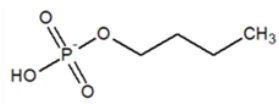

Adipate
[AD]

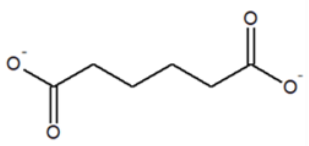

Salicylate
[SA]

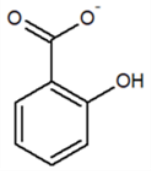

Aspartate
[AS]

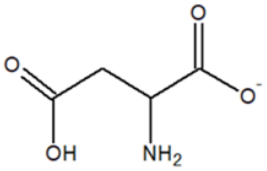

Glutamate
[GL]

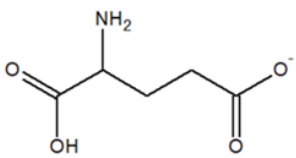

Sulphonate
[SO_3]

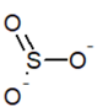

Phosphate
[PO_3]

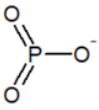

Heptadecane benzene sulfonyl
[$C_{17}BS$]

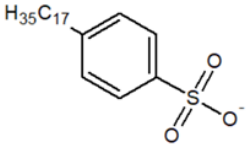

Histidine
[HT]

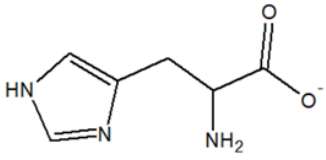

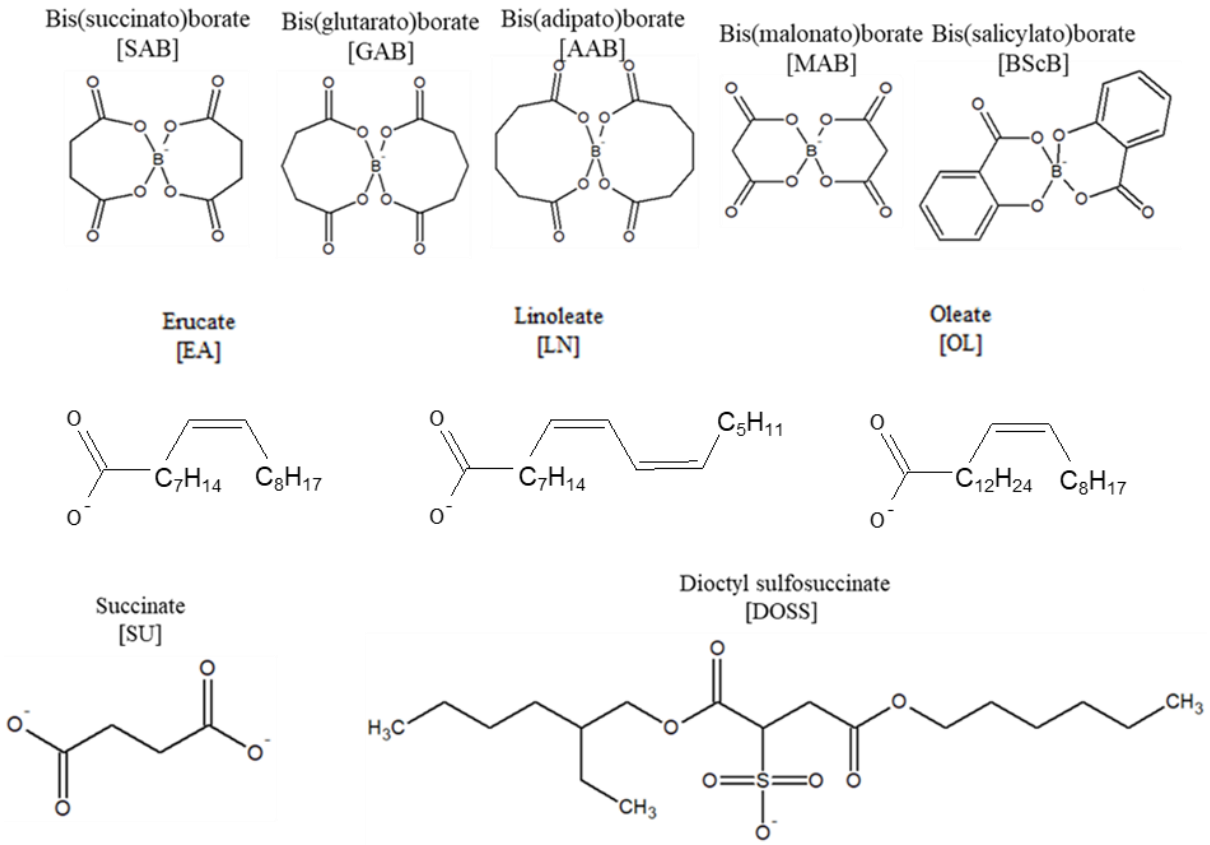

Figure 1.2. Structures of the cations and anions reviewed on this paper.

Table 1.1. Overview of the studied systems, according to the cation.

Cation	R	Anions	Amount/ wt.%	Base stock	System	Ref
Imidazolium	R^1=methyl, R^2=butyl, [C_4MIM]	[PF_6]	1	Polyurea grease (PUG)	Steel/ Steel (S/S)	[27]
		[PF_6]	0.1	Graphene (GO)	S/S	[28]
		[BF_4]	0.1	GO	S/S	[28]
		[NTf_2]	0.1	GO	S/S	[28]
		[TfO]	2	Polyethylene glycol (PEG)	S/Si	[29]
		[DCA]	2	PEG	S/Si	[29]
	R^1=methyl, R^2=hexyl, [C_6MIM]	[PF_6]	1	PUG	S/S	[27]
			2	PEG	S/S	[30]
		[BF_4]	1	PUG	S/S	[27]
		[NTf_2]	0.1	GO	S/S	[28]
	R^1=methyl, R^2=octyl, [C_8MIM]	[PF_6]	1	PUG	S/S	[27]
		[BF_4]	5	Isoparaffinic base oil+GO	S/sapphire	[31]
	R^1=methyl, R^2=decyl, [C_{10}MIM]	[PF_6]	1	PUG	S/S	[27]
	R^1=methyl, R^2=hydroxyethyl, [C_2OHMIM]	[BF_4]	1	GO+Water	S/S	[32]
		[NTf_2]	1	GO+Water	S/S	[32]
	R^1=methyl, R^2=ethyl, [C_2MIM]	[BF_4]	1	Propylene Glycol Dioleate (PGDO)	S/Al	[33]

	R	Anions	Amount/ wt.%	Base stock	System	Ref
	R^1=methyl, R^2=ethyl, [C_2MIM]	[NTf_2]	1	PGDO	S/Al	[33]
		[$MeSO_4$]	0.63, 2.5, 6	Glycerol	S/S	[34]
		[$BuSO_4$]	0.63, 2.5, 6	Glycerol	S/S	[34]
		[$OcSO_4$]	0.63, 2.5, 6	Glycerol	S/S	[34]
		[TfO]	2	PEG	S/Si	[29]
		[$EtSO_4$]	2	PEG	S/Si	[29]
	R^1=methyl, R^2=hexadecyl, [C_{12}MIM]	[BF_4]	0.1-2	Liquid paraffin	S/S	[35]
	R^1=methyl, R^2=1-(3,5-ditert-butyl-4-hydroxybenzyl), [BHTMIM]	[PF_6]	1	PEG	S/S	[36]
			2	PEG, PUG	S/S	[30]
		[BF_4]	1	PEG	S/S	[36]
		[NTf_2]	1	PEG	S/S	[36]
	R^1=methyl, R^2=3-((1H-benzo[d][1,2,3] triazol-1-yl)methyl)-1-methyl-1H, [BTAMIM]	[PF_6]	2	PEG, PUG	S/S	[30,37]
					S/Cu	[38]
		[BF_4]	2	PEG, PUG	S/S	[37]
		[NTf_2]	2	PEG, PUG	S/S	[37]
	R^1=methyl, R^2=2,6-di-tert-butyl-4-(chloromethyl) phenol	[PF_6]	2	PEG	S/S	[30]
	R^1=methyl, R^2=1-(chloromethyl)-1H-benzo[d][1,2,3]triazole	[PF_6]	2	PEG	S/S	[30]
	R^1=vinyl, R^2=ethyl, [EVIM]	[$EtSO_4$]	2	PEG	S/Si	[29]

	R	Anions	Amount/ wt.%	Base stock	System	Ref
	R^1=methyl, R^2=1-((1H-benzo[d][1,2,3]triazol-1-yl)methyl)	$[PF_6]$	2	PEG	S/S	[30]
	R^1=methyl, R^2=1-(2-hydroxyethyl), [C_2OHMIM]	[TfO]	2	PEG	S/Si	[29]
		[DCA]	2	PEG	S/Si	[29]
	R^1=methyl, R^2=1-allyl, [AMIM]	[TfO]	2	PEG	S/Si	[29]
	R^1= methyl, R^2=triethylene glycol, [MIM-TEG-MIM]	$[Cl]_2$	1	Polypropylene glycol, PPG	S/S	[39]
		$[NTf]_2$	1	PPG	S/S	[39]
		$[MeSO_3]_2$	1	PPG	S/S	[39]
	R^1=methyl, R^2=H, R^3=pentyl, [MIM(C_5)MIM]	[BScB	2	PEG200	S/S	[40]
	R^1=R^2=methyl, R^2=pentyl, [DMIM(C_5)DMIM]	[BScB]	2	PEG200	S/S	[40]
	R^1=butyl, R^2=H, R^3=pentyl, [C_4MIM(C_5)C_4MIM]	[BScB]	2	PEG200	S/S	[40]
Phosphonium	R^1=R^2=R^3=hexyl, R^4=tetradecyl, [P_{66614}]	[BTMPP]	5	Polyalphaolefin (PAO), 10W, 10W30	S/Fe	[41]
			6*	SAE 15W40	Fe/Fe	[42,43]
			0.25, 0.5, 1	YUBASE™	S/S	[44]
			1	Gas-to-liquids base oil (GTL)	S/Fe	[45]
		[BEHP]	5	PAO, 10W, 10W30	S/Fe	[41]
			1	Zinc di-alkyl di-thiophosphate (ZDDP)	S/S	[46]
			1	ZDDP	Si_3N_4/S	[46]

	R	Anions	Amount/ wt.%	Base stock	System	Ref
	R^1=R^2=R^3=hexyl, R^4=tetradecyl, [P_{66614}]	[BEHP]	1.03	PAO4	S/Fe	[47]
			1.04	GTL 4 cSt	S/Fe	[48]
			6*	SAE 15W40	Fe/Fe	[42,43]
			0.25, 0.5, 1	YUBASE™	S/S	[44]
			1.04	GTL	S/Fe	[45]
			1	0.1 wt.% boron nitride nanoparticles (h-BN)+ PAO 32	S/S	[49]
		[BTMPP]	1	0.1 wt.% h-BN + PAO 32	S/S	[49]
		[DEP]	1	VO, BPE, TMP, TTM	S/S	[50]
		[FAP]	1	VO, BPE, TMP, TTM	S/S	[50]
		[DBP]	5	PAO, 10W, 10W30	S/Fe	[41]
		[BTMPDTP]	5	PAO, 10W, 10W30	S/Fe	[41]
		[DPP]	0.7-0.9	Safflower oil (SO)	S/S	[51]
		[CA]	1.65	PAO4	S/Fe	[47]
		[DC]	-	PAO4	S/Fe	[47]
		[ST]	1.98	PAO4	S/Fe	[47]
		$[SO_3]^{2-}$	2.44	PAO4	S/Fe	[47]
		[BTMPP]	0.1	60 wt.% solvent neutral 150W + 40 wt.% bright stock 90W	S/S	[52]
		$[NTf_2]$	0.1	150W+90W	S/S	[52]

	R	Anions	Amount/ wt.%	Base stock	System	Ref
	R^1= R^2=R^3=butyl, methyl, R^4=ethyl, [P_{4442}]	[DEP]	1	0.1 wt.% h-BN + PAO 32	S/S	[49]
			1	VO, BPE, TMP, TTM	S/S	[50]
			2	0.1 wt.% h-BN + TTM, 0.1 wt.% graphene nanoplatelets (GnPs) + TTM	S/S	[53]
		[FAP]	1	VO, BPE, TMP, TTM	S/S	[50]
	R^1=methyl, R^2=R^3=R^4=butyl, [P_{1444}]	[DPP]	0.7-0.9	SO	S/S	[51]
		[DMP]	0.7-3.4	[C_2im][TBB], [aim][TBB], [C_4MIM][NTf_2]	S/S	[54]
			0.1	150W+90W	S/S	[52]
	R^1=R^2=R^3=R^4=butyl, [P_{4444}]	[BEHP]	0.75	PAO4	S/Fe	[47]
			1.04	GTL 4 cSt	S/Fe	[48]
		[DEDTP]	0.1	150W+90W	S/S	[52]
	R^1=methyl, R^2=R^3=R^4=octyl, [P_{1888}]	[DBP]	5	FVA3	S/S	[55]
		[BTMPP]	5	FVA3	S/S	[55]
	R^1=R^2=R^3=R^4=octyl, [P_{8888}]	[BEHP]	1.04	GTL 4 cSt	S/Fe	[48]
	R^1=R^2=R^3=octyl, R^4=tetradecyl, [P_{44414}]	[BEHP]	1.04	GTL 4 cSt	S/Fe	[48]
	R^1=R^2=R^3= butyl, R^4=octyl, [P_{4448}]	[BEHP]	1.04	GTL 4 cSt	S/Fe	[48]
Ammonium	R^1=ethyl, R^2=R^3=methyl, R^4=methoxyethyl, [$N_{2112OCH3}$]	[FAP]	1	PAO6	CrN PVD, TiN PVD coatings	[56,57]

	R	Anions	Amount/ wt.%	Base stock	System	Ref
	$R^1=R^2= CH_2CH_2OH$, $R^3=R^4=H$, $[N_{22HHOH}]_2$	[AD]	1	PAO6	Cu/Cu	[58]
	$R^1=R^2= CH_2CH_2OH$, $R^3=R^4=H$, $[N_{22HHOH}]$	[SA]	-	PAO6	Cu/Cu	[58]
		[OL]	-	PAO6	Cu/Cu	[58]
		[SU]	1	Water	Sapphire/S	[59]
	R^1=octadecyl, $R^2=R^3=R^4=H$, $[N_{18HHH}]$	$[C_{17}BS]$	2	PAO10	S/S	[60]
	R^1=dodecyl, $R^2=R^3=R^4=H$, $[N_{12HHH}]$	$[C_{17}BS]$	2	PAO10	S/S	[60]
	R^1=methyl, $R^2=R^3=R^4$=octyl, $[N_{1888}]$	[DOSS]	1	PAO	S/S S/Cu	[61]
		[DBP]	5	FVA3	S/S	[55]
		[BTMPP]	5	FVA3	S/S	[55]
	R^1=methyl, $R^2=R^3=R^4$=dodecyl, $[N_{1121212}]$	[DOSS]	1	PAO	S/S S/Cu	[61]
		[DBP]	5	FVA3	S/S	[55]
		[BTMPP]	5	FVA3	S/S	[55]
	$R^1=R^2=R^3$=octyl, $R^4=H$, $[N_{888H}]$	[BEHP]	1.74	Low viscosity base oil + Exp. Base oil	S/Fe	[62]
		[BEHP]	1.04	GTL	S/Fe	[45]
	$R^1=R^2=R^3$=propyl, R^4=pentyl, $[N_{3335}]$	[BScB]	2	PEG200	S/S	[40]
	$R^1=R^2=R^3$=octyl, R^4=pentyl, $[N_{8885}]$	[BScB]	2	PEG200	S/S	[40]
	$R^1=R^2$=methyl, R^3=cyclohexane, $R^4= Cy_{65}$, $[N_{11Cy65}]$	[BScB]	2	PEG200	S/S	[40]

	R	Anions	Amount/ wt.%	Base stock	System	Ref
	$R^1=R^2=R^3=R^4$=octyl, [N_{8888}]	[BEHP]	2.04	Low visc. base oil + Exp. Base oil	S/Fe	[62]
		[DOSS]	1	PAO	S/S S/Cu	[61]
		[PO_3]	0.5, 1, 2, 3	PAO10	S/S	[63]
	$R^1=R^2=R^3$=nonyl, R^4=octyl, [N_{9998}]	[PO_3]	0.5, 1, 2, 3	PAO10	S/S	[63]
	$R^1=R^2=R^3$=decyl, R^4=octyl, [$N_{1010108}$]	[PO_3]	0.5, 1, 2, 3	PAO10	S/S	[63]
	$R^1=R^2=R^3$=octyl, R^4=dodecyl, [N_{88812}]	[PO_3]	0.5, 1, 2, 3	PAO10	S/S	[63]
	$R^1=R^2=R^3$=nonyl, R^4=dodecyl [N_{99912}]	[PO_3]	0.5, 1, 2, 3	PAO10	S/S	[63]
	$R^1=R^2=R^3$=decyl, R^4=dodecyl [$N_{10101012}$]	[PO_3]	0.5, 1, 2, 3	PAO10	S/S	[63]
	R^1=methyl, $R^2=R^3=R^4$=octyl, [N_{1888}]	[BEHP]	1.78	Low visc. base oil + Exp. Base oil	S/Fe	[62]
		[DOSS]	1	PAO	S/S, S/Cu	[61]
	$R^1=R^2=R^3=R^4$=butyl, [N_{4444}]	[AS]	0.15, 0.3, 1, 1.5, 2, 3	Solvent neutral N-150	S/S	[64]
		[GL]		N-150	S/S	[64]
		[DOSS]	1	PAO	S/S, S/Cu	[61]
		[DBP]	0.5	P106, PAO10 + PAO40, EO	S/Al	[65]
		[MAB]	0.5, 1, 2	PEG200	S/S	[66]
		[SAB]	0.5, 1, 2	PEG200	S/S	[66]
		[GAB]	0.5, 1, 2	PEG200	S/S	[66]
		[AAB]	0.5, 1, 2	PEG200	S/S	[66]
		[ST]	2	Polyol Ester (PE)	S/S	[67]

	R	Anions	Amount/ wt.%	Base stock	System	Ref
	R^1=butyl, R^2=R^3=R^4=H, [N_{4HHH}]	[OL]	2	PE	S/S	[67]
		[LN]	2	PE	S/S	[67]
		[AS]	2	PE	S/S	[68]
		[GL]	2	PE	S/S	[68]
		[DBP]	0.5	P106, PAO10 + PAO40, EO	S/Al	[65]
	R^1=R^2=R^3=R^4=hexyl, [N_{6666}]	[CA]	0,5, 2	PE	S/S	[69]
		[PAL]	0.5, 2	PE	S/S	[69]
	R^1=R^2=butyl, R^3=R^4=H, [N_{44HH}]	[BP]	0.1-5	PEG	S/S	[70]
		[EP]	0.1-5	PEG	S/S	[70]
	R^1=R^2=R^3=dodecyl, R^4=$C_3H_6PO(OC_2H_5)_2$, [$N_{121212C3POOC2}$]	[DOSS]	1, 2, 3	PAO10	S/S	[71]
		[LATS]	1, 2, 3	PAO10	S/S	[71]
	R^1=R^2=R^3=methyl, R^4= hexadecyl, [N_{11116}]	[BEHP]	1	PAO10	S/S	[72]
	R^1=R^2=R^3=methyl, R^4=hexadecyl, [N_{11116}]$_2$	[BEHP]$_2$	1	PAO10	S/S	[72]
	R^1=R^2=R^3=ethyl, R^4= methyl, [N_{2221}]	[$MeSO_4$]	0.625, 2.5, 8	Glycerol	S/S	[73]
	R^1=R^2=H, R^3=R^4= C_2H_4OH, [N_{22HHOH}]$_2$	[SU]	1	Water	S/S	[74]
Pyrrolidinium and Pyridinium	R^1=butyl, R^2=methyl, [C_4C_1-pyrr]	[FAP]	Neat	PAO	TiN, CrN, DLC coatings	[75]
	R^1=butyl, R^2= methyl, [C_4C_1-pyr]	[NTf_2]	5	PAO	S/S	[76]
		[$MeSO_4$]	0.625, 2.5, 8	Glycerol	S/S	[73]
	R^1=methyl, R^2=TEG, [C_1-pyrr-TEG-C_1-pyrr]	[Cl]$_2$	1	PPG	S/S	[39]

	R	Anions	Amount/ wt.%	Base stock	System	Ref
	R^1=methyl, R^2=TEG, [C_1-pyrr-TEG-C_1-pyrr]	$[NTf_2]_2$	1	PPG	S/S	[39]
		$[MeSO_3]_2$	1	PPG	S/S	[39]
	R^1=methyl, R^2=R^3=R^4= H, [C_1-pyr]	$[MeSO_4]$	0.25, 0.5, 1.0	Glycerol	S/S	[77]
		$[NTf_2]$	0.25, 0.5, 1.0	Glycerol	S/S	[77]
	R^1=methyl, R^2=R^3=R^4= CH_2OCH_2, [C_1-pyr$(CH_2OCH_2)_3C_1$-pyr]	$[MeSO_4]_2$	0.25, 0.5, 1.0	Glycerol	S/S	[77]
		$[NTf_2]_2$	0.25, 0.5, 1.0	Glycerol	S/S	[77]
Guanidinium	R^1=R^2=R^3=R^4=methyl, [TMG]	[CA]	0.05, 0.1, 0.5, 1, 1.5	N-150	S/S	[78]
		[MA]	0.05, 0.1, 0.5, 1, 1.5	N-150	S/S	[78]
		[OL]	0.05, 0.1, 0.5, 1, 1.5	N-150	S/S	[78]
		[EA]	0.05, 0.1, 0.5, 1, 1.5	N-150	S/S	[78]
		[LN]	0.05, 0.1, 0.5, 1, 1.5	N-150	S/S	[78]
		[HT]	0.5, 1, 2, 3	PEG200	S/S	[79]
		[GL]	0.5, 1, 2, 3	PEG200	S/S	[79]
		[AS]	0.5, 1, 2, 3	PEG200	S/S	[79]
Miscellaneo	$[Li(C_3N_3(OR)_3)]$	$[NTf_2]$	0.1-1	Multiply-alkylated cyclopentanes (MACs)	S/S	[80]

	R	Anions	Amount/ wt.%	Base stock	System	Ref
	$[Li(P_3N_3(OR)_6]$	$[NTf_2]$	0.1-1	MACs	S/S	[80]
	[Li(BTAG3)]	$[BF_4]$	1	MACs	S/S	[80]
		$[PF_6]$	1	MACs	S/S	[80]
		[TfO]	1	MACs	S/S	[80]
		$[NTf_2]$	1	MACs	S/S	[80]
	[Li(glyme)]	$[NTf_2]$	1, 3, 5	PEG400	S/S	[81]
	[Ch]	[BEHP]	0.1	150W+90W	S/S	[52]
		[DBDTP]	0.1	150W+90W	S/S	[52]
	PANI-doped $[C_4$-3-MIM]	$[PF_6]$	0.2 0.3	PAO PUG	S/S	[82]
		$[BF_4]$	0.2 0.3	PAO PUG	S/S	[82]

*vol.%

1.3.1.1 Imidazolium-based additives

Imidazolium-based ILs are probably the most used additives since the initial works in the years 2004-2009.[8,83–85] In the beginning of the present decade, the group of Liu studied the effect of adding imidazolium-based ILs to poly(ethylene glycol) (PEG) and polyurea grease (PUG) on the lubrication of steel/steel and steel/copper pairs at room and high temperatures. They found great friction and wear reduction, which was attributed to the formation of boundary lubrication films. Several kinds of ILs composed by the anions tetrafluoroborate [BF_4], hexafluorophosphate [PF_6] and bis(tri fluoro methyl sulfonyl) imide [NTf_2], and by imidazolium-based cations containing alkyl groups,[27] sterically hindered phenol groups,[36] a benzotriazole group [37,38] and both phenol and benzotriazole groups [30] were tested. The bi-functional ILs investigated in the latter work were able to overcome the corrosion problems associated with the hydrolysis of perfluoro anions and, when added to PEG400, revealed better tribological properties than the commonly used IL-additive P106 (1-methyl-3-hexyl-imidazolium hexafluorophosphate). XPS analysis suggested the formation of protective films by tribochemical reaction leading to iron-containing compounds, but physical adsorption leading to nitrogen double-bond compounds could not be ruled out.

Jiménez and Bermúdez studied the effect of adding short alkyl chain imidazolium ILs to propylene glycol dioleate in the lubrication of aluminum alloys and found reduction of wear but no alteration in friction.[33] Alternatively, Zhang *et al*.[35] synthesized a long alkyl chain imidazolium IL liquid crystal, which was used as an additive to liquid paraffin in the lubrication of steel/steel contacts. They found a decrease both in CoF and wear due to the formation of a protective film on the steel surface, which underwent a transition to a mesophase due to friction-induced heating.

Pejaković *et al*.[34] studied the behavior of 1-ethyl-3-methylimidazolium sulfates, with different alkyl chain lengths in the anion, as additives to glycerol. The lubrication tests using steel/steel pairs demonstrated that the anion n-butyl sulfate was better than the anions methyl and octyl sulfate for low-speed conditions. When compared to octyl sulfate, this could be due to the larger number of molecules of 1-ethyl-3-methylimidazolium n-butyl sulfate able to form the protective surface layer, since the solutions contained the same weight ratio of ILs. The same group found that, at high temperatures, the maximum efficacy of these additives was obtained at very small concentrations (<0.63 w%) and should be related with the possibility of the sulfate group interacting with the steel surface to form a sulfidic species, rather than with the length of the anion alkyl chain.[86]

Several authors studied the possibility of associating imidazolium-based ILs to graphene to achieve additives with good efficiency. Fan and Wang[28] modified sheets of graphene oxide (GO) and graphene (G) with 1-butyl-3-methylimidazolium tetrafluoroborate [C_4-3-MIM][BF_4], 1-butyl-3-methylimidazolium hexafluorophosphate [C_4-3-MIM][PF_6], and 1-hexyl-3-

methylimidazolium bis(tri fluoro methyl sulfonyl)imide [C_6-3-MIM][NTf_2] and added them on multialkylated cyclopentanes to lubricate steel contacts. They found considerable reduction of friction and wear, which was attributed to the formation of films by physical adsorption of GO and G and tribo-chemical reactions between the functional groups of ILs and the surfaces. Sanes *et al*.[31] used the IL 1-octyl-3-methylimidazolium tetrafluoroborate [C_8-3-MIM][BF_4], graphene and graphene+IL as additives in an isoparaffinic base oil at room temperature and a fully-formulated base oil at 150 °C. The tribological tests were performed with a sapphire-stainless steel system. In the case of isoparaffinic base oil, the best performance was obtained with graphene+IL because the IL contributed for the separation of the sliding surfaces. No tribo-corrosion was observed in any case when the IL was present as additive; moreover, the presence of the IL could prevent oxidation of the wear tracks on the surface. In the case of the tests performed with the fully-formulated base oil at 150 °C, the addition of a small amount of graphene was sufficient to reduce the CoF up to 73%, which was attributed to the formation of a protective graphene-containing layer on the surface. Recently, Gan *et al*. used two ILs based on the cation 1-(2-hydroxyethyl)-3-methylimidazoium [C_2OHMIM] and the anions [BF_4] and [NTf_2] as coupling agents to functionalize GO, which was then dispersed in water.[32] The obtained dispersions were used in the lubrication of steel pairs and exhibited excellent anti-wear properties. The authors attributed this behavior to electrostatic adsorption of a self-healing and self-wetting film on the interface region.

More recently, Amorim *et al*.[29] reported imidazolium based additives to lubricate silicon surfaces. The studied ionic liquids were 1-ethyl-3-metylimidazolium triflate [C_2MIM][TfO], 1-butyl-3-methylimidazolium triflate [C_4MIM][TfO], 1-(2-hydroxyethyl)-3-methylimidazolium triflate [C_2OHMIM][TfO], allyl methylimidazolium triflate [AMIM][TfO], 1-butyl-3-methylimidazolium dicyanamide [C_4MIM][DCA], 1-(2-hydroxyethyl)-3-methylimidazolium dicyanamide [C_2OHMIM][DCA], 1-ethyl-3-methylimidazolium ethyl sulfate [C_2MIM][$EtSO_4$] and 1-ethyl-3-vinylimidazolium ethyl sulfate [evim][$EtSO_4$] as 2 wt.% additives to PEG 200. The structures of the studies ILs and the results of the tribological experiments are presented in Figure 1.3. A decrease in the CoF was observed for all the ILs added to PEG 200 when comparing to the neat base oil. ILs containing the anion ethyl sulfate yielded the best results, while the ILs with triflate anion led to the worst. XPS analysis confirmed that the interaction of the anion ethyl sulfate with the silicon surface was stronger than that of the anion triflate. The efficiency of ethyl sulfate to reduce friction was previously reported in the literature, in studies involving ILs as neat lubricants.[87,88]

(A)

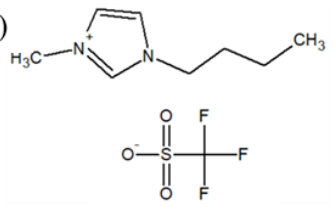

[C_4MIM][TfO]

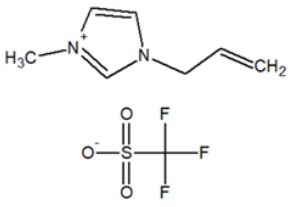

[AMIM][TfO]

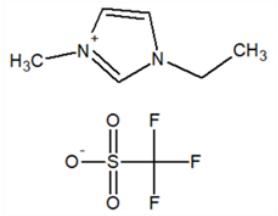

[C_2MIM][TfO]

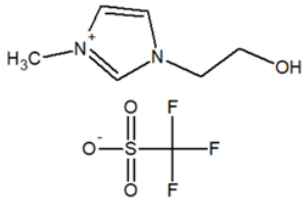

[C_2OHMIM][TfO]

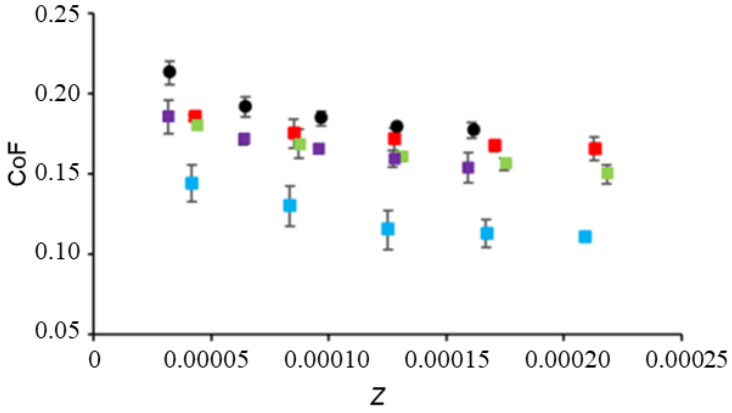

(B)

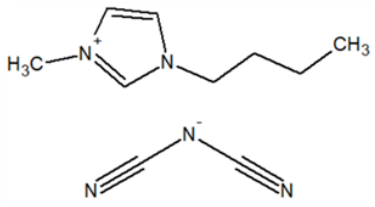

[C_4MIM][DCA]

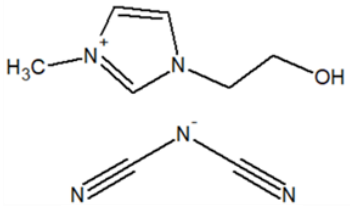

[C_2OHMIM][DCA]

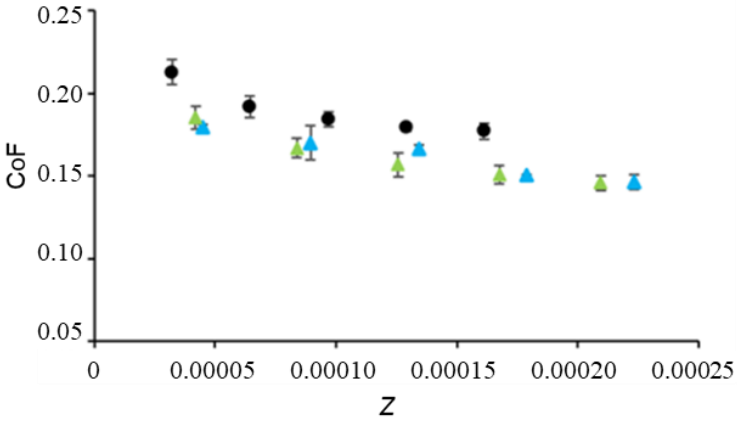

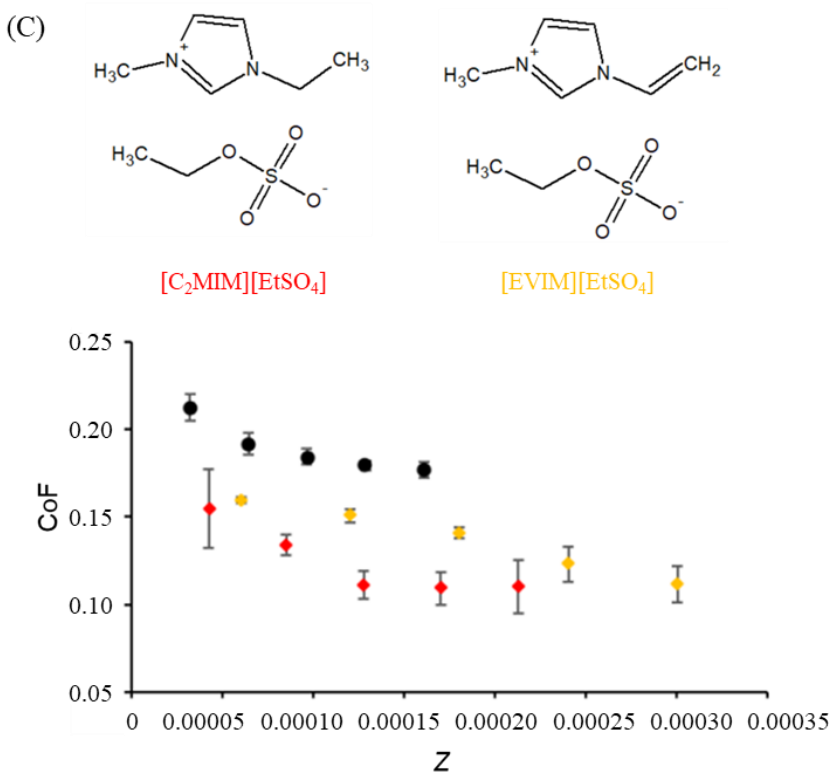

Figure 1.3. Structures of the studied ILs and CoF *vs. Z* for the best performing dry liquids according to the anion: (A) [TfO] based: PEG + [C4MIM][TfO] (blue squares), PEG + [AMIM][TfO] (purple squares), PEG + [C2MIM][TfO] (red squares), PEG + [C2OHMIM][TfO] (green squares); (B) [DCA] based: PEG + [C4MIM][DCA] (blue triangles), PEG + [C2OHMIM][DCA] (green triangles) and (C)][EtSO4] based: PEG + [C2MIM][EtSO4] (red diamonds), PEG + [EVIM][EtSO4] (yellow diamonds). The black circles correspond to dry PEG 200, for comparison purposes. Adapted from reference [29].

1.3.1.2 Phosphonium-based additives

The first study concerning the use of phosphonium-based ILs as lubricant additives was published in 2006,[89] but only over the past decade, there was a significant effort in the investigation of this IL family.

Yu *et al.*[41] studied the lubrication of steel-cast iron pairs with ILs involving the cation tri hexyl(tetradecyl)phosphonium [P66614] and the anions bis(2,4,4-trimethylpentyl) phosphinate [BTMPP], bis(2-ethyl-hexyl) phosphate [BEHP], di butyl phosphate [DBP] and bis(2,4,4-trimethylpentyl) dithiophosphinate [BTMPDTP]. ILs containing phosphonium cations showed higher thermal stability than the commonly used lubricants PAO, 10W and 10W30. General significant friction and wear reduction was observed upon the addition of 5 wt.% of these IL additives to the base oils. The good tribological performance of [P66614][BEHP] was also reported in steel-steel and Si3N4-steel contacts by Cai *et al.*[46] In steel-steel contacts, this IL

outperformed zinc di-alkyl di-thiophosphate (ZDDP) in terms of anti-wear properties. However, in the ceramic contact the observed results were the opposite, with the IL leading to greater wear.

Somers *et al*.[26] investigated the solubility of various types of phosphonium-based ILs in polar and non-polar lubricant oils. They found that the ILs sharing the long alkyl chain phosphonium cation [P_{66614}] were soluble in polar base oils, while ILs comprising this cation and phosphate (bis(2-ethylhexyl)phosphate [BEHP] or phosphinate [BTMPP] anions, both with long alkyl chains, were soluble in polar and non-polar base oils. The blends of additives and non-polar base oils led to large wear reduction of aluminum surfaces and, among them, the blend of [P_{66614}][BTMPP] with mineral oil was the most efficient at high load. XPS analysis of the worn surfaces suggested that the ability of the IL to adsorb, both physically and chemically, on the surface dictates its tribological performance.

Khemchandani *et al*.[51] reported biocompatible ILs containing the anion di phenyl phosphate [DPP] and the cations tri butyl(methyl) phosphonium [P_{1444}] and [P_{66614}], as additives with anti-wear properties. The behavior of [P_{1444}][DPP] and [P_{66614}][DPP] as additives in sunfflower oil (SO), polyol ester (PE) and trimethylolpropane (TMP) was compared to that of the neat oils. Amine phosphate (AF), a commonly used anti-wear additive in biodegradable lubricants, and anti-oxidant additives (AO) were also added. Among the three base oils, SO showed the highest wear track diameter and CoF, which was decreased by almost 50% upon the addition of AF+AO. In contrast, these additives practically did not affect the tribological behavior of PE and TMP. The addition of the ILs to all base fluids led to a significant reduction in the CoF. Both ILs showed a similar decrease in the CoF and [P_{66614}][DPP] and demonstrated significant wear reduction. However, since this IL is less biocompatible, further studies were conducted only with [P_{1444}][DPP]. The CoF results are presented in Figure 1.4. In the case of SO+AP+AO the formed tribofilm broke down at 200N, resulting in wear at higher loads. On the other hand, SO+AP+AO+ [P_{66614}][DPP] ensured a stable tribofilm, which protected the surface from wear until 350N, proving the greater load carrying capacity of this IL. The sample containing [P_{66614}][DPP] when compared to neat SO led to a reduction of nearly 50% in the wear track diameter for high loads. Surface analysis by SEM-EDS and XPS confirmed the formation of a phosphorous tribofilm on the metal surface, limiting the tribocorrosion. Further AFM studies revealed a smooth surface after lubrication with SO+AP+AO [P_{66614}][DPP], which is an indication of the formation of a good boundary lubrication film.

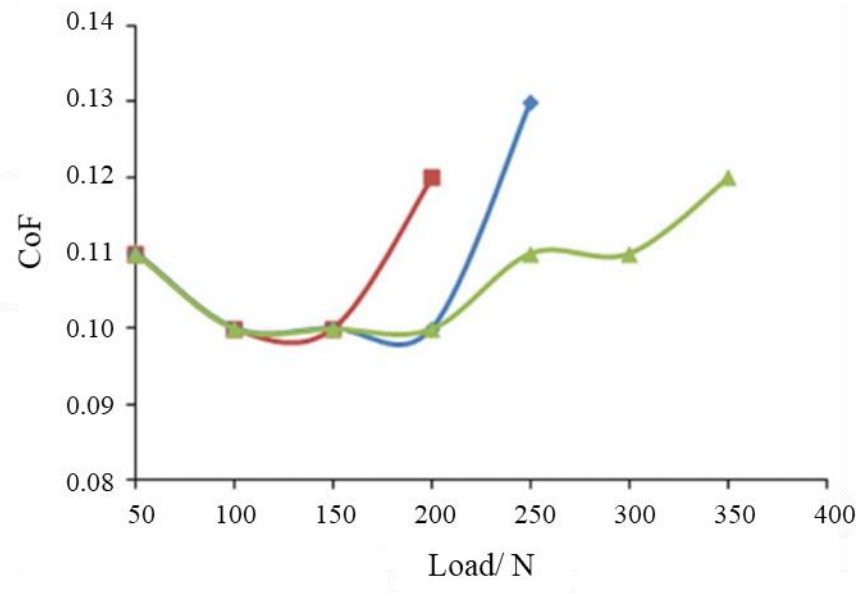

Figure 1.4. Friction coefficient results for SO (red square), SO+AP+AO (blue diamond) and SO+AP+AO+ [P_{1444}][DPP] (green triangle). Adapted from reference [51].

Later studies carried out by Zhou *et al*.[47] in 2014 evaluated the tribological performance of ILs resulting from the combination of the cations tetra butyl phosphonium [P_{4444}] and [P_{66614}] with the anions [BEHP], organophosphate, carboxylate and sulphonate. The addition of these ILs to PAO4 did not imply a significant reduction of the CoF. However, all the IL blends demonstrated effective anti-wear behavior, with sulphonate-based ILs being the most effective, followed by carboxylate and organophosphate-based ILs. Analysis of the tribofilms showed that their formation resulted mostly from the interaction of the anions with the cast iron surfaces.

In the same year, Totolin *et al*.[54] focused on a phosphonium phosphate IL as additive to alkylborane-imidazole complexes to lubricate steel-steel contacts. The chosen IL was [P_{1444}][DMP], which was dispersed in the base oils 1-ethylimidazole tributylborane [C_2im][TBB], 1-allylimidazole tributylborane [aim][TBB] and [C_4MIM][NTf_2] in a 0.7 to 3.4 wt.% proportion. The results were very promising, with friction reduction and anti-wear properties in comparison to the reference [C_4MIM][NTf_2]. Phosphate-based tribofilms showed to be more effective regarding surface protection and have the advantage of being non-corrosive and moisture stable, contrary to the fluorine-based IL used as reference. Besides, the synthesized IL revealed a high load carrying capacity to loads up to 150 N.

Fernández *et al*.[50] studied [P_{66614}] and [P_{4442}]-based ILs with anions diethylphosphate [DEP] and tri(pentafluoroethyl)-trifluorophosphate [FAP], respectively, to lubricate steel/ steel contacts. The ILs were added at 1 wt.% concentration to several base oils: a vegetable oil (VO) which is a high oleic sunflower oil, and three syntectic esters (a biodegradable polymeric ester, BPE, a trimethylol propane trioleate, TMP, and isotridecyl trimellitate, TTM). In general,

[P_{4442}][DEP] showed greater improvement in the tribological properties than [P_{66614}][FAP], which was more significant when the ILs were dispersed in TMP and VO. These results were explained by the formation of a phosphorous-containing tribofilm on the surface, which did not occur with IL [P_{66614}][FAP].

Barnhill *et al*.[48] compared the physicochemical properties and the tribological behavior of ILs containing the anion [BEHP] and the following phosphonium-based cations: tetra octyl phosphonium [P_{8888}], tri butyl(octyl)phosphonium [P_{4448}], tri butyl(tetradecyl)phosphonium [P_{44414}], [P_{66614}], and [P_{4444}]. More symmetrical cations with smaller alkyl chains led to ILs having higher density, thermal stability and viscosity, while larger cations (minimum of six carbons) increased the solubility in the GTL 4 cSt base oil. In terms of corrosion, none of the ILs attacked the cast iron surfaces. The CoFs of the blends [P_{8888}][BEHP] + GTL 4 and [P_{66614}][BEHP] + GTL 4, containing 1.04 wt.% of IL, decreased ~10% when compared to the base oil. Besides, the rapid increase of the CoF observed in the beginning of the friction tests with the neat base oil, an indication of previously referred scuffing,[90,91] did not occur with the IL additives. The same blends were found to effectively protect the surface from wear, with the symmetric cation slightly outperforming the asymmetric one. The same group [45] investigated the synergistic effect of the previously studied phosphonium-alkylphosphate ILs and the commercial anti-wear additive ZDPP added to GTL 4 cSt. The IL [P_{8888}][BEHP] combined with ZDPP and added to GTL led to a reduction of 30% on the CoF and more than 70% on the wear volume. Other ILs sharing the same anion or cation were tested but this synergy happened only for phosphonium-alkyl phosphate ILs.

Anand *et al*.[42,43] studied phosphonium-based ILs as lubricant additives to engine oils in cast iron systems that simulate the piston ring-cylinder liner contact. The chosen ILs, [P_{66614}][BEHP] and [P_{66614}][BTMPP], were added to engine-aged and fresh lubricants in 6 vol.%. Friction and wear decreased upon addition of the ILs due to the formation of boundary films, which reduced the effect of plastic deformation and abrasive wear; the effect was more important in engine-aged lubricants. The boundary film revealed a higher concentration of phosphorous, indicating the involvement of the ILs in the formation of the boundary film.

González *et al*.[44] reported the use of [P_{66614}][BTMPP] and [P_{66614}][BEHP] as additives in a base oil and compared their tribological performance with that of ZDDP in steel-steel contacts. The ILs were dispersed in the oil in various concentrations and other mixtures using ZDDP, with similar concentrations of phosphorous, were prepared. All mixtures yielded CoF values lower than the base oil, being the lowest values obtained with ZDDP. In terms of wear, the mixtures showed a clear reduction when compared to the neat base oil, with an increase in concentration yielding improved anti-wear behavior. Surface analysis suggested the existence of plastic deformation and adhesive wear mechanism, as well as the presence of phosphorus at the surface, especially in the case of [P_{66614}][BTMPP] and ZDDP.

More recently, in 2020, the group of Fernández reported the use of boron nitride nanoparticles[49,53] and graphene nanoplatelets[53] with phosphonium-based ILs, as efficient

hybrid additives. Hexagonal boron nitride (h-BN) nanosheets were added at 0.1 wt.% to ILs [P_{66614}][BEHP], [P_{4442}][DEP] and [P_{66614}][BTMPP], which were, in turn, dispersed at 1 wt.% in the base oil PAO 32. The hybrid additives showed improved tribological performance, both in terms of friction and wear, when compared to the single IL additives, proving the synergy between the ILs and the nanoparticles.[49] The synergic effect between boron nitride nanoparticles (0.1 wt.%) was also assessed with the IL [P_{4442}][DEP] dispersed in base oil TTM at 2 wt.%. Graphene nanoplatelets (GnPs) were added to this system of IL+base oil (0.1 wt.%) and allowed to reduce the CoF in 33% and the diameter of the wear track in 44% when compared to the neat base oil.[53]

1.3.1.3 Ammonium-based additives

ILs containing ammonium-based cations were first investigated as lubricant additives in 2006.[92] Later, in 2011, Blanco *et al*. published two papers describing the properties of ethyl-dimethyl-2-methoxyethylammonium tris(pentafluoroethyl) trifluorophosphate, [(NEMM)MOE][FAP], as additive to polyalphaolefin (PAO 6) to lubricate CrN PVD and TiN PVD coatings.[56,57] Although the IL reduced friction and wear, the results were not very promising compared with those obtained with the traditional oil additive ZDDP.

Espinosa *et al*.[58] synthesized ammonium carboxylate ILs to lubricate copper and used the most efficient containing adipate [AD] anion, [N_{22HHOH}]$_2$[AD], as additive to base oil PAO 6. The CoF decreased by 20% and wear by 34%, in comparison with PAO 6. This group used the IL composed by the same cation ([N_{22HHOH}]) with succinate [SU] anion as additive in water (1 wt.%) to lubricate sapphire/steel systems.[59] The neat IL allowed a decrease of 88% in the CoF when compared to water, and the mixture water+IL yielded CoF values of 0.0001, which corresponded to a reduction of 97% comparing to water and 78% comparing to the neat IL.

In 2013, Zhao *et al*.[60] synthesized two protic ILs, N-octadecyl amine linear alkyl benzene sulfonic acid (18A-LABSA) and N-dodecyl amine linear alkyl benzene sulfonic acid (12A-LABSA), to be used as additives in PAO10 base oil. The structures of the ILs are presented in Figure 1.5.

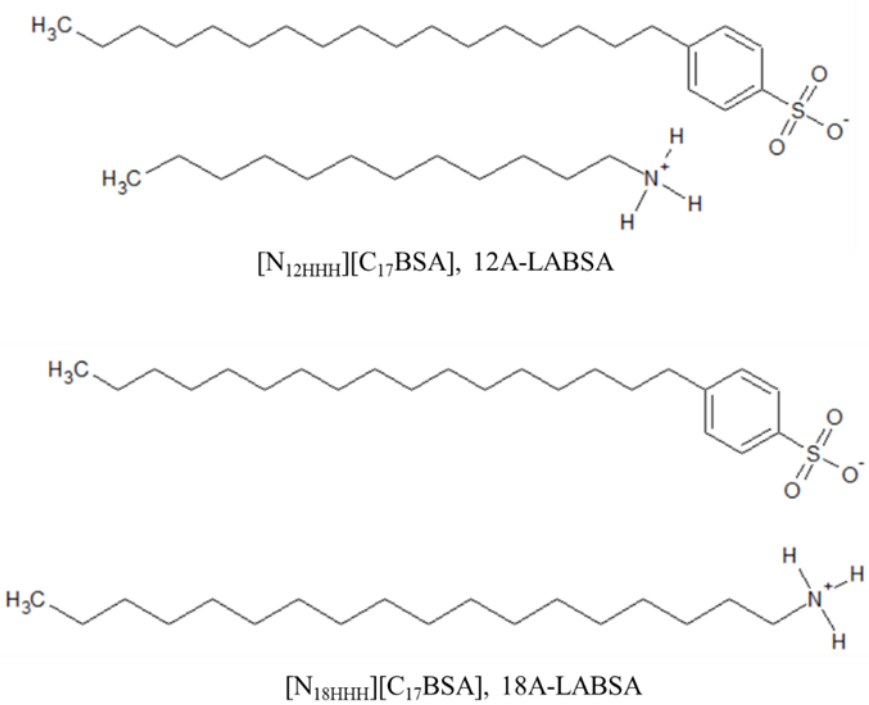

Figure 1.5. Structures of the studied ionic liquids: 12A-LABSA and 18A-LABSA.

The reported ILs showed excellent friction reduction and anti-wear abilities when added to PAO. Comparing the two additives, the longer chain amine revealed better anti-wear properties, which could be related to the better packing due to van der Waals interactions. The surface lubricated by PAO showed signs of deep grooves, wide cracks, and big pits while the surfaces lubricated with the ILs as additives were uniform and smooth with relatively narrow and shallow tracks. This behavior might be explained by the formation of a tribofilm composed by organic amines resulting from the ammonium salts of the ILs and a chemically adsorbed film due to the interactions between the sulfonate anions and the metallic atoms of the steel surface.

In the same year, Khatri *et al.*[64] introduced ILs based on amino acids as additives to mineral lubricant oil N-150. Later, they studied the same ILs containing the cation [N_{4444}] and two anions derived from the amino acids aspartic acid [AS] and glutamic acid [GL], as additives of a non-conventional polyol ester base oil.[67] The studied ILs showed improved anti-friction and anti-wear performance. These are very important findings as amino acid-based ILs are biocompatible and biodegradable and have reduced toxicity, making them suitable as bio-additives for machinery lubrication.[93–97]

Qiao *et al.*[65] published in 2014 a study where ILs composed of different cations, [N_{4HHH}] and [N_{4444}], and the same anion, [DBP], were tested as additives for the lubrication of steel-aluminum contacts. The ILs were dispersed in formulated base oils in 0.5 wt. %. Three base oils were chosen: the widely studied IL P106, a mixture of PAO10 and PAO40, and EO that is

a blend of NM3986 with pentaerythritol oleate (PEO). The tribological performance of the ILs dispersed in the base oils was evaluated through CoF and wear measurements. The ILs' polarity demonstrated to have a great impact on their tribological behavior, particularly on the anti-wear properties. Regarding the CoF, the ILs as additives to EO have shown the best results, followed by P106 and PAO blend. The improvements in the friction performance was attributed to the synergy between the well-ordered adsorbed layers and the films formed due to the tribochemical reaction between the ILs and the metal substrate.

Also in 2014, Fan *et al.*[61] and Gusain *et al.*[40] reported halogen-free ammonium-based ILs with better tribological properties than the conventional ones containing halogens. The former group investigated a wide variety of ILs containing dioctyl sulfosuccinate [DOSS] anion, which were added to PAO to lubricate steel/steel and steel/copper contacts. All the synthesized ILs were non-corrosive and improved the anti-friction and anti-wear behavior of PAO. The latter group studied bis(salicylato)borate [BScB] ammonium and imidazolium ILs with variable alkyl chains and cyclic ring structures, as additives to PEG200, to lubricate steel/steel systems. The structures of the cations are presented in Figure 1.6. All the ILs were non-corrosive, contrarily to the analogues with the commonly used [PF_6] anion, and showed improved tribological properties, which was attributed to the formation of an absorbed film.

Halogen-free ILs based on ammonium and phosphonium cations were also reported by Westerholt *et al.*[55] in 2015, as additives to FVA3, a reference oil of the Forschungsver-einigung Antriebstechnik e.V. The ILs [N_{1888}][DBP], [$N_{1121212}$][DBP], [N_{1888}][BTMPP], [$N_{1121212}$][BTMPP], [P_{1888}][DBP] and [P_{1888}][BTMPP] were compared to the commonly reported IL [P_{66614}][BTMPP], showing improved anti-friction and anti-wear performance due to the formation of a protective layer on the steel surfaces. The most promising ILs were [N_{1888}][DBP] and [P_{1888}][DBP], which demonstrated good anti-corrosion properties, particularly for brass surfaces, which are very interesting for industrial applications.

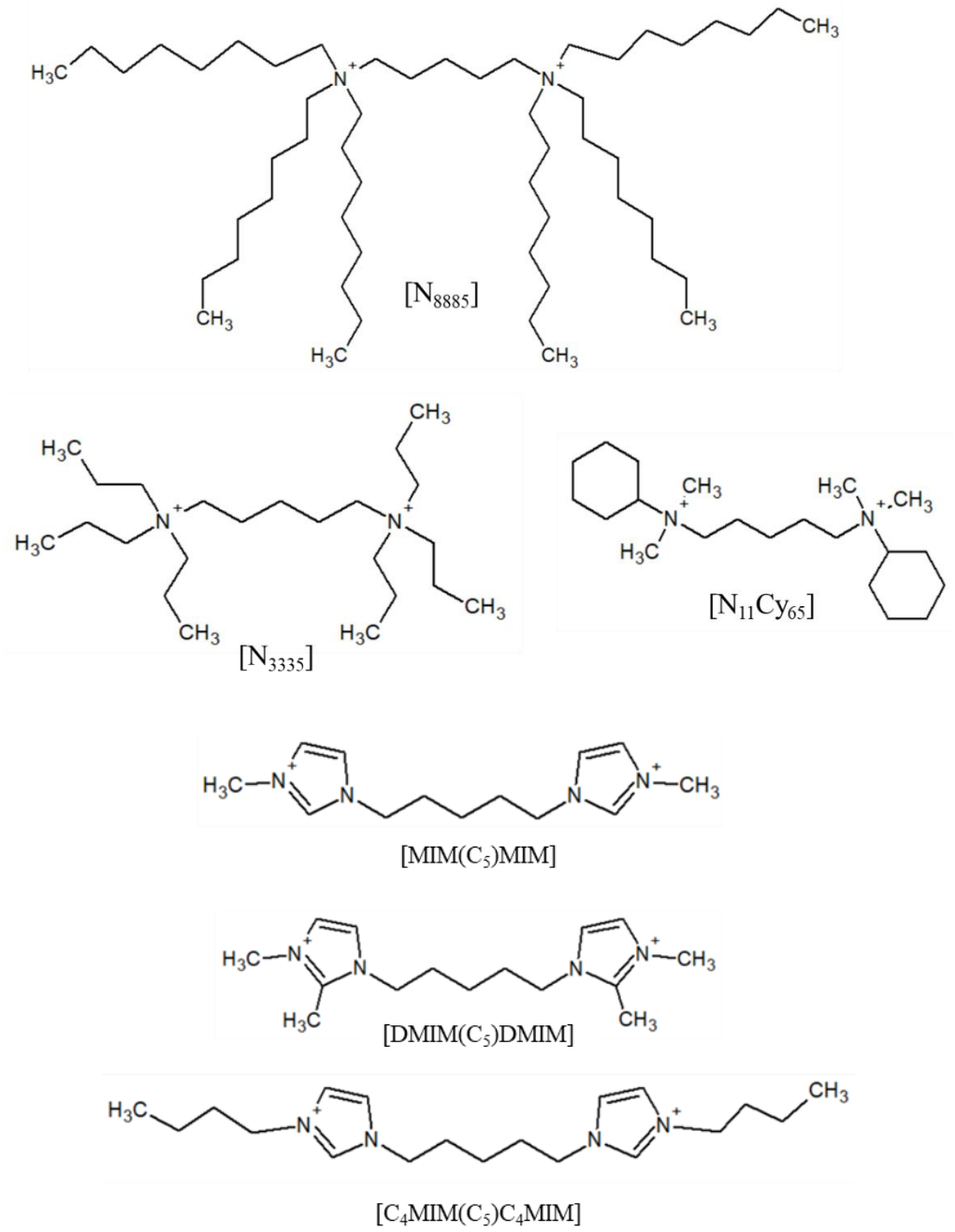

Figure 1.6. Ammonium and imidazolium cations studied in reference [40].

In the same year, Fu *et al.*[63] performed a tribological study with the ILs [N_{8888}][PO_3], [N_{9998}][PO_3], [$N_{1010108}$][PO_3], [N_{88812}][PO_3], [N_{99912}][PO_3] and [$N_{10101012}$][PO_3], all containing the anion phosphite. The ILs demonstrated better anti-friction and anti-wear properties for steel/steel contacts when compared to ZDDP and performed better under extreme pressure. The improved tribological characteristics were attributed to the formation of polyphosphates due to the ILs decomposition, which prevents the direct contact of the asperities on the metal surface.

In 2016, several authors investigated the tribological behavior of ammonium containing IL additives. Barnhill *et al*.[62] tested protic and aprotic ammonium-phosphate ILs with the anion [BEHP], as additives to an engine oil. Slight pitting corrosion was observed on the cast iron surfaces with aprotic ILs, while protic ILs showed no corrosion attack. Both protic and aprotic additives eliminated scuffing failure observed with the neat engine oil. The protic IL tri octyl ammonium [N_{888H}][BEHP] outperformed the aprotic ILs, tetra octyl ammonium [N_{8888}][BEHP] and methyl tri octyl imidazolium [N_{1888}][BEHP], in terms of wear and friction reduction. The best tribological performance of [N_{888H}][BEHP] was evident from the surface characterization which revealed a tribofilm layer composed of iron phosphates and iron oxides. Khatri *et al*.[66] studied the anti-wear and friction-reducing properties of ILs based on the tetrabutyl ammonium cation, [N_{4444}], and dicarboxylic acid derived orthoborate anions, as additives to PEG200 to lubricate steel–steel contacts. All ILs revealed good tribological properties, but the best results were obtained with the shortest alkyl chain anion. ILs involving phosphonate anions are known to be good lubricants, which led Han *et al*.[70] to compare the behavior of the ILs containing the cation dibutylammonium [N_{44HH}] and the anions O-butyl phosphonate, [BP], and O-ethyl phosphonate, [EP], with that of [C_4MIM][BP], as additives in PEG to lubricate steel surfaces. [N_{44HH}][EP] demonstrated the best tribological performance, which was attributed to its higher affinity with the steel surface.

Gusain *et al*.[67] investigated the use of fatty acid ILs based on [N_{4444}], as additives to polyol ester base oil, to lubricate steel surfaces. The ILs [N_{4444}][ST], [N_{4444}][OL] and [N_{4444}][LN], containing respectively, the anions stearate, oleate and linoleate, were chosen because they are green compounds, derived from vegetable oils. The anion [ST] is fully saturated with all methylene units, while anions [OL] and [LN] contain one and two double bonds, respectively. The fatty acid anions interact with the steel surface decreasing both friction and wear under boundary lubrication conditions. [N_{4444}][OL] exhibited the largest decrease in the CoF, while the most considerable wear reduction was observed for [N_{4444}][ST]. EDX analysis of the formed tribofilms revealed that [N_{4444}][ST] interacts with steel through the carboxylate group, and the methylene units in neighboring stearate anions interact with each other, through weak van der Waals interactions, forming a stable well-organized structure. In the case of [N_{4444}][OL] and [N_{4444}][LN], the existence of unsaturation sites distorts the structure and the methylene units cannot interact with nearby units, providing a loosely-oriented structure with worse anti-wear properties.

Huang *et al*.[71] synthesized two quaternary ammonium ILs composed by the common cation [$(C_{12}H_{25})_3NC_3H_6PO(OC_2H_5)_2$] and two anions: [DOSS] and laurate [LATS]. They were added as additives to PAO 10 and used to lubricate steel/steel contacts. Both ILs revealed good capacity to reduce friction and wear resulting from their tendency to interact with the contacting surfaces. At low load, the cation with long alkyl chains should play the most important role, leading to the formation of a densely packed adsorbed film. At high load,

besides ions adsorption, there should also be chemical reaction between the ILs and the surfaces leading to the formation of a resistant film.

In 2019, Yu *et al*.[72] investigated the tribological and corrosion behavior of $[N_{11116}]$[BEHP] and $[N_{11116}]_2$[BEHP] dispersed in PAO10 (1 wt.%). In Figure 1.7 the structures of the ILs are given. The CoF results obtained at room temperature and 100 °C indicated that the addition of 1 wt.% of these ILs to PAO10 significantly reduced CoF and improved anti-wear performance. The surface analysis demonstrated that the improved tribological performance was due to the formation of a $FePO_4$ or nitrogen-containing tribofilm that protected the surface. When comparing the two ILs, $[N_{11116}]$[BEHP] exhibited better lubricity properties since, as it is less sterically hindered than $[N_{11116}]_2$[BEHP], it may form a more stable boundary lubrication film on the surface.

In the same year, Avilés *et al*.[74] used a new diprotic IL containing two cations [bis(2-hydroxyethyl)ammonium], $[N_{HH22OH}]$, and the anion [SU] as additive to water in the lubrication of steel surfaces and found a reduction in friction and wear, which was attributed to the formation of a thin film after water evaporation

More recently, Sernaglia *et al*.[69] added two fatty acid ILs based on the cation $[N_{6666}]$ and the anions caprylate [CA] and palmitate [PAL] to polyol ester but did not find a significant improvement of the tribological performance.

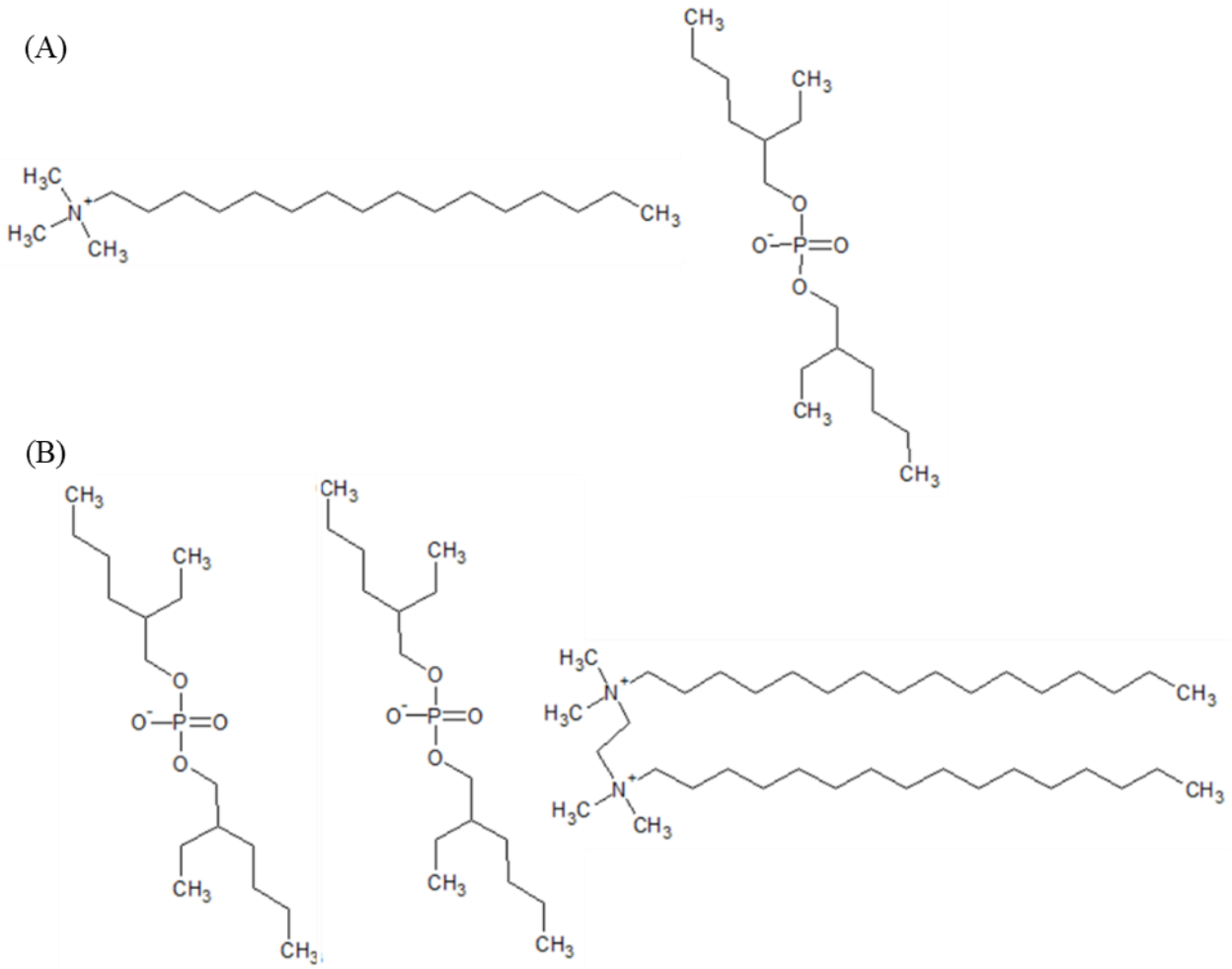

Figure 1.7. Structures of the studied ionic liquids: (A) [N_{11116}][BEHP] and (B) [N_{11116}]$_2$[BEHP]. Adapted from reference [72].

1.3.1.4 Pyrrolidinium and pyridinium-based additives

The group of Hernández-Battez has long studied the tribological properties of ILs based on the cation 1-butyl-1-methylpyrrolidinium [C_4C_1-pyrr] as additives to base oils. They found that addition of 1-butyl-1-methylpyrrolidinium tris(pentafluoroethyl) trifluorophosphate ([C_4C_1-pyrr][FAP]) into polyalphaolefin to lubricate TiN, CrN and DLC coatings [75] slightly decreased the CoF, being a more significant improvement obtained with the neat IL. In contrast, the presence of the additive did not reduce wear. Furthermore, no improvement of the tribological behavior was observed when comparing with the performance of traditional additive ZDDP.[98] The same group compared the performance of [C_4C_1-pyrr][FAP] with that of ethyl-dimethyl-2-methoxyethylammonium tris(pentafluoroethyl), [(NEMM)MOE][FAP], as additives to a mineral hydrocracking oil to lubricate steel-steel pairs.[99] Both ILs revealed anti-friction and anti-wear properties, but [C_4C_1-pyr][FAP] was more efficient. XPS analysis of the wear tracks demonstrated that the IL reacted with the steel surface to form phosphates and

fluorine–iron compounds. In another work,[76] the authors studied the tribological properties of mixtures of polyalphaolefin-based and mineral oil-based lubricants with two ILs composed of the cations [C_4C_1-pyr] and [Choline], and the anion [NTf_2]. Friction and wear of steel surfaces were reduced in the presence of both additives, more significantly in the case of [C_4C_1-pyr][NTf_2]. Surprinsingly, Somers *et al*.[100] reported a null miscibility of [C_4C_1-pyr][NTf_2] and [C_4C_1-pyr][FAP] in vegetable oil, two polyol esters, a mineral oil and a polyalphaolefin, which hindered their use as additives in these oils. [C_4C_1-pyr][NTf_2] was also added to a mineral fully-formulated wind turbine gear oil leading to a small friction reduction but a significant wear decrease.[101]

Pejaković *et al*.[73] compared the tribological behavior of two ILs based on the anion methyl sulfate, [C_4C_1-pyr][$MeSO_4$] and tri ethyl methyl ammonium methyl sulfate [N_{2221}][$MeSO_4$], as additives in a glycerol model lubricant. The use of these ILs as additives yielded a reduction on the CoF and wear of steel contacts when compared to neat glycerol, but, when compared to the pure ILs, the additives showed worse anti-friction and anti-wear properties. The addition of ILs to glycerol reduced abrasion but increased tribo-corrosion. In the case of pure ILs, a thick protective tribochemical film was formed, which was responsible for the enhanced tribological properties. Although non-toxic, the IL [C_4C_1-pyr][$MeSO_4$] demonstrated poor biodegradability, which implies limited application in lubrication, especially as a pure lubricant.[102]

Dicationic ILs formed by oligoethylene glycols linking two cationic moieties based on either N-methylpyrrolidinium or N-methylimidazolium[39] were studied as neat lubricants and additives. While longer chains improved the tribological performance of the neat lubricants, in the case of the additives they correspond to a smaller number of IL molecules in the mixture (at constant weight percentage) and led to worst tribological behavior. Later studies carried out by the same group[77] evaluated the lubricating properties of mono and dicationic ILs incorporating PEG chains linking two alkylpyridinium moieties. The ILs methyl pyridinium methyl sulfate [C_1-pyr][$MeSO_4$], methyl pyridinium bis(tri fluoro methyl sulfonyl)imide [C_1-pyr][NTf_2], 1,13-di(N-methylpyridinium-2′-yl)-4,7,10-trioxatridecane methyl sulfate [C_1-pyr(CH_2OCH_2)$_3$$C_1$-pyr][$MeSO_4$]$_2$ and 1,13-di(N-methylpyridinium-2′-yl)-4,7,10-trioxatridecane bis(tri fluoro methyl sulfonyl)imide [C_1-pyr(CH_2OCH_2)$_3$$C_1$-pyr][$NTf_2$]$_2$ were dispersed in glycerol (0.25, 0.5 and 1.0 wt.%). The additives based on the anion [$MeSO_4$] did not affect the CoF, while ILs with [NTf_2] showed significant improvements in the CoF. A concentration of 1.0 wt.% of [C_1-pyr][NTf_2] led to a reduction in the CoF. In the case of [C_1-pyr(CH_2OCH_2)$_3$$C_1$-pyr][$NTf_2$]$_2$, the results were even more promising, with CoF decreasing up to 72% when compared to that of neat PEG, for the same concentration. In terms of wear, only glycerol with 0.25 wt.% [C_1-pyr(CH_2OCH_2)$_3$$C_1$-pyr][$MeSO_4$]$_2$ had better performance than pure glycerol. For the other mixtures, wear was found to increase with increasing IL concentration, which was attributed by the authors to tribocorrosion.

1.3.1.5 Guanidinium-based additives

The research on guanidinium-based ILs as lubricant additives is very recent and only a few papers have been published so far. The first one by Khatri *et al.*[78] appeared in 2018 and describes the tribological behavior of ILs containing the cation 1,1,3,3-tetramethylguanidinium [TMG] and fatty-acid anions with different alkyl chain length and degree of saturation: [CA], myristate [MA], erucate [EA], [OL] and [LN]. All ILs led to a significant reduction in the friction coefficient and wear of steel/steel contacts when added to the base oil N-150. ILs with longer alkyl chains led to blends with better anti-wear and friction-reduction properties. An increase in the unsaturation degree was associated to lower friction reduction but did not influence wear. Figure 1.8 shows the variations on the CoF and wear track diameter for all the IL blends, at a constant chosen concentration of 5 wt.%, as well as the base oil for comparison purposes. SEM and EDX analysis of the worn surfaces indicated the presence of adsorbed ILs which formed boundary films.

More recently, the same group reported a new series of ILs based on the same cation combined with other amino acids such as L-histidine, L-glutamic acid and L-aspartic acid to form [TMG][HT], [TMG][GL] and [TMG][AS], respectively.[79] The ILs were dispersed in PEG200 in 0.5, 1, 2 and 3 wt.% concentrations and their tribological properties for steel/steel contacts were assessed. In general, increasing the IL concentration resulted in better anti-friction properties, with the optimal results reached for 2 wt.% dosage, which allowed the formation of a compact thin layer that reduced shear strength and, in consequence, the CoF. All ILs demonstrated excellent anti-wear properties when added to the base oil, with almost no corrosion. [TMG][GL] was the most promising anti-corrosion IL, followed by [TMG][AS] and [TMG][HT], which suggested that the presence of a carboxylic group is important for anti-corrosion properties. The best performing ILs in terms of friction and wear were [TMG][AS] and [TMG][GL], which was attributed by the authors to the strong affinity of the two carboxylic units present on the anions to the metal surface.

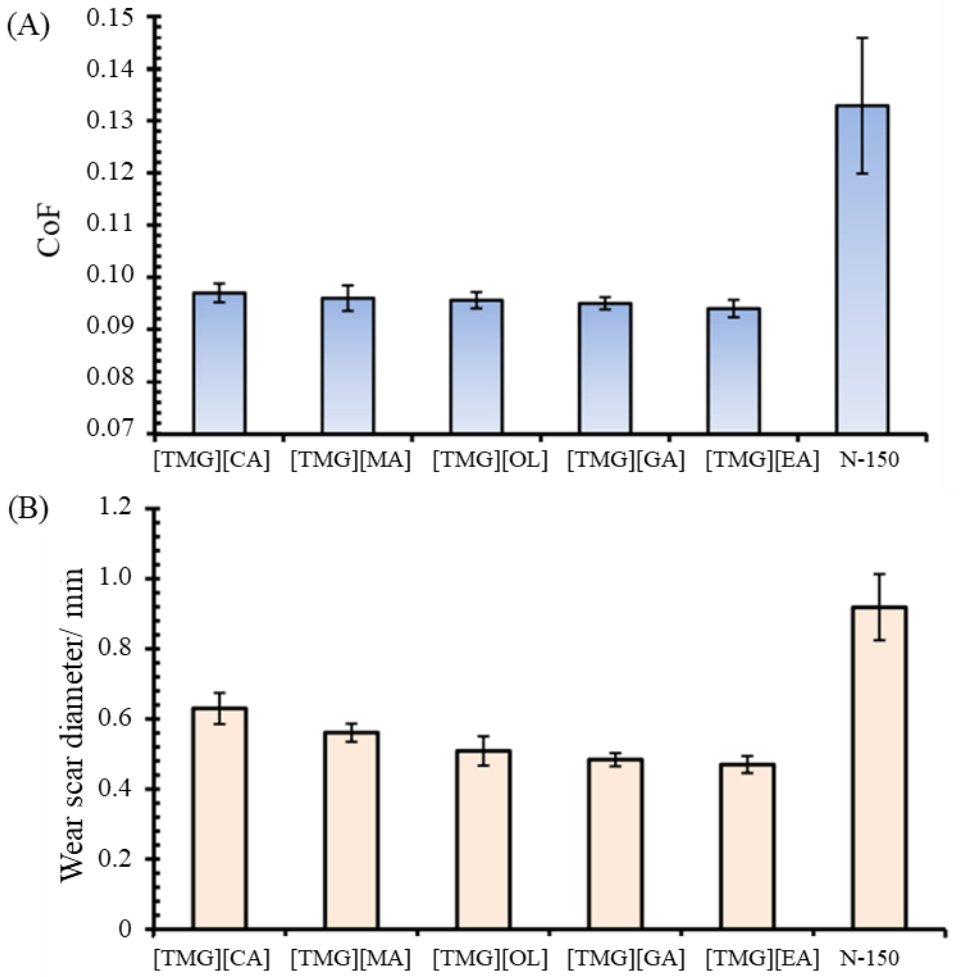

Figure 1.8. CoF (A) and wear track diameter (B) obtained with the IL blends for a concentration of 5 wt.%. The results of the base oil are also included. Adapted from reference [78].

1.3.1.6 Miscellaneous Ionic Liquid additives

This section is dedicated to studies performed with ILs that are not composed of the previously mentioned cations or have those cations combined with other chemical species.

One example are lithium-based ILs. Song *et al.*[80] studied [Li][NTf_2]-based ILs blended with tri(methoxyethoxyethoxyethoxy)triazine [$C_3N_3(OR)_3$] and hexa(methoxyethoxyethoxyethoxy)cyclotriphosphazene [$P_3N_3(OR)_6$], as additives to multiply alkylated cyclopentanes (MACs) to lubricate steel-steel contacts. All the synthesized ILs showed better anti-friction and anti-wear properties, as well as higher load-carrying capacity, when compared to the commonly used lubricant ZDDP. This phenomenon is explained by the interaction between the ILs and the metal surface, forming a protective film. The same group synthesized methoxy tris-ethoxy methylene benzotriazole [BTAG3], which added to the

lithium salts, $LiBF_4$, $LiPF_6$, LiTfO and $LiNTf_2$, led to the ILs: [Li(BTAG3)][BF_4], [Li(BTAG3)][PF_6], [Li(BTAG3)][TfO] and [Li(BTAG3)][NTf_2]. These ILs were added to MACs to lubricate steel-steel contacts and their anti-corrosion properties in comparison to the commonly used IL [C_4-3-MIM][BF_4] were evaluated.[103] Copper strip corrosion tests were carried out by immersion of the copper sheets in the ILs for 10 days. The results are presented in Figure 1.9, where it can be easily seen that the copper sheet soaked in [C_4-3-MIM][BF_4] suffered severe corrosion while the ones immersed in the functionalized ILs suffered only a slight corrosion, with little color change. This is more evident in the case of [Li(BTAG3)][NTf_2], which was the IL with the best anti-corrosion properties. Moreover, all ILs presented much better anti-wear and friction-reduction properties than ZDDP.

More recently, Yang *et al.*[81] have reported lithium-based IL additives to lubricate steel/steel contacts. The IL [Li(glyme)][NTf_2] was added to PEG 400 in 1, 3 and 5 wt.% proportions and the tribological performance of these blends was assessed at several lubrication regimes and temperatures. The authors concluded that, in the elasto-hydrodynamic regime, the presence of the additives led to higher lubricant film thickness. In the mixed lubrication regime, increasing the IL concentration reduced friction and wear because of the formation of an adsorbed tribofilm. The authors also suggested that viscosity may aid on the formation of a more stable tribofilm, thus the additives were less efficient at high temperature.

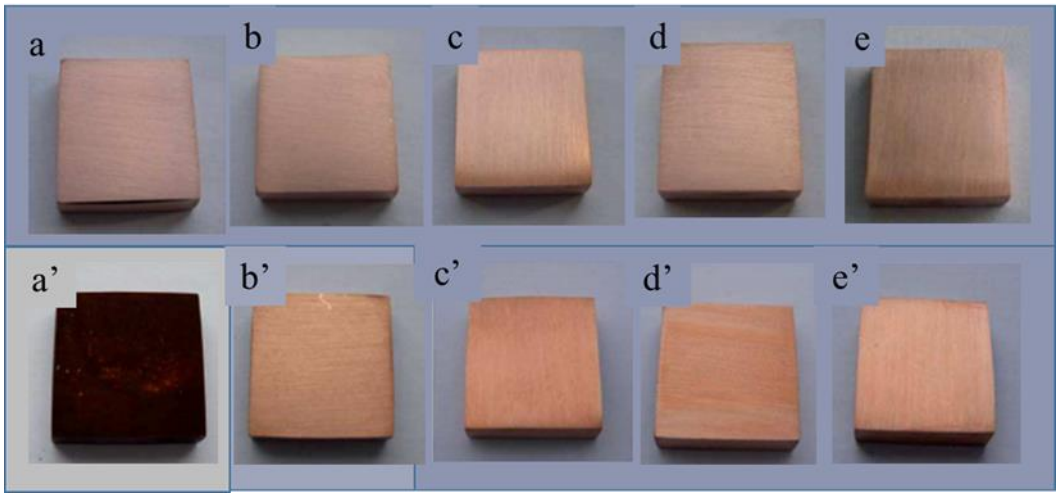

Figure 1.9. Copper sheets before (a,b,c,d,e) and after (a',b',c',d',e') the corrosion tests: [C_4-3-MIM][BF_4] (a and a'), [Li(BTAG3)][BF_4] (b and b'), [Li(BTAG3)][PF_6] (c and c'), [Li(BTAG3)][TfO] (d and d') and [Li(BTAG3)][NTf_2] (e and e'). Adapted from reference [103].

In 2016, Sharma *et al.*[52] studied the tribological behavior of choline-based ILs. Six ILs, containing P on the cation, the anion or both, were tested as 0.1 wt.% additives to group I mineral base oil. The chosen ILs were [Ch][BEHP], [Ch][DBDTP], [P_{66614}][BTMPP], [P_{66614}][NTf_2], [P_{1444}][DMP] and [P_{4444}][DEDTP]. ZDDP was also studied for comparison

purposes. All the studied ILs showed variations in the CoF values while ZDDP presented very stable results. The lowest CoF was obtained for [Ch][BEHP]. In terms of wear, [Ch][BEHP] and [P_{66614}][NTf_2] presented similar or better anti-wear properties than ZDDP, but all the other ILs performed worst. In an earlier study performed by the same group, the mechanism of tribofilm formation of ILs [Ch][BEHP] and [Ch][DBDTP], and ZDDP revealed to be very similar.[104] The ZDDP-based additives led to the formation of Zn polyphosphates, while the ILs studied in this paper yielded Fe polyphosphates. The results suggested that the underlying substrate reacts with the decomposition products of the ILs, yielding the protective films. The sulfur present in the phosphate anions demonstrated to be crucial to the reduction in friction and wear.

A few years later, Cao *et al*.[82] reported the commonly studied ionic liquids [C_4-3-MIM][PF_6] and [C_4-3-MIM][BF_4] doped with PANI as additives to PAO and PUG. The idea was to combine the anticorrosion properties of PANI with the tribological performance of the ILs. The ILs were dispersed in PAO in 0.2 wt.% concentration and in 0.3 wt.% in PUG but the greatest CoF reduction was obtained for a concentration of 0.2 wt.% in PAO. Both PANI-doped ILs revealed close CoF values, lower than those obtained with pure PAO and PAO+0.2 wt.% of the non-doped ILs. The same tendency was observed in comparison to PUG. These excellent tribological results were explained by the formation of a physically adsorbed film of PANI-doped ILs, which could avoid the direct contact between the friction surfaces. The wear tests were also very promising, showing a significantly reduction of the wear volume. Besides, these ILs exhibited excellent anti-corrosion properties.

1.4 Deep Eutectic Solvents as Lubricants

Deep Eutectic Solvents (DESs) are mixtures composed of two or three components capable of self-association through hydrogen bond interactions (hydrogen bond donors, HBDs, and hydrogen bond acceptors, HBAs, presented in Figure 1.10). The term DES was first proposed by Abbott *et al*.[105] to describe the mixture of choline chloride and urea (1:1 or 1:2). For the definition of DES, a significant decrease on the melting point of the mixture comparing to the original individual components should be observed. In this context, differential scanning calorimetry (DSC) is an important characterization technique to proof the DES formation. The depression of the melting point is due to the low lattice energy resulting from the charge delocalization, which occurs through hydrogen bonding involving the large and asymmetric ions usually present in DESs.[105,106] At this point, it is important to stress that there is some confusion in the literature about the definition of DES. In strict terms, DES should refer to eutectic mixtures with an eutectic point lower than that of the ideal mixture and variable composition, as long as it remains liquid at operating temperature.[107]

DESs share with ILs some unusual properties such as almost negligible vapor pressure, non-flammability and high ionic conductivity. They also allow tuning of their physico-chemical

properties such as viscosity, conductivity and surface tension through the combination of different HBDs and HBAs.[108,109] DES emerged as green alternatives to ILs because they are cheaper, easier to prepare and their preparation method is more efficient and environmentally friendly. In general, DES are easy to synthetize by mixing several proportions of HBA and HBD (with heating) by a trial and error approach.[120] In the last few years, DES have been applied as alternative solvents in organic chemistry and material science, in metal processing, electroplating and other electrochemistry applications and, more recently, as lubricants in the field of Tribology.[109,110] Since the application of DES in lubrication has emerged recently as a new research area, the number of publications is very small and enabled a more detailed analysis of each paper than in the case of IL additives.

Hydrogen Bond Donors (HBDs)

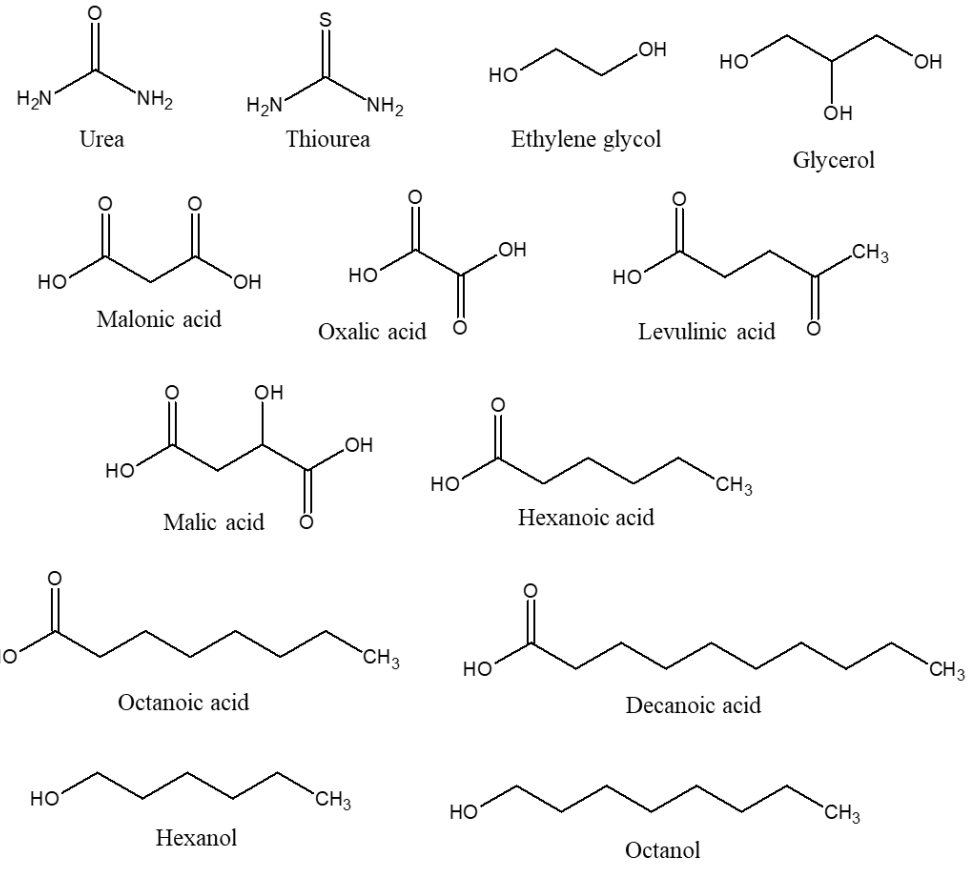

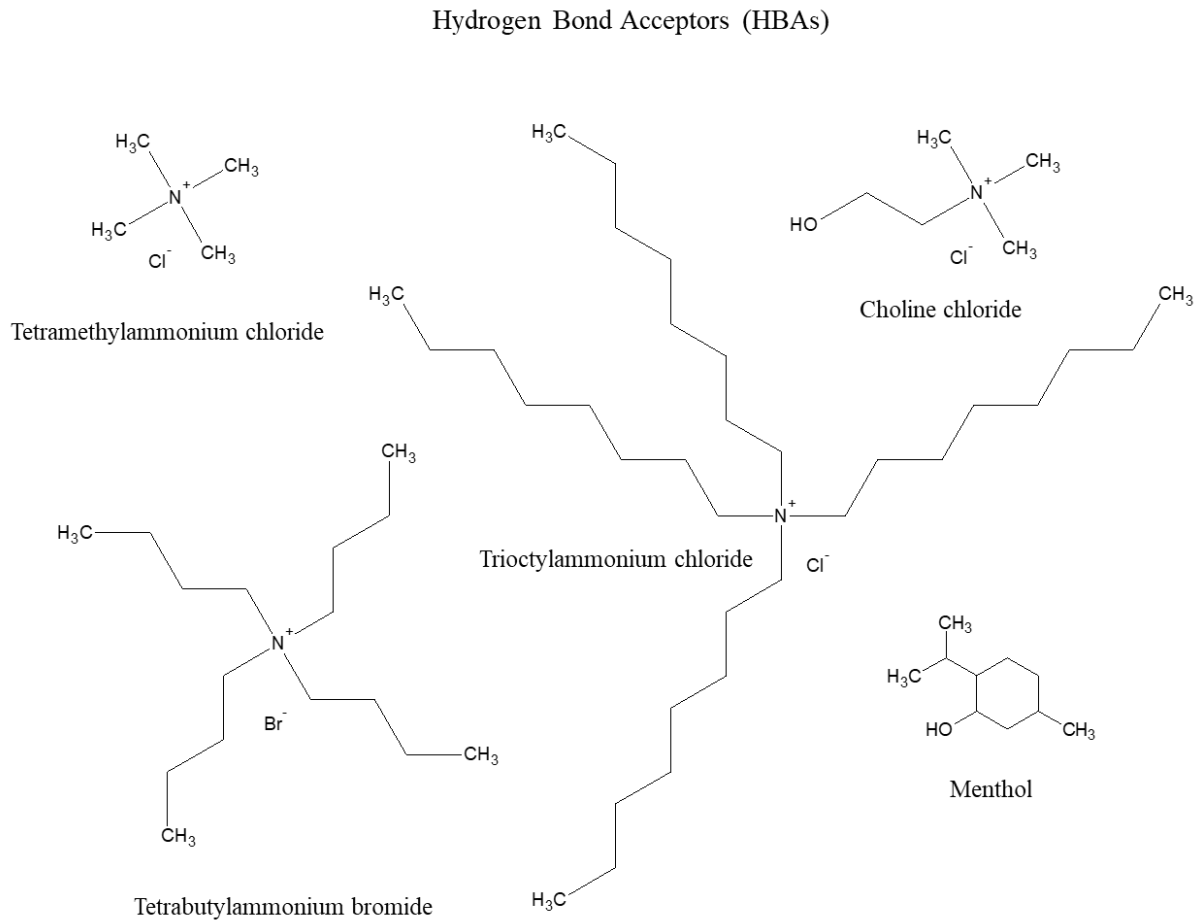

Figure 1.10. Most common Hydrogen Bond Donors and Acceptors (HBDs and HBAs).

DES were first proposed for the lubrication of steel/steel contacts in 2010 by Lawes *et al.*,[111] using the choline chloride [Ch]Cl salt in combination with two HBDs (urea and ethylene glycol, EG) in a 1:2 molar ratio. Both mixtures were prepared by mixing the two components under heating (50 °C) and stirring until a homogeneous and colorless liquid was obtained. The authors proposed a comparative study of lubricant retention in three types of steel surfaces with different surface roughness. Tribological tests were performed with and without lubricant (dry test) on surfaces of average roughness (R_a): 8 nm, 70 nm and 200 nm. The counter-body was a 2.5 mm radius steel sphere. Two conditions were used for the tests: low speed and high load and high speed and low load. SAE 5W30 reference lubricant was tested under the same conditions.

The obtained CoF values varied between ~0.2 for SAE 5W30 and 0.8 in dry conditions. For the two DES, the CoF was low (around the value of the reference lubricant) at the beginning of the test but increased, after a certain sliding distance, to values similar to the one obtained in the dry conditions. The authors attributed this fact to the loss of the boundary lubrication film in

the sliding contact. The sliding distance prior to the loss of lubricant varied with the testing conditions and the surface roughness. This parameter was used by the authors to classify the lubricant performance. In all cases, [Ch]Cl:urea (1:2) exhibited better performance, which was attributed by the authors to its higher viscosity.

In 2014, Abbott *et al*.[112] investigated water miscible DES as potential lubricants. This study was motivated by the problem of marine environment contamination by the commonly used mineral oils. The authors chose [Ch]Cl:urea (1:2), [Ch]Cl:EG (1:2), [Ch]Cl:glycerol (1:2) and [Ch]Cl:oxalic acid (1:1) and compared their viscosities, viscosity indexes, densities, surface tensions, corrosion rates and friction coefficients with those of a reference oil used for marine applications (Mobil Therm 605). The results of viscosity (at 40 and 100 °C), viscosity index (VI), density (at 25 °C), freezing temperature (T_f) and surface tension for all studied mixtures are presented in Table 1.2. The viscosity index refers to the extent of viscosity change with temperature and the obtained values for all DESs are equal or higher than that of the reference oil. Most DESs also have lower freezing points, which suggests better performance at low temperatures. However, the high freezing point of DES [Ch]Cl:urea (1:2) and the tendency of urea to decompose and form ammonia at high temperatures[113,114] make this mixture undesirable for general use. In contrast, [Ch]Cl:glycerol could be an interesting marine lubricant given its characteristics of non-toxicity and complete miscibility with water. On the other hand, [Ch]Cl:EG is suitable for operation at high and low temperatures due to its high viscosity index and low freezing temperature.

Table 1.2. Values of viscosity, viscosity index (VI), density, freezing temperature (T_f) and surface tension obtain for all studied fluids. Values obtained in reference [112].

Fluids	Viscosity/ $mm^2 \cdot s^{-1}$		VI	Density/ $g \cdot cm^{-3}$	T_f/ °C	Surface tension/ $mN \cdot m^{-1}$
	40 °C	100 °C				
Mobil Therm 605	30	5	100	0.87	-9	30.6
[Ch]Cl:EG (1:2)	20	5	191	1.12	-61	49.2
[Ch]Cl:glycerol (1:2)	118	23	147	1.19	-35	55.4
[Ch]Cl:urea (1:2)	218	24	121	1.20	12	86.4
[Ch]Cl:oxalic acid (1:1)	149	28	144	1.20	-18	75.3

The authors determined the corrosion rates in mild steel by two methods: linear sweep voltammetry (LSV) and electrochemical impedance spectroscopy (EIS). The results presented in Table 1.3 show that the corrosion rates are very low except for [Ch]Cl:oxalic acid (1:1), which the authors justify by the presence of an insulating film on the metal surface on the latter case.

Table 1.3. Corrosion rate of mild steel obtained by the LSV and EIS methods for all studied fluids. Values obtained in reference [112].

Fluids	Corrosion of mild steel/ μm per year	
	LSV	EIS
Reference oil Mobil Therm 605	-	-
[Ch]Cl:EG (1:2)	1.9	5.02
[Ch]Cl:glycerol (1:2)	0.4	2.2
[Ch]Cl:urea (1:2)	2.5	2.7
[Ch]Cl:oxalic acid (1:1)	176	65

To simulate real marine conditions, the authors added 1 wt% water containing 3 wt% NaCl (similar to sea water) to the reference oil and two DES. The final solutions were placed on the mild steel surfaces to assess if corrosion occurred. An analogous experiment was made with [Ch]Cl instead of NaCl. According to Figure 1.11, for the reference oil severe corrosion of the mild steel was observed for the two cases, while in the case of [Ch]Cl:EG (1:2) and [Ch]Cl:glycerol (1:2), no visible signs of corrosion were observed even after 6 months of immersion.

The influence of water on the corrosion rate of iron, nickel and aluminum was also assessed. The low corrosion rates measured with glycol-based DES, even at high water contents, indicate that they would be suitable lubricants in marine environments.

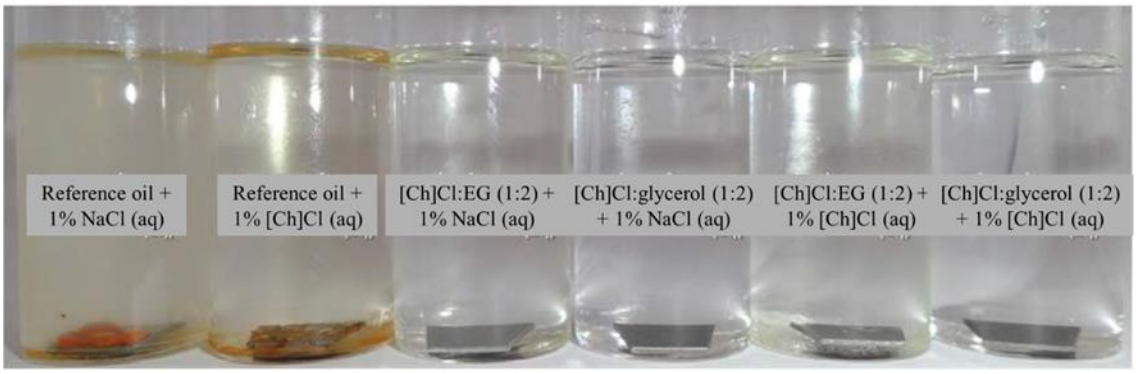

Figure 1.11. Corrosion experiments of mild steel after 2 weeks of immersion in the reference oil and the DES containing 1% NaCl (aq) and 1% [Ch]Cl (aq). Adapted from reference [112].

The tribological performance of the DES was assessed using several types of surfaces (Al, bronze, Cu, mild steel, stainless steel) and a stainless steel counter-body.[112,115] The obtained friction coefficients are presented in Table 1.4.

Table 1.4. Coefficient of kinetic friction of the studied deep eutectic solvents and the reference oil for several types of contacts with stainless steel as counter-body. Values obtained in references [112,115].

Fluids	Surfaces				
	Al	Bronze	Cu	Mild steel	SS
Mobil Therm 605	0.12	0.23	0.37	0.40	0.55
[Ch]Cl:EG (1:2)	0.31	0.26	0.21	0.32	0.30
[Ch]Cl:glycerol (1:2)	0.15	0.58	0.59	0.30	0.31
[Ch]Cl:urea (1:2)	0.55	0.40	0.45	0.28	0.35
[Ch]Cl:oxalic acid (1:1)	0.25	0.29	0.18	0.38	0.30

Clearly, the improved tribological performance of the DES with respect to the mineral oil was observed only for iron-based alloys. The authors tried to explain these results through the ability of the liquids to wet the different surfaces. A mineral oil made from hydrocarbons should interact weakly with the metal surfaces by van der Waals forces while the polar functional groups present in DES enable the adsorption on the surface through hydrogen bonds or chemical reaction. This adsorption leads to the formation of a thin layer or film of lubricant on the metal surface, reducing friction coefficient and wear.[115] However, no explanation was given for the opposite tribological behavior observed with DES and mineral oil on the other metals.

In fact, correlations between the substrate wettability and the tribological performance are hard to establish.[116] For example, Borruto *et al*.[117] found that water lubrication in a boundary/mixed regime was more efficient when the substrates were very hydrophobic and the counter-bodies very hydrophilic.

More recently, Garcia *et al*.[118] tested graphene-containing DES to lubricate steel/steel contacts. Graphene is a promising solid lubricant when used alone[119–121] or added to IL lubricants.[74,122–125] This was the main motivation for the authors to study mixtures of low toxicity DES, namely [Ch]Cl:urea (1:2), [Ch]Cl:EG (1:2) and [Ch]Cl:malic acid, with graphene. (1:1). Commercial synthetic base oil Synfluid PAO6 was selected as the comparative reference. In terms of tribological performance, all tested DES with or without graphene addition yielded lower CoFs when compared to the reference oil (see Figure 1.12). The results were particularly relevant for [Ch]Cl:EG (1:2) and [Ch]Cl:urea (1:2), with added graphene. In the former case, the value of CoF ~0.01 indicates that almost no friction was reached.

After the tribological tests, the surfaces were imaged by optical microscopy and SEM to assess wear. The optical microscopy images of the wear tracks (not shown) revealed that adding graphene to the lubricants made the wear tracks smoother. The exception was [Ch]Cl:malic acid, which led to very wide and irregular wear tracks, even in the presence of graphene.

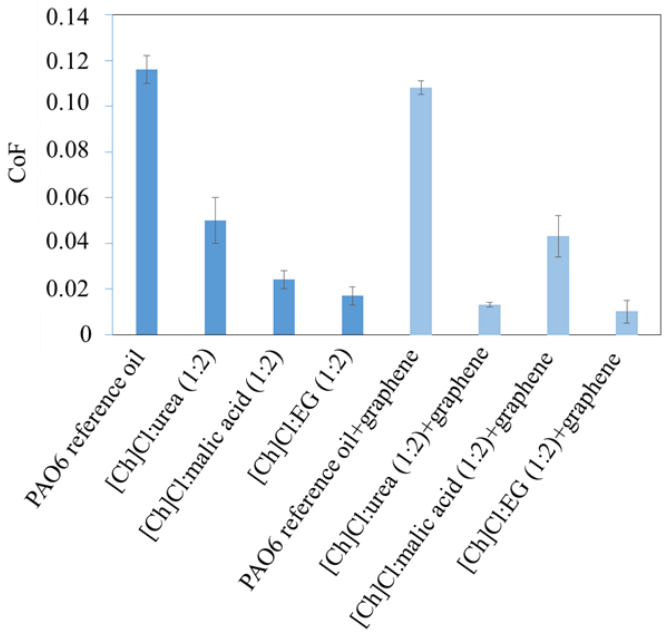

Figure 1.12. CoF results obtained for the studied fluids with and without added graphene. Adapted from reference [118].

The SEM images presented in Figure 1.13, allow a deeper examination of the surfaces. Figure 1.13a, c and g show cavities on the wear tracks containing lubricant residues which are typical of adhesive wear. In contrast, Figure 1.13e, relative to [Ch]Cl:malic acid, shows a very rough surface attacked by severe corrosion, which affects the accurate measurement of the depth of the wear tracks. Figure 1.13b, d and h, which correspond to the lubricants with the graphene additive, reveal that the mechanism changed from adhesion to abrasive wear, with much less pits and less damaged wear tracks.

These results suggest that the addition of graphene to the reference oil and to [Ch]Cl:urea (1:2) and [Ch]Cl:EG (1:2) prevented the formation and consequent detachment of wear particles. Although in most cases the addition of graphene meant less corrosion, in the case of [Ch]Cl:malic acid (1:1), it seems to have enhanced the damage caused by corrosion of the steel surface (see Figure 1.13f). The measured wear rates are presented in Figure 1.14 and show that graphene addition promoted the decrease in the wear rate, with the greater reduction being observed for the reference oil. The exception is [Ch]Cl:malic acid (1:1), where the large errors bars in the wear rate values do not allow to conclude about the effect of graphene.

The overall results of this study are very promising because they demonstrated that it is possible to decrease friction and wear by addition of graphene to the lubricants. Adsorption of graphene sheets to the steel surface to form a protective film[126,127] was suggested as the explanation for this behavior. Furthermore, the traditional oil may be substituted by [Ch]Cl:EG which is biodegradable and not harmful for the environment.

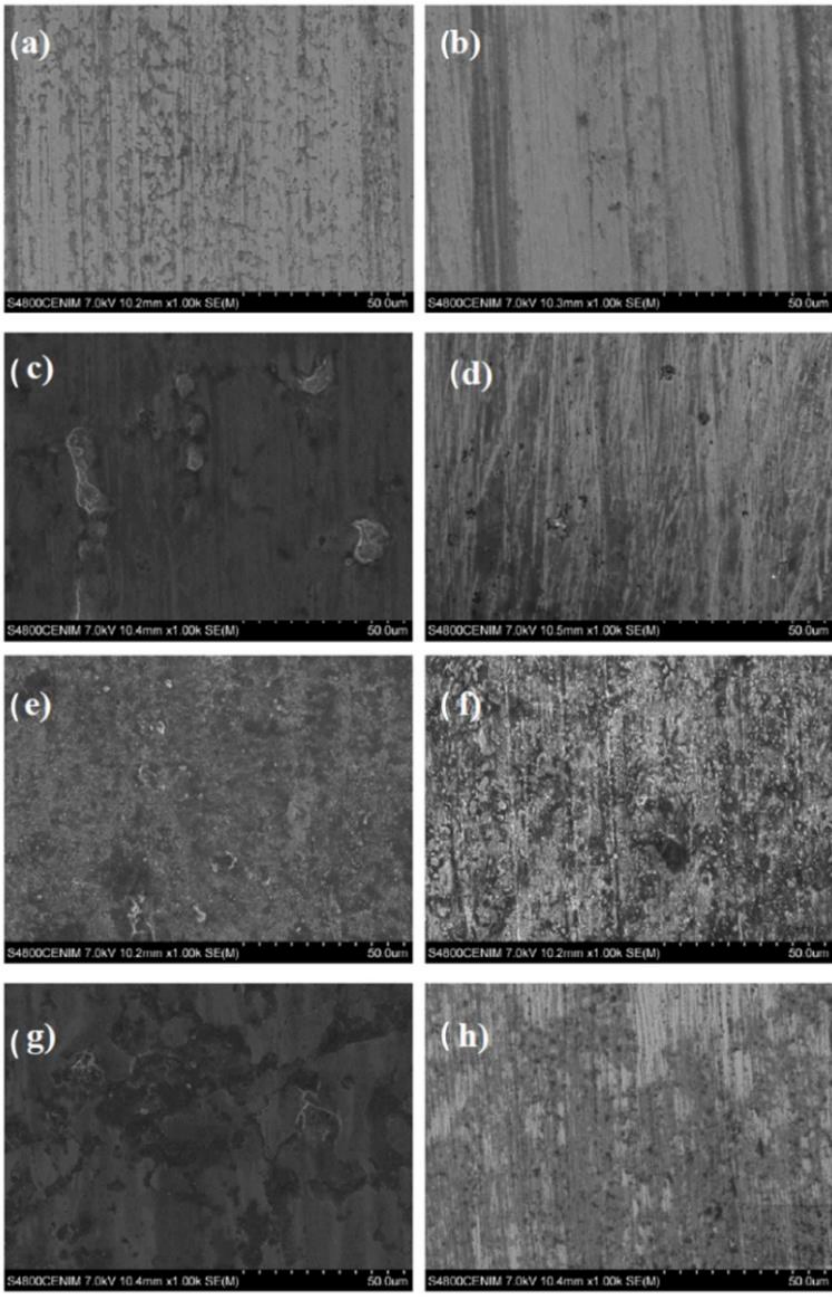

Figure 1.13. SEM images (1000× magnification) of the wear tracks in the surfaces after the tribological tests with the different lubricants: (a) reference oil PAO6, (b) reference oil PAO6 + graphene, (c) [Ch]Cl:urea (1:2), (d) [Ch]Cl:urea (1:2) + graphene, (e) [Ch]Cl:malic acid (1:1), (f) [Ch]Cl:malic acid (1:1) + graphene, (g) [Ch]Cl:EG (1:2) and (h) [Ch]Cl:EG (1:2) + graphene. Adapted from reference [118].

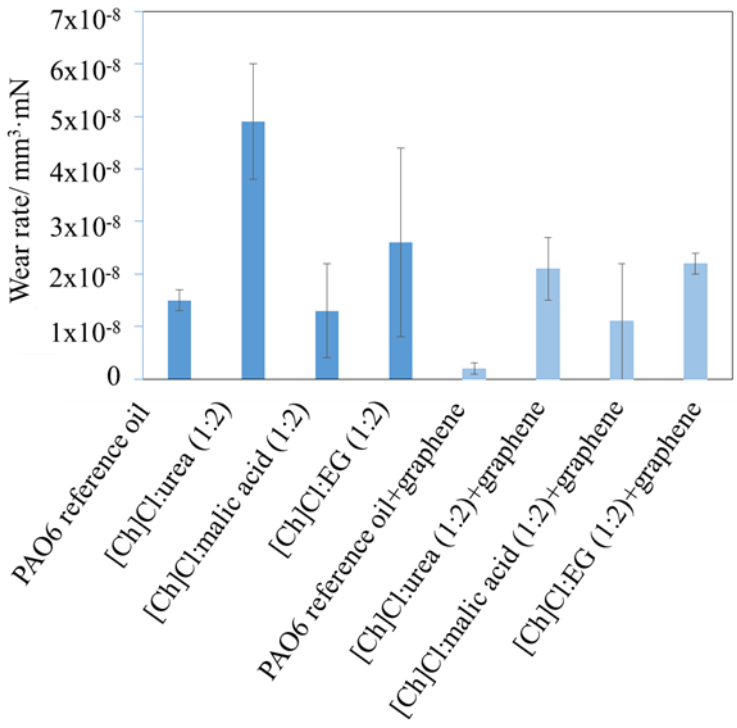

Figure 1.14. Average wear rate of the steel surface for each lubricating fluid. Adapted from reference [118].

Another study involving the use of DES as lubricants appeared in 2019 by Antunes *et al*.[110] The motivation for this study was related to the recent rise of nano and microelectromechanical systems (NEMs and MEMs) and the need for an efficient lubrication of silicon contacts.[128–131] Silicon is a very fragile material and a non-adequate lubrication may lead to adhesion, friction and wear problems. The authors prepared four new DES based on sulfur containing ions: dibutyl-ethylsulfonium ethylsulfate [S_{442}][$EtSO_4$]:PEG 200, ethyl-tetrahydrotiophene ethylsulfate [C_2-THT][$EtSO_4$]:PEG 200, 1-ethyl-3-methylimidazolium (*S*)-camphorsulfonate [C_2MIM][(*S*)-CSA]:PEG 200 and 1-methyl-3-picolinium methylsulfate [C_1-3-pic][$MeSO_4$]:PEG 200. This choice was based on previous knowledge of the good tribological performance of ILs with sulfur units to lubricate silicon surfaces.[29,87] For comparison purposes, model lubricant PEG 200 and three previously reported DES were also studied: [N_{4442}]Br:Sulf, [Ch]Cl:PEG 200 and [N_{4444}]Br:PEG 200. The mixtures were analyzed by DSC, viscosity and wettability measurements. Table 1.5 shows the glass transition temperature (T_g) of the mixtures and their components and the viscosity of the DES at room temperature. The values of T_g for the mixtures were below that of the pure components, except for [S_{442}][$EtSO_4$]:PEG 200 and [C_2-THT][$EtSO_4$]:PEG 200. All the mixtures were considered as eutectics because one single peak was observed in the thermograms, although, in some cases, T_g was above that of the pure components.

Table 1.5. Glass transition temperature and viscosity of the studied fluids. Values obtained in reference [110].

	Fluids	T_g/ °C	Viscosity/ mPa·s
Deep Eutectic Solvents	[Ch]Cl:PEG	-20.0[a]	122±3
	$[N_{4444}]$Br:Sulf	-78.2	139±3
	$[N_{4444}]$Br:PEG 200	-81.1	153±3
	$[S_{442}][EtSO_4]$:PEG 200	-81.4	146±4
	$[C_2$-THT$][EtSO_4]$:PEG 200	-80.7	163.5±0.3
	$[C_2$MIM$][(S)$-CSA]:PEG 200	-76.3	130.6±0.1
	$[C_1$-3-pic$][MeSO_4]$:PEG 200	-74.2	185.9±0.3
DESs components	[Ch]Cl	302.0[a]	-
	$[N_{4444}]$Br	-	-
	Sulfolane	26.0[b]	-
	$[S_{442}][EtSO_4]$	-86.3	307±1
	$[C_2$-THT$][EtSO_4]$	-86.1	413±4
	$[C_2$MIM$][(S)$-CSA]	-32.9	11506±20
	$[C_1$-3-pic$][MeSO_4]$	-70.7	1432.5±2.0
	PEG 200	-56.0[c]	60.0±0.1

[a] Freezing temperature taken from reference [132], [b] Freezing temperature taken from reference [133], [c] Freezing temperature taken from reference [134]

The DES are moderately viscous, although considerably more than PEG 200. The contact angles obtained on silicon surfaces were very similar and varied between 34° for $[C_2$MIM$][(S)$-CSA]:PEG 200 and 43 ° for [Ch]Cl:PEG 200. The tribological behavior of the DES and reference lubricant PEG 200 was assessed with the tribopair steel ball/silicon surface for 400 cycles and the results are presented in Figure 1.15.

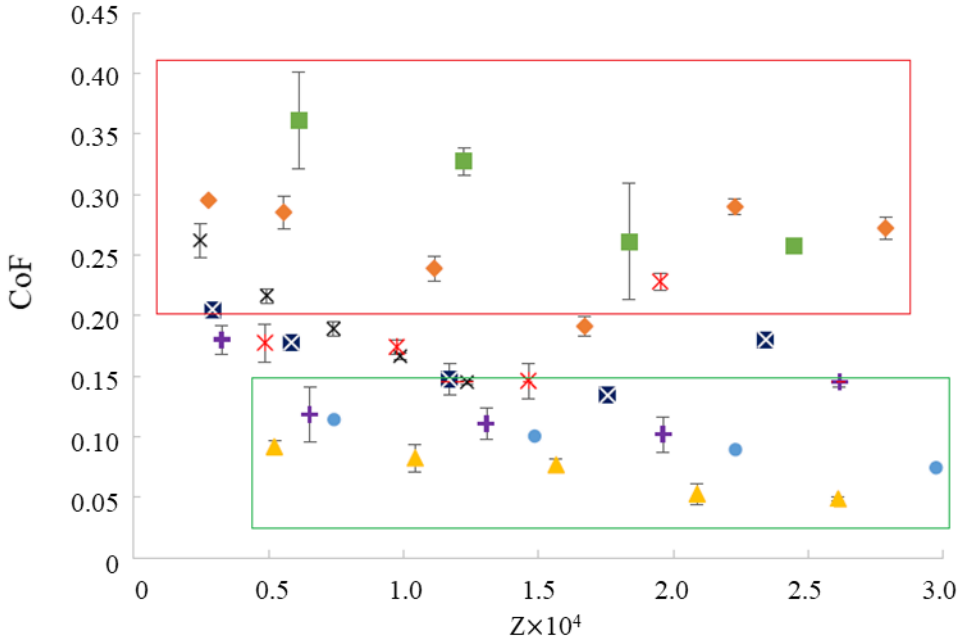

Figure 1.15. CoF *vs.* *Z* for 400 cycles and a force of 15 mN (× PEG200, ✳ [Ch]Cl:PEG, ◆ [N_{4444}]Br:Sulf, ■ [N_{4444}]Br:PEG, ⊠ [S_{442}][$EtSO_4$]:PEG, ✚ [C_2-THT][$EtSO_4$]:PEG, ▲ [C_2MIM][(*S*)-CSA]:PEG and ● [C_1-3-pic][$MeSO_4$]:PEG). The error bars correspond to the standard deviations. Adapted from reference [110].

The best performing liquids were [C_1-3-pic][$MeSO_4$]:PEG 200 and [C_2MIM][(*S*)-CSA]:PEG 200 whose CoF values totally lie within the rectangle in green. The worst results, lying within the rectangle in red, were obtained with [N_{4444}]Br:Sulf and [N_{4444}]Br:PEG. Longer tribological tests (3100 cycles) were done with PEG200 and the best DES using two forces (15 and 30 mN) and the obtained Stribeck curves (CoF *vs.* *Z*) are presented in Figure 1.16. Since the CoFs measured with the DES were similar at both forces, the lubrication regime should be mixed or elastohydrodynamic. In contrast, the significant dependence of CoF on the force observed for PEG200 indicates a boundary lubrication.

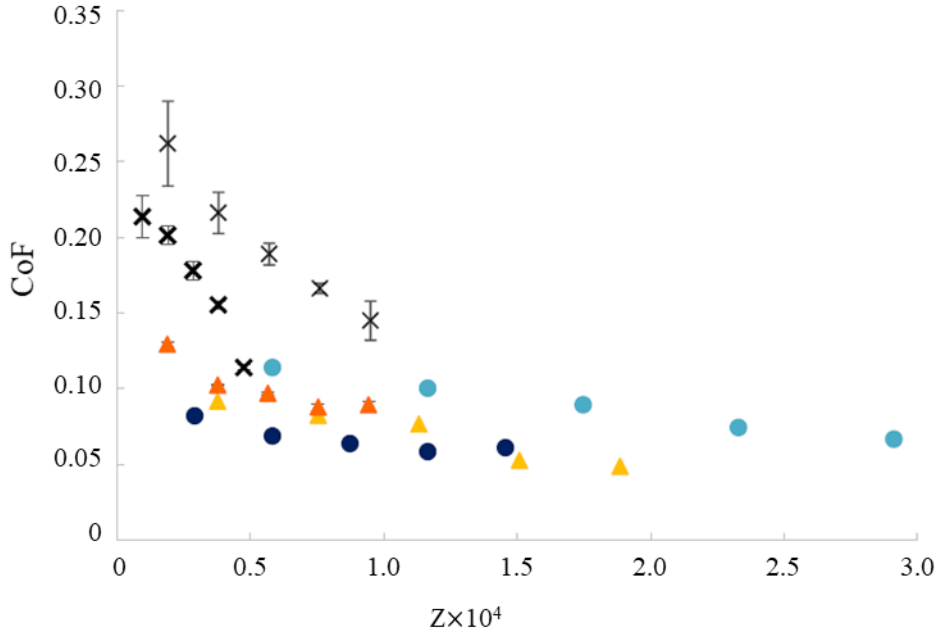

Figure 1.16. CoF *vs.* *Z* for 3100 cycles and the two forces: 15 mN (× PEG200, ▲ [C_2MIM][(*S*)-CSA]:PEG, ● [C_1-3-pic][$MeSO_4$]:PEG) and 30 mN (✕ PEG200, ▲ [C_2MIM][(*S*)-CSA]:PEG, ● [C_1-3-pic][$MeSO_4$]:PEG). The error bars correspond to the standard deviations. Adapted from reference [110].

The AFM images of the silicon surfaces before and after the tribological tests with the best DES are shown in Figure 1.17 and it is clear that no wear occurred. The better tribological behavior of [C_1-3-pic][$MeSO_4$]:PEG 200 and [C_2MIM][(*S*)-CSA]:PEG 200 suggests that, besides the interaction between the sulfur atoms in the anions and the silicon, the interactions of imidazolium and picolinium cations with the surface should also contribute for the formation of a tribofilm. Although deeper research is needed to evaluate the performance of the mixtures in more realistic conditions, the present data are very encouraging with regard to future application of DES based on sulfur as alternative lubricants for MEMs and NEMs.

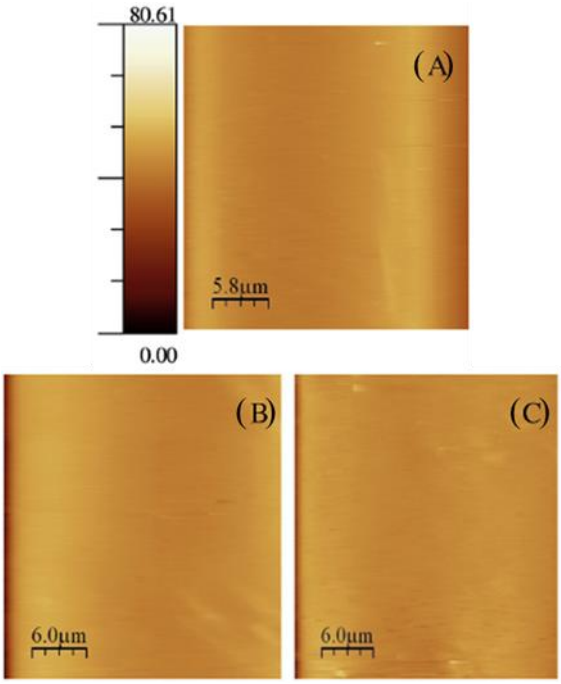

Figure 1.17. AFM images of the Si surface after the long tribological tests (3100 cycles, v = 4·mm·s^{-1} and F = 15 mN) before (A) and after the tribological tests for the best performing lubricants: [C_2MIM][(*S*)-CSA]:PEG (B) and [C_1-3-pic][$MeSO_4$]:PEG (C). Adapted from reference [110].

Recently, Hallet *et al*.[135] studied the frictional behavior of nanoscale films of [Ch]Cl:EG confined between two atomically smooth mica surfaces. They tested samples with different amounts of water: dry, humid (equilibrated with the ambient environment) and with 30% and 50% of added water. Figure 1.18 shows the kinetic friction force, F_S, as a function of the normal force, F_N, and the correspondent CoF, μ, obtained with the four samples. Surprisingly, two types of common behavior were found: dry DES and DES with 50% of water revealed superlubricity at all measured loads; humid DES and DES with 30% water led to very low friction coefficients at low loads that increased up to 0.12 for high loads. The authors suggested the following explanation based on Neutron diffraction measurements. A small amount of water enhances the hydrogen bond network in DES resulting in a film with higher resistance to sliding. In contrast, addition of more than 42% of water disrupts the DES structure leading to the segregation of water layers, which favor the in-plane fluidity and ensure superlubricity.

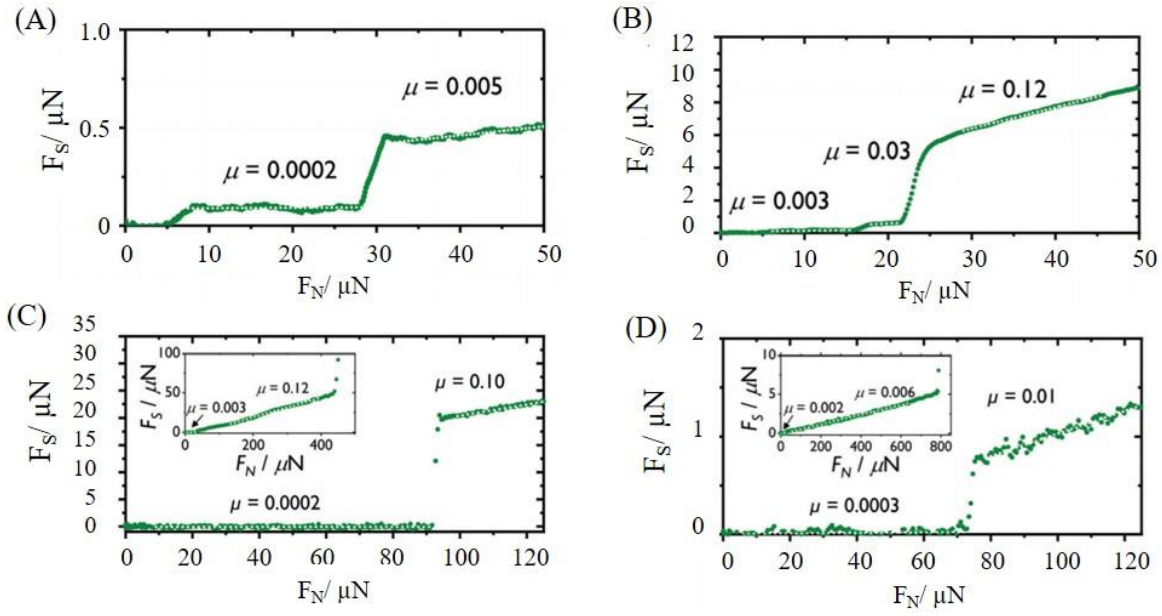

Figure 1.18. Kinetic friction force *vs*. normal force and the corresponding friction coefficient for the four samples: (A) dry, (B) humid, (C) with 30% of added water and (D) with 50% of added water. Adapted from reference [135].

1.5 Problems and Objectives

The growing concern with environmental issues and the rapid development of new engines in the past few decades accentuated the need for more efficient lubrication. There are several ways to improve lubrication properties, such as surface deposition or modification, or by using lubricants, which can be solid (graphite, graphene, Teflon ®, molybdenum and tungsten disulfide), semi-solid (greases) or liquid lubricants (oils or water).

The scientific community has been trying to develop new and competitive lubricants with anti-friction and anti-wear properties, which are more enviormentally friendly. With that in mind, ionic liquids have shown very interesting results.

The main objective of the work presented in this thesis is to synthesize new ionic liquids and prepare deep eutectic solvents, characterize them in terms of physical and chemical properties and assess their tribological performance. Ionic Liquids and Deep Eutectic Solvents have several interesting properties and, depending on the cation/anion or HBA/HBD combination, allow tuning of their properties, making them task-specific compounds with potentially good lubricating capabilities. This thesis focuses particularly in finding liquid lubricants for NEMs and MEMs (nano and microelectromechanical devices) which are miniturized devices made of silicon, a very fragile material which lacks efficient lubrication. NEMs and MEMs have great impact in our day-to-day lives and are used in components of sensors, accelerometers

(airbags), micromotors, microgears, etc. The efficient lubrication of NEMs and MEMs, when they involve moving parts (type IV NEMS/MEMS), is of great importance since, at a smaller scale, forces of adhesion, capillarity, electrostatic and surface tension become more important, creating major issues in the technology of those devices. The operating conditions of these devices usually range from loads of milinewtons to newtons and speeds from $\mu m \cdot s^{-1}$ to $mm \cdot s^{-1}$. Si/Si tribological pairs that mimic the contact in NEMs and MEMs were the ultimate goal of the study. Steel contacts are also studied briefly, as bearing steel is widely used in several extremely important industrial applications such as in rollings and bearings of turbines, engines and varied manufacturing equipment. Steel bearings are usually lubricated with mineral oils with or without additives (such as ZDDP) and their operating loads are in the order of magnitude of Newton, with speeds ranging from $mm \cdot s^{-1}$ to $m \cdot s^{-1}$.

The results obtained in this work complete the study of Ionic Liquids as lubricant additives and opens the path to the use of Deep Eutectis Solvents as lubricants for future studies, moving towards a more sustainable world using more environmentally friendly approaches, namely in the synthesis and application of lubricants.

1.6 References

[1] K. Holmberg, A. Erdemir, Influence of Tribology on Global Energy Consumption, Costs and Emissions. *Friction* **2017**, *5* (3), 263–284. https://doi.org/10.1007/s40544-017-0183-5

[2] T. A. Harris, M. N. Kotzalas, *Essential Concepts of Bearing Technology*, 5th ed.; CRC Press, **2006**.

[3] A. Somers, P. Howlett, D. MacFarlane, M. A. Forsyth, Review of Ionic Liquid Lubricants. *Lubricants* **2013**, *1* (1), 3–21. https://doi.org/10.3390/lubricants1010003

[4] F. Zhou, Y. Liang, W. Liu, Ionic Liquid Lubricants: Designed Chemistry for Engineering Applications. *Chem. Soc. Rev.* **2009**, *38*, 2590–2599. https://doi.org/10.1039/B817899M

[5] B. Bhushan, *Introduction to Tribology*, 1st ed.; Wiley, J., Ed.; Wiley: New York, **2002**; Vol. 17.

[6] D. R. MacFarlane, M. Kar, J. M. Pringle, *Fundamentals of Ionic Liquids*. Wiley-VCH Verlag GmbH & Co. KGaA, Ed.; Wiley, **2017**.

[7] C. E. Tucker, D. A. Jaeger, Diels-Alder Reactions in Ethylammonium Nitrate, a Low-Melting Fused Salt. *Tetrahedron Letters* **1989**, *30* (14), 1785–1788. https://doi.org/10.1016/S0040-4039(00)99579-0

[8] Y. Zhou, J. Qu, Ionic Liquids as Lubricant Additives: A Review. *Applied Materials & Interfaces* **2017**, *9*, 3209–3222. https://doi.org/10.1021/acsami.6b12489

[9] G. Tiago, J. Restolho, A. Forte, R. Colaço, Novel Ionic Liquids for Interfacial and Tribological Applications. *Colloids and Surfaces A : Physicochemical and Engineering Aspects* **2015**, *472*, 1–8. https://doi.org/10.1016/j.colsurfa.2015.02.030

[10] H. Sakaebe, H. Matsumoto, N-Methyl-N-Propylpiperidinium Bis(Trifluoromethanesulfonyl)Imide (PP13-TFSI) - Novel Electrolyte Base for Li Battery. *Electrochemistry Communications* **2003**, *5* (7), 594–598. https://doi.org/10.1016/S1388-2481(03)00137-1

[11] J. J. Xu, H. Ye, J. Huang, Novel Zinc Ion Conducting Polymer Gel Electrolytes Based on Ionic Liquids. *Electrochemistry Communications* **2005**, *7* (12), 1309–1317. https://doi.org/10.1016/j.elecom.2005.09.011

[12] V. M. Kobryanskii, S. A. Arnautov, Chemical Synthesis of Polyphenylene in an Ionic Liquid. *Synthetic Metals* **1993**, *55* (2–3), 924–929. https://doi.org/10.1016/0379-6779(93)90176-W

[13] M. J. Earle, P. B. McCormac, K. R. Seddon, Regioselective Alkylation in Ionic Liquids. *Chemical Communications* **1998**, No. 20, 2245–2246. https://doi.org/10.1039/a806328a

[14] J. G. Huddleston, H. D. Willauer, R. P. Swatloski, A. E. Visser, R. D. Rogers, Room Temperature Ionic Liquids as Novel Media for "clean" Liquid-Liquid Extraction. *Chemical Communications* **1998**, No. 16, 1765–1766. https://doi.org/10.1039/A803999B

[15] M. J. Earle, P. B. McCormac, K. R. Seddon, Diels–Alder Reactions in Ionic Liquids. *Green Chemistry* **1999**, *1* (1), 23–25. https://doi.org/10.1039/a808052f

[16] R. L. Vekariya, A Review of Ionic Liquids: Applications towards Catalytic Organic Transformations. *Journal of Molecular Liquids* **2017**, *227*, 44–60. https://doi.org/10.1016/j.molliq.2016.11.123

[17] C. Ye, W. Liu, Y. Chen, L. Yu, Room-Temperature Ionic Liquids: A Novel Versatile Lubricant. *Chem. Commun.* **2001**, *21*, 2244–2245. https://doi.org/10.1039/B106935G

[18] Z. Tang, S. Li, A Review of Recent Developments of Friction Modifiers for Liquid Lubricants (2007-Present). *Current Opinion in Solid State and Materials Science* **2014**, *18* (3), 119–139. https://doi.org/10.1016/j.cossms.2014.02.002

[19] S. A. S. Amiril, E. A. Rahim, S. Syahrullail, A Review on Ionic Liquids as Sustainable Lubricants in Manufacturing and Engineering: Recent Research, Performance, and Applications. *Journal of Cleaner Production* **2017**, *168*, 1571–1589. https://doi.org/10.1016/j.jclepro.2017.03.197

[20] H. Xiao, Ionic Liquid Lubricants: Basics and Applications. *Tribology Transactions* **2017**, *60* (1), 20–30. https://doi.org/10.1080/10402004.2016.1142629

[21] M. Cai, Q. Yu, W. Liu, F. Zhou, Ionic Liquid Lubricants: When Chemistry Meets Tribology. *Chemical Society Reviews* **2020**, *49* (21), 7753–7818. https://doi.org/10.1039/d0cs00126k

[22] T. Naveed, R. Zahid, R. A. Mufti, M. Waqas, M. T. Hanif, A Review on Tribological Performance of Ionic Liquids as Additives to Bio Lubricants. *Proceedings of the Institution of Mechanical Engineers, Part J: Journal of Engineering Tribology* **2020**. https://doi.org/10.1177/1350650120973805

[23] P. Iglesias, M. D. Bermúdez, F. J. Carrión, G. Martínez-Nicolás, Friction and Wear of Aluminium-Steel Contacts Lubricated with Ordered Fluids-Neutral and Ionic Liquid Crystals as Oil Additives. *Wear* **2004**, *256* (3–4), 386–392. https://doi.org/10.1016/S0043-1648(03)00442-3

[24] A. E. Jiménez, M. D. Bermúdez, P. Iglesias, F. J. Carrión, G. Martínez-Nicolás, 1-N-Alkyl-3-Methylimidazolium Ionic Liquids as Neat Lubricants and Lubricant Additives in Steel-Aluminium Contacts. *Wear* **2006**, *260*, 766–782. https://doi.org/10.1016/j.wear.2005.04.016

[25] A. E. Jiménez, M. D. Bermúdez, F. J. Carrión, G. Martínez-Nicolás,. Room Temperature Ionic Liquids as Lubricants Additives in Steel-Aluminium Contacts: Influence of Sliding Velocity, Normal Load and Temperature. *Wear* **2006**, *261*, 347–359. https://doi.org/10.1016/j.wear.2005.11.004

[26] A. E. Somers, B. Khemchandani, P. C. Howlett, J. Sun, D. R. MacFarlane, N.Forsyth, Ionic Liquids as Antiwear Additives in Base Oils: Influence of Structure on Miscibility and Antiwear Performance for Steel on Aluminum. *Appl. Mater. Interfaces* **2013**, *5*, 11544–11553. https://doi.org/10.1021/am4037614

[27] M. Cai, Z. Zhao, Y. Liang, F. Zhou, W. Liu, Alkyl Imidazolium Ionic Liquids as Friction Reduction and Anti-Wear Additive in Polyurea Grease for Steel/Steel Contacts. *Tribol. Lett.* **2010**, *40*, 215–224. https://doi.org/10.1007/s11249-010-9624-2

[28] X. Fan, L. Wang, High-Performance Lubricant Additives Based on Modified Graphene Oxide by Ionic Liquids. *J. Colloid Interface Sci.* **2015**, *452*, 98–108. https://doi.org/10.1016/j.jcis.2015.04.025

[29] P. M. Amorim, A. M. Ferraria, R. Colaço, L. C. Branco, B. Saramago, Imidazolium-Based Ionic Liquids Used as Additives in the Nanolubrication of Silicon Surfaces. *Beilstein Journal of Nanotechnology* **2017**, *8*, 1961–1971. https://doi.org/10.3762/bjnano.8.197

[30] M. Cai, Y. Liang, F. Zhou, W. Liu, A Novel Imidazolium Salt with Antioxidation and Anticorrosion Dual Functionalities as the Additive in Poly(Ethylene Glycol) for Steel/Steel Contacts. *Wear* **2012**, *306* (1–2), 197–208. https://doi.org/10.1016/j.wear.2012.09.001

[31] J. Sanes, M. D. Avilés, N. Saurín, T. Espinosa, F. J. Carrión, M. D. Bermúdez, Synergy between Graphene and Ionic Liquid Lubricant Additives. *Tribology International* **2017**, *116* (August), 371–382. https://doi.org/10.1016/j.triboint.2017.07.030

[32] C. Gan, T. Liang, W. Li, X. Fan, X. Li, D. Li, M. Zhu, Hydroxyl-Terminated Ionic Liquids Functionalised Graphene Oxide with Good Dispersion and Lubrication Function. *Tribol. Int.* **2020**, *148*, 106350. https://doi.org/10.1016/j.triboint.2020.106350

[33] A. E. Jiménez, M. D. Bermúdez, Short Alkyl Chain Imidazolium Ionic Liquid Additives in Lubrication of Three Aluminium Alloys with Synthetic Ester Oil. *Tribology - Materials, Surfaces and Interfaces* **2012**, *6* (3), 109–115. https://doi.org/10.1179/1751584X12Y.0000000011

[34] V. Pejaković, M. Kalin, Frictional Behavior of Imidazolium Sulfate Ionic Liquid Additives under Mixed Slide-to-Roll Conditions: Part 1 - Variation of Mixtures with Identical Weight Ratio of Ionic Liquid Additive. *Lubrication Science* **2015**, *27*, 463–477. https://doi.org/10.1002/ls.1289

[35] C. Zhang, S. Zhang, L. Yu, P. Zhang, Z. Zhang, Z. Wu, Tribological Behavior of 1-Methyl-3-HexadecylimidazoliumTetrafluoroborate Ionic Liquid Crystal as a Neat Lubricantand as an Additive of Liquid Paraffin. *Tribol. Lett.* **2012**, *46*, 49–54. https://doi.org/10.1007/s11249-012-9917-8

[36] M. Cai, Y. Liang, M. Yao, Y. Xia, F. Zhou, W. Liu, Imidazolium Ionic Liquids As Antiwear and Antioxidant Additive in Poly(Ethylene Glycol) for Steel/Steel Contacts. *ACS Appl. Mater. Interfaces* **2010**, *2*, 870–876. https://doi.org/10.1021/am900847j

[37] M. Cai, Y. Liang, F. Zhou, W. Liu, Tribological Properties of Novel Imidazolium Ionic Liquids Bearing Benzotriazole Group as the Antiwear/Anticorrosion Additive in Poly(Ethylene Glycol) and Polyurea Grease for Steel/Steel Contacts. *ACS Appl. Mater. Interfaces* **2011**, *3*, 4580–4592. https://doi.org/10.1021/am200826b

[38] M. Cai, Y. Liang, F. Zhou, W. Liu, Anticorrosion Imidazolium Ionic Liquids as the Additive in Poly(Ethylene Glycol) for Steel/Cu-Sn Alloy Contacts. *Faraday Discussions* **2012**, *156*, 147–157. https://doi.org/10.1039/c2fd00124a

[39] F. Pagano, C. Gabler, P. Zare, M. Mahrova, N. Dörr, R. Bayon, X. Fernandez, W. H. Binder, M. Hernaiz, E. Tojo, A. Igartua, Dicationic Ionic Liquids as Lubricants. Proc I Mech E Part J. *J. Engineering Tribology* **2012**, *226*, 952–964. https://doi.org/10.1177/1350650112458873

[40] R. Gusain, P. Gupta, S. Saran, O. P. Khatri, Halogen-Free Bis(Imidazolium)/ Bis(Ammonium)-Di[Bis(Salicylato)Borate] Ionic Liquids as Energy-Efficient and Environmentally Friendly Lubricant Additives. *ACS Appl. Mater. Interfaces* **2014**, *6*, 15318–15328. https://doi.org/10.1021/am503811t

[41] B. Yu, D. G. Bansal, J. Qu, X. Sun, H. Luo, S. Dai, P. J. Blau, B. G. Bunting, G. Mordukhovich, D. J. Smolenski, Oil-Miscible and Non-Corrosive Phosphonium-Based Ionic Liquids as Candidate Lubricant Additives. *Wear* **2012**, *289*, 58–64. https://doi.org/10.1016/j.wear.2012.04.015

[42] M. Anand, M. Hadfield, J. L. Viesca, B. Thomas, R. González, R. Cantrill, A. H. Battez, Assessing Boundary Film Forming Behavior of Phosphonium Ionic Liquids as Engine Lubricant Additives. *Lubricants* **2016**, *4* (2). https://doi.org/10.3390/lubricants4020017

[43] M. Anand, M. Hadfield, J. L. Viesca, B. Thomas, A. H. Battez, S. Austen, Ionic Liquids as Tribological Performance Improving Additive for In-Service and Used Fully-Formulated Diesel Engine Lubricants. *Wear* **2015**, *334–335*, 67–74. https://doi.org/10.1016/j.wear.2015.01.055

[44] R. González, M. Bartolomé, D. Blanco, J. L. Viesca, A. Fernández-González, A. H. Battez, Effectiveness of Phosphonium Cation-Based Ionic Liquids as Lubricant Additive. *Tribology International* **2016**, *98*, 82–93. https://doi.org/10.1016/j.triboint.2016.02.016

[45] J. Qu, W. C. Barnhill, H. Luo, H. M. Meyer, D. N. Leonard, A. K. Landauer, B. Kheireddin, H. Gao, B. L. Papke, S. Dai, Synergistic Effects between Phosphonium-Alkylphosphate Ionic Liquids and Zinc Dialkyldithiophosphate (ZDDP) as Lubricant Additives. *Advanced Materials* **2015**, *27* (32), 4767–4774. https://doi.org/10.1002/adma.201502037

[46] Z. Cai, H. M. Meyer, C. Ma, M. Chi, H. Luo, J. Qu, Comparison of the Tribological Behavior of Steel-Steel and Si3N4-Steel Contacts in Lubricants with ZDDP or Ionic Liquid. *Wear* **2014**, *319* (1–2), 172–183. https://doi.org/10.1016/j.wear.2014.08.002

[47] Y. Zhou, J. Dyck, T. W. Graham, H. Luo, D. N. Leonard, J. Qu, Ionic Liquids Composed of Phosphonium Cations and Organophosphate, Carboxylate, and Sulfonate Anions as Lubricant Antiwear Additives. *Langmuir* **2014**, *30* (44), 13301–13311. https://doi.org/10.1021/la5032366

[48] W. C. Barnhill, J. Qu, H. Luo, H. M. Meyer, C. Ma, M. Chi, B. L. Papke, Phosphonium-Organophosphate Ionic Liquids as Lubricant Additives: Effects of Cation Structure on

Physicochemical and Tribological Characteristics. *ACS Applied Materials and Interfaces* **2014**, *6* (24), 22585–22593. https://doi.org/10.1021/am506702u

[49] K. I. Nasser, J. M. Liñeira del Río, E. R. López, J. Fernández, Synergistic Effects of Hexagonal Boron Nitride Nanoparticles and Phosphonium Ionic Liquids as Hybrid Lubricant Additives. *Journal of Molecular Liquids* **2020**, *311*, 113343. https://doi.org/10.1016/j.molliq.2020.113343

[50] I. Otero, E. R. López, M. Reichelt, M. Villanueva, J. Salgado, J. Fernández, Ionic Liquids Based on Phosphonium Cations As Neat Lubricants or Lubricant Additives for a Steel/Steel Contact. *ACS Appl. Mater. Interfaces* **2014**, *6*, 13115–13128. https://doi.org/10.1021/am502980m

[51] B. Khemchandani, A. Somers, P. Howlett, A. K. Jaiswal, E. Sayanna, M. A. Forsyth, New Biocompatible Ionic Liquid as an Antiwear Additive for Biodegradable Lubricants. *5th World Tribology Congress, WTC 2013* **2013**, *4*, 2786–2789. https://doi.org/10.1016/j.triboint.2014.04.016

[52] V. Sharma, N. Doerr, P. B. Aswath, Chemical-Mechanical Properties of Tribofilms and Their Relationship to Ionic Liquid Chemistry. *RSC Adv.* **2016**, *6*, 22341–22356. https://doi.org/10.1039/C6RA01915C

[53] J. M. Liñeira del Río, E. R. López, J. Fernández, Synergy between Boron Nitride or Graphene Nanoplatelets and Tri(Butyl)Ethylphosphonium Diethylphosphate Ionic Liquid as Lubricant Additives of Triisotridecyltrimellitate Oil. *Journal of Molecular Liquids* **2020**, *301*. https://doi.org/10.1016/j.molliq.2020.112442

[54] V. Totolin, I. Minami, C. Gabler, J. Brenner, N. Dörr, Lubrication Mechanism of Phosphonium Phosphate Ionic Liquid Additive in Alkylborane-Imidazole Complexes. *Tribology Letters* **2014**, *53* (2), 421–432. https://doi.org/10.1007/s11249-013-0281-0

[55] A. Westerholt, M. Weschta, A. Bosmann, S. Tremmel, Y. Korth, M. Wolf, E. Shlucker, N. Wehrum, A. Lennert, M. Uerdingen, W. Holweger, S. Wartzack, P. Wasserscheid, Halide-Free Synthesis and Tribological Performance of Oil-Miscible Ammonium and Phosphonium-Based Ionic Liquids. *ACS Sustainable Chemistry Engineering* **2015**, *3* (2), 54–67. https://doi.org/doi.org/10.1021/sc500517n

[56] D. Blanco, A. H. Battez, J. L. Viesca, R. González, A. Fernández-González, Lubrication of CrN Coating With Ethyl-Dimethyl-2-Methoxyethylammonium Tris(Pentafluoroethyl) Trifluorophosphate Ionic Liquid as Additive to PAO 6. *Tribol. Lett. Lett.* **2011**, *41*, 295–302. https://doi.org/10.1007/s11249-010-9714-1

[57] D. Blanco, R. González, A. H. Battez, J. L. Viesca, A. Fernández-González, Use of Ethyl-Dimethyl-2-Methoxyethylammonium Tris(Pentafluoroethyl) Trifluorophosphate as Base Oil Additive in the Lubrication of TiN PVD Coating. *Tribol. Int.* **2011**, *44*, 645–650. https://doi.org/10.1016/j.triboint.2011.01.004

[58] T. Espinosa, J. Sanes, A. E. Jiménez, M. D. Bermúdez, Protic Ammonium Carboxylate Ionic Liquid Lubricants of OFHC Copper. *Wear* **2013**, *303*, 495–509. https://doi.org/10.1016/j.wear.2013.03.041

[59] T. Espinosa, M. Jimenez, J. Sanes, A. E. Jimenez, M. Iglesias, M. D. Bermudez, Ultra-Low Friction with a Protic Ionic Liquid Boundary Film at the Water-Lubricated Sapphire-Stainless Steel Interface. *Tribology Letters* **2014**, *53* (1), 1–9. https://doi.org/10.1007/s11249-013-0238-3

[60] Q. Zhao, G. Zhao, M. Zhang, X. Wang, W. Liu, Tribological Behavior of Protic Ionic Liquids with Ammonium Salts Modified LABSA as Lubricants and Additives. *Lubrication Science* **2013**, *25*, 217–230. https://doi.org/10.1002/ls.1204

[61] M. Fan, D. Yang, X. Wang, W. Liu, H. Fu, DOSS- Based QAILs: As Both Neat Lubricants and Lubricant Additives with Excellent Tribological Properties and Good Detergency. *Industrial and Engineering Chemistry Research* **2014**, *53* (46), 17952–17960. https://doi.org/10.1021/ie502849w

[62] W. C. Barnhill, H. Luo, H. M. Meyer, C. Ma, M. Chi, B. L. Papke, J. Qu, Tertiary and Quaternary Ammonium-Phosphate Ionic Liquids as Lubricant Additives. *Tribology Letters* **2016**, *63* (2). https://doi.org/10.1007/s11249-016-0707-6

[63] X. Fu, L. Sun, X. Zhou, Z. Li, T. Ren, Tribological Study of Oil-Miscible Quaternary Ammonium Phosphites Ionic Liquids as Lubricant Additives in PAO. *Tribology Letters* **2015**, *60* (2), 1–12. https://doi.org/10.1007/s11249-015-0596-0

[64] P. K. Khatri, G. D. Thakre, S. L. Jain, Tribological Performance Evaluation of Task-Specific Ionic Liquids Derived from Amino Acids. *Ind. Eng. Chem. Res.* **2013**, *52* (45), 15829–15837. https://doi.org/10.1021/ie402141v

[65] D. Qiao, H. Wang, D. Feng, Tribological Performance and Mechanism of Phosphate Ionic Liquids as Additives in Three Base Oils for Steel-on-Aluminum Contact. *Tribology Letters* **2014**, *55* (3), 517–531. https://doi.org/10.1007/s11249-014-0377-1

[66] P. K. Khatri, C. Joshi, G. D. Thakre, S. L. Jain, Halogen-Free Ammonium-Organoborate Ionic Liquids as Lubricating Additives: The Effect of Alkyl Chain Lengths on the Tribological Performance. *New Journal of Chemistry* **2016**, *40* (6), 5294–5299. https://doi.org/10.1039/c5nj02225h

[67] R. Gusain, S. Dhingra, O. P. Khatri, Fatty-Acid-Constituted Halogen-Free Ionic Liquids as Renewable, Environmentally Friendly, and High-Performance Lubricant Additives. *Industrial and Engineering Chemistry Research* **2016**, *55* (4), 856–865. https://doi.org/10.1021/acs.iecr.5b03347

[68] P. Nagendramma, P. K. Khatri, G. D. Thakre, S. L. Jain, Lubrication Capabilities of Amino Acid Based Ionic Liquids as Green Bio-Lubricant Additives. *Journal of Molecular Liquids* **2017**, *244*, 219–225. https://doi.org/10.1016/j.molliq.2017.08.115

[69] M. Sernaglia, D. Blanco, A. H. Battez, R. González, A. Fernández-González, M. Bartolomé, Two Fatty Acid Anion-Based Ionic Liquids - Part II: Effectiveness as an

Additive to Polyol Ester. *J. Mol. Liq.* **2020**, *310*, 113158. https://doi.org/10.1016/j.molliq.2020.113158

[70] Y. Han, D. Qiao, Y. Guo, D. Feng, L. Shi, Influence of Competitive Adsorption on Lubricating Property of Phosphonate Ionic Liquid Additives in PEG. *Tribology Letters* **2016**, *64* (2), 1–12. https://doi.org/10.1007/s11249-016-0749-9

[71] G. Huang, Q. Yu, Z. Ma, M. Cai, W. Liu, Probing the Lubricating Mechanism of Oil-Soluble Ionic Liquids Additives. *Tribology International* **2017**, *107* (June 2016), 152–162. https://doi.org/10.1016/j.triboint.2016.08.027

[72] Q. Yu, C. Zhang, R. Dong, Y. Shi, Y. Wang, Y. Bai, J. Zhang, M. Cai, F. Zhou, Novel N-, P-Containing Oil-Soluble Ionic Liquids with Excellent Tribological and Anti-Corrosion Performance. *Tribol. Int.* **2019**, *132*, 118–129. https://doi.org/10.1016/j.triboint.2018.12.002

[73] V. Pejaković, M. Kronberger, M. Mahrova, M. Vilas, E. Tojo, M. Kalin, Pyrrolidinium Sulfate and Ammonium Sulfate Ionic Liquids as Lubricant Additives for Steel/Steel Contact Lubrication. *Journal of Engineering Tribology* **2012**, *226* (11), 923–932. https://doi.org/10.1177/1350650112448978

[74] M. D. Avilés, F. J. Carrión-Vilches, J. Sanes, M. D. Bermúdez, Diprotic Ammonium Succinate Ionic Liquid in Thin Film Aqueous Lubrication and in Graphene Nanolubricant. *Tribology Letters* **2019**, *67* (1), 0. https://doi.org/10.1007/s11249-019-1138-y

[75] R. González, A. H. Battez, D. Blanco, J. L. Viesca, A. Fernández-González, Lubrication of TiN, CrN and DLC PVD Coatings with 1-Butyl-1-Methylpyrrolidiniumtris(Pentafluoroethyl) Trifluorophosphate. *Tribol. Lett.* **2010**, *40*, 269–277. https://doi.org/10.1007/s11249-010-9674-5

[76] R. Monge, R. González, A. Hernández Battez, A. Fernández-González, J. L. Viesca, A. García, M. Hadfield, Ionic Liquids as an Additive in Fully Formulated Wind Turbine Gearbox Oils. *Wear* **2015**, *328–329*, 50–63. https://doi.org/10.1016/j.wear.2015.01.041

[77] M. Mahrova, F. Pagano, V. Pejakovic, A. Valea, M. Kalin, A. Igartua, E. Tojo, Pyridinium Based Dicationic Ionic Liquids as Base Lubricants or Lubricant Additives. *Tribology International* **2015**, *82* (PA), 245–254. https://doi.org/10.1016/j.triboint.2014.10.018

[78] P. K. Khatri, M. S. Aathira, G. D. Thakre, S. L. Jain, Synthesis and Tribological Behavior of Fatty Acid Constituted Tetramethylguanidinium (TMG) Ionic Liquids for a Steel/Steel Contact. *Materials Science and Engineering C* **2018**, *91* (May), 208–217. https://doi.org/10.1016/j.msec.2018.05.038

[79] A. M. Sadanandan, P. K. Khatri, R. C. Saxena, S. L. Jain, Guanidine Based Amino Acid Derived Task Specific Ionic Liquids as Noncorrosive Lubricant Additives for Tribological Performance. *J. Mol. Liq.* **2020**, *313*, 1–10. https://doi.org/doi.org/10.1016/j.molliq.2020.113527

[80] Z. Song, Y. Liang, M. Fan, F. Zhou, W. Liu, Lithium-Based Ionic Liquids as Novel Lubricant Additives for Multiply Alkylated Cyclopentanes (MACs). *Friction* **2013**, *1* (3), 222–231. https://doi.org/10.1007/s40544-013-0019-x

[81] S. Yang, J. S. S. Wong, F. Zhou, Ionic Liquid Additives for Mixed and Elastohydrodynamic Lubrication. *Tribology Transactions* **2018**, *61* (5), 816–826. https://doi.org/10.1080/10402004.2018.1426802

[82] Z. Cao, Y. Xia, C. Chen, Fabrication of Novel Ionic Liquids-Doped Polyaniline as Lubricant Additive for Anti-Corrosion and Tribological Properties. *Tribology International* **2018**, *120* (January), 446–454. https://doi.org/10.1016/j.triboint.2018.01.009

[83] A. E. Jiménez, M. D. Bermúdez, F. J. Carrión, G. Martínez-Nicolás, Room Temperature Ionic Liquids as Lubricant Additives in Steel-Aluminium Contacts: Influence of Sliding Velocity, Normal Load and Temperature. *Wear* **2006**, *261* (3–4), 347–359. https://doi.org/10.1016/j.wear.2005.11.004

[84] A. E. Jiménez, M. D. Bermúdez, Imidazolium Ionic Liquids as Additives of the Synthetic Ester Propylene Glycol Dioleate in Aluminium-Steel Lubrication. *Wear* **2008**, *265*, 787–798. https://doi.org/10.1016/j.wear.2008.01.009

[85] A. H. Battez, R. Gonzalez, J. L. Viesca, D. Blanco, E. Asedegbega, A. Osorio, Tribological Behavior of Two Imidazolium Ionic Liquids as Lubricant Additives for Steel/Steel Contacts. *Wear* **2009**, *266*, 1224−1228. https://doi.org/10.1016/j.wear.2009.03.043

[86] V. Pejaković, C. Tomastik, N. Dörr, M. Kalin, Influence of Concentration and Anion Alkyl Chain Length on Tribological Properties of Imidazolium Sulfate Ionic Liquids as Additives to Glycerol in Steel-Steel Contact Lubrication. *Tribology International* **2016**, *97*, 234–243. https://doi.org/10.1016/j.triboint.2016.01.034

[87] J. Cosme, P. D. A. Bastos, I. Catela, D. Silva, R. Colaço, L. C. Branco, B. Saramago, Task–Specific Ionic Liquids Based on Sulfur for Tribological Applications. *ChemistrySelect* **2016**, *1* (13), 3612–3617. https://doi.org/10.1002/slct.201600880

[88] S. Perkin, J. Klein, T. Albrecht, Layering and Shear Properties of an Ionic Liquid , 1-Ethyl-3-Methylimidazolium Ethylsulfate , Confined to Nano-Films between Mica Surfaces. *Physical Chemistry Chemical Physics* **2010**, *12*, 1243–1247. https://doi.org/10.1039/b920571c

[89] L. J. Weng, X. Q. Liu, Y. M. Liang, Q. J. Xue, Effect of Tetraalkylphosphonium Based Ionic Liquids as Lubricants on the Tribological Performance of a Steel-on-Steel System. *Tribology Letters* **2006**, *26* (1), 11–17. https://doi.org/10.1007/s11249-006-9175-8

[90] S. Odi-Owei, B. J. Roylance, L. Z. Xie, Experimental Study of Initial Scuffing and Recovery in Sliding Wear Using a Four-Ball Machine. *Wear* **1987**, *117*, 267–287. https://doi.org/10.1016/0043-1648(87)90149-9

[91] J. Qu, J. J. Truhan, P. J. Blau, Detecting the Onset of Localized Scuffing in a Pin-on-Twin Fuel-Lubricated Test for Heavy-Duty Diesel Fuel Injectors. *International Journal of Engine Research* **2005**, *6* (1), 1–9. https://doi.org/10.1243/146808705X7356

[92] J. Qu, J. J. Truhan, S. Dai, H. Luo, P. J. Blau, Ionic Liquids with Ammonium Cations as Lubricants or Additives. *Tribology Letters* **2006**, *22* (3), 207–214. https://doi.org/10.1007/s11249-006-9081-0

[93] M. Nawshad, M. Zakaria, A. B. Mohamad, C. D. Wilfred, M. M. I. Abdul, S. Rafiq, Thermophysical Properties of Some Amino Acid-Based Ionic Liquids. *Research Journal of Chemistry and Environment* **2011**, *15* (2), 772–778.

[94] H. Ohno, K. Fukumoto, Amino Acid Ionic Liquids. *Accounts of Chemical Research* **2007**, *40* (11), 1122–1129. https://doi.org/10.1021/ar700053z

[95] Z. F. Zhang, J. G. Li, Q. G. Zhang, W. Guan, J. Z. Yang, Enthalpy of Solution of Amino Acid Ionic Liquid 1-Ethyl-3-Methylimidazolium Ammonioacetate. *Journal of Chemical and Engineering Data* **2008**, *53* (5), 1196–1198. https://doi.org/10.1021/je700599z

[96] N. Muhammad, Z. B. Man, M. A. Bustam, M. I. A. Mutalib, C. D. Wilfred, S. Rafiq, Synthesis and Thermophysical Properties of Low Viscosity Amino Acid-Based Ionic Liquids. *Journal of Chemical and Engineering Data* **2011**, *56* (7), 3157–3162. https://doi.org/10.1021/je2002368

[97] R. K. Singh, S. Pandey, R. C. Saxena, G. D. Thakre, N. Atray, S. S. Ray, Derivatizing L-Histidine to Develop a Novel Additive for a Polyol-Based Biolubricant. *New Journal of Chemistry* **2015**, *39* (7), 5354–5359. https://doi.org/10.1039/c5nj00467e

[98] J. L. Viesca, M. Anand, D. Blanco, A. Fernández-González, A. García, M. Hadfield, Tribological Behavior of PVD Coatings Lubricated with a FAP- Anion-Based Ionic Liquid Used as an Additive. *Lubricants* **2016**, *4* (1). https://doi.org/10.3390/lubricants4010008

[99] J. L. Viesca, A. García, A. Hernández Battez, R. González, R. Monge, A. Fernández-González, M. Hadfield, FAP- Anion Ionic Liquids Used in the Lubrication of a Steel-Steel Contact. *Tribology Letters* **2013**, *52* (3), 431–437. https://doi.org/10.1007/s11249-013-0226-7

[100] A. E. Somers, B. Khemchandani, P. C. Howlett, J. Sun, D. R. MacFarlane, M. Forsyth, Ionic Liquids as Antiwear Additives in Base Oils: Influence of Structure on Miscibility and Antiwear Performance for Steel on Aluminum. *ACS Applied Mater Interfaces* **2013**, *5*, 11544–11553. https://doi.org/10.1021/am4037614

[101] C. M. C. G. Fernandes, A. H. Battez, R. González, R. Monge, J. L. Viesca, A. García, R. C. Martins, J. H. O. Seabra, Torque Loss and Wear of FZG Gears Lubricated with Wind Turbine Gear Oils Using an Ionic Liquid as Additive. *Tribology International* **2015**, *90*, 306–314. https://doi.org/10.1016/j.triboint.2015.04.037

[102] S. Stolte, S. Steudte, O. Areitioaurtena, F. Pagano, J. Thöming, P. Stepnowski, A. Igartua, Ionic Liquids as Lubricants or Lubrication Additives: An Ecotoxicity and Biodegradability Assessment. *Chemosphere* **2012**, *89* (9), 1135–1141. https://doi.org/10.1016/j.chemosphere.2012.05.102

[103] Z. Song, M. Cai, Y. Liang, M. Fan, F. Zhou, W. Liu, In Situ Preparation of Anti-Corrosion Ionic Liquids as the Lubricant Additives in Multiply-Alkylated Cyclopentanes. *RSC Adv.* **2013**, *3*, 21715–21721. https://doi.org/10.1039/C3RA42092B

[104] V. Sharma, C. Gabler, N. Doerr, P. B. Aswath, Mechanism of Tribofilm Formation with P and S Containing Ionic Liquids. *Tribology International* **2015**, *92*, 353–364. https://doi.org/10.1016/j.triboint.2015.07.009

[105] A. P. Abbott, G. Capper, D. L. Davies, H. L. Munro, R. K. Rasheed, V. Tambyrajah, Preparation of Novel, Moisture-Stable, Lewis-Acidic Ionic Liquids Containing Quaternary Ammonium Salts with Functional Side Chains. *Chemical Communications* **2001**, *1* (19), 2010–2011. https://doi.org/10.1039/b106357j

[106] E. L. Smith, A. P. Abbott, K. S. Ryder, Deep Eutectic Solvents (DESs) and Their Applications. *Chem. Rev.* **2014**, *114*, 11060–11082. https://doi.org/10.1021/cr300162p

[107] M. A. R. Martins, S. P. Pinho, J. A. P. Coutinho, Insights into the Nature of Eutectic and Deep Eutectic Mixtures. *Journal of Solution Chemistry* **2019**, *48* (7), 962–982. https://doi.org/10.1007/s10953-018-0793-1

[108] A. P. Abbott, D. Boothby, G. Capper, D. L. Davies, R. K. Rasheed, Deep Eutectic Solvents Formed between Choline Chloride and Carboxylic Acids: Versatile Alternatives to Ionic Liquids. *J. Am. Chem. Soc.* **2004**, *126*, 9142–9147. https://doi.org/10.1016/j.energy.2016.08.057

[109] E. L. Smith, A. P. Abbott, K. S. Ryder, Deep Eutectic Solvents (DESs) and Their Applications. *Chemical Reviews* **2014**, *114* (21), 11060–11082. https://doi.org/10.1021/cr300162p

[110] M. Antunes, A. S. Campinhas, M. de Sá Freire, F. Caetano, H. P. Diogo, R. Colaço, L. C. Branco, B. Saramago, Deep Eutectic Solvents (DES) Based on Sulfur as Alternative Lubricants for Silicon Surfaces. *Journal of Molecular Liquids* **2019**, *295*. https://doi.org/10.1016/j.molliq.2019.111728

[111] S. D. A. Lawes, S. V. Hainsworth, P. Blake, K. S. Ryder, A. P. Abbott, Lubrication of Steel/Steel Contacts by Choline Chloride Ionic Liquids. *Tribology Letters* **2010**, *37* (2), 103–110. https://doi.org/10.1007/s11249-009-9495-6

[112] A. P. Abbott, E. I. Ahmed, R. C. Harris, K. S. Ryder, Evaluating Water Miscible Deep Eutectic Solvents (DESs) and Ionic Liquids as Potential Lubricants. *Green Chemistry* **2014**, *16* (9), 4156–4161. https://doi.org/10.1039/c4gc00952e

[113] S. D. Yim, S. J. Kim, J. H. Baik, I. S. Nam, Y. S. Mok, J. H. Lee, B. K. Cho, S. H. Oh, Decomposition of Urea into NH3 for the SCR Process. *Industrial and Engineering Chemistry Research* **2004**, *43* (16), 4856–4863. https://doi.org/10.1021/ie034052j

[114] S. Tischer, M. Börnhorst, J. Amsler, G. Schoch, O. Deutschmann, Thermodynamics and Reaction Mechanism of Urea Decomposition. *Physical chemistry chemical physics : PCCP* **2019**, *21* (30), 16785–16797. https://doi.org/10.1039/c9cp01529a

[115] E. I. Ahmed, A. P. Abbott, K. S. Ryder, Lubrication Studies of Some Type III Deep Eutectic Solvents (DESs). In *6th Int. Conf. Work. Basic Appl. Sci. AIP*; 2017. https://doi.org/10.1063/1.5004283

[116] P. M. Amorim, A. M. Ferraria, R. Colaço, L. C. Branco, B. Saramago, Imidazolium-Based Ionic Liquids Used as Additives in the Nanolubrication of Silicon Surfaces. *Beilstein Journal of Nanotechnology* **2017**, *8* (1), 1961–1971. https://doi.org/10.3762/bjnano.8.197

[117] A. Borruto, G. Crivellone, F. Marani, Influence of Surface Wettability on Friction and Wear Tests. *Wear* **1998**, *222* (1), 57–65. https://doi.org/10.1016/S0043-1648(98)00256-7

[118] I. Garcia, S. Guerra, J. de Damborenea, A. Conde, Reduction of the Coefficient of Friction of Steel-Steel Tribological Contacts by Novel Graphene-Deep Eutectic Solvents (DESs) Lubricants. *Lubricants* **2019**, *7* (4). https://doi.org/10.3390/lubricants7040037

[119] D. Berman, A. Erdemir, A. V. Sumant, Graphene: A New Emerging Lubricant. *Materials Today* **2014**, *17* (1), 31–42. https://doi.org/10.1016/j.mattod.2013.12.003

[120] O. Penkov, H. J. Kim, D. E. Kim, Tribology of Graphene: A Review. *International Journal of Precision Engineering and Manufacturing* **2014**, *15* (3), 577–585. https://doi.org/10.1007/s12541-014-0373-2

[121] M. A. Arenas, J. I. Ahuir-Torres, I. García, H. Carvajal, J. de Damborenea, Tribological Behavior of Laser Textured Ti6Al4V Alloy Coated with MoS2 and Graphene. *Tribology International* **2018**, *128* (April), 240–247. https://doi.org/10.1016/j.triboint.2018.07.031

[122] X. Fan, L. Wang, High-Performance Lubricant Additives Based on Modified Graphene Oxide by Ionic Liquids. *Journal of Colloid and Interface Science* **2015**, *452*, 98–108. https://doi.org/10.1016/j.jcis.2015.04.025

[123] R. Pamies, M. D. Avilés, J. Arias-Pardilla, T. Espinosa, F. J. Carrión, J. Sanes, M. D. Bermúdez, Antiwear Performance of Ionic Liquid+graphene Dispersions with Anomalous Viscosity-Temperature Behavior. *Tribology International* **2018**, *122* (January), 200–209. https://doi.org/10.1016/j.triboint.2018.02.020

[124] W. Zhao, Z. Zeng, S. Peng, X. Wu, Q. Xue, J. Chen, Fabrication and Investigation the Microtribological Behaviors of Ionic Liquid-Graphene Composite Films. *Tribology Transactions* **2013**, *56* (3), 480–487. https://doi.org/10.1080/10402004.2012.754071

[125] B. Yu, Z. Liu, F. Zhou, W. Liu, Y. Liang, A Novel Lubricant Additive Based on Carbon Nanotubes for Ionic Liquids. *Materials Letters* **2008**, *62* (17–18), 2967–2969. https://doi.org/10.1016/j.matlet.2008.01.128

[126] H. Kinoshita, Y. Nishina, A. A. Alias, M. Fujii, Tribological Properties of Monolayer Graphene Oxide Sheets as Water-Based Lubricant Additives. *Carbon* **2014**, *66*, 720–723. https://doi.org/10.1016/j.carbon.2013.08.045

[127] Y. B. Guo, S. W. Zhang, The Tribological Properties of Multi-Layered Graphene as Additives of PAO2 Oil in Steel-Steel Contacts. *Lubricants* **2016**, *4* (3). https://doi.org/10.3390/lubricants4030030

[128] Z. Rymuza, Control Tribological and Mechanical Properties of MEMS Surfaces. Part 1: Critical Review. *Microsystem Technologies* **1999**, *5* (4), 173–180. https://doi.org/10.1007/s005420050160

[129] H. Liu, B. Bhushan, Nanotribological Characterization of Molecularly Thick Lubricant Films for Applications to MEMS/NEMS by AFM. *Ultramicroscopy* **2003**, *97* (1–4), 321–340. https://doi.org/10.1016/S0304-3991(03)00058-5

[130] J. J. Nainaparampil, K. C. Eapen, J. H. Sanders, A. A. Voevodin, Ionic-Liquid Lubrication of Sliding MEMS Contacts: Comparison of AFM Liquid Cell and Device-Level Tests. *Journal of Microelectromechanical Systems* **2007**, *16* (4), 836–843. https://doi.org/10.1109/JMEMS.2007.901628

[131] J. Y. Leong, J. Zhang, S. K. Sinha, A. Holmes, H. Spikes, T. Reddyhoff, Confining Liquids on Silicon Surfaces to Lubricate MEMS. *Tribology Letters* **2015**, *59* (1), 1–11. https://doi.org/10.1007/s11249-015-0541-2

[132] A. P. Abbott, G. Capper, D. L. Davies, R. K. Rasheed, V. Tambyrajah, Novel Solvent Properties of Choline Chloride/Urea Mixtures. *Chemical Communications* **2003**, *9* (1), 70–71. https://doi.org/10.1039/b210714g

[133] *National Center for Biotechnology Information, PubChem Compound Database; CID=31347.*

[134] R. Majumdar, K. S. Alexander, A. T. Riga, Physical Characterization of Polyethylene Glycols by Thermal Analytical Technique and the Effect of Humidity and Molecular Weight. *Pharmazie* **2010**, *65* (5), 342–346. https://doi.org/10.1691/ph.2010.9280

[135] J. E. Hallett, H. J. Hayler, S. Perkin, Nanolubrication in Deep Eutectic Solvents. *Physical Chemistry Chemical Physics* **2020**, *22* (36), 20253–20264. https://doi.org/10.1039/d0cp03787g

2

IONIC LIQUIDS AS LUBRICANT ADDITIVES FOR MEMS/NEMS

2.1

PICOLINIUM-BASED IONIC LIQUIDS AS ADDITIVES

This chapter presents the results obtained using picolinium-based Ionic Liquids as additives and it is based on the published paper: **M. T. Donato**, F. Caetano, R. Colaço, L. C. Branco, B. Saramago, Picolinium-Based Hydrophobic Ionic Liquids as Additives to PEG200 to Lubricate Steel-Silicon Contacts, *Chemistry Select* **2020**, *5* (20), 5864-5872.

2.1.1 Introduction

Surface lubrication technology is still a recurring problem, which justifies the increasing demand for new and improved lubricant oils.[1] In particular, several improvements in specific equipment depend on the development of new efficient lubricants. In all lubricant applications, there is always a drive for reduced emissions, increased durability and chemical or thermal stability of the lubricant as well as for reduced friction of the involved surfaces. In recent years, ionic liquids (ILs) have been largely reported as an alternative generation of lubricants,[2–8] due to their excellent lubricant properties when compared with common lubricant oils. ILs are organic salts with low melting points (below 100 °C) composed by cation-anion pairs. The main properties of ILs include low volatility, high thermal and chemical stability, non-flammability, broad electrochemical window, miscibility with organic compounds and electric conductivity. The cations are usually bulky organic structures, and the anions, usually organic or inorganic, can be classified as hydrophilic or hydrophobic, depending on its hydration capacity. ILs have a wide range of applications,[9] such as alternative solvents, media for catalytic reactions, liquid-liquid extractions, and electrolytes in batteries,[10–14] and also as lubricating oils.[4–8] One limitation to the use of ILs in lubrication is their price; however, this problem may be solved by adding ILs as additives in commercial oils. Several reports in the literature revealed that a small amount of IL added to lubricant oils may improve significantly their tribological properties.[15–20] Most studies involve aluminum and steel surfaces, which are the most common for industrial applications. Silicon is another important material used in the manufacture of micro and nanoelectromechanical systems (MEMS/NEMS), where the demand for conductive lubricants has increased.[21] Several research groups have been successfully testing the performance of pure ILs as lubricants for Si surfaces[22–26] but, to our knowledge, the only reports on the efficient behavior of ILs as oil additives to lubricate Si were recently published by the group of T. Atkin.[27,28]

Sulfur-based organic salts were tested in our laboratory as additives in the base oil polyethylene glycol (PEG200) to lubricate Si substrates aiming at a future application in MEMS/NEMS, which involve moving parts. Imidazolium, guanidinium, and pyridinium-based cations were coupled with the anions methylsulfate [$MeSO_4$], ethyl sulfate [$EtSO_4$], and methanesulfonate [$MeSO_3$] leading to excellent tribological properties.[29] This behavior was attributed to the strong interaction between sulfur and the Si surface ensuring the formation of a stable surface layer that hinders the contact between the sliding surfaces. The objective of the present work is twofold: 1) to test a more sustainable IL synthetic method based on microwave irradiation; 2) to study the tribological behavior of three new ILs based on picolinium, as additives to model lubricant PEG200. The series 1-hexyl-2, 3 or 4-picolinium trifluoromethanesulfonate [C_6-x-pic][TfO] where x=2, 3 and 4 was compared with 1-hexyl-3-methylimidazolium trifluoromethanesulfonate [C_6MIM][TfO] and 1-hexylpyridinium trifluoromethanesulfonate [C_6pyr][TfO]. Figure 2.1.1 illustrates the chemical structures of the

synthesized ILs. The study of that series of ILs may shed some light on the influence of the stereo chemistry on the lubrication capacity of the additives. In fact, previous studies revealed that stereo chemical differences among ILs with similar cations (different chain length of the alkane chain) would account for different redox and thermal stability, being the symmetric cation [C_n-4-pic] the most stable. Other study showed that the addition of small amounts of more basic ILs (e.g. ammonium and pyridinium cations) to organic solvents lead to smaller changes in the solvent polarity compared with the addition of acidic imidazolium-based ones.[30] Thus, we may expect that the polarity of PEG200 when mixed with [C_6MIM][TfO] is higher than with [C_6-x-pic][TfO]. In this context, we selected the moderately hydrophobic anion trifluoromethanesulfonate [TfO] in order to minimize hydration when exposed to humid atmosphere.

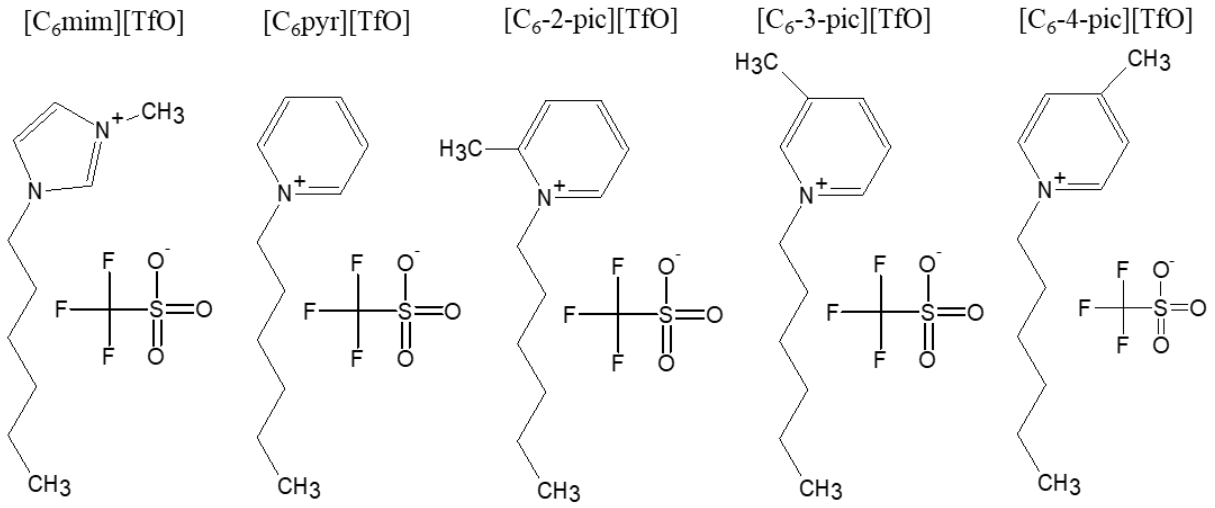

Figure 2.1.1. Chemical structures of the studied salts.

All synthetized salts were characterized by spectroscopic techniques (^{1}H, ^{13}C and ^{19}F-NMR and FTIR-ATR). The viscosity and contact angle of the mixtures of the ILs with the model lubricant PEG200, were measured and tribological studies involving steel spheres rubbing against silicon surfaces were performed. The tribological behavior of the additives of the series [C_6-x-pic][TfO] was compared to [C_6pyr][TfO] and [C_6MIM][TfO] in order to understand the role of the structure of cation on the lubrication efficiency. The effects of the water content in the lubricants and the roughness of the steel counter-bodies on the lubrication mechanism were assessed.

2.1.2 Experimental

2.1.2.1 Materials

The reagents used to synthetize the salts are listed in Table 2.1.1. The solvents were acetonitrile 99.8% from Merck (Germany), methanol 99.8% from Sigma-Aldrich (USA), ethanol 99.8% and diethyl ether ≥99.8% from Honeywell (USA), and deuterated dimethylsulfoxide 99.8% from Eurisotop (France). Polyethylene glycol (MW 200) – PEG200 was from Sigma-Aldrich (USA), with water content <0.5 %. Distilled and deionized (DD) water was obtained with a Millipore Milli-Q system (resistivity ≥ 18.2 M cm).
The substrates used for tribological tests and contact angle measurements were square samples (1×1 cm^2) cut from Si b100N wafers with 0.5 mm of thickness, roughness RMS=1 nm and hardness of 71 HRC. Two types of stainless steel spheres were used as counter-bodies: 316L (BC Precision, USA) with 3 mm of diameter, RMS= 20 ± 0.4 nm and hardness 55-61 HRC, designated by rough spheres, and 440C (McMaster-Carr, USA) with 2.28 mm of diameter, roughness RMS = 6 ± 0.6 nm and hardness of 60 HRC, designated by smooth spheres. 316L stainless steel spheres present low carbon levels and are composed of Fe, Cr (16-18%), Ni (10-14%), Mo (2-3%), Mn (up to 2%) and small amounts of several other elements such as Si, N, S, P. 440 C stainless steel spheres have high carbon levels and are composed of Cr (16%-18%) and Ni (75%), with traces of Mn, Si, Cu, Mo, P and S.

Table 2.1.1. Reagents used to synthesize the salts.

Reagent	Supplier	Purity/ %
Bromohexane	Acrös Organics	99
Methyl imidazole	Alfa Aesar (USA)	99
Pyridine	Merck (USA)	p.a.
2-Methylpyridine	Solchemar (Portugal)	>98
3-Methylpyridine	Solchemar (Portugal)	99
4-Methylpyridine	Alfa Aesar (USA)	98
Sodium triflate	Solchemar (Portugal)	>98
Potassium triflate	Solchemar (Portugal)	>98

2.1.2.2 Methods

The preparation of the picolinium based ILs was performed by microwave (MW) irradiation process as a more sustainable synthetic method. Comparing to conventional synthetic process, MW methodology allowed higher reaction yields and purity levels as well as reduced reaction

times. In this case, it is important to mention about the possibility to reduce 24h to 30-35 minutes to achieve the desired compounds. All alkylation reactions were performed without organic solvent, simplifying the further purification process. In the second step, the bromide salts were exchanged to triflate salts using an optimized reaction methodology. In order to check the chemical structures and purities, all compounds were characterized by NMR and elemental analysis (see details in Annex A.1).

The ILs were added to PEG200 using the weight percentage of 2% because preliminary tests using 1%, 2% and 5% w/w showed similar CoFs for 2% and 5% w/w.[29] The water content of all testing liquids, after being submitted to the vacuum drying process, was checked by Karl–Fischer coulometric titration (Metrohom, Switzerland).

The viscosity of the liquids was measured with a viscometer, model DVII+Pro from Brookfield (USA), in the temperature range 15 °C to 50 °C. The uncertainties in temperature and in dynamic viscosity were, respectively, ±0.02K, and ±3.0%. The Newtonian behavior of the fluids was evaluated with rheological tests (shear stress *vs*. the shear velocity).

The wettability of the Si substrates by the liquid mixtures was assessed by the sessile drop method at room temperature. The Si substrates were carefully cleaned using the following protocol: 2 × 15 min sonication in Dextran® solution intercalated with 10 min sonication in water, followed by 3×10 min sonication in water, rinsing with DD water, drying with nitrogen, and left inside a vacuum oven at room temperature, for, at least, two hours. The drops were deposited on the Si surfaces inside an ambient chamber model 100-07-00 (Ramé-Hart, Succasunna, NJ, USA) with a 2.5 mL micro syringe (Hamilton, Switzerland). The images of drops were obtained with a video camera (jAi CV-A50, Barcelona, Spain) mounted on a microscope Wild M3Z (Leica Microsystems, Wetzlar, Germany) and they were analyzed by running the ADSA software (Axisymmetric Drop Shape Analysis, Applied Surface Thermodynamics Research Associates, Toronto, Canada). The measurements were done under a dry nitrogen gentle flow to avoid water absorption by the liquids. A minimum of seven drops were analyzed for each mixture.

The tribological tests were done with a nanotribometer (CSM Instruments, Peseux, Switzerland) using PEG200 and PEG200+ILs as lubricants. The Si substrates and the steel spheres were cleaned according to the procedure described above. The steel spheres were glued on a medium load cantilever. The stroke of the reciprocal movement of the counterbodies was 0.5 mm, the normal forces applied varied between 15 mN and 150 mN (476 MPa to 1 GPa maximum contact pressure, respectively), and the frequency varied in the range 4 - 20 hertz, corresponding to sliding velocities of 4 – 20 $mm \cdot s^{-1}$. The number of cycles was 400, which corresponded to 400 mm of total sliding distance, while for the best lubricating mixture, longer tribological tests were performed (11000 cycles, sliding distance 11000 mm) with a sliding speed of 8 $mm \cdot s^{-1}$. The experiments were done, at least, in triplicate, at room temperature, under a flow of dry nitrogen. The results were analyzed with the software TriboX.

The surfaces of the Si substrates and of the steel spheres were imaged before and after the tribological tests. In the latter case, the cleaning protocol described above was slightly changed by substituting sonication in Dextran® solution by sonication in chloroform to ensure the removal of eventual traces of adsorbed ILs. An atomic force microscope (AFM) (NanoSurfEasyscan 2) was used with Si tips (force constant of 0.2 $N \cdot m^{-1}$) at a constant contact force of 20 nN, in contact mode. The images were obtained through the WSxM 5.0 Develop 4.0 software.

2.1.3 Results and Discussion

2.1.3.1 Effect of the cation

The CoF values (F=15 mN, rough spheres) obtained with [C_6MIM][TfO], [C_6pyr][TfO] and the pyridinium-based ILs are compared with those previously reported for other imidazolium-based ILs[29] in Figure 2.1.2. The data are presented as Stribeck curves plotting CoF as a function of the Sommerfeld parameter, Z, defined as:

$$Z = \frac{\eta v r}{N} \qquad \text{Eq. 2.1}$$

where η is the lubricant viscosity (Pa·s), v is the sliding speed ($m \cdot s^{-1}$), r is the counter-body radius (m) and F is the applied load (N). The values of CoF for PEG200 are included for comparison purposes.

It is clear from the figure, that the cations containing hexyl or butyl side chain lead to lower CoF values than the cations with shorter side chains, which demonstrates the importance of lateral van der Waals interactions between the side chains leading to more compact adsorbed layers. Among the cations with one hexyl side chain, [C_6-4-pic] stands out as the most efficient in the CoF reduction. The symmetry of this cation, previously reported as being responsible for its higher thermal stability, may lead to a more ordered structure of the adsorbed layer, which implies smaller energy dissipation and lower friction. The reduction in CoF depends on the interactions between the adsorbate and the sliding surfaces but also on the shape of the adsorbed molecules. The film of PEG200 should be weakly bonded to the Si surface through dipole interactions between PEG200 and Si-O groups. Differently, the additives chemically adsorb to the Si through the bonding of the S-O group of the [TfO] anion to the non-oxidized Si of the surface forming S-O-Si bonds. Besides these bonds, the less sterically hindered CH groups of the aromatic ring of the cation would be responsible for hydrogen bonding with the oxidized Si.

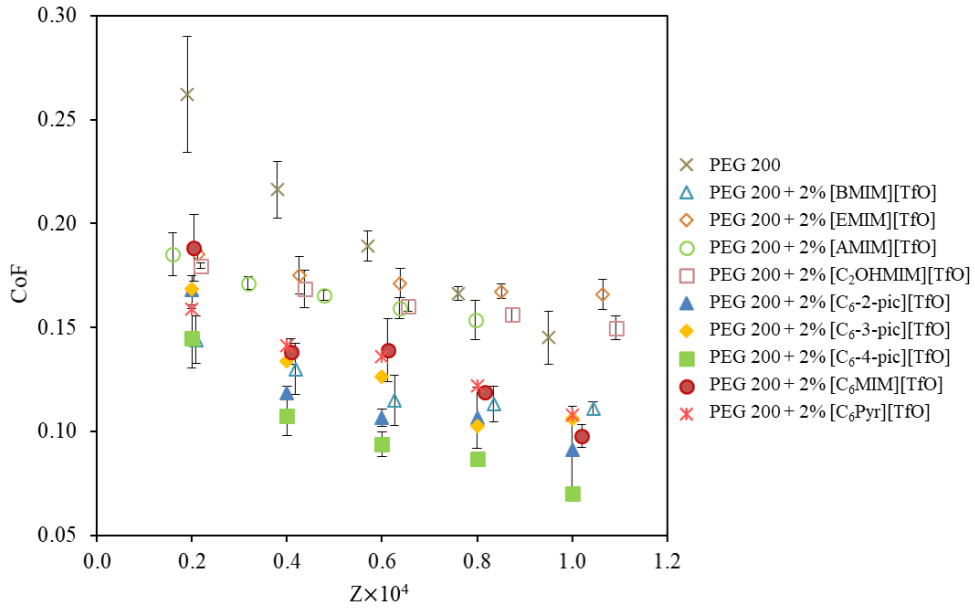

Figure 2.1.2. CoF *vs.* Sommerfeld parameter, Z, for PEG200 and its mixtures for a load of 15 mN and sliding speeds varying between 4 and 20 mm·s^{-1}. The errors are ± standard deviations (n ≥ 3).

The water content, viscosity at 25 °C and the contact angle on Si of PEG200 and its mixtures are presented in Table 2.1.2. The values of the viscosity for all mixtures are very similar, and higher than that of neat PEG200, except for [AMIM][TfO]+PEG200. The contact angles vary between 15° and 41°, but no correlation may be found with the tribological performance: the best wettability of [C$_2$OHMIM][TfO]+PEG200 does no ensure a low CoF. In principle, a good wettability of the substrates should be important to reduce friction in boundary/mixed lubrication regime; however, the influence of wettability is complex and hard to predict. For example, Borruto *et al*. found that water lubrication in the mixed/hydrodynamic regime was most effective when the discs were very hydrophobic and the counter-bodies, very hydrophilic.[31]

Table 2.1.2. Properties of PEG200 and IL+PEG200 mixtures. [a] Data taken from reference [29].

Liquids	Water content/ ppm	η/ mPa·s	Contact angle/ °
PEG200[a]	200-500	40	31±3
PEG 200 + 2% [EMIM][TfO][a]	568	53	24±2
PEG 200 + 2% [BMIM][TfO][a]	675	52	27±2
PEG 200 + 2% [AMIM][TfO][a]	406	40	17±1
PEG 200 + 2% [C_2OHMIM][TfO][a]	466	55	15±1
PEG 200 + 2% [C_6-2-pic][TfO]	206	50	36±1
PEG 200 + 2% [C_6-3-pic][TfO]	496	50	41±2
PEG 200 + 2% [C_6-4-pic][TfO]	242	50	36±1
PEG 200 + 2% [C_6Pyr][TfO]	376	49	47±1
PEG 200 + 2% [C_6MIM][TfO]	555	51	30±3

2.1.3.2 Effect of water content

Although the studied ILs are based on the hydrophobic anion [TfO], they are very hygroscopic, as well as the hydrophilic base oil PEG200, and the water content of the PEG200+IL mixtures may increase during the tribological applications at ambient conditions. The influence of water on the tribological performance of PEG200 and its mixtures with 1-ethyl-3-methylimidazolium trifluoromethanesulfonate ([EMIM][TfO]) and 1-butyl-3-methylimidazolium trifluoromethanesulfonate ([BMIM][TfO]) was studied in a previous work.[29] It was demonstrated that water saturated PEG200 led to a slight increase of the friction coefficient (CoF), while the CoF values obtained with the IL mixtures were independent of the water content. In the present work, the CoF of the mixture [C_6-4-pic][TfO]+PEG200 was measured as a function of the water content (F=30 mN, 600 MPa maximum contact pressure, v = 4, 8, 12, 16 and 20 mm·s^{-1}), from the dry state to the saturation level achieved after several days exposure at ambient atmosphere, and the results are shown in Figure 2.1.3.

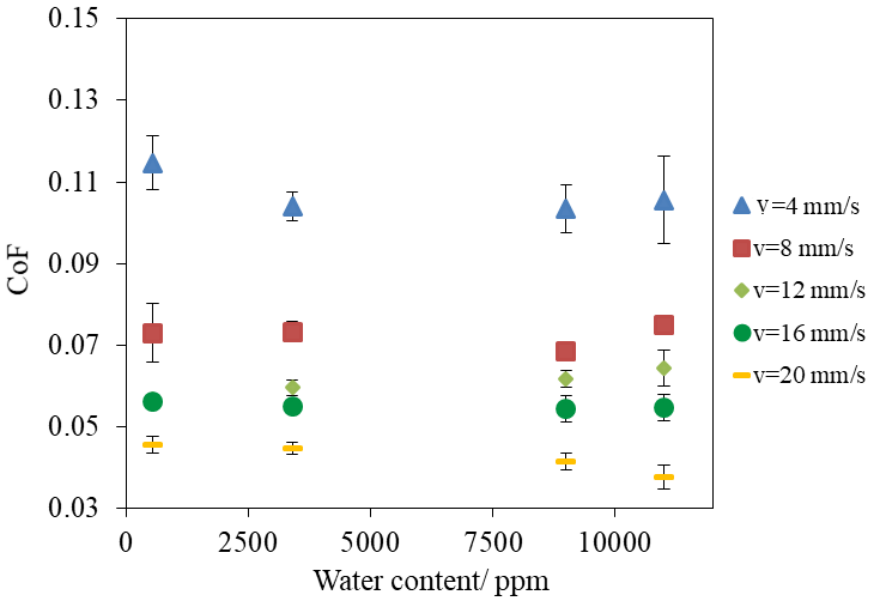

Figure 2.1.3. CoF of [C_6-4-pic][TfO]+2% PEG200 for a load of F=30 mN and varying speeds, as a function of humidity.

These results show that CoF is independent of the water content, in agreement with the previous report.[29] In the literature, the results concerning the effect of water on the lubrication performance of ILs are contradictory. Arcifa *et al*.[32] found that tests done with hydrophobic imidazolium-based ILs using silica/silicon pairs, at a small applied load (0.5 N), in humid air led to an increase of wear and friction, which was attributed to the disruption of lubricant film. However, the same research group reported a decrease in friction and wear when studying the behavior of [EMIM][$EtSO_4$] in humid conditions with the same tribological pair, at high load (4.5 N).[33] This effect was attributed to the smoothing of the silica surface due to the formation of a ductile layer of hydrated silica.

The effect of water content on the viscosity and the contact angle of [C_6-4-pic][TfO]+PEG200 on the Si surface was assessed and the results are given in Figure A.1.2 (Annex A.1). The viscosity decreased only for the highest water content (saturated [C_6-4-pic][TfO]+PEG200), which may be attributed, in part, to the small value of the viscosity of water compared to the values of PEG200 and its mixture. The random changes observed for the contact angles cannot be considered significant.

2.1.3.3 Effect of the counter-body roughness

In order to understand the effect of the counter-body roughness on the lubrication mechanism, we compare the tribological behavior of the pairs rough sphere/Si and smooth sphere/Si. The CoF values obtained using the lubricant [C_6-4-pic][TfO]+PEG200 in a wide range of loads, at a constant sliding speed of 8 mm·s^{-1}, are presented in Figure 2.1.4.

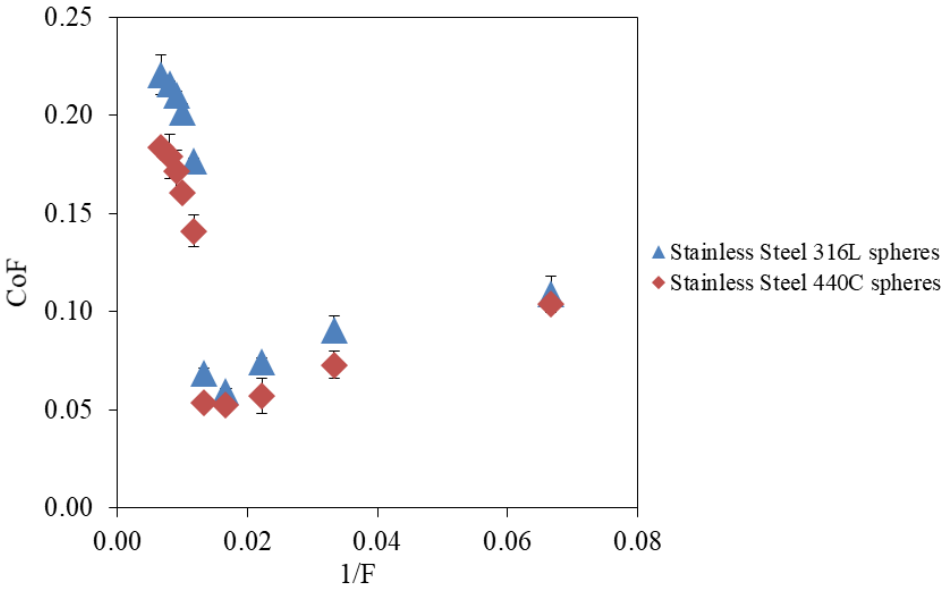

Figure 2.1.4. CoF values obtained with [C_6-4-pic][TfO]+PEG200, using rough and smooth steel spheres with loads of 15 mN, 30 mN, 45 mN, 60 mN, 75 mN, 85 mN, 100 mN, 110 mN, 125 mN and 150 mN at constant velocity (8 mm·s^{-1}) and 400 cycles.

The CoF values followed a typical Stribeck curve where the three lubrication regimes are visible: boundary lubrication at high loads, mixed/elastohydrodynamic for medium loads, and hydrodynamic for low loads. Furthermore, the CoF values decrease when the roughness of the counter-body is reduced in the boundary and mixed/ elastohydrodynamic regimes, which means that the surfaces of the tribological pair are only partially separated by the lubricant.

In the absence of experimental values for the thickness of the lubricant film, which could help in the understanding of the lubrication mechanism, we applied the elastohydrodynamic theory of lubrication (EHL) to estimate the theoretical minimum film thickness, *h*, to nonconformal geometry of ball-on-disc contact.[34,35] The details of the calculation are given in Annex A.1 of the Supporting Information. The values of the film thickness calculated for elastohydrodynamic conditions (loads 45 mN, 60 mN and 75 mN, corresponding, respectively, to 687, 756 and 814 MPa maximum contact pressures, at average sliding speed of 8 mm·s^{-1}) varied between ~1.7 nm for smooth spheres and ~2.1 nm for rough spheres. Comparison of the film thickness with the composite surface roughness, defined as $\left(\sigma_{ball}^2 + \sigma_{disc}^2\right)^{1/2}$ which, in the present case, corresponds to approximately 20 ± 0.4 nm for the rough sphere and 6 ± 0.6 nm for the smooth sphere, shows that the film is not thick enough to separate the two sliding surfaces and that contact between asperities will always occur during sliding. Here we must point out that EHL theory may lead to unreliable values for film thickness when the lubricating films are of the order of some nanometers. In the case of ILs, other authors found

inconsistencies between the observed lubrication regime and the one compatible with the film thickness predicted by the EHL theory.[33,36] However, a thin film may be compatible with EHL conditions if the sliding surfaces are protected by a thin layer of adsorbed IL ions.

To check the occurrence of eventual wear of the sliding surfaces, long tribological tests (11000 cycles equivalent to 11000 mm of sliding distance under a load of 150 mN) were done using the smooth and the rough counter-bodies. The CoF was plotted as a function of time in Figure A.1.3 and Figure A.1.4 (Annex A.1) for PEG200 and [C_6-4-pic][TfO]+PEG200, respectively. The values of CoF increased to around 0.2, independently of the lubricant composition or the roughness, and remained practically constant during the testing time. The fact that the CoF values do not change with time suggests the absence of wear. To confirm this hypothesis and further investigate the lubrication mechanism, the surfaces of the Si substrates and the steel spheres were imaged with AFM, before and after being submitted to the tribological tests, and carefully washed.

The AFM images of the Si surfaces, before and after being submitted to the tribological tests and carefully washed, using PEG and [C_6-4-pic][TfO]+PEG200, as lubricants, and rough and smooth steel spheres, as counter-bodies, are shown in Figure 2.1.5. No wear tracks could be detected using both rough and smooth spheres. However, the roughness of Si decreased considerably after the tests with PEG200 and kept the same order of magnitude after the tests with [C_6-4-pic][TfO]+PEG200, using both types of spheres.

The AFM images of the rough and smooth steel spheres, before and after being submitted to the tribological tests and carefully washed, using PEG200 and [C_6-4-pic][TfO]+PEG200 as lubricants, are shown in Figure 2.1.6. In the case of the smooth spheres, no significant changes of roughness were observed after the tribological tests with both lubricants. In contrast, the roughness of the rough spheres was considerably reduced after the test with PEG200 and remained approximately constant after the test with [C_6-4-pic][TfO]+PEG200.

The analysis of the surface roughness demonstrates the role of the IL on the protection of both surfaces during the sliding process. In presence of neat PEG200, the tests done under boundary lubrication (high load) involved contact of the steel sphere with the Si surface and led to accommodation of both surfaces. This effect is more evident for the Si surface whose roughness was reduced in ~ 83%, after the tests with both soft and rough spheres. The average roughness of the spheres decreased significantly (about 60%) only for the rough ones. In contrast, when the lubricant was [C_6-4-pic][TfO]+PEG200, the average roughness of both surfaces (spheres and Si substrates) did not change significantly after the tests. The overall results confirm that a complex lubrication mechanism, designated by mixed or adsorption lubrication,[35] where the load is supported by the liquid film retained among the asperities of the opposing surfaces and by the layer adsorbed on the asperities.

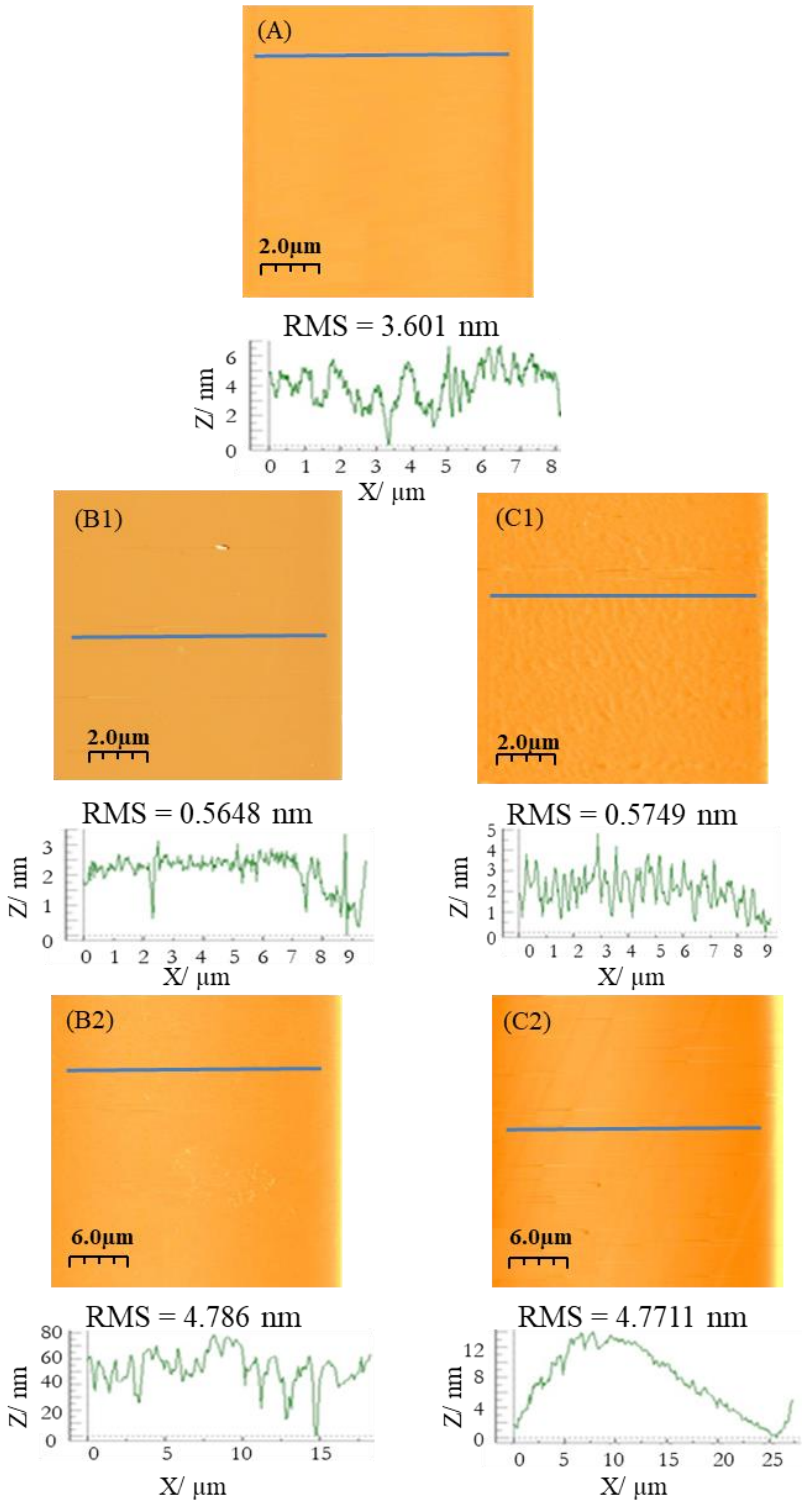

Figure 2.1.5. AFM images of the Si surfaces before (A) and after being submitted to long tribological tests (load of 150mN), and carefully washed, using PEG200 (B1 and B2) and [C_6-4-pic][TfO]+PEG200 (C1 and C2) as lubricants and the counter-bodies: rough steel spheres (left) and smooth steel spheres (right).

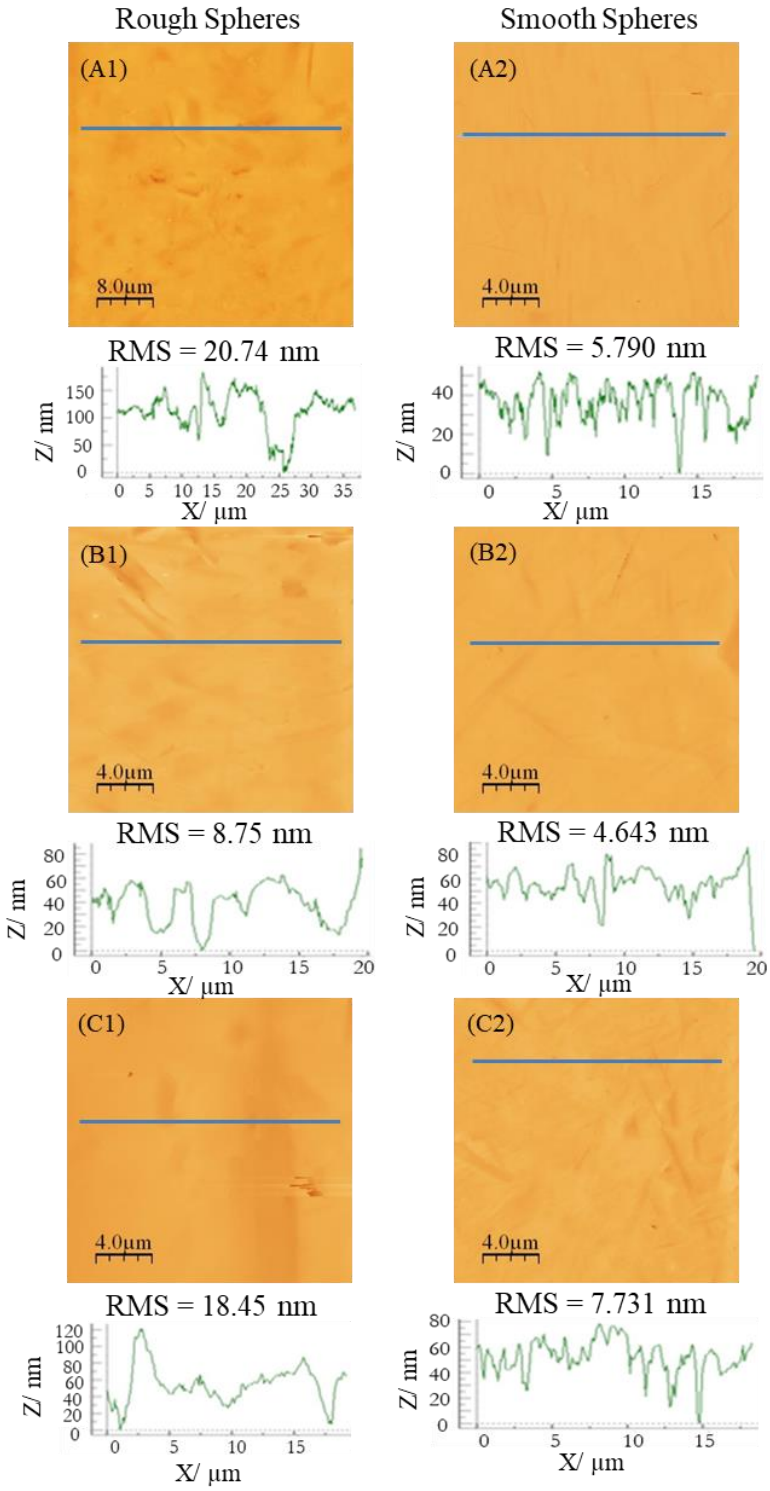

Figure 2.1.6. AFM images of steel spheres before (A1 and A2) and after being submitted to long tribological tests (load of 150 mN) and carefully washed using PEG (B1 and B2) and [C_6-4-pic][TfO]+PEG200 (C1 and C2) as lubricants: rough steel spheres (left) and smooth steel spheres (right).

Figure 2.1.7 shows a schematic representation of the lubrication films of PEG200 and [C6-4-pic][TfO]+PEG200 formed between the surfaces of the rough steel sphere and the silicon substrate under boundary lubrication (150 mN).
In the case of neat PEG200, the asperities of the counter-body were in contact and suffered deformation, while addition of [C6-4-pic][TfO] resulted in the chemical adsorption of the anions to the silicon surface. The symmetric nature of the [C6-4-pic] enhanced the layering of the ions, which led to an adsorbed film able to keep the sliding surfaces separated during the sliding process.

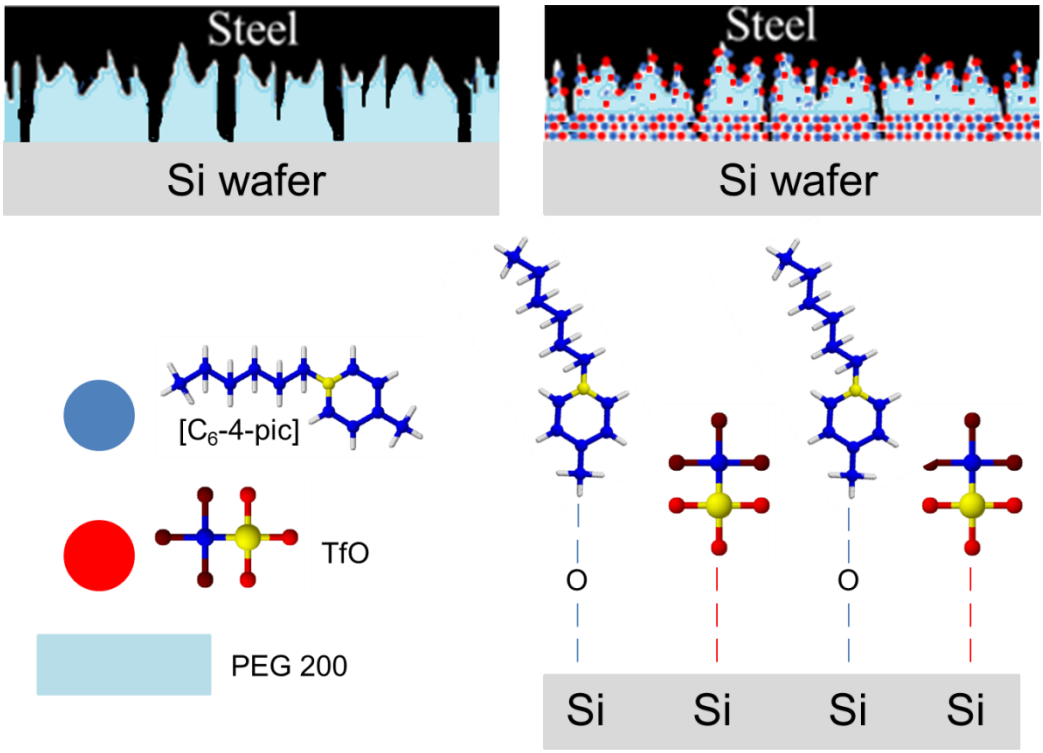

Figure 2.1.7. Schematic representation of the lubrication mechanism of rough steel spheres sliding on Si surfaces using neat PEG200 and the mixture [C6-4-pic][TfO]+PEG200 under a high load: in the presence of PEG200, elastic deformation of the steel asperities occurred(top left image); [C6-4-pic][TfO]+PEG200 protects the surfaces due to the formation of an adsorbed, layered film of the IL ions (right images). Adsorption on steel is a plausible hypothesis.

2.1.4 Conclusions

Three new ILs based on picolinium were successfully synthesized using microwave process as more sustainable method: [C6-x-pic] [TfO] where x=2, 3 and 4. The performance of these ILs as additives to model lubricant oil PEG200 was evaluated and compared with that of other ILs sharing the same hydrophobic anion, using the tribological pair steel sphere/Si substrate. The

lowest CoF values were obtained with ILs based on cations containing one hexyl or butyl side chain. [C_6-4-pic][TfO] was the most efficient additive, which may be attributed to the symmetry of the cation leading to an ordered adsorbed layer. Thus, the lubrication ability depends not only on the adsorption strength of the additive but also on the ordered arrangement of the molecules within the adsorbed layer. No effect of the water content of the lubricants on friction was found. Wear of the Si substrates under boundary lubrication conditions (high load) was not observed in any case, indicating a mixed or adsorption lubrication regime, where the load is supported by the liquid film retained among the asperities of the opposing surfaces and by the layer adsorbed on the asperities.

2.1.5 References

[1] T. Mang, C. Bush, in *Lubricants and Lubrication* (Eds.: Wilfried Dresel, T. Mang), Wiley-VCH Verlag GmbH & Co. KGaA, Germany, **2017**, 11–30.

[2] W. Zhou, F. Liang, Y. Liu, Ionic liquid lubricants: designed chemistry for engineering applications. *Chem. Soc. Rev.* **2009**, *38*, 2590–2599. https://doi.org/10.1039/B817899M

[3] M. D. Bermúdez, A. E. Jiménez, J. Sanes, F. J. Carrión, Ionic Liquids as Advanced Lubricant Fluids. *Molecules* **2009**, *14*, 2888–2908. https://doi.org/10.3390/molecules14082888

[4] I. Minami, Ionic Liquids in Tribology. *Molecules* **2009**, *14*, 2286–2305. https://doi.org/10.3390/molecules14062286

[5] M. D. Bermúdez, Introduction to the Ionic Liquids Special Issue. *Tribol. Lett.* **2010**, *40*, 213. https://doi.org/10.1007/s11249-010-9707-0

[6] N. Dörr, Special Issue on Ionic Liquids as Lubricants. *Proc. Ins. Mech. Eng. Part J: J. Eng. Tribol.* **2012**, *226*, 889–890. https://doi.org/10.1177/1350650112464332

[7] Y. Kondo, T. Koyama, S. Sasaki, in *Ionic Liquids- New Aspects for the Future*, (Ed.: J. Kadowaka), InTech, Rijeka, **2013**.

[8] A. E. Somers, P. C. Howlett, D. R. MacFarlane, M. Forsyth, A Review of Ionic Liquid Lubricants. *Lubricants* **2013**, *1*, 3–21. https://doi.org/10.3390/lubricants1010003

[9] M. Freemantle, *An Introduction to Ionic Liquids.*, RSC Publishing, Cambridge, **2009**.

[10] C. A. M. Afonso, J. P. S. G. Crespo, *Green Separation Processes: Fundamentals and Applications*, Weinheim, **2005**.

[11] P. Wasserscheid, *Ionic Liquids in Synthesis.*, WILEY-VCH Verlag GmbH , Co. KGaA, Weinheim, **2007**.

[12] S. Werner, M. Haumann, P. Wasserscheid, Ionic Liquids in Chemical Engineering. *Annu. Rev. Chem. Biom. Eng.* **2010**, *1*, 203–230. https://doi.org/10.1146/annurev-chembioeng-073009-100915

[13] J. P. Hallett, T. Welton, Room-Temperature Ionic Liquids. Solvents for Synthesis and Catalysis. *Chem. Rev.* **2011**, *111*, 3508–3576. https://doi.org/10.1021/cr1003248

[14] L. Yu, G. Z. Chen, Ionic Liquid-Based Electrolytes for Supercapacitor and Supercapattery. *Front. Chem.* **2019**, 2–25. https://doi.org/10.3389/fchem.2019.00272

[15] M. Cai, Y. Liang, F. Zhou, W. Liu, Tribological Properties of Novel Imidazolium Ionic Liquids Bearing Benzotriazole Group as the Antiwear/Anticorrosion Additive in Poly(ethylene glycol) and Polyurea Grease for Steel/Steel Contacts. *ACS Appl. Mater. Interfaces* **2011**, *3*, 4580–4592. https://doi.org/10.1021/am200826b

[16] A. E. Jiménez, M. D. Bermúdez, Short Alkyl Chain Imidazolium Ionic Liquid Additives in Lubrication of Three Aluminium Alloys With Synthetic Ester Oil. *Tribol. Surf. Interfaces* **2012**, *6*, 109–115. https://doi.org/10.1179/1751584X12Y.0000000011

[17] M. Cai, Y. Liang, F. Zhou, W. Liu, A Novel Imidazolium Salt With Antioxidation and

Anticorrosion Dual Functionalities as the Additive in Poly (Ethylene Glycol) for Steel/Steel Contacts. *Wear* **2013**, *306*, 197–208. https://doi.org/10.1016/j.wear.2012.09.001

[18] R. Gusain, P. Gupta, S. Saran, O. P. Khatri, Halogen-Free Bis (Imidazolium)/Bis (Ammonium)-di [Bis (Salicylato) Borate] Ionic Liquids as Energy-Efficient and Environmentally Friendly Lubricant Additives. *ACS Appl. Mater. Interfaces* **2014**, *6*, 15318–15328. https://doi.org/10.1021/am503811t

[19] M. A. Gutierrez, M. Haselkorn, P. Iglesias, The Lubrication Ability of Ionic Liquids as Additives for Wind Turbine Gearboxes Oils. *Lubricants* **2016**, *4*, 14–26. https://doi.org/10.3390/lubricants4020014

[20] R. Gusain, P. S. Bakshi, S. Panda, O. P. Sharma, R. Gardas, O. P. Khatri, Physicochemical and Tribophysical Properties of Trioctylalkylammonium Bis (Aalicylato) Borate (N_{888} n-BScB) Ionic Liquids: Effect of Alkyl Chain Length. *Phys. Chem. Chem. Phys.* **2017**, *19*, 6433–6442. https://doi.org/10.1039/C6CP05990B

[21] B. Bhushan, in *Nanotribology Nanomechanics - An Introduction.* (Ed.: B. Bhushan), Springer International Publishing AG, **2017**, pp. 797–907.

[22] B. Yu, F. Zhou, Z. Mu, Y. M. Liang, W. M. Liu, Tribological Properties of Ultra-Thin Ionic Liquid Films on Single-Crystal Silicon Wafers with Functionalized Surfaces. *Tribol. Inter.* **2006**, *39*, 879–887. https://doi.org/10.1016/j.triboint.2005.07.039

[23] Y. Mo, W. Zhao, M. Zhu, M. Bai, Nano/Microtribological Properties of Ultrathin Functionalized Imidazolium Wear-Resistant Ionic Liquid Films on Single Crystal Silicon. *Tribol. Lett.* **2008**, *32*, 143–151. https://doi.org/10.1007/s11249-008-9371-9

[24] G. Xie, Q. Wang, L. Si, S. Liu, G. Li, Tribological Characterization of Several Silicon-Based Materials Under Ionic-Liquids Lubrication. *Tribol. Lett.* **2009**, *36*, 247–257. https://doi.org/10.1007/s11249-009-9480-0

[25] Y. Mo, F. Huang, F. Zhao, Functionalized Imidazolium Wear-Resistant Ionic Liquid Ultrathin Films for MEMS/NEMS Applications. *Surf. Interface Anal.* **2011**, *43*, 1006–1014. https://doi.org/10.1002/sia.3684

[26] J. Cosme, P. D. A. Bastos, I. Catela, D. Silva, R. Colaço, L. C. Branco, B. Saramago, Task–Specific Ionic Liquids Based on Sulfur for Tribological Applications. *ChemistrySelect* **2016**, *1*, 3612–3617. https://doi.org/10.1002/slct.201600880

[27] H. Li, P. K. Cooper, A. E. Somers, M. W. Rutland, P. C. Howlett, M. Forsyth, R. Atkin, Ionic Liquid Adsorption and Nanotribology at the Silica–Oil Interface: Hundred-Fold Dilution in Oil Lubricates as Effectively as the Pure Ionic Liquid. *J. Phys. Chem. Lett.* **2014**, *5*, 4095–4099. https://doi.org/10.1021/jz5021422

[28] H. Li, A. E. Somers, P. C. Howlett, M. W. Rutland, M. Forsyth, R. Atkin, Addition of Low Concentrations of an Ionic Liquid to a Base Oil Reduces Friction Over Multiple Length Scales: A Combined Nano-and Macrotribology Investigation. *Phys. Chem. Chem. Phys.* **2016**, *18*, 6541–6547. https://doi.org/10.1039/C5CP07061A

[29] P. M. Amorim, A. M. Ferraria, R. Colaço, L. C. Branco, B. Saramago, Imidazolium-Based

Ionic Liquids Used as Additives in the Nanolubrication of Silicon Surfaces. *Beilstein J. Nanotechnol.* **2017**, *8*, 1961–1971. https://doi.org/10.3762/bjnano.8.197

[30] R. M. Couto, C. Lourenço, P. C. Simões, L. C. Branco, Task Specific Ionic Liquids as Polarity Shifting Additives of Common Organic Solvents. *New J. Chem.* **2014**, *38*, 5559–5565. https://doi.org/10.1039/C4NJ00781F

[31] A. Borruto, G. Crivellone, F. Marani, Influence of Surface Wettability on Friction and Wear Tests. *Wear* **1998**, *222*, 57–65. https://doi.org/10.1016/S0043-1648(98)00256-7

[32] A. Arcifa, A. Rossi, R. M. Espinosa-Marzal, N. D. Spencer, Influence of Environmental Humidity on the Wear and Friction of a Silica/Silicon Tribopair Lubricated With a Hydrophilic Ionic Liquid. *ACS Appl. Mater. Interfaces* **2016**, *8*, 2961–2973. https://doi.org/10.1021/acsami.5b09370

[33] A. Arcifa, A. Rossi, R. M. Espinosa-Marzal, N. D. Spencer, Environmental Influence on the Surface Chemistry of Ionic-Liquid-Mediated Lubrication in a Silica/Silicon Tribopair. *J. Phys. Chem. C* **2014**, *118*, 29389–29400. https://doi.org/10.1021/jp505998k

[34] B. J. Hamrock, D. Dowson, Isothermal Elastohydrodynamic Lubrication of Point Contacts: Part III—Fully Flooded Results. *J. Lubr. Technol.* **1977**, *99*, 264–275. https://doi.org/10.1115/1.3453074

[35] G. Stachowiak, A. Batchelor, *Engineering Tribology* Butterworth-Heinemann., Oxford, U.K., **2013**.

[36] H. Xiao, D. Guo, S. Liu, G. Pan, X. Lu, Film Thickness of Ionic Liquids Under High Contact Pressures as a Function of Alkyl Chain Length. *Tribol Lett.* **2011**, *41*, 471–477. https://doi.org/10.1007/s11249-010-9729-7

2.2

PROTIC IONIC LIQUIDS AS ADDITIVES

This chapter presents the results obtained using a set of protic Ionic Liquids as additives and it is based on the published paper: **M. T. Donato**, J. Deuermeier, R. Colaço, L. C. Branco, B. Saramago, New Protic Ionic Liquids as Potential Additives to Lubricate Si-based MEMS/NEMS, *Molecules* **2023**, *28* (6), 2678.

2.2.1 Introduction

Protic ionic liquids (PILs) are a subclass of ionic liquids, which are composed of Brønsted acids and bases. The unique properties of these PILs result from the presence of proton-donor and proton-acceptor sites, which are responsible for the formation of dense hydrogen bonding leading to bi-continuous sponge-like nanostructures.[1] Greaves and Drummond first reviewed the properties and applications of PILs in 2008 [2] and reported only one study on the lubricant properties of a series of alkylammonium PILs.[3] The authors of that study compared the tribological properties of PILs and imidazolium aprotic ILs with those of mineral oils and found reduced friction and wear of steel-aluminum contacts with the PILs, in particular, with the monoprotic trioctylammonium bis(trifluoromethylsulfonyl)imide ([N_{888H}][NTf_2]). This PIL added to a commercial mineral oil eliminated the known adhesion problems in the aluminum sliding surfaces, which was attributed to the fast reaction of the IL with aluminum leading to a protective boundary film. Since then, several authors have been studying the application of ammonium and phosphonium-based PILs as neat lubricants or additives to lubricate metallic contacts.[4–13] Ammonium-based PILs demonstrated excellent performance as lubricants of magnetic thin films,[4] as additives in lithium complex grease to lubricate steel-steel pairs [5] and both as pure lubricants or oil additives in the lubrication of copper-copper contacts.[6] Ultra-low friction was obtained with water containing 2-hydroxyethylammonium succinate to lubricate sapphire-stainless steel contacts.[7] 2-Hydroxyethylammonium formiate and pentanoate were tested as lubricants of aluminum-steel contacts and were demonstrated to be effective in wear reduction, although they did not improve friction in comparison with commercial oils.[8] Similar behavior was observed with other ammonium-based PILs containing the oleate cation: tribological tests with alumina/aluminum pair demonstrated that the only advantages compared to the commercial lubricant were the low price and low toxicity as well as the higher chemical stability.[9] The PIL tri-[bis(2-hydroxyethyl)ammonium] citrate was successfully applied as an additive to mineral oil in the lubrication of aluminum-steel [10] and steel-steel contacts,[11] while di[bis(2-hydroxyethyl)ammonium] succinate was used as an additive in water and as base lubricant for graphene dispersions to lubricate alumina/steel pairs.[12] Kahn *et al*. synthesized fatty-acid-derived PILs based on the phosphonium cation, which decreased friction and wear of the steel tribopair when added to lube oil.[13] It is also important to emphasize that PILs are easily prepared by simple protonation of the cation using appropriate acid, as well as cheaper compared to other ILs.

To our knowledge, the capacity of PILs to lubricate silicon surfaces was never reported in the literature, except in a recent publication by our group,[14] as described later in this section. The high demand for the efficient lubrication of micro and nanoelectromechanical systems (MEMS and NEMS), which are traditionally made of silicon, derives from the fact that silicon is a very fragile material and non-adequate lubrication may lead to adhesion, friction and wear problems.[15] These problems occur only when MEMS and NEMS have moving parts, such as

in optical switches, magnetic storage devices, resonators, gyroscopes and micro pumps, among others. The peculiar properties of ILs, including their high electrical conductivity which ensures low contact resistance between sliding parts, represent important advantages compared to conventional lubricants in this type of application. Even used as lubricant additives, ILs were found to increase the conductivity of the solvent.[16,17]

The investigation of the performance of ILs as neat lubricants or additives in the lubrication of silicon dates back to 2006 when Yu *et al*. demonstrated that films of vinyl groups functionalized ILs reduced the friction and wear of hydroxyl-terminated Si surfaces.[18] Bhushan *et al*.[19] evaluated the nanoscale tribological performance of two imidazolium-based ILs deposited on Si wafers. The partially bonded coatings demonstrated the best tribological behavior as they combined the bonded lubricant with a mobile fraction. Zhu *et al*.[20] and Mo *et al*.[21,22] investigated the lubrication capacity of a thin film of ILs deposited on single crystal Si wafers. They found that the nano and microtribological properties were dependent on the structure of both the anions and the cations, wettability and environment. Pu *et al*.[23] used the same type of approach with crown-type phosphate ILs to lubricate silicon surfaces modified with self-assembled monolayers. The group of Spencer [24] studied the lubrication of the silicon/silica pair by two ILs based on the 1-ethyl- and 1-hexyl-3-methylimidazolium cations combined with tris(pentafluoroethyl) tris(perfluoroalkyl)trifluorophosphate anions, respectively, [C_2MIM][FAP] and [C_6MIM][FAP], with a pin-on-disc tribometer. They found that varying the environmental humidity affected the mechanism of lubrication in different ways depending on the applied load. Later, they used 1-ethyl-3-methylimidazolium ethylsulfate ([C_2MIM][$EtSO_4$]) in similar studies and claimed that the presence of water in the IL induced decreases in wear and roughness of the sliding surfaces, minimizing the formation of debris. [25] In 2017, the same authors reported a comparison of the lubrication of the silicon/silica tribopair with 1-ethyl-, 1-hexyl- and 1-dodecyl-3-methylimidazolium bis(trifluoromethylsulfonyl)imide, ([C_2MIM][NTf_2], [C_6MIM][NTf_2] and [C_{12}MIM][NTf_2]), under boundary conditions, with the results obtained using [C_2MIM][$EtSO_4$] and the FAP-based ILs.[26] Raman and XPS spectra of the worn surfaces revealed mechanical wear as the prevailing form when the lubricants were the ILs based on the [$EtSO_4$] and the [NTf_2] anions but not with the ILs containing the [FAP] anion. Our group investigated the use of ILs as additives in the model lubricant polyethylene glycol (PEG200) to lubricate the pair steel ball/Si surface.[14,27,28] A series of imidazolium-based ILs were tested and a significant reduction in the friction coefficient (CoF) was obtained with PEG200 + 2% [C_2MIM][$EtSO_4$], which was attributed to the strong interaction of the anion with the Si surface.[25] Picolinium-based ILs, namely 1-hexyl-2, 3 or 4-picolinium trifluoromethanesulfonate, were also tested in similar studies and [C_6-4-pic][TfO] demonstrated the best tribological performance which was explained by the ordered adsorbed layer formed by the symmetric cation.[26] Sulfur-based ILs and organic salts, some liquids and other solids at room temperature, were used as additives in the base oil PEG200.[14] Excellent tribological properties were achieved with ILs containing

the methylsulfate ([$MeSO_4$]) and the mesylate ([$MeSO_3$]) anions. This performance was attributed to the formation of chemical bonds between the S atoms of the anions and the Si surface leading to the formation of a compact adsorbed film. The behavior of aprotic ILs was compared to two PILs such as methylimidazolium mesylate ([MIMH][$MeSO_3$]) and tetramethylguanidinium mesylate ([TMGH][$MeSO_3$]). The PILs outperformed the aprotic ILs in the reduction in friction compared to the model lubricant (PEG200), except in the case of 1-methyl-3-picolinium methylsulfate ([C_1-3-pic][$MeSO_4$]). However, more extensive studies are needed to confirm the promising results obtained with the investigated PILs.

In this work, we synthesized ten PILs based on the combination of the methylimidazolium ([MIMH]), 4-picolinium ([4-picH]), pyridinium ([PyrH]), 1,8-diazabicyclo[5.4.0]-undec-7-ene-8-ium ([DBUH]) and tetramethylguanidinium ([TMGH]) cations with hydrogen sulfate ([HSO_4]) and [$MeSO_3$] anions. The molecular structures of these ions are presented in Figure 2.2.1. Among these salts, [4-picH][$MeSO_3$], [PyrH][HSO_4], [DBUH][HSO_4] and [MIMH][HSO_4], are liquid and the remaining ones are solids at room temperature. The idea was to ally the good lubrication capacity of the anions based on sulfur units with the presence of proton donors in the cations. The PILs were tested as additives to PEG200 in the proportion of 2% in weight. The viscosity and wettability of the mixtures were measured and their lubrication capacity was assessed using two tribopairs: steel sphere/Si surface and Si sphere/Si surface. A first screening of the additives was conducted with the steel spheres, and then the more expensive Si spheres were used to compare the behavior of the worst and the best-performing liquids in the lubrication of Si contacts that better mimic dynamic MEMS/NEMS, most frequently made of silicon. Friction and wear were determined and the worn sliding surfaces were imaged and chemically analyzed in order to understand the wear mechanisms.

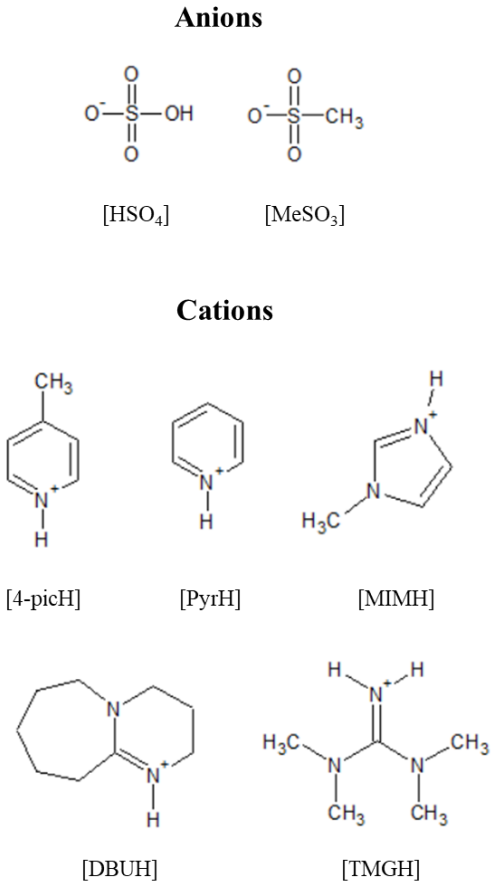

Figure 2.2.1. Molecular structures of the studied anions and cations.

2.2.2 Experimental

2.2.2.1 Materials

All reagents for the synthesis of the PILs were purchased and used without additional purification. The list of reagents is the following: 4-methylpyridine 98%, methylimidazole 99% and tetramethylguanidine 99% from Alfa Aesar (Tewksbury, MA, USA); pyridine p.a. and sulfuric acid 95–97% from Merck (Rahway, NJ, USA); 1,8-diazabicyclo(5.4.0)undec-7-ene 98% and methanesulfonic acid 99% from Sigma-Aldrich (Rahway, NJ, USA).

The solvents were acetonitrile 99.8% from Merck (Darmstadt, Germany) and deuterated water 99.9% from Eurisotop (Gif sur Yvette, France). Polyethylene glycol (MW 200)—PEG200 was from Sigma-Aldrich (Rahway, NJ, USA), with water content < 0.5%. Distilled and deionized water (DD) was obtained with a Millipore system.

Si b100N wafers (Si-Mat, Kaufering, Germany), with 0.5 mm of thickness, 1 nm of root mean square (RMS) roughness and 1121–1428 HV of hardness, were cut in squares (1×1 cm^2) to be used in the tribological tests and the contact angle measurements. Spheres of stainless steel

(SS) AISI 316L grade 100 (Atlas Ball and Bearing Co. Ltd., Walsall, UK) with 6 mm of diameter, roughness RMS = 1 μm and hardness of 260–390 HV and Si spheres (J. Hauser GMBH and Co., Solms, Germany) with 6 mm of diameter, 15 nm of RMS roughness and 1412 HV of hardness were used as counter-bodies.

2.2.2.2 Methods

The syntheses of the PILs are described in detail in the Supporting Information. In order to check the chemical structures and purities, all compounds were characterized by ^{1}H and ^{13}C NMR, FTIR and elemental analysis (see NMR and FTIR spectra in Figure A.2.1 in Annex A.2). The syntheses of [MIMH][$MeSO_3$], [TMGH][$MeSO_3$] and [DBUH][HSO_4] were described in previous works.[14,0]

The choice of the optimal concentration of the PIL was based on the comparison of the CoF obtained with mixtures of [4-picH][HSO_4] and PEG200 using three concentrations: 1%, 2% and 5% (w/w) (Figure A.2.2). The best performance was obtained with 2% (w/w), which was adopted for all PILs. The mixtures were dried under a vacuum and their water content was determined by Karl–Fischer coulometric titration (Metrohm, Herisau, Switzerland). The chemical stability of the formulations was checked by ^{1}H-NMR comparing the original spectra of the components (PEG200 and PILs) as well as the mixtures PEG200 + 2%PILs after 6 months of preparation. In general, it is possible to conclude that the formulations are chemically stable. In order to prove the chemical stability, ^{1}H-NMR of the mixture PEG200 + 2%[4-picH][HSO_4] was included in Annex A.2 (see Figure A.2.3).

The viscosity was measured at 25 °C using a rheometer MCR 92 (Anton Paar, Graz, Austria). The results are average values obtained from three measurements. The contact angles of the studied liquids on the Si surface were measured by the sessile drop method at room temperature.[30] The Si substrates were cleaned according to the following protocol: (1) 2×15 min sonication in Dextran® solution intercalated with 10 min sonication in water; (2) 3×10 min sonication in water; (3) rinsing with DD water. After being flushed with nitrogen, and dried in a vacuum oven at room temperature for, at least two hours, the substrates were placed inside an environmental chamber 100-07-00 (Ramé-Hart, Succasunna, USA). The images of the sessile drops were captured with a camera jAi CV-A50 (Infaimon, Barcelona, Spain) coupled to a microscope Wild M3Z (Leica Microsystems, Wetzlar, Germany), and the software ADSA (Applied Surface Thermodynamics Research Associates,Toronto, Canada) was used for image analysis. The reported contact angles were average values obtained from measurements performed on at least four drops of each liquid.

The tribological tests were conducted with a tribometer TRB3 (Anton Paar, Graz, Switzerland) in the configuration reciprocating ball-on-flat at room temperature (~25 °C) and relative humidity (~45%). The tribopairs were SS spheres/Si substrates and Si spheres/Si substrates. After cleaning both spheres and substrates, using the protocol described in the previous

section, the sphere was placed on the tribometer arm and the Si substrate was glued to a metallic container. Several drops of liquid were added to ensure the full coverage of the surfaces. Two types of tests were conducted with the different tribopairs. The SS spheres were used in short-duration tests (85 cycles, corresponding to 0.68 m of sliding distance), under a low normal force of 1 N, and sliding speeds varying between 1 and 20 $mm \cdot s^{-1}$. The Hertz contact stress was 584.5 MPa. The Si spheres were used in short and long tests (2375 cycles, corresponding to 19 m of sliding distance), under the normal load of 1 N and higher normal loads of 2 N and 4 N, at a constant speed of 8 $mm \cdot s^{-1}$. The amplitude of the reciprocal movement of the counter-body was always 4 mm. The Hertz contact stresses varied between 584.5 MPa for 1 N and 927.9 MPa for 4 N. The results were analyzed using the software TriboX. The reported values for CoF represent the average of at least three results obtained in independent experiments.

After the tribological tests, the Si spheres and the Si substrates were carefully cleaned with acetone and dried with nitrogen, to remove any traces of adsorbed material. A Scanning Electron Microscope (SEM) JSM7001F (JEOL, Tokyo, Japan) was used to analyze the surfaces of both Si spheres and Si substrates after the tribological tests. The surfaces of the Si substrates were also imaged using an optical profilometer Profilm 3D (Filmetrics, San Diego, California, USA) and for each track, the worn volume was estimated by multiplying the track length by the average of the cross-sectional areas of the worn track determined by numerical integration of the 2D profiles (3–5 measurements per track).

The elemental composition of the wear tracks on the Si spheres and Si substrates was studied by X-ray photoelectron spectroscopy (XPS), using a spectrometer Axis Supra (Kratos Analytical Ltd., Manchester, UK). A monochromatic Al Kα source was run at 225W. The detailed spectra were acquired at a pass energy of 20 eV through an aperture of 110 μm. Data analysis was conducted with CasaXPS. Atomic percentages were calculated assuming a homogenous distribution of elements, using the Kratos relative sensitivity factors.

In order to assess the thickness of the film remaining on the Si substrate after the long tribological test at 1 N, the excess liquid was removed with absorbing paper and dried with a nitrogen flow. The tracks left on the adsorbed film were analyzed using an atomic force microscope (NanoSurf Easyscan 2, Liestal, Switzerland) with Si tips ($c = 0.2\ N \cdot m^{-1}$, $f_0 = 25$ kHz) in contact mode (contact force of 50 nN), using the software WSxM 5.0 Develop 4.0.

2.2.3 Results and Discussion

2.2.3.1 Water content, viscosity and wettability of the PILs

Rheological studies were made at 25 °C and variable shear rate, which showed that the liquid mixtures present a Newtonian behavior. The water content, the viscosity at 25 °C and the contact angle on Si of PEG200 and of the mixtures PEG 200 + 2% PILs are given in Table 2.2.1. All

mixtures present moderate viscosity, varying between 49 mPa·s and 64 mPa·s, higher than pure PEG200. The additives based on the anion [$MeSO_3$] lead to higher viscosity than those with the anion [HSO_4] when sharing the same cation. The PEG200 and all the mixtures exhibited good wettability on the Si surface.

Table 2.2.1. Water content, viscosity, η, at 25 °C and equilibrium contact angle on Si substrates of PEG200 and the mixtures. The standard deviations correspond to n = 3 for viscosity and n ≥ 4 for contact angle.

Liquids	Water content/ ppm	η/ mPa·s	Contact angle/ °
PEG200	175	41 ± 1	28 ± 2
PEG 200 + 2% [MIMH][HSO_4]	75	50 ± 1	26 ± 3
PEG 200 + 2% [MIMH][$MeSO_3$]	62	56 ± 1	28 ± 2
PEG 200 + 2% [4-picH][HSO_4]	88	49 ± 1	27 ± 4
PEG 200 + 2% [4-picH][$MeSO_3$]	375	53 ± 1	28 ± 4
PEG 200 + 2% [PyrH][HSO_4]	62	48 ± 1	26 ± 4
PEG 200 + 2% [PyrH][$MeSO_3$]	486	63 ± 1	28 ± 4
PEG 200 + 2% [DBUH][HSO_4]	138	50 ± 1	22 ± 2
PEG 200 + 2% [DBUH][$MeSO_3$]	75	54 ± 1	28 ± 4
PEG 200 + 2% [TMGH][HSO_4]	112	49 ± 1	18 ± 2
PEG 200 + 2% [TMGH][$MeSO_3$]	2875	58.7 ± 0.5	27 ± 4

2.2.3.2 Tribological tests with the tribopair SS/Si

The first experiments aimed at a previous evaluation of the lubrication capacity of the prepared PILs using the tribopair SS sphere/Si substrate in short tests under a low load (1 N). These conditions were chosen in order to avoid wear, which complicates the interpretation of the friction results, thus allowing a first screening of the PILs. The Stribeck curves (CoF *vs*. Sommerfeld parameter, Z) for the two sets of PILs sharing the same anions, [HSO_4] and [$MeSO_3$], are shown in Figure 2.2.2. The parameter Z is defined as:

$$Z = \frac{\eta v r}{N} \qquad \text{Eq. 2.2}$$

where η is the lubricant viscosity (Pa·s), v is the sliding speed (m·s^{-1}), r is the counter-body radius (m) and F is the applied load (N). Stribeck curves allow for the identification of the lubrication regimes that exist between contacting surfaces. In this case, two different regimes can be identified: boundary regime, in which the asperities of the surfaces in relative motion come into physical contact and adhesion and/or abrasion occur; boundary/mixed regime,

which is an intermediate regime where there is some contact between asperities but the lubricant film already plays an important role in supporting the applied load. In the first regime ($Z\times10^5 < 0.3$), CoF decreases sharply with speed, while in the second one ($Z\times10^5 > 0.3$), CoF is almost constant.

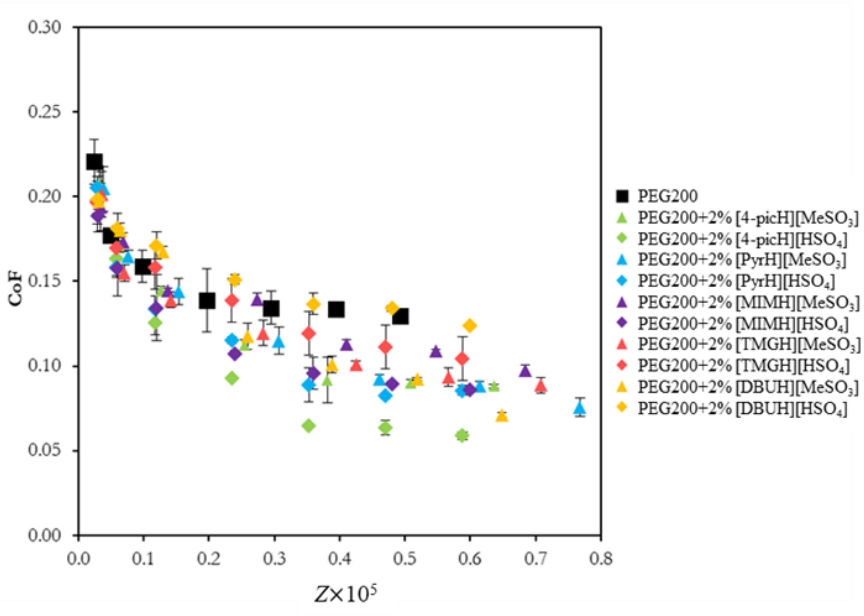

Figure 2.2.2. CoF *vs*. Sommerfeld parameter, *Z*, for the pair SS sphere/Si substrate using neat PEG200 and the mixtures PEG200 + 2% PIL as lubricants. The errors are ±standard deviation (n ≥ 3).

Apart from [DBUH][HSO_4], the addition of the PILs to PEG200 led to a decrease in CoF. Most PILs present a similar behavior, but [4-picH][HSO_4] stands out as the best one. Figure A.2.4 compares the Stribeck curves obtained for the PILs grouped according to the anion, [HSO_4] and [$MeSO_3$], respectively. Among the PILs based on the same anion, it is possible to identify significant differences, which seems to indicate that the cation possesses a more important role in determining the lubrication capacity. The small, symmetric cation [4-picH] may interact with the Si surface through hydrogen bonds established between NH and CH groups of the picolinium ring and the oxidized Si, leading to the formation of a compact adsorbed layer. A similar behavior was observed by the authors with 1-methyl-3-picolium methylsulfate ([C_1-3-pic][$MeSO_4$]). [14] In contrast, the cation [DBUH] has a large size, low symmetry and stronger delocalized charge,[31] which do not favor the interaction with the Si surface. The [HSO_4] anion may also contribute to the formation of the stable lubrication film through the interaction of the S-O groups with the non-oxidized Si, while the hydroxyl groups interact with the Si-O. Thus, the best tribological behavior obtained with [4-picH][HSO_4] should result from the synergy of the two ions.

We must stress that the tribological behavior of the mixtures PEG 200 + 2% [MIMH][$MeSO_3$] and PEG 200 + 2% [TMGH][$MeSO_3$] was previously tested with the same tribopair under different conditions (loads of 15 mN and 30 mN).[14] They led to significant decreases in CoF when compared to PEG200 and to other mixtures of PEG200 with aprotic ILs. However, Figure 2.2.2 shows that the tribological behavior of the former mixtures under 1 N of load was clearly outperformed by PEG 200 + 2% [4-picH][HSO_4]. The additive [4-picH][HSO_4] reduced 55% the CoF of PEG200 (v = 20 mm·s^{-1}), while the reductions with [MIMH][$MeSO_3$] and [TMGH][$MeSO_3$] were 25% and 31%, respectively.

2.2.3.3 Tribological tests with the tribopair Si/Si

The best and the worst additives tested with the tribological pair SS/Si, respectively, [4-picH][HSO_4] and [DBUH][HSO_4], were further studied using the tribopair Si sphere/Si substrate. To better assess the role of the anion, the results are compared with those obtained with the two other PILs sharing the same cations but with the anion [$MeSO_3$]: [4-picH][$MeSO_3$] and [DBUH][$MeSO_3$]. Figure 2.2.3 shows CoF *vs*. Z for neat PEG200 and the mixtures of these additives with PEG200 obtained with short tests under the load of 1 N. When these results are compared with the previous ones obtained with the tribopair SS/Si, a significant reduction in the CoF is observed for all mixtures. This decrease may be attributed to the smaller roughness of the Si spheres (RMS = 15 nm) compared to the SS spheres (RMS = 1 μm).

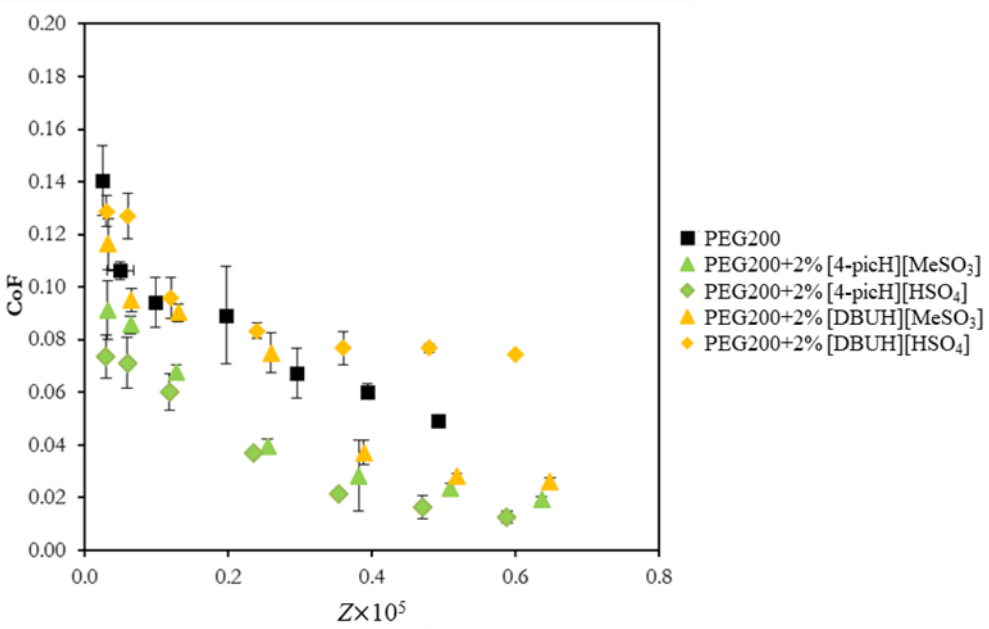

Figure 2.2.3. CoF *vs*. Sommerfeld parameter, Z, for the pair Si sphere/Si substrate using neat PEG200 and the mixtures PEG200 + 2% PIL as lubricants in short tests under load of 1 N. The errors are ±standard deviation (n ≥ 3).

The tribological behavior of the tested PILs follows a similar pattern to that obtained with the SS spheres but with a slight difference: [DBUH][HSO_4] is still the worst additive but the lubrication capacities of [4-picH][HSO_4] and [4-picH][$MeSO_3$] are almost the same. A possible justification for this behavior should lie in different interactions between these anions and the SS or Si spheres. It seems that the anion [HSO_4] may react with steel to produce a protective layer more efficiently than [$MeSO_3$], thus justifying the better behavior of [4-picH][HSO_4] for the SS/Si pair.

The influence of the load and the number of cycles on the CoF was investigated and the results obtained with forces of 1 N, 2 N and 4 N, at the sliding speed of 8 mm·s^{-1} are presented in Figure 2.2.4. The choice of this value was based on the analysis of the Stribeck curves (Figure 2.2.3), which show that for this intermediate speed, the lubrication regime may be considered boundary/mixed (low Sommerfeld parameter). To confirm the lubrication regime, the value of the thickness of the lubricant film should be compared with the composite surface roughness, defined as $\left(\sigma_{ball}^2 + \sigma_{disc}^2\right)^{1/2}$, which in the present case is approximately 15 nm. Although we do not have direct experimental access to that thickness, we may have an estimation through the AFM analysis of the film that remained on the Si surface, following the tribological experiments. Figure A.2.5 (Annex A.2) shows the surface of the Si substrate at the end of the test with PEG200 + 2% [4-picH][HSO_4] (2375 cycles, 1 N) after removing the excess liquid: outside the track an adsorbed layer approximately 4.5 nm high is visible. The observed track should be the result of the continuous removal of this layer during the sliding movement of

the tribological pair. Furthermore, we estimated the theoretical minimum film thickness by applying the elastohydrodynamic theory of lubrication (EHL) to a nonconformal geometry of ball-on-disc contact.[32] The value of the film thickness obtained for the load of 1 N (condition of Figure 2.2.3) and sliding speed of 8 mm·s^{-1} (details of the calculation in Annex A.2) is ~2 nm. We must stress that the calculated value of the film thickness must be taken with care, because the EHL theory of lubrication does not strictly apply when the film thickness is in the order of nanometers, and inconsistencies were found when applying the EHL theory to ILs.[33] Nevertheless, the consistency between the calculated minimum film thickness and the thickness measured with AFM allows concluding that the film is not thick enough to separate the two sliding surfaces, confirming a boundary/mixed lubrication regime, where the load is carried mainly by the surface asperities or partially by the asperities and the lubricant film.

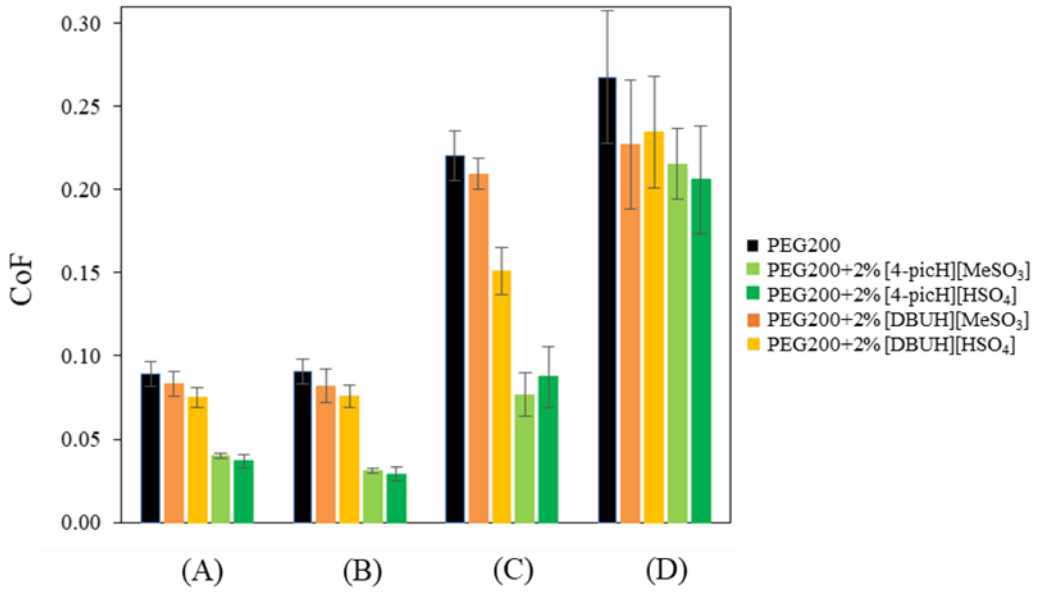

Figure 2.2.4. Average CoF values obtained with the pair Si sphere/Si substrate using neat PEG200 and the mixtures PEG200 + 2% PIL as lubricants: short tests under the load of 1 N (A) and long tests under the loads of 1 N (B), 2 N (C) and 4 N (D). The errors are ±standard deviation ($n \geq 3$).

At low load, the value of the CoF is constant throughout all the sliding distances of the tribological test: the average values obtained with 2375 cycles are not significantly different from those obtained with 85 cycles. In contrast, increasing the load led to increasing values of CoF, with a larger scatter, indicating the existence of wear. In all cases, there is a tendency for a decrease in the average CoF after adding the additives, but the larger decreases occurred with [4-picH][HSO_4] and [4-picH][$MeSO_3$]. As expected, after the short tests, no wear of the Si substrates could be detected, but the situation changed for the longer tests. Figure 2.2.5 shows the wear volumes obtained in long tests under loads of 1 N, 2 N and 4 N.

The most remarkable results were obtained with the additives [4-picH][HSO_4] and [4-picH][$MeSO_3$] at 2 N: the wear volumes became almost negligible. For the lower load (1 N), the wear volumes were small for all mixtures, while for the higher load (4 N), the large scatter of the results does not allow a meaningful comparison, although [4-picH][HSO_4] still demonstrated the best behavior. The analysis of the time dependence of the CoF in the long tests helps to understand the dispersion of the CoF and the wear values. Figure A.2.6 presents examples of the variation of CoF with time, obtained during long tests with $v = 8\ mm \cdot s^{-1}$ for 1 N, 2 N and 4 N. The CoF values remained constant without the presence of any running-in period for the tests under 1 N, indicating the stability of the lubricant film. Under the load of 2 N, only the test with PEG200 + 2% [4-picH][HSO_4] led to a constant value, although the variation was very slight with PEG200 + 2% [4-picH][$MeSO_3$]. The tests under 4 N led to some instability with sporadic peaks in the CoF values for all mixtures giving evidence to the existence of three-body wear. The CoF is slightly decreasing with time, which may be attributed to the rolling and sliding of debris particles that absorb deformation energy.[34] The same behavior can be detected in the tests under 2 N using PEG200 and their mixtures with [DBUH][HSO_4] and [DBUH][$MeSO_3$]. Silicon is known to have good mechanical properties but its low toughness results in adhesive wear where the first debris are formed, followed by third-body wear.[35,36] The local variations of the surface morphology should be responsible for the observed fluctuations in the friction coefficient. The additives [4-picH][HSO_4] and [4-picH][$MeSO_3$] strongly adsorb on the Si surfaces of the body and the counter-body minimizing the contact between the sliding surfaces during the tribological tests under loads of 1 N and 2 N. For the highest load (4 N), the additives could no longer protect the surfaces from contact and third-body wear occurs, as shown in the SEM images in Figure 2.2.6. The images of the worn surface of the Si balls clearly show signs of three-body abrasive wear where the black dots correspond to debris. These small black particles of angular shape result from the oxidation of Si fragments detached during the first cycles of the tribological tests and oxidized by the action of heat and pressure. It is clear from the figure that the three-body abrasive wear is more intense for PEG200 and has the lowest intensity when using the additive [4-picH][HSO_4]. The width of the wear tracks on the Si substrates confirms these results: the narrowest track is observed for [4-picH][HSO_4].

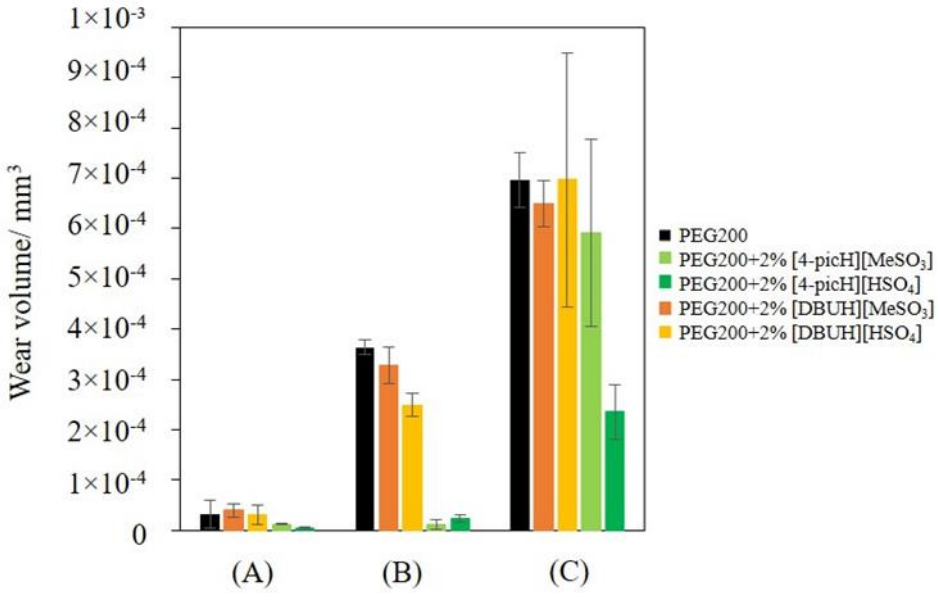

Figure 2.2.5. Average wear volumes obtained with the pair Si sphere/Si substrate using neat PEG200 and the mixtures PEG200 + 2% PIL as lubricants in long tests under loads of 1 N (A), 2 N (B) and 4 N (C). The errors are ±standard deviation (n ≥ 3).

The profiles of the wear tracks on the Si substrates were obtained with a profilometer and are presented in Figure 2.2.7. PEG200 led to a deep, wide wear profile, while the profile obtained with [4-picH][HSO_4] is the shallowest. This behavior is typical of well-lubricated surfaces of the same material moving relative to each other. The moving surfaces deform and the ball penetrates slightly on the underlying substrate leading to a wide, shallow wear track.

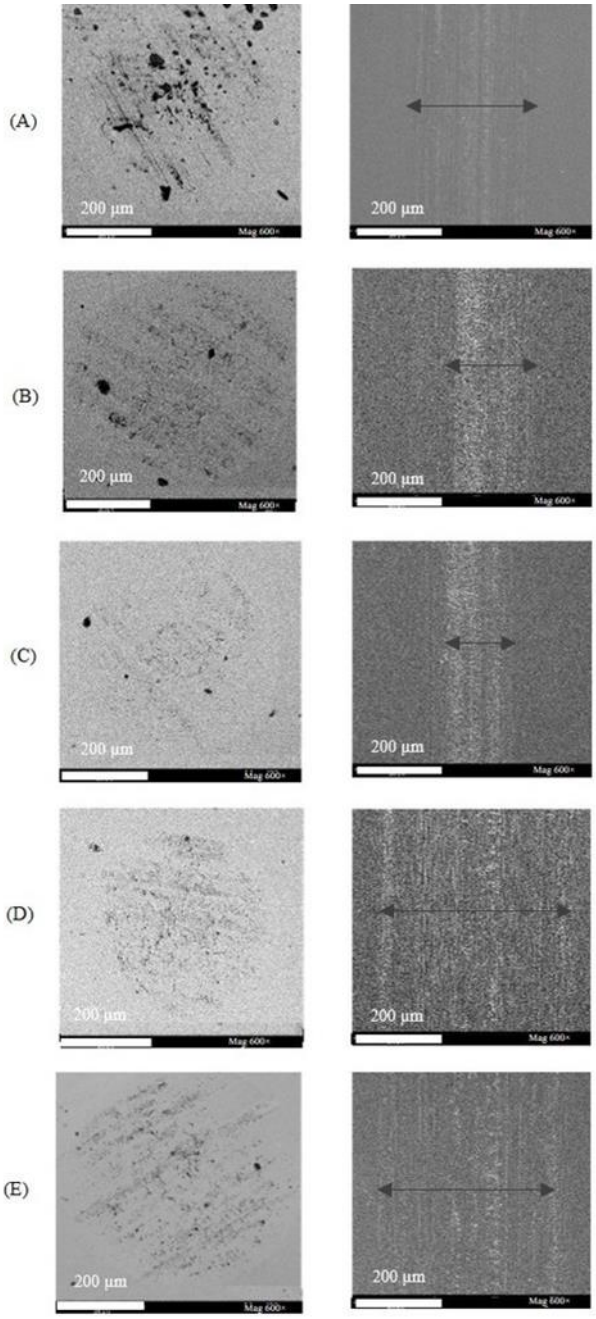

Figure 2.2.6. SEM images with 600× magnification of the worn surfaces of the Si balls (left) and the Si substrates (right) after long tribological tests under the load of 4 N using as lubricants: PEG200 (A), PEG200 + 2% [4-picH][$MeSO_3$] (B), PEG200 + 2% [4-picH][HSO_4] (C), PEG200 + 2% [DBUH][$MeSO_3$] (D) and PEG200 + 2% [DBUH][HSO_4] (E). The black arrows mark the limits of the wear tracks.

The elemental composition of the Si substrates inside and outside the wear tracks (under the load of 4 N) obtained with XPS analysis is presented in Table 2.2.2. The most striking result is the presence of nitrogen inside and outside the track for PEG200 + 2% [4-picH][HSO_4], the best

lubricating mixture. This confirms that [4-picH][HSO_4] is the PIL with a higher tendency to adsorb on the Si surface. Surprisingly, no sign of sulfur could be detected indicating that the interaction of this PIL with the surface occurs mostly through the cation. When comparing the atomic percentages inside the wear tracks, the percentages of Si are higher and those of oxygen and carbon are lower for the worst additives, which are the ones based on the [DBUH] cation.

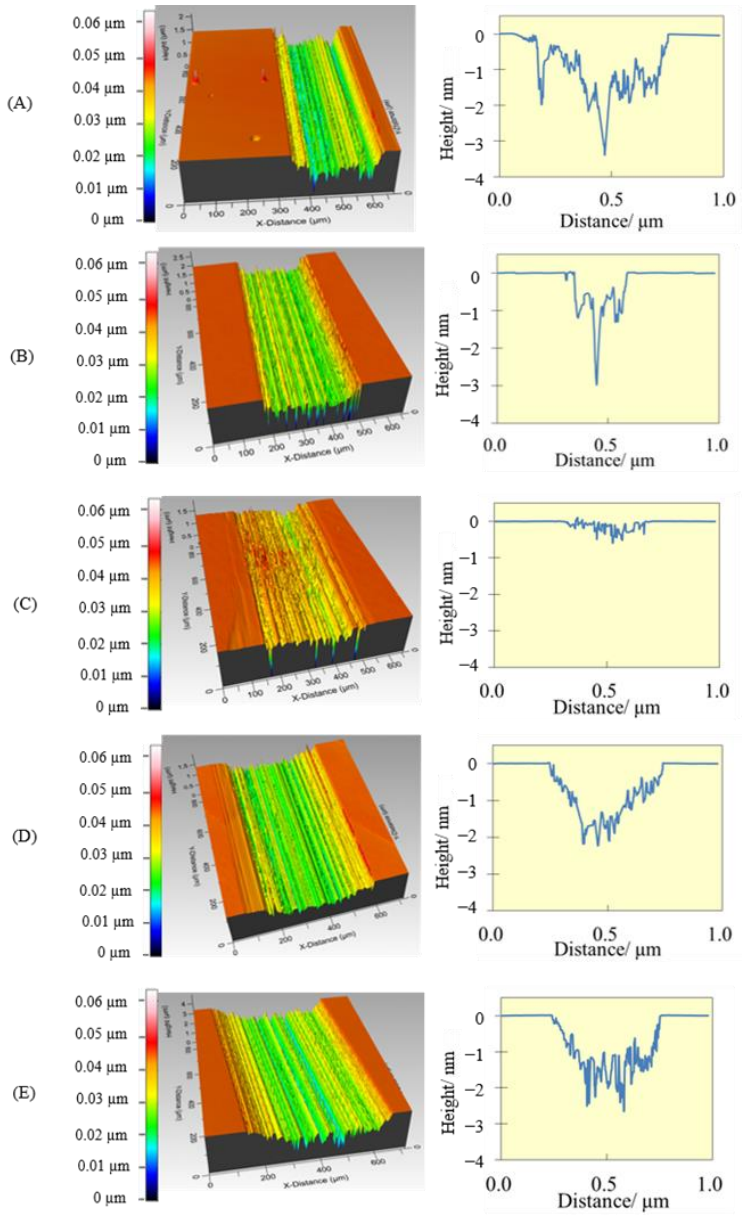

Figure 2.2.7. Wear tracks of the Si substrates (profilometer images with 20×magnification) after long tribological tests under the load of 4 N using as lubricants: PEG200 (A), PEG200 + 2% [4-picH][$MeSO_3$] (B), PEG200 + 2% [4-picH][HSO_4] (C), PEG200 + 2% [DBUH][$MeSO_3$] (D) and PEG200 + 2% [DBUH][HSO_4] (E).

This is in agreement with the fact that the films of adsorbed [DBUH][$MeSO_3$] and [DBUH][HSO_4] are less resistant to wear and are removed more easily from the surface during the sliding process. Comparison of the Si 2p percentages inside and outside the wear tracks reveals slightly lower values inside, with the exception of the [DBUH][HSO_4], which suggests that the sliding process helps in the spreading of the lubrication film on the Si substrate. In the case of O 1s and C 1s, the data are difficult to interpret because these elements may derive from different sources, including ambient contamination.

Table 2.2.2. Relative surface atomic concentrations inside and outside the wear tracks (shown in Figure 2.2.6).

Lubricant	Relative Atomic Percentages							
	Si 2p		O 1s		C 1s		N 1s	
	In	Out	In	Out	In	Out	In	Out
PEG200	37.4	45.4	31.8	35.9	30.8	18.7	-	-
PEG200 + 2% [4-picH][$MeSO_3$]	36.4	48.3	32.2	33.3	31.4	18.4	-	-
PEG200 + 2% [4-picH][HSO_4]	37.8	41.6	34.1	33.3	27.7	24.6	0.4	0.5
PEG200 + 2% [DBUH][$MeSO_3$]	49.2	52.1	27.7	34.9	23.1	13.0	-	-
PEG200 + 2% [DBUH][HSO_4]	48.7	45.5	28.2	21.1	23.1	33.4	-	-

The XPS spectra of the Si substrates inside the wear tracks (regions limited by the segments between arrows in Figure 2.2.6) are compared with the ones outside the wear tracks, in Figure 2.2.8. The relative amount of Si^{4+} compared to Si^0 provides an indication for surface oxidation of the silicon. The quantification was conducted via fitting over a Shirley background, using Si 2p duplets with a line shape of LA (1.5,3,90) for Si^0 and GL(30) for Si^{4+}. The Si substrates outside the wear tracks all have a similar Si^{4+} contribution. After application of the load, the presence of oxidized silicon is most pronounced with the lubricants containing [4-picH]. This strongly indicates the wear-induced formation of silicon dioxide, which offers additional protection against wear. In fact, the Young modulus of SiO_2 (66–75 MPa) is much smaller than that of Si (130–169 MPa), which makes the oxidized silicon easier to deform. Note, that the superior resistance to wear not only depends on the surface oxidation by the cation [4-picH] but also on the right anion: the combination [4-picH][HSO_4] allows for better protection of the sliding surfaces, which may be related to its higher chemical adsorption.

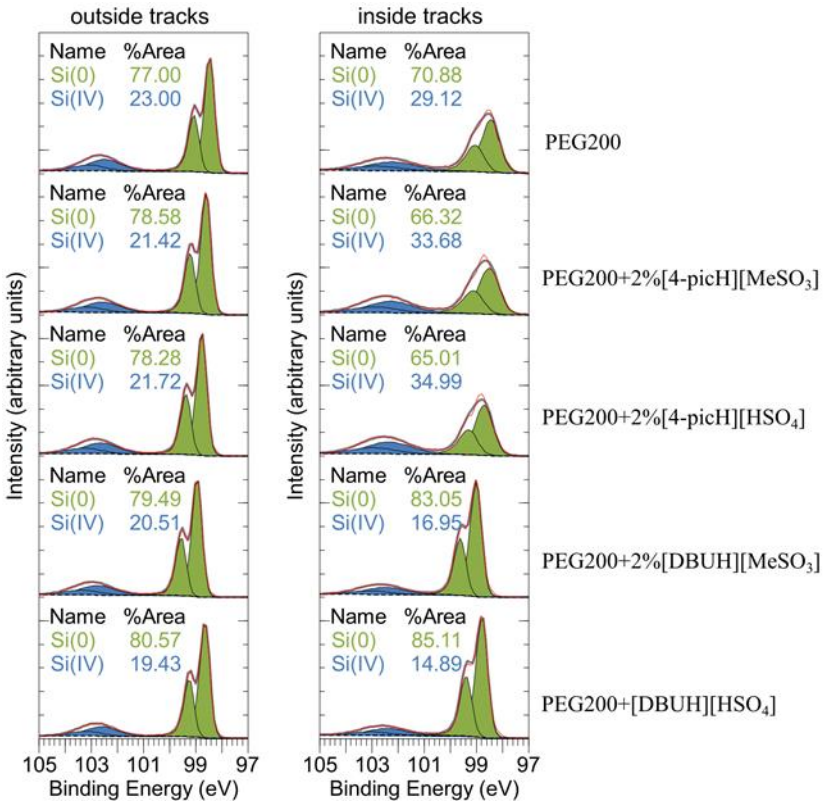

Figure 2.2.8. XPS Si 2p emission from outside (left) and inside (right) of the wear tracks (shown in Figure 2.2.6). Red: original data, dashed black line: background, green: Si^0 components, blue: Si^{4+} components, grey: envelope. Each silicon oxidation state is fitted with two components of the same color, cor-responding to the Si $2p_{3/2}$ and Si $2p_{1/2}$ doublets, separated by 0.6 eV and with identical line width, respectively.

A schematic representation of the possible lubrication process during the tribological tests under high load with PEG200 and the mixture PEG200 + 2% [4-picH][HSO_4] is proposed in Figure 2.2.9. The three-body abrasive wear leads to the formation of debris and surface cracks, which occurs when the lubricant PEG200 is minimized in the presence of the mixture. The PIL adsorbs to the sliding surfaces avoiding direct contact between the body and counter-body which becomes slightly deformed under the load.

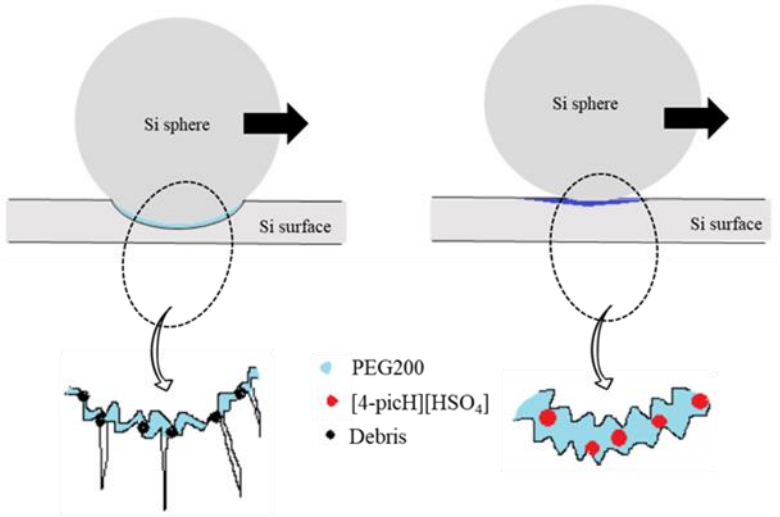

Figure 2.2.9. Schematic representation of the lubrication process during the tribological tests under high load.

2.2.4 Conclusions

The tribological properties of ten PILs based on the hydrogen sulfate [HSO_4] and meyslate [$MeSO_3$] anions as additives to model lubricant PEG200 were evaluated first in steel/Si and afterwards in Si/Si contacts. From the initial screening, two cations were chosen, which led to the best ant the worst lubrication, respectively, [4-picH] and [DBUH]. The lubrication capacity of [4-picH][HSO_4], [4-picH][$MeSO_3$], [DBUH][HSO_4] and [DBUH][$MeSO_3$] was further assessed using Si/Si pairs to mimic the behavior of MEMS and NEMS. The best additive was [4-picH][HSO_4], which revealed excellent lubrication capacity and minimized third-body abrasive wear. The most striking results were the wear reductions observed at loads of 2 N and 4 N: 15 times and three times lower than that with neat PEG200, respectively. Chemical and image analysis of the wear tracks demonstrated that this PIL, composed of the symmetric cation [4-picH] and the anion [HSO_4], was able to adsorb strongly on the Si surface leading to the formation of a protective film on the sliding surfaces. We conclude that, through an adequate cation/anion combination, it is possible to prepare PILs that are very promising additives to lubricate efficiently Si-based MEMS/NEMS.

2.2.5 References

[1] R. Hayes, S. Imberti, G. G. Warr, R. Atkin, R. The Nature of Hydrogen Bonding in Protic Ionic Liquids, *Angew. Chem. Int*. **2013**, *52*, 4623–4627. https://doi.org/10.1002/anie.201209273

[2] T. L. Greaves, C. J. Drummond, Protic Ionic Liquids: Properties and Applications, *Chem. Rev.* **2008**, *108*, 206–237. https://doi.org/10.1021/cr068040u

[3] J. J. Qu, J.J. Truhan, S. Dai, H. Luodan, P. J. Blau, Ionic Liquids With Ammonium Cations as Lubricants or Additives. *Tribol. Lett*. **2006**, *22*, 207–214. https://doi.org/10.1007/s11249-006-9081-0

[4] H. Kondo, Protic Ionic Liquids With Ammonium Salts as Lubricants for Magnetic Thin Film Media. *Tribol. Lett.* **2008**, *31*, 211–218. https://doi.org/10.1007/s11249-008-9355-9

[5] Q. Zhao, G. Zhao, M. Zhang, X. Wang, W. Liu, Tribological Behavior of Protic Ionic Liquids With Dodecylamine Salts of Dialkyldithiocarbamate as Additives in Lithium Complex Grease. *Tribol. Lett*. **2012**, *48*, 133–144. https://doi.org/10.1007/s11249-012-0011-z

[6] T. Espinosa, J. Sanes, A. E. Jiménez, M. D. Bermúdez, Protic Ammonium ACrboxylate Ionic Liquid Lubricants of OFHC Copper. *Wear* **2013**, *303*, 495–509. https://doi.org/10.1016/j.wear.2013.03.041

[7] T. Espinosa, M. Jiménez, J. Sanes, A. E. Jiménez, M. Iglesias, M. D. Bermúdez, Ultra-Low Friction With a Protic Ionic Liquid Boundary Film at the Water-Lubricated Sapphire – Stainless Steel Interface. *Tribol. Lett*. **2014**, *53*, 1–9. https://doi.org/10.1007/s11249-013-0238-3

[8] M. R. Ortega, V. Karine, P. Leandro, B. Ramos, U. Boff, S. Mattedi, L. Schaeffer, C. F. Malfatti, Protic Ionic Liquids Used as Metal-Forming Green Lubricants for Aluminum: Effect of Anion Chain Length. *Mater. Res*. **2017**, *20*, 675–687. https://doi.org/10.1590/1980-5373-MR-2016-0626

[9] M. R. Vega, J. Ercolani, S. Mattedi, C. Aguzzoli, C. A. Ferreira, A. S. Rocha, C. F. Malfatti, Oleate-Based Protic Ionic Liquids as Lubricants for Aluminum 1100. *Eng. Chem. Res*. **2018**, *57*, 12386–12396. https://doi.org/10.1021/acs.iecr.8b02426

[10] A. Patel, H. Guo, P. Iglesias, P. Study of the Lubricating Ability of Protic Ionic Liquid on an Aluminum–Steel Contact. *Lubricants* **2018**, *6*, 66. https://doi.org/10.3390/lubricants6030066

[11] H. Guo, P. Iglesias, Tribological Behavior of Ammonium-Based Pionic Liquid as Lubricant Additive. *Friction* **2021**, *9*, 169–178. https://doi.org/10.1007/s40544-020-0378-z

[12] M. D. Gonzalez, F. Vilches, J. Sanes, M. D. Bermúdez, Diprotic Amonium Succinate Ionic Liquid in Thin Film Aqueous Lubrication and in Graphene Nanolubricant. *Tribol. Lett*. **2019**, *67*, 26. https://doi.org/10.1007/s11249-019-1138-y

[13] A. Khan, R. Gusain, M. Sahai, O. P. Khatria, Fatty Acids-Derived Protic Ionic Liquids as Lubricant Additive to Synthetic Lube Base Oil For Enhancement of Tribological Properties. *J. Mol. Liq*. **2019**, *293*, 111444. https://doi.org/10.1016/j.molliq.2019.111444

[14] M. Antunes, M. T. Donato, V. Paz, F. Caetano, L. Santos, R. Colaço, L. C. Branco, B. Saramago, Improving the Lubrication of Silicon Surfaces Using Ionic Liquids as Oil Additives: The Effect of Sulfur-Based Functional Groups. *Tribol. Lett*. **2020**, *68*, 70. https://doi.org/10.1007/s11249-020-01308-7

[15] Z. Rymuza, Control Tribological and Mechanical Properties of MEMS Surfaces. Part 1: Critical Review. *Microsyst. Technol*. **1999**, *5*, 173–180. https://doi.org/10.1007/s005420050160

[16] A. Filippov, N. Azancheev, A. Gibaydullin, S. Bhattacharyya, O. N. Antzutkin, F. U. Shah, Dynamic Properties of Imidazolium Orthoborate Ionic Liquids Mixed with Polyethylene Glycol Studied by NMR Diffusometry and Impedance Spectroscopy. *Magn. Reson. Chem*. **2018**, *56*, 113–119. https://doi.org/10.1002/mrc.4636

[17] T. Y. Wu, H. C. Wang, S. G. Su, S. T. Gung, M. W. Lin, C. B. Lin, Characterization of Ionic Conductivity, Viscosity, Density, and Self-Diffusion Coefficient For Binary Mixtures of Polyethyleneglycol (or Polyethyleneimine) Organic Solvent With Room Temperature Ionic Liquid $BMIBF_4$ (or $BMIPF_6$). *J. Taiwan Inst. Chem. Eng.* **2010**, *41*, 315–325. https://doi.org/10.1016/j.jtice.2009.10.003

[18] B. Yu, F. Zhou, Z. Mu, Y. M. Liang, W. M. Liu, Tribological Properties of Ultra-Thin Ionic Liquid Films on Single-Crystal Silicon Wafers With Functionalized Surfaces. *Tribol. Inter*. **2006**, *39*, 879–887. https://doi.org/10.1016/j.triboint.2005.07.039

[19] B. Bhushan, M. Palacio, B. Kinzig, AFM-Based Nanotribological and Electrical Characterization of Ultrathin Wear-Resistant Ionic Liquid Films. *J. Colloid Interface Sci*. **2008**, *317*, 275–287. https://doi.org/10.1016/j.jcis.2007.09.046

[20] M. Zhu, J. Yan, Y. Mo, M. Bai, Effect of the Anion on the Tribological Properties of Ionic Liquid Nano-Films on Surface-Modified Silicon Wafers. *Tribol. Lett*. **2008**, *29*, 177–183. https://doi.org/10.1007/s11249-007-9294-x

[21] Y. Mo, W. Zhao, M. Zhu, M. Bai, Nano/Microtribological Properties of Ultrathin Functionalized Imidazolium Wear-Resistant Ionic Liquid Films on Single Crystal Silicon. *Tribol. Lett*. **2008**, *32*, 143–151. https://doi.org/10.1007/s11249-008-9371-9

[22] Y. Mo, F. Huang, F. Zhao, Functionalized Imidazolium Wear-Resistant Ionic Liquid Ultrathin Films for MEMS/NEMS Applications. *Surf. Interface Anal*. **2011**, *43*, 1006–1014. https://doi.org/10.1002/sia.3684

[23] J. Pu, D. Jiang, Y. Mo, L. Wang, Q. Xue, Micro/Nano-Tribological Behaviors of Crown-Type Phosphate Ionic Liquid Ultrathin Films on Self-Assembled Monolayer Modified Silicon. *Surf. Coat. Technol.* **2011**, *205*, 4855–4863. https://doi.org/10.1016/j.surfcoat.2011.04.089

[24] A. Arcifa, A. Rossi, R. M. Espinosa-Marzal, N. D. Spencer, Environmental Influence on the Surface Chemistry of Ionic-Liquid-Mediated Lubrication in a Silica/Silicon Tribopair. *J. Phys. Chem. C* **2014**, *118*, 29389–29400. https://doi.org/10.1021/jp505998k

[25] A. Arcifa, A. Rossi, R. M. Espinosa-Marzal, N. D. Spencer, Influence of Environmental Humidity on the Wear and Friction of a Silica/Silicon Tribopair Lubricated With a Hydrophilic Ionic Liquid. *ACS Appl. Mater. Interfaces* **2016**, *8*, 2961–2973. https://doi.org/10.1021/acsami.5b09370

[26] A. Arcifa, A. Rossi, N. D. Spencer, Adsorption and Tribochemical Factors Affecting the Lubrication of Silicon-Based Materials by (Fluorinated) Ionic Liquids. *J. Phys. Chem. C* **2017**, *121*, 7259–7275. https://doi.org/10.1021/acs.jpcc.6b13028

[27] P. M. Amorim, A. M. Ferraria, R. Colaço, L. C. Branco, B. Saramago, Imidazolium-Based Ionic Liquids Used as Additives in Nanolubrication of Silicon Surfaces. *Beilstein J. Nanotechnol*. **2017**, *8*, 1961–1971. https://doi: 10.3762/bjnano.8.197

[28] M. T. Donato, F. Caetano, R. Colaço, L. C. Branco, B. Saramago, Picolinium-Based Hydrophobic Ionic Liquids as Additives to PEG200 to Lubricate Steel-Silicon Contacts. *ChemistrySelect* **2020**, *5*, 5864–5872. https://doi.org/10.1002/slct.202000613

[29] A. A. Cândido, T. C. Rozada, A. M. F. Rozada, J. R. B. Souza, E. J. Pilau, F. A. Rosa, E. A. Basso, G. F. Gauze, Mechanistic Investigation of DBU-Based Ionic Liquids for Aza-Michael Reaction: Mass Spectrometry and DFT Studies of Catalyst role. *J. Braz. Chem. Soc*. **2020**, *31*, 1796–1804. https://doi.org/10.21577/0103-5053.20200066

[30] J. Restolho, J. L. Mata, B. Saramago, On the Interfacial Behavior of Ionic Liquids: Surface Tensions and Contact Angles, *J. Colloid Interface Sci*. **2009**, *340*, 82–86. https://doi.org/10.1016/j.jcis.2009.08.013

[31] J. Nowicki, M. Muszyńskia, J. P. Mikkola, Ionic Liquids Derived From Organosuperbases: En Route to Superionic Liquids. *RSC Adv*. **2016**, *6*, 9194–9208. https://doi.org/10.1039/C5RA23616A

[32] G. Stachowiak, A. Batchelor, *Engineering Tribology Butterworth-Heinemann*, 4th ed.; Butterworth-Heinemann: Oxford, UK, 2014.

[33] H. Xiao, D. Guo, S. Liu, G. Pan, X. Lu, Film Thickness of Ionic Liquids under High Contact Pressures as a Function of Alkyl Chain Length. *Tribol. Lett.* **2011**, *41*, 471–477. https://doi.org/10.1007/s11249-010-9729-7

[34] I. L. Singer, How Third-Body Processes Affect Friction and Wear. *MRS Bull.* **1998**, *23*, 37–40. https://doi.org/10.1557/S088376940003061X

[35] G. Subhash, A. D. Corwin, M. P. Boer, Evolution of Wear Characteristics and Frictional Behavior in MEMS Devices. *Tribol. Lett.* **2011**, *41*, 177–189. https://doi.org/10.1007/s11249-010-9696-z

[36] D. H. Alsem, M. T. Dugger, E. A. Stach, R. O. Ritchie, Micron-Scale Friction and Sliding Wear of Polycrystalline Silicon Thin Structural Films in Ambient Air. *J. Microelectrom. Syst*. **2008**, *17*, 1144–1154. https://doi.org/10.1109/JMEMS.2008.927751

3

DEEP EUTECTIC SOLVENTS AS LUBRICANTS FOR MEMS/NEMS

3.1

EUTECTIC SYSTEMS

This chapter presents the results obtained using Eutectic Systems as lubricants and it is based on the published paper **M. T. Donato**, L. Santos, H. P. Diogo, R. Colaço, L. C. Branco, B. Saramago, Eutectic systems containing an ionic liquid and PEG200 as lubricants for silicon surfaces: effect of the mixture's molar ratio, *Journal of Molecular Liquids* **2022**, *350*, 118572.

3.1.1 Introduction

Deep Eutectic Solvents (DESs) are mixtures which show a significant decrease on the melting point comparing to the original individual components due to the hydrogen bonding involving the large and asymmetric ions usually present.[1,2] However, there is some confusion in the literature about the magnitude of the decrease that qualifies the eutectic as deep. According to Martins *et al*.,[3] the designation of DES should apply to an eutectic mixture with the eutectic point lower than that predicted for the ideal mixture and variable composition, as long as it remains liquid at operating temperature. Thus, we will use the term eutectic system (ES) to designate eutectic mixtures in general, without the requirement of a deep eutectic.

ESs are combinations of H-bond donors (HBDs) with H-bond acceptors (HBAs), which allow tuning of their physicochemical properties through the adequate choice of the components and their molar ratios.[2,4] The properties of ESs are similar to those of ionic liquids (ILs), namely very low vapor pressure, non-flammability, and high ionic conductivity, but they are cheaper and their preparation method is easier, more efficient and environmentally friendly. In the last few years, ESs have been applied as green alternatives to ILs in organic chemistry, electrochemistry, engineering, pharmaceutical and material sciences.[2]

ESs were first proposed as lubricants in 2010 by Lawes *et al*.,[5] who tested the choline chloride ([Ch]Cl) salt combined with urea and ethylene glycol (EG) in a 1:2 molar ratio, to lubricate steel/steel contacts. In 2014, Abbott *et al.* compared the tribological behavior of [Ch]Cl:urea (1:2), [Ch]Cl:EG (1:2), [Ch]Cl:glycerol (1:2) and [Ch]Cl:oxalic acid (1:1) with that of a reference oil used for marine applications.[6] Among the various metallic surfaces tested, only the iron-based alloys led to improved tribological performance of the ESs with respect to the mineral oil.

Garcia *et al*.[7] tested the effect of addition of graphene to [Ch]Cl:urea (1:2), [Ch]Cl:EG (1:2) and [Ch]Cl:malic acid (1:1) on the lubrication of steel/steel contacts. The authors used a commercial synthetic base oil as the comparative reference. All tested ESs, with or without graphene, yielded lower values for the coefficients of friction (CoF) when compared to the reference oil. However, the greater reduction in the wear rate was observed when graphene was added to the commercial oil.

Recently, Hallet *et al*.[8] studied the frictional behavior of nanoscale films of [Ch]Cl:EG (1:2) confined between two atomically smooth mica surfaces. The authors found that addition of water (more than 42%) led to the segregation of water layers, which ensured superlubricity.

In 2019, our group developed a new type of ESs based on the combination of ILs with polyethylene glycol (MW 200), PEG200, to lubricate silicon surfaces.[9] The motivation for this study was to take advantage of the lubricating properties of ILs based on sulfur containing ions, while using PEG200 as a green and low cost HBD. Silicon is a very fragile material used in nano and microelectromechanical systems (NEMs and MEMs), which need an efficient

lubrication.[10-13] The fact that ILs are electrically conductive, in contrast with the conventional lubricants, makes them attractive as ES components for microelectronics lubrication because they can reduce the contact resistance between sliding surfaces [14-19] and their tribological performance may be improved through the application of external electric fields.[20] Four ESs were prepared: dibutyl-ethylsulfonium ethylsulfate [S_{442}][$EtSO_4$]:PEG200 (1:4), ethyl-tetrahydrotiophene ethylsulfate [C_2-THT][$EtSO_4$]:PEG200 (1:4), 1-ethyl-3-methylimidazolium (S)-camphorsulfonate [C_2MIM][(*S*)-CSA]:PEG200 (1:4) and 1-methyl-3-picolinium methylsulfate [C_1-3-pic][$MeSO_4$]:PEG200 (1:4). The best tribological behavior was obtained for [C_1-3-pic][$MeSO_4$]:PEG200 and [C_2MIM][(*S*)-CSA]:PEG200 suggesting that, besides the interaction between the sulfur atoms in the anions and the silicon, the interactions of imidazolium and picolinium cations with the surface should also contribute for the formation of a tribofilm.

In the present work, the tribological behavior of eutectic mixtures in several proportions of PEG200 with 1-hexyl-4-picolinium trifluoromethanesulfonate, [C_6-4-pic][TfO], is studied. The choice of this IL was based on its good lubrication capacity of the pair steel ball/silicon substrate demonstrated in a previous work.[21] The objective of this investigation is to understand the effect that the composition of the eutectic mixture may have in its tribological performance. In general, ESs are prepared by mixing several proportions of HBA and HBD (with heating) by a trial and error approach. If mixtures are clear and transparent, indicating complete miscibility, they are considered ESs, but the eutectic composition is rarely presented. In fact, mixtures of components which are liquid at room temperature and do not crystalize but, instead, present glass transition temperatures, are very difficult to characterize by differential scanning calorimetry (DSC). In this work, besides DSC, we used FTIR and monodimensional and bidimensional NMR spectra to analyze the mixtures [C_6-4-pic][TfO]:PEG200 (1:2, 1:4, 1:8 and 1:16 molar ratios) and tried to correlate the molecular interactions with friction and wear obtained when using these systems as lubricants of the pair steel ball/Si substrate.

3.1.2 Experimental

3.1.2.1 Materials

All reagents for the synthesis IL were purchased and used without additional purification. Polyethylene glycol (MW 200) – PEG200 – was from Sigma-Aldrich (USA), with water content <0.5 %. Distilled and deionized (DD) water was obtained with a Millipore Milli-Q system (resistivity ≥ 18.2 M cm).

The silicon substrates were square samples (1×1 cm^2) cut from Si b100N wafers with 0.5 mm of thickness, roughness RMS=1 nm and hardness of 71 HRC. The counter-bodies were stainless

steel AISI 316L grade 100 spheres (Atlas Ball & Bearing Co. Ltd., UK) with 6 mm of diameter, roughness RMS=1 μm and hardness of 60 HRC.

3.1.2.2 Methods

The IL was synthesized according to the procedure described in our previous work.[21]
The ESs were prepared by mixing the IL and PEG200, in the molar ratios 1:2, 1:4, 1:8 and 1:16, under vigorous stirring for 24h at 60 °C. The products were dried in vacuum for two days and analyzed by FTIR-ATR (Nicolet 5700 FTIR spectrometer, Thermo Electron Corporation, USA), 4 cm^{-1} resolution and 128 scans and ^{1}H-NMR (Bruker 400MHz, model Avance III, USA).
The water content of the ESs was checked by Karl–Fischer coulometric titration (Metrohom, Switzerland).
The pure components and the mixtures were analyzed by differential scanning calorimetry (2820 Modulated DSC TA Instruments, USA). The samples were sealed in aluminum crucibles under an inert atmosphere. One cycle in the temperature range -110 °C to 70 °C with a heating/cooling rate of 5 °C/min, was done. Temperature and enthalpy DSC calibration were performed as previously described.[22] The thermograms were analyzed with the *software* Universal Analysis 2000 TA Instruments.
The viscosity was measured at 25 °C using a rheometer (MCR 92, Anton Paar, Austria). The contact angles of the ESs on the silicon substrates were determined by the sessile drop method at room temperature.[23] The Si substrates were cleaned according to the following procedure: 2×15 min sonication in Dextran® solution (0.2% v/v in water) intercalated with 10 min sonication in water, followed by 3×10 min sonication in water, rinsing with DD water, flushing with nitrogen, and drying overnight in a vacuum oven at room temperature. The measurements were made inside an ambient chamber model 100-07-00 (Ramé-Hart, Succasunna, NJ, USA), under a weak flow of dry nitrogen to avoid water absorption by the liquids. The images of drops were obtained with a video camera (jAi CV-A50, Barcelona, Spain) mounted on a microscope Wild M3Z (Leica Microsystems, Wetzlar, Germany) and they were analyzed by running the ADSA (Axisymmetric Drop Shape Analysis, Applied Surface Thermodynamics Research Associates, Toronto, Canada) software.
The coefficients of friction were measured with a ball-on-disc tribometer (TRB^{3}, Anton Paar, Switzerland). The counter-bodies were 316-L stainless steel spheres, which were rubbed against flat Si surfaces. Both the spheres and the silicon surfaces were cleaned using the above mentioned protocol. The spheres were placed on the tribometer arm and the Si surfaces were glued to a metallic container, to which a sufficient amount of liquid was added to ensure the full coverage of the surfaces. The amplitude of the reciprocal movement of the counter-body was 4 mm. A low normal force of 1 N was applied for the short duration tests (85 cycles, corresponding to 0.68 m of sliding distance) to minimize the wear of the surfaces and thus allowing easier interpretation of friction data. For each of these tests, the sliding speed varied

between 1 and 20 $mm \cdot s^{-1}$. Higher normal loads of 2, 4 and 8 N were also applied for the longer tests (2375 cycles, corresponding to 19 m of sliding distance) in order to study wear. For these tests, a speed of 8 $mm \cdot s^{-1}$ was chosen. The Hertz contact stresses varied between 584.5 MPa for 1N and 1169.1 MPa for 8N. All the experiments were done at room temperature, at least in triplicate. The results were analyzed using the software TriboX. After the long tribological tests, the surfaces of the silicon substrates were imaged using an optical profilometer (Profilm 3D, Filmetrics, USA) and their worn volumes were assessed. For each track, the worn volume was estimated by multiplying the track length by the average of the cross-sectional areas of the worn track determined by numerical integration of the 2D profiles (3-5 measurements per track).
The steel balls were observed using a Scanning Electron Microscope (SEM) JEOL JSM7001F (Tokyo, Japan).

3.1.3 Results and Discussion

3.1.3.1 Thermal analysis, viscosity and wettability of the ESs

The water content of PEG200, the IL and the ESs was less than 1000 ppm. Analysis of the DSC thermograms obtained with the starting components and the ESs reveals, in all cases, a glass transition temperature (T_g) varying between -84 °C (PEG200) and -81 °C (IL). Besides T_g, an exothermic event attributed to a cold crystallization followed by a melting peak can be identified in the heating cycles of the IL and the ESs (Figure A.3.1 in Annex A.3). The values of T_g (T_{onset}), the temperature of cold crystallization (T_{max}), and the temperature of the melting peak (T_{max}) are presented in Table 3.1.1. Although no direct evidence supports the existence of ESs, the presence of a single T_g value in the thermograms of the ESs is compatible with the formation of an eutectic mixture. The mixture 1:2 presents the largest supercooled liquid region of the compounds under analysis with an incipient crystallization near 34 °C in clear contrast with the other mixtures (Figure A.3.1).

Table 3.1.1. Thermal analysis of PEG200, [C_6-4-pic][TfO], and their mixtures, including glass transition temperature (T_g), temperature of cold crystallization ($T_{cold\ cristalization}$), and temperature of the melting peak ($T_{melting}$).

Liquids	T_g/ °C	$T_{cold\ cristalization}$/ °C	$T_{melting}$/ °C
[C_6-4-pic][TfO]	-81	16	34
PEG200	-84	29	62
[C_6-4-pic][TfO]:PEG200 (1:2)	-84	34	45
[C_6-4-pic][TfO]:PEG200 (1:4)	-81	22	45
[C_6-4-pic][TfO]:PEG200 (1:8)	-80	25	51
[C_6-4-pic][TfO]:PEG200 (1:16)	-82	21	46

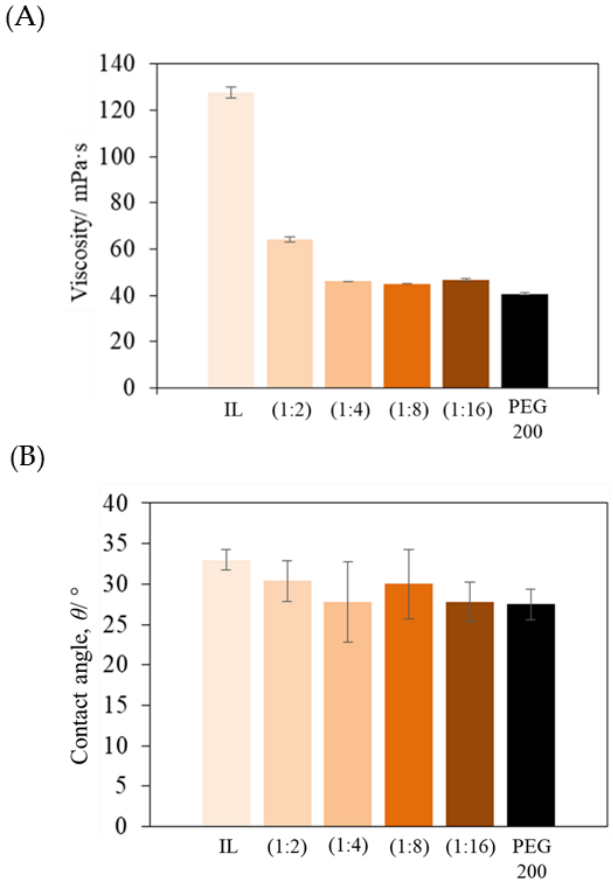

Figure 3.1.1. Viscosity (A) and equilibrium contact angle on Si substrates (B), at 25 °C, of the pure components and the ESs with decreasing amounts of IL (from left to right). The errors are ± standard deviations (n = 3) for viscosity and (n ≥ 4) for contact angle.

The viscosities at 25 °C and the contact angles on the Si surface of the ESs and the pure components are shown in Figure 3.1.1 and in Table A.3.1 (Annex A.3).

The IL is much more viscous than PEG200 and the mixtures. Amongst the ESs, the mixture 1:2 stands out as the most viscous, while the viscosities of the other mixtures are not significantly different. The non-ideal dependence of viscosity on molar fraction may be attributed to the competition between the two main mechanisms involved: the association mechanism via hydrogen bonding and the interstitial accomodation.[24,25] Furthermore, small differences in the water content of the mixtures may contribute to some dispersion in the results.

3.1.3.2 FTIR and NMR spectroscopy

FTIR spectra of the ESs and the pure components are presented in Figure A.3.2 in Annex A.3. Figure 3.1.2 shows a comparison between the spectra of PEG200 and the IL with the spectra of the ESs in different wavenumber ranges. These ranges include the broad band around 3407 cm^{-1} corresponding to O-H in the spectrum of PEG200, which also appears in the spectrum of the IL, although shifted to higher wavenumbers and shallower (Figure 3.1.2A). The presence of water traces in the IL may be responsible for it. Thus, the bands observed in the mixtures in this range (3407-3500 cm^{-1}) derive from the superposition of the O-H bands of both components.

In Figure 3.1.2B we observe the effect of PEG in the 1635 cm^{-1} band, assigned to C=N vibration of the picolinium cation. A blue shift occurs for the ES 1:2 and 1:4 spectra, indicating stronger interactions for these compositions. The same effect can be observed in the C-F bonds of pure IL (Figure 3.1.2C), where the 1214 cm^{-1} and 1143 cm^{-1} bands, assigned to the asymmetric and symmetric extension of C-F in the [TfO] anion, respectively,[26] shift to the blue. In fact a maximum shift is observed for 1:2 molar ratio (1143 cm^{-1} to 1157 cm^{-1} and 1214 cm^{-1} to 1225 cm^{-1}). Furthermore, the 1242 cm^{-1} and 1018 cm^{-1} bands of IL, corresponding to S=O vibrations, are also affected, especially for the 1:2 ratio (Figure A.3.2). These strong interactions observed in the 1:2 ratio suggest that this particular composition could be close to the eutectic. Although the hydrogen bonds established between PEG200 and the IL should induce longer bonds in the involved ions, with a consequent decrease in bond strength and frequency, the formation of new hydrogen bonds may involve both blue and red shifts, according with the electron density distribution, which depends on the electron affinity of atoms involved.[27] Furthermore, assigning vibrational modes for ES using FTIR alone has limitations and should be complemented by Density Functional Theory simulations.[28]

The molar ratios of the prepared ESs were confirmed by the analysis of the ^{1}H-NMR spectra shown in Figure A.3.3. In order to detect the preferential interactions between PEG200 and the cation of the IL in the ES 1:2, a two-dimensional Nuclear Overhauser Effect Spectroscopy (2D NOESY) experiment was performed (Figure 3.1.3). As can be seen from the spectrum, the most intense peak corresponding to PEG200 interacts with the middle CH_2 from the aliphatic chain of the cation – corresponding to the first three signals highlighted in black – and the aromatic

carbons – corresponding to the last two signals highlighted in back. This is proof that there is, in fact, a preferential interaction of the eutectic mixture 1:2 with PEG200.

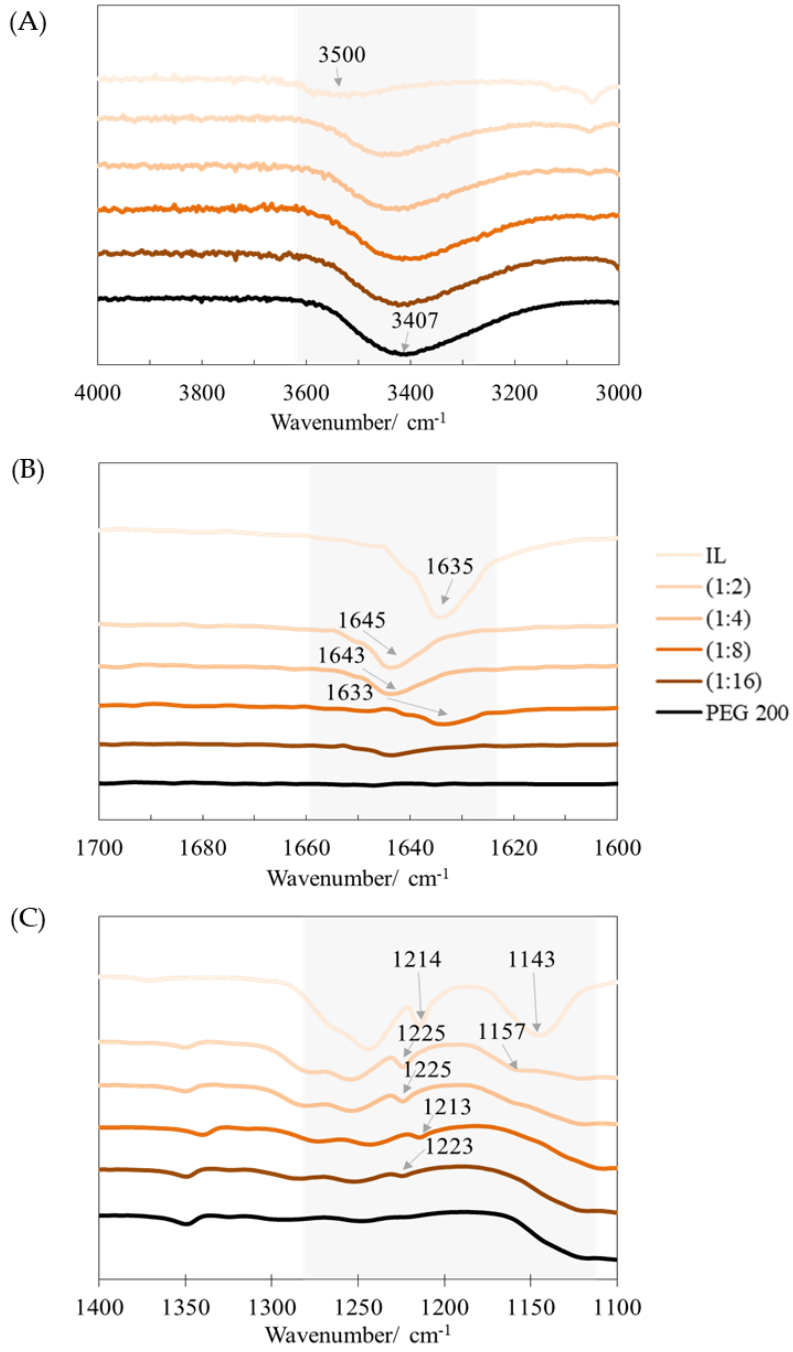

Figure 3.1.2. FTIR spectra of PEG200, [C_6-4-pic][TfO] and the ESs 1:2, 1:4, 1:8 and 1:16 in three wavenumber ranges which include the vibrations of the following groups: (A) O-H; (B) C=N; (C) S=O and C-F.

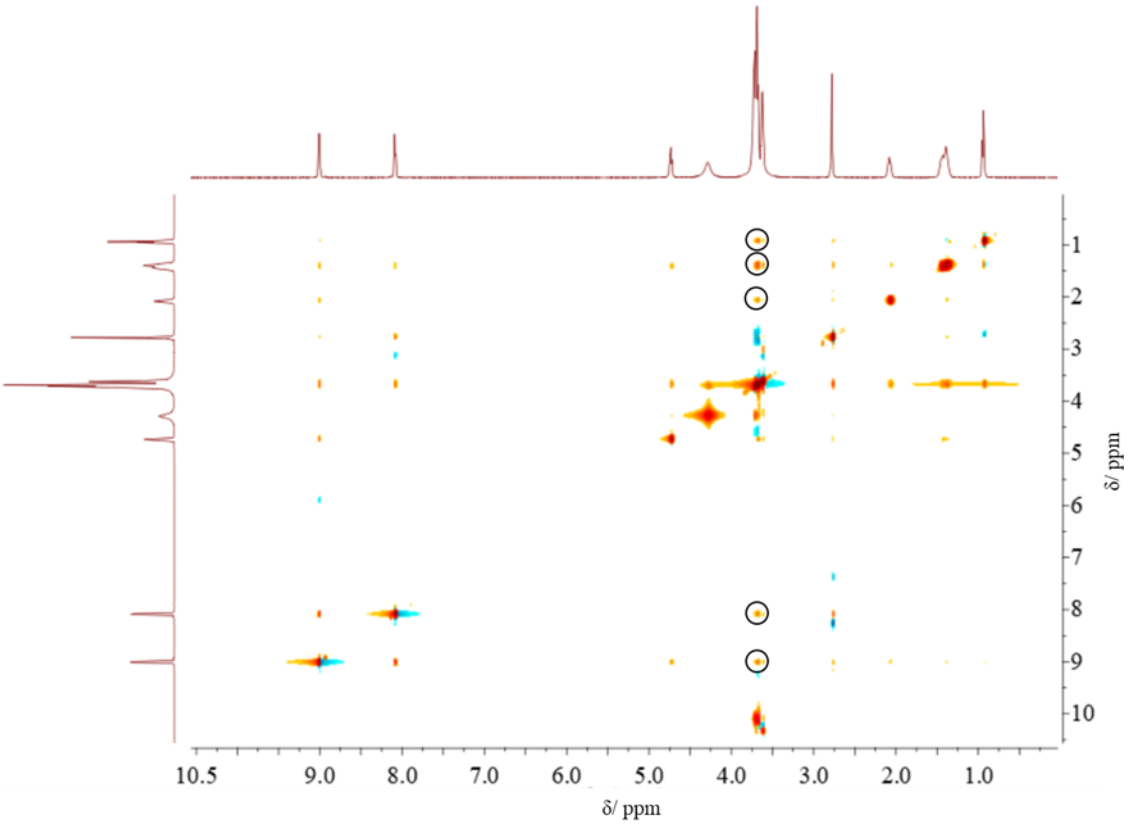

Figure 3.1.3. 2D NOESY experiment performed for ES 1:2.

3.1.3.3 Tribological tests

The tribological behavior was assessed in two types of tests. First, the CoFs were obtained with a normal force of 1N and 85 cycles, to avoid the occurrence of wear. The CoF values are plotted as a function of the Sommerfeld parameter, Z (Figure 3.1.4) which is defined as:

$$Z = \frac{\eta v r}{N} \qquad \text{Eq. 3.1}$$

where η is the lubricant viscosity (Pa·s), v is the sliding speed (m·s^{-1}), r is the counter-body radius (m) and F is the applied load (N).

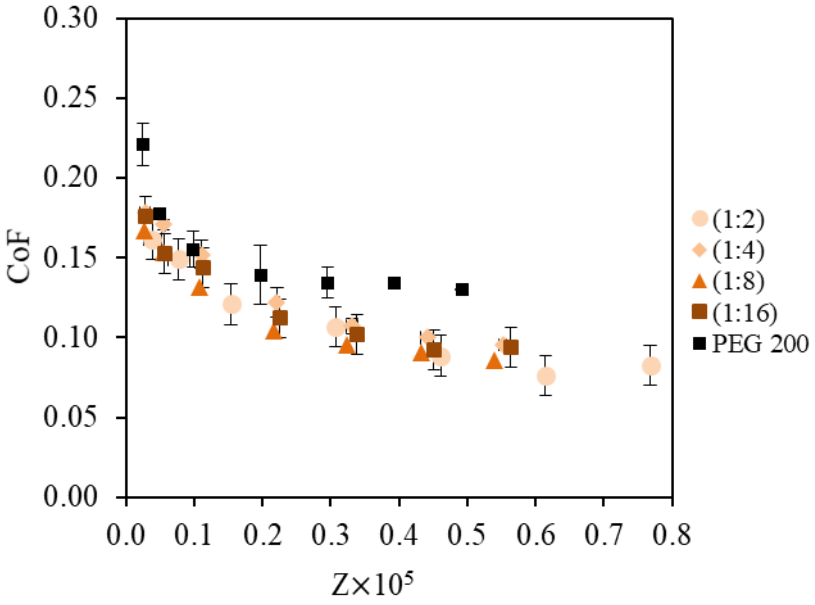

Figure 3.1.4. CoF *vs.* Sommerfeld parameter, *Z*, obtained with PEG200 and the ESs in tribological tests with the pair steel/Si under a normal force of 1N and 85 cycles. The errors are ± standard deviation (n ≥ 3).

The CoF values obtained with the ESs are lower than those of PEG200, the model lubricant, and among the various molar ratios the differences are not significant. We must point out that higher values for the Sommerfeld parameters were attained with the ES 1:2 because it is the most viscous lubricant. The lubrication regime may be considered boundary/mixed (low Sommerfeld parameters) where the load is carried mainly by the surface asperities or partially by the asperities as well as the lubricant film. The second type of tests was made under increased normal forces (2, 4 and 8 N) and longer periods of time (2375 cycles) at a constant sliding speed of 8 mm·s^{-1}, to understand the behavior of ESs in the eventual minimization of wear. The CoF values remained constant with time (Figure A.3.4) without the presence of any running-in period. Figure 3.1.5 and Table A.3.2 present the average CoF values and the average wear volumes obtained with PEG200 and the ESs. The effect of the applied load on friction is not clear, but a tendency for increased CoF at higher loads may be identified and the lubrication regime changes to boundary. The reduction in friction observed when PEG200 was replaced by the ESs is more evident at 8N. For the three tested forces, [C$_6$-4-pic][TfO]:PEG200 (1:2) led to the lowest CoF.

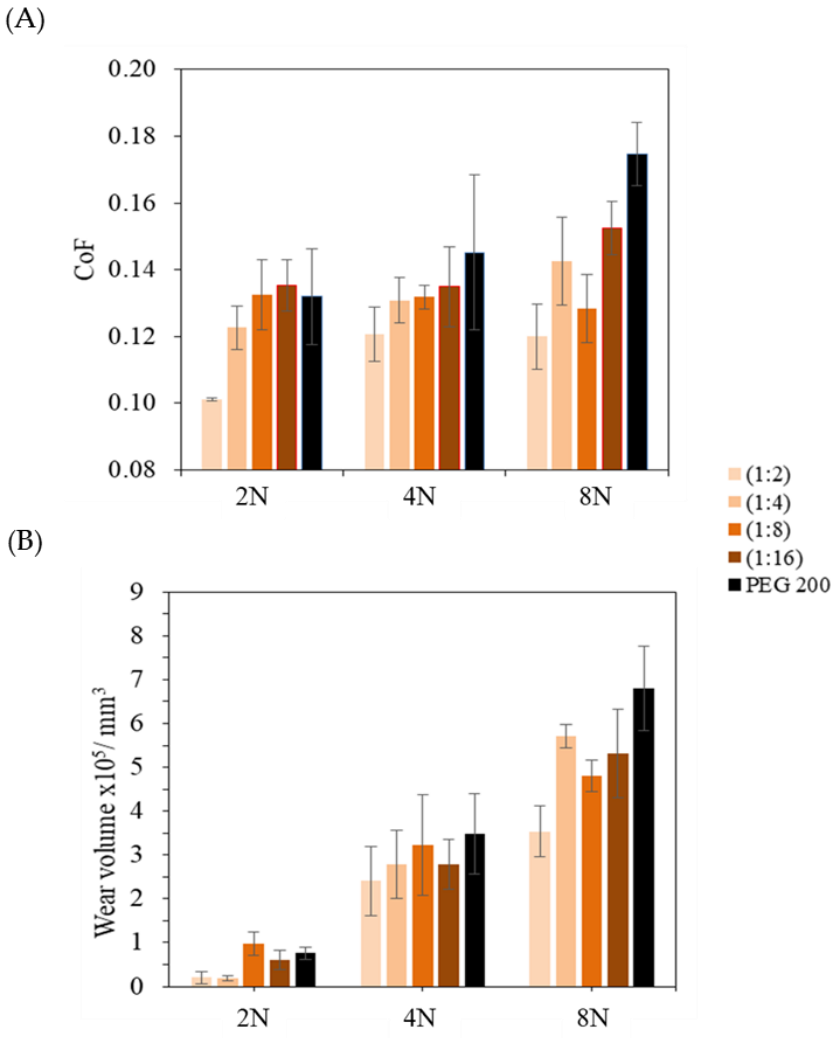

Figure 3.1.5. Average CoF values (A) and average wear volumes (B) obtained with PEG200 and the ESs in tribological tests with the pair steel/Si under normal forces of 2N, 4N and 8N and 2375 cycles. The errors are ± standard deviation (n ≥ 3) for CoF and (n ≥ 3) for wear.

Due to the brittleness of the Si surface, the wear tracks present a wide variability, and the errors associated with the wear measurements are large; even though, it is possible to conclude that wear increases as the normal force increases and the most significant differences are observed for the largest force (8 N). In this case, wear was maximum for PEG200 and minimum for ES [C_6-4-pic][TfO]:PEG200 (1:2).

The wear scars on the Si surface and the steel ball for a load of 8N are shown in Figure 3.1.6.

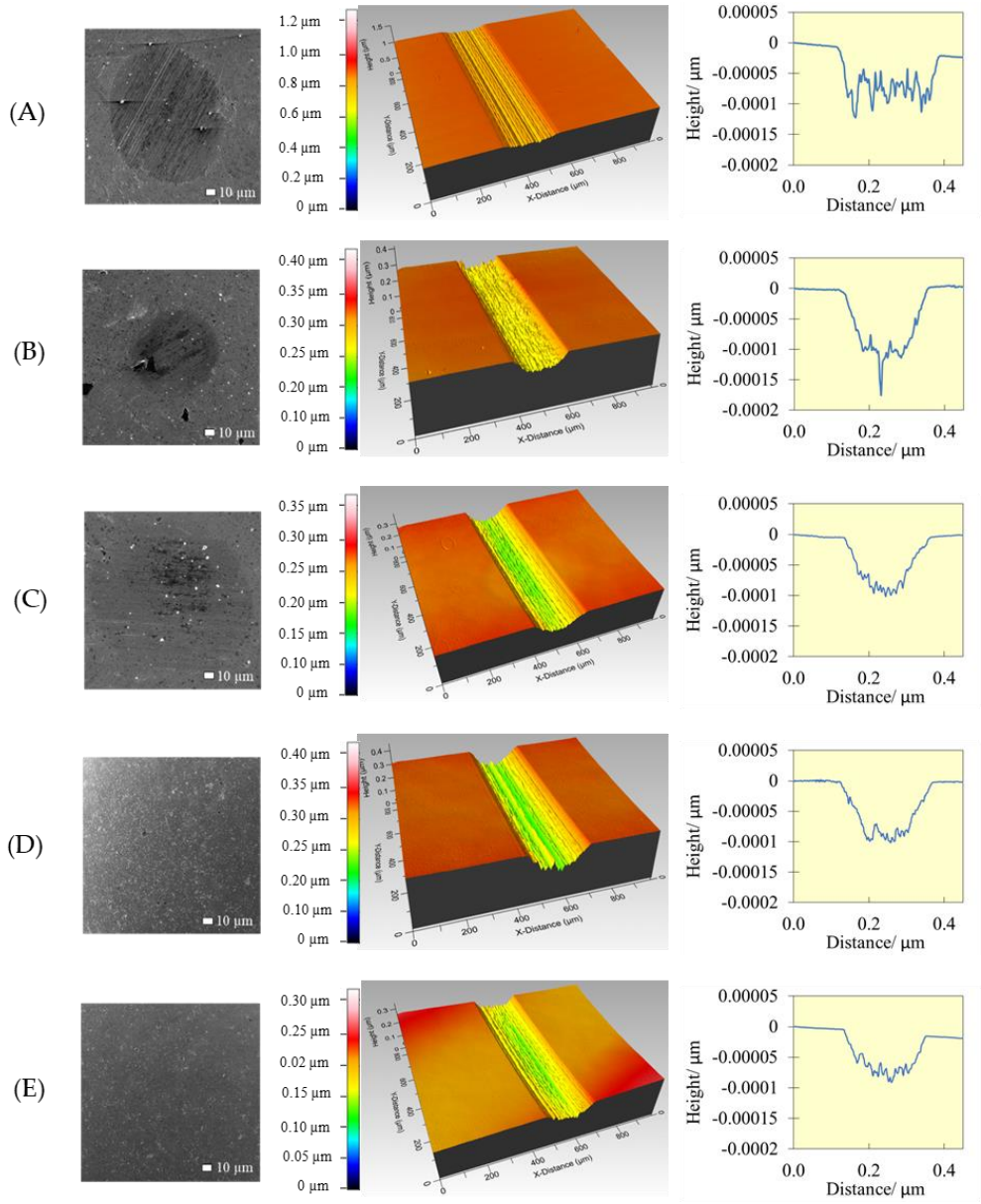

Figure 3.1.6. Worn surfaces of the steel ball (SEM images with 300× magnification, left) and the Si surface (profilometer images 20× magnification, right) after the tribological tests using as lubricants: PEG200 (A), 1:16 (B), ES 1:8 (C), ES 1:4 (D) and ES 1:2 (E).

The SEM images of the worn spheres show a maximum wear for PEG200 which decreases for increasing concentration of the IL. No wear can be detected when using the ESs 1:4 and 1:2. The cross-section profiles of the wear tracks on the Si substrates are wider for PEG200, while the ES 1:2 yielded the least deep profile, in agreement with the results of Figure 3.1.5B for the load of 8N.

Altogether, the tribological results indicate that the ESs present better lubrication properties than PEG200. A possible explanation for this behavior may be attributed to the chemical

adsorption of the ions at the Si surface. While the molecules of PEG200 weakly bond to Si through dipole interactions with the Si-O groups, the sulfur atom in the [TfO] anion may interact with non-oxidized Si leading to S-O-Si bonds, and the less sterically hindered CH groups of the aromatic ring of the picolinium cation may establish hydrogen bonding with the oxidized Si. However further studies are necessary to prove this proposed explanation.

The main objective of this work was to investigate a possible correlation between the composition of the ESs, namely the proximity of the eutectic point, and their lubrication capacity. Although we could not unequivocally demonstrate that the composition 1:2 is the eutectic point, the results of the characterization of the mixtures with different techniques converge on the conclusion that stronger interactions exist between the IL and PEG200 for this composition. The ES 1:2 presented the largest supercooled liquid region, the highest viscosity and the largest shifts in the peaks characteristic of the FTIR spectrum. Also, from the results of 2D-NMR experiment for this composition, it is clear that hydrogen bonds are formed between the cation of the IL and PEG200.

Among the various molar ratios investigated, the ES 1:2 presents the best lubrication capacity for the most severe conditions (higher load and longer time). This behavior may be attributed to the highest viscosity of this ES which ensures the formation of a thicker lubricant film. Furthermore, the stronger interactions detected between PEG200 and the IL for this particular composition, could also contribute for a higher stability of the film. The strong hydrogen bond network established around the eutectic composition, which prevents crystallization, ensures a favorable packing in the ES. This effect may result in the increase of the stability of the adsorbed boundary layer formed on the sliding surfaces, which leads to the decrease in friction and wear under high load. These results are in agreement with the optimum tribological performance of DES based on quaternary ammonium salts, at the eutectic composition, previously reported by Abbott *et al*.[5]

3.1.4 Conclusions

In this work the tribological behavior of eutectic systems composed by PEG200 and [C_6-4-pic][TfO] with several molar ratios (1:2, 1:4, 1:8 and 1:16) was investigated to look for an eventual correlation between the composition and the lubrication performance. The optimum tribological performance was found for the composition 1:2, which is the ratio associated with stronger interactions between the mixture components. The mixture with this molar ratio packs in order to maximize the hydrogen bonds and leads to the formation of a stable tribofilm which ensures the lowest values of CoF and wear of the Si surface for the highest applied load. Further studies are needed using other types of ESs with well-known eutectic points, to fully understand the mechanism of Si lubrication by ESs and the role of their composition.

3.1.5 References

[1] A. P. Abbott, G. Capper, D. L. Davies, H. L. Munro, R. K. Rasheed, V. Tambyrajah, Preparation of Novel, Moisture-Stable, Lewis-Acidic Ionic Liquids Containing Quaternary Ammonium Salts With Functional Side Chains, *Chem. Commun*. **2001**, *1*, 2010–2011. https://doi.org/10.1039/b106357j

[2] E. L. Smith, A. P. Abbott, K. S. Ryder, Deep Eutectic Solvents (DESs) and Their Applications, *Chem. Rev*. **2014**, *114*, 11060–11082. https://doi.org/10.1021/cr300162p

[3] M. A. R. Martins, S. P. Pinho, J. A. P. Coutinho, Insights Into the Nature of Eutectic and Deep Eutectic Mixtures, *J. Solution Chem*. **2019**, *48*, 962–982. https://doi.org/10.1007/s10953-018-0793-1

[4] A. P. Abbott, D. Boothby, G. Capper, D. L. Davies, R. K. Rasheed, Deep Eutectic Solvents Formed Between Choline Chloride and Carboxylic Acids: Versatile Alternatives to Ionic Liquids, *J. Am. Chem. Soc*. **2004**, *126*, 9142–9147. https://doi.org/10.1016/j.energy.2016.08.057

[5] S. D. A. Lawes, S. V. Hainsworth, P. Blake, K. S. Ryder, A. P. Abbott, Lubrication of Steel/Steel Contacts by Choline Chloride Ionic Liquids, *Tribol. Lett*. **2010**, *37*, 103–110. https://doi.org/10.1007/s11249-009-9495-6

[6] A. P. Abbott, E. I. Ahmed, R. C. Harris, K. S. Ryder, Evaluating Water Miscible Deep Eutectic Solvents (DESs) and Ionic Liquids as Potential Lubricants, *Green Chem*. **2014**, *16*, 4156–4161. https://doi.org/10.1039/c4gc00952e

[7] I. Garcia, S. Guerra, J. de Damborenea, A. Conde, Reduction of the Coefficient of Friction of Steel-Steel Tribological Contacts by Novel Graphene-Deep Eutectic Solvents (DESs) Lubricants, *Lubricants* **2019**, *7*, 37. https://doi.org/10.3390/lubricants7040037

[8] J. E. Hallett, H. J. Hayler, S. Perkin, Nanolubrication in Deep Eutectic Solvents, *Phys. Chem. Chem. Phys.* **2020**, *22*, 20253–20264. https://doi.org/10.1039/d0cp03787g

[9] M. Antunes, A. S. Campinhas, M. de Sá Freire, F. Caetano, H. P. Diogo, R. Colaço, L. C. Branco, B. Saramago, Deep Eutectic Solvents (DES) Based on Sulfur as Alternative Lubricants For Silicon Surfaces, *J. Mol. Liq*. **2019**, *295*, https://doi.org/10.1016/j.molliq.2019.111728

[10] Z. Rymuza, Control Tribological and Mechanical Properties of MEMS Surfaces. Part 1: Critical Review, *Microsyst. Technol*. **1999**, *5*, 173–180. https://doi.org/10.1007/s005420050160

[11] H. Liu, B. Bhushan, Nanotribological Characterization of Molecularly Thick Lubricant Films for Applications to MEMS/NEMS by AFM, *Ultramicroscopy* **2003**, *97*, 321–340. https://doi.org/10.1016/S0304-3991(03)00058-5

[12] J. J. Nainaparampil, K. C. Eapen, J. H. Sanders, A. A. Voevodin, Ionic-Liquid Lubrication of Sliding MEMS Contacts: Comparison of AFM Liquid Cell and Device-Level Tests, *J. Microelectromechanical Syst*. **2007**, *16*, 836–843.

https://doi.org/10.1109/JMEMS.2007.901628

[13] J. Y. Leong, J. Zhang, S. K. Sinha, A. Holmes, H. Spikes, T. Reddyhoff, Confining Liquids on Silicon Surfaces to Lubricate MEMS, *Tribol. Lett*. **2015**, *59*, 1–11. https://doi.org/10.1007/s11249-015-0541-2

[14] B. Yu, F. Zhou, Z. Mu, Y. M. Liang, W. M. Liu, Tribological Properties of Ultra-Thin Ionic Liquid Films on Single-Crystal Silicon Wafers With Functionalized Surfaces, *Tribol. Inter.* **2006**, *39*, 879-887. https://doi.org/10.1016/j.triboint.2005.07.039

[15] Y. Mo, W. Zhao, M. Zhu, M. Bai, Nano/Microtribological Properties of Ultrathin Functionalized Imidazolium Wear-Resistant Ionic Liquid Films on Single Crystal Silicon, *Tribol. Lett.* **2008**, *32*, 143-151. https://doi.org/10.1007/s11249-008-9371-9

[16] B. G. Xie, Q. Wang, L. Si, S. Liu, G. Li, Tribological Characterization of Several Silicon-Based Materials Under Ionic-Liquids Lubrication, *Tribol. Lett*. **2009**, *36*, 247-257. https://doi.org/ 10.1007/s11249-009-9480-0

[17] M. Palacio, B. A. Bhushan, A Review of Ionic Liquids for Green Molecular Lubrication in Nanotechnology, *Tribol. Lett*. **2010**, *40*, 247-268. https://doi.org/ 10.1007/s11249-010-9671-8

[18] Y. Mo, F. Huang, F. Zhao, Functionalized Imidazolium Wear-Resistant Ionic Liquid Ultrathin Films for MEMS/NEMS Applications, *Surf. Interface Anal*. **2011**, *43*, 1006-1014. https://doi.org/10.1002/sia.3684

[19] W. Zhao, J. Pu, Q. Yu, Z. Zeng, X. Wu, Q. Xue, A Novel Strategy to Enhance Micro/Nano-Tribological Properties of DLC Film by Combining Micro-Pattern and Thin Ionic Liquids Film, *Colloids Surf. A* **2013**, *428*, 70-78. https://doi.org/10.1016/j.colsurfa.2013.03.047

[20] G. Xie, J. Luo, D. Guo, S. Liu, Nanoconfined Ionic Liquids Under Electric Fields, *Appl. Phys. Lett.* **2010**, *96*, 043112. https://doi.org/10.1063/1.3292213

[21] M. T. Donato, F. Caetano, R. Colaço, L. C. Branco, B. Saramago, Picolinium-Based Hydrophobic Ionic Liquids as Additives to Lubricate Steel-Silicon Contacts, *Chemistry Select* **2020**, *5*, 5864-5872. https://doi.org/10.1002/slct.202000613

[22] J. J. Moura Ramos, R. Taveira-Marques, H. P. Diogo, Estimation of the Fragility Index of Indomethacin by DSC Using the Heating and Cooling Rate Dependency of the Glass Transition, *J. Pharm. Sci*. **2004**, *93*, 1503-1507. https://doi.org/ 10.1002/jps.20061

[23] J. Restolho, J. L. Mata, B. Saramago, On the Interfacial Behavior of Ionic Liquids: Surface Tensions and Contact Angles, *J. Colloid Interface Sci*. **2009**, *340*, 82-86. https://doi.org/10.1016/j.jcis.2009.08.013

[24] Q. Zhang, K. O. Vigier, S. Royer, F. Jérôme, Deep Eutectic Solvents: Syntheses, Properties and Applications, *Chem. Soc. Rev*. **2012**, *41*, 7108–7146. https://doi.org/10.1039/C2CS35178A

[25] R. Haghbakhsh, A. R. C. Duarte, S. Raeissi, Viscosity Investigations on the Binary Systems of (1 ChCl:2 Ethylene Glycol) DES and Methanol or Ethanol, *Molecules* **2021**, *26*, 5513. https://doi.org/10.3390/molecules26185513

[26] B. C. Smith, Infrared Spectral Interpretation – A Systematic Approach. CRC Press, Boca Raton, **1998**.

[27] J. Joseph, E. Jemmis, Red-, Blue-, or No-Shift in Hydrogen Bonds: A Unified Explanation, *J. Am. Chem. Soc*. **2007**, *129*, 4620-32. https:// doi.org/ 10.1021/ja067545z

[28] R. Gautam, N. Kumar, J. G. Lynam, Theoretical and Experimental Study of Choline Chloride-Carboxylic Acid Deep Eutectic Solvents and Their Hydrogen Bonds, *J. Mol. Struct*. **2020**, *1222*, 128849. https://doi.org/10.1016/j.molstruc.2020.128849

3.2

HYDROPHOBIC DEEP EUTECTIC SOLVENTS AS LUBRICANTS

This chapter presents the results obtained using Deep Eutectic Solvents as lubricants and it is based on the submitted paper **M. T. Donato**, H. P. Diogo, J. Deuermeier, R. Colaço, L. C. Branco, B. Saramago, Hydrophobic Deep Eutectic Solvents with anti-wear properties for NEMs/MEMs, ACS Applied Materials & Interfaces, **2023**.

3.2.1 Introduction

In the last decade, investigation on the properties and applications of eutectic systems (ESs) increased exponentially. Among the ESs, those characterized by a large melting point depression, the so-called deep eutectic solvents (DES), deserved special attention. They have in common with ionic liquids (ILs) the possibility of tuning their properties by changing the combination of hydrogen bond donor (HBD) and hydrogen bond acceptor (HBA). DES can be used in almost all applications of ILs, with the advantage of being cheaper, less toxic and easier to prepare. The majority of the studied DES are hydrophilic and loose their integrity in water.[1] In 2015, the group of Kroon presented the first hydrophobic DES.[2] They consisted of a fatty acid (decanoic acid) as HBD, and, as HBA, the ammonium salts: tetrabutylammonium chloride ($[N_{4444}][Cl]$), methyltrioctylammonium chloride ($[N_{8881}][Cl]$ also designated as [Aliquat]Cl), tetraheptylammonium chloride ($[N_{7777}][Cl]$), tetraoctylammonium chloride ($[N_{8888}][Cl]$), methyltrioctylammonium bromide ($[N_{8881}][Br]$) and tetraoctylammonium bromide ($[N_{8888}][Br]$). These new solvents proved to have high extraction efficiency for volatile fatty acids from aqueous solutions and gave rise to a new research line in the field of DES. In the same year, a second type of hydrophobic DES was proposed by the group of Marrucho, composed by two neutral compounds, DL-menthol and carboxylic acids.[3] Since then, the number of publications on hydrophobic DES steadily increased, and their potential use in extraction of bioactive and medical compounds, contaminant removal, metal extraction, CO_2 capture, reaction media, formation of hydrogels and membranes, photoluminescence and dye sensitized solar cells and even Covid-19 control, has been investigated.[4-6] Besides the low solubility in water, the hydrophobicity of DES leads to somewhat peculiar properties. The hydrophobic DES are less thermally stable than the hydrophilic DES, and are slightly less dense than water, in contrast with the hydrophilic ones. The melting point depression and the viscosity of hydrophobic DES vary over a wide range: high values may be achieved for DES composed by salts due to extensive hydrogen bonding, while small values are usual for those composed by neutral components. It is possible to tune the viscosity through the size of the HBD or HBA chains; for example, in the case of DES based on tetraalkyl quaternary ammonium salts, the viscosity increases with the increase of the alkyl chains, but the existence of long branched chains leads to a decrease in viscosity due to the shielding of the charge in the nitrogen atom.[7]

Among the numerous applications of hydrophilic DES, lubrication is one of the least explored. The group of Abbott [8-10] reported good capacity of DES to lubricate steel/steel contacts but a less satisfying performance with aluminum surfaces, which are moderately hydrophobic. Lawes [8] found that DES based on choline chloride combined with urea and ethylene glycol are better lubricants of steel/steel contacts in the early stages of lubrication than mineral oils, but friction increased after a short period. Our group prepared new DES from salts based on sulfur-containing anions and polyethylene glycol (PEG200) to lubricate the pair steel ball/Si

substrate.[11,12] The best lubricants were the DES composed by the salts: 1-hexyl-4-picolinium trifluoromethanesulfonate [C_6-4-pic][TfO], 1-ethyl-3-methylimidazolium (S)-camphorsulfonate ([C_2MIM][(*S*)CSA], and 1-methyl-3-picolinium methyl sulfate ([C_1-3-pic][$MeSO_4$]). Their lubrication capacity was attributed to the formation of adsorbed ordered layers that support the load together with the liquid film retained among the asperities of the opposing surfaces. All mixtures led to lower friction coefficients than the model lubricant, PEG200.

To our knowledge, there are no studies reported in the literature about the lubricating properties of hydrophobic DES. However, the fact that the miscibility of the lubricant with water during operation in ambient conditions is undesirable, makes hydrophobic DES particularly adequate for this application. In this work, the performance of both ionic and non-ionic hydrophobic DES as lubricants of the tribological pairs steel ball/Si surface and Si ball /Si surface was assessed. The importance of the investigation of Si surfaces results from the fact that micro and nanoelectromechanical systems (MEMS and NEMS) are traditionally made of Si. When MEMS and NEMS involve motion, an efficient lubrication is fundamental to avoid adhesion, friction and wear problems since Si is a very fragile material.[13,14] Two families of hydrophobic DES using different HBAs were tested: one based on non-ionic menthol component; other based on ionic quaternary ammonium salts. Menthol was chosen because it is a cheap, natural component with a very low solubility in water, while hydrophobic DES based on quaternary ammonium salts are the most studied. All prepared DES (see Figure 3.2.1) have been previously reported in the literature, as follows: menthol:hexanoic acid (1:1),[15] menthol:octanol (1:1),[16] [N_{4444}][Br]:hexanoic acid (1:1),[17] [N_{4444}][Br]:octanol (1:2),[18] [Aliquat][Cl]:hexanoic acid (1:1),[17] [Aliquat][Cl]:octanoic acid (1:1),[17] [Aliquat][Cl]:decanoic acid (1:2),[2] [Aliquat][Cl]:octanol (1:1),[17] [Aliquat][Cl]:hexanol (1:2)[19] and [Aliquat][Cl]:menthol (1:2).[19,20] The relevant physicochemical properties of the DES for tribological application were measured. The lubrication capacity of these mixtures was compared to hexadecane, a mineral oil considered as the model lubricant of MEMS/NEMS. The initial screening of all DES was made with steel spheres, while the most expensive Si spheres were used to test the best performing liquids. The sliding surfaces were imaged after the tribological tests using profilometry and Scanning Electron Microscopy (SEM) and chemically analyzed with X-ray Photoelectron Spectroscopy (XPS). The behavior of the best lubricants was further investigated through thermal analysis and hot stage polarization microscopy.

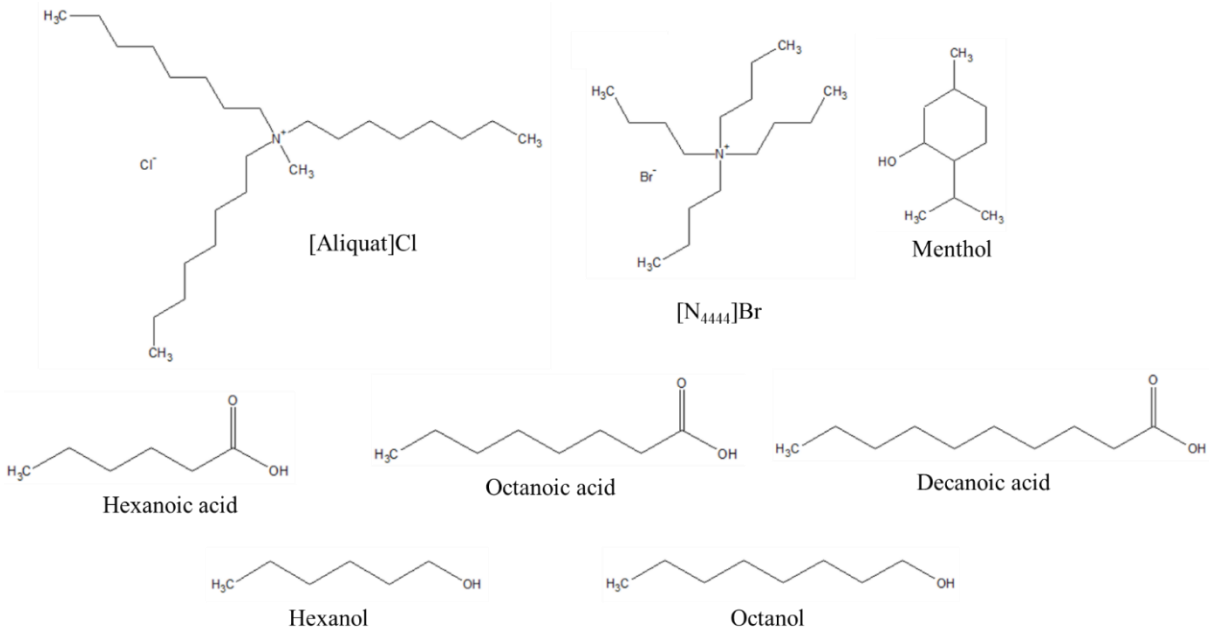

Figure 3.2.1. Molecular structures of the components (HBA or HBD) of the studied eutectic systems.

Finally, the effects of the presence of small amounts of water absorbed from ambient were tackled, considering that DES are hygroscopic and contact with humid atmosphere in all industrial applications. The impact of water on the physicochemical properties and supramolecular network of DES has been recently addressed by several authors.[21-24] NMR studies and molecular simulation were used to understand the changes in structural and transport properties of hydrophobic DESs exposed to water vapor.[24] The results obtained with [N_{4444}][Cl]:decanoic acid (1:2) indicated that very small amounts of water break the hydrogen bonding network and enhance mobility leading to a decrease in viscosity. Furthermore, the hydrated chloride ions become free and make the solvent more acidic as well as more corroding. In the present work, changes in the physicochemical properties of [Aliquat]Cl:octanol (1:1) and [Aliquat]Cl:menthol (1:2) and their tribological behavior induced by the presence of water were assessed.

3.2.2 Experimental

3.2.2.1 Materials

The reagents used for the preparation of the DESs were the following: trioctylmethylammonium chloride [Aliquat]Cl from Alfa Aesar (USA), hexanoic acid ≥98% from Sigma-Aldrich (USA), octanoic acid >98% from Sigma Aldrich (USA), decanoic acid 99% from Alfa Aesar (USA), 1-hexanol 99% from Sigma-Aldrich (USA), 1-octanol 99% from Alfa

Aesar (USA), menthol >98% from Sigma Aldrich (USA) and tetramethylammonium bromide [N_{4444}]Br 98% from Alfa Aesar (USA). Hexadecane 99% was obtained from Sigma-Aldrich. The solvents were deuterated water 99.9% and deuterated chloroform 99.9% from Eurisotop (France). Distilled and deionized water (DD) was obtained with a Millipore system.
Si b100N wafers (Si-Mat, Germany), with 0.5 mm of thickness, 1 nm of root mean square (RMS) roughness and 1121-1428 HV of hardness, were cut in squares (1×1 cm^2) to be used in the tribological tests and the contact angle measurements. Spheres of stainless steel (SS) AISI 316L grade 100 (Atlas Ball & Bearing Co. Ltd., UK) with 6 mm of diameter, roughness RMS=1 μm and hardness of 260-390 HV and Si spheres with 6 mm of diameter and 15 nm of RMS roughness (J. Hauser GMBH &Co., Germany) were used as counter-bodies.

3.2.2.2 Methods

The DESs were prepared by mixing the HBD and HBA components, in the indicated molar ratios, under vigorous stirring for 24h and their HBD:HBA proportion was checked by ^{1}H-NMR experiments (Bruker 400MHz, model Avance III, USA). The ^{1}H-NMR spectra are presented in Figure A.4.1 in Annex A.4. The DES samples were used without further treatment. Wet DES samples were prepared by the addition of 2% (w/w) of water. This amount of water was chosen because it was the highest attainable water content that kept the solutions homogeneous. The water content was measured with a HB43-S Halogen Moisture Analyzer (Mettler Toledo, Greifensee, Switzerland). The thermal behavior of DES with and without water was determined through thermal analysis using a differential scanning calorimeter (2820 Modulated DSC TA Instruments, New Castle DE, USA). The samples were sealed in aluminum crucibles and submitted to one cycle in the temperature range -105 °C to 50 °C with a heating/cooling rate of 5 °C/min. The thermograms were analyzed with the software Universal Analysis 2000 TA Instruments. HSPM observations were performed on a BX51 Optical Microscope (Olympus, Florida, USA). The temperature changes and stabilization were set by a Linkam LTS360 liquid nitrogen cooled cryostage and were measured with a Pt resistance thermometer. Observations were carried out in the temperature range from ambient temperature to 120 °C at a heat rate of 15 °C·min^{-1}, using an Olympus SC-30 camera for picture record.
The viscosities were measured at 25 °C using a rheometer (MCR 92, Anton Paar, Austria). The contact angles of the liquids on the Si substrates were determined by the sessile drop method at room temperature.[25] The Si substrates were cleaned according to the following procedure: 2×15 min sonication in Dextran® solution (0.2% v/v in water) intercalated with 10 min sonication in water, followed by 3×10 min sonication in water, rinsing with DD water, flushing with nitrogen, and drying overnight in a vacuum oven at room temperature. The measurements were made inside an ambient chamber model 100-07-00 (Ramé-Hart,

Succasunna, NJ, USA), under a weak flow of dry nitrogen to avoid water absorption by the liquids. The images of drops were obtained with a video camera (jAi CV-A50, Barcelona, Spain) mounted on a microscope Wild M3Z (Leica Microsystems, Wetzlar, Germany) and they were analyzed by running the ADSA (Axisymmetric Drop Shape Analysis, Applied Surface Thermodynamics Research Associates, Toronto, Canada) software.

The friction coefficients of the DESs and hexadecane, a model lubricant, were measured using a tribometer (TRB^3, Anton Paar, Switzerland) in the configuration reciprocating ball-on-flat. The 316-L stainless steel spheres (6 mm radius) were used as counter-bodies in the preliminary tests for the DES screening, and afterwards, they were substituted by Si spheres (6 mm radius). Both types of spheres were rubbed against flat Si surfaces. The spheres and the Si surfaces were cleaned using the above mentioned protocol. The spheres were placed on the tribometer arm and the Si substrates were glued to a metallic container, to which a determined amount of liquid was added in order to guarantee the full coverage of the surfaces. The amplitude of the reciprocal movement of the counter-body was 4 mm. A low normal force of 1 N was applied for the short duration tests (85 cycles, corresponding to 0.68 m of sliding distance) to minimize the wear of the surfaces. For each of these tests, the sliding speed varied between 1 and 20 mm·s^{-1}. With the objective of studying wear, longer tests (2375 cycles, corresponding to 19 m of sliding distance) were carried out with higher loads of 2, 4, 8, 10 and 12N and a constant speed of 8 mm·s^{-1}. For these tests, the Hertz contact stresses varied between 0.7 GPa for 2N and 1.3 GPa for 12N. All the experiments were done at room temperature (~25 °C) and relative humidity ~ 45%, at least in triplicate, and the results were analyzed using the software TriboX. After the long tribological tests, the Si substrates and the Si spheres were carefully cleaned with acetone to remove any trace of DES and then dried with nitrogen. The surfaces of the Si substrates were imaged using an optical profilometer (Profilm 3D, Filmetrics, USA) and their worn volumes were assessed. For each track, the worn volume was estimated by multiplying the track length by the average of the cross-sectional areas of the worn track determined by numerical integration of the 2D profiles (3-5 measurements per track). A Scanning Electron Microscope (SEM) JEOL JSM7001F (Tokyo, Japan) was used for imaging, at higher magnification, the clean surfaces of the Si substrates and the spheres after the tribological tests. The elemental composition of the wear tracks on the Si substrates and the Si spheres was studied by X-ray photoelectron spectroscopy (XPS), using an Axis Supra spectrometer from Kratos Analytical (Manchester, UK). A monochromatic Al Kα source was run at 225W. The detailed spectra were acquired at a pass energy of 20 eV through an aperture of 110 μm. Data analysis was done with CasaXPS software. Atomic percentages were calculated assuming a homogenous distribution of elements, using the Kratos relative sensitivity factors. Due to the occurrence of slight differential charging, the Si 2p$_{3/2}$ binding energy of elemental silicon was used for charge referencing to 99.35 eV.

The corrosive behavior was assessed through the comparison of the Si substrates before and after being exposed to 5 μL of DES and wet DES samples during two weeks at room temperature (~25 °C), inside a sealed vessel containing a saturated aqueous solution of potassium carbonate, which ensures a relative humidity of 45%. The Si surfaces were analyzed by visual inspection and by SEM, after being carefully cleaned with acetone and dried with nitrogen.

3.2.3 Results and Discussion

3.2.3.1 Characterization of the DESs

The viscosity was measured, at constant temperature, as a function of the shear rate and all liquids exhibited Newtonian behavior. The water content, the viscosity at 25 °C and the contact angle on Si of hexadecane and the DESs are given in Table 3.2.1. The viscosities of the liquids vary significantly between them: it is possible to distinguish low viscous (hexadecane, menthol:hexanoic acid (1:1) and menthol:octanol (1:1)), moderate viscous ([Aliquat]Cl:hexanol (1:2) and [N_{4444}]Br:octanol (1:2)) and highly viscous ([Aliquat]Cl:hexanoic acid (1:1), [Aliquat]Cl:octanoic acid (1:1), [Aliquat]Cl:decanoic acid (1:2), [Aliquat]Cl:octanol (1:1), [Aliquat]Cl:menthol (1:2) and [N_{4444}]Br:hexanoic acid (1:1)). The viscosity depends on the molar ratio of the components and, for the same molar ratio, increases with the length of the alkyl chains present on each component. The lack of agreement with the values found in the literature is not surprising because these were obtained in different/ unknown conditions and viscosity is strongly dependent on temperature and water content. The best wettability of the Si surface was observed for hexadecane and menthol:octanol (1:1), but all DES exhibited low contact angles.

Table 3.2.1. Viscosity, η, at 25 °C and equilibrium contact angle on Si substrates of hexadecane and the DESs. The standard deviations correspond to n = 3 for viscosity and n ≥ 4 for contact angle. The viscosity values found in literature are included.

Lubricants	Water content/ %	η/ mPa·s	Contact angle/ °
Hexadecane	0.3	2.6±0.2; 3.0[a]	14±2
[Aliquat]Cl:hexanoic acid (1:1)	4.6	338±2	24±1
[Aliquat]Cl:octanoic acid (1:1)	2.4	548±1	29±3
[Aliquat]Cl:decanoic acid (1:2)	0.3	259±1; 783.41 [2][b]	24±3
[Aliquat]Cl:hexanol (1:2)	4.2	115±1	24±2
[Aliquat]Cl:octanol (1:1)	1.6	278±1	22±3
[Aliquat]Cl:menthol (1:2)	2.1	400±1; 257.6 [20][c]	28±2
[N_{4444}]Br:octanol (1:2)	5.5	108±1	33±3
[N_{4444}]Br:hexanoic acid (1:1)	2.0	366±5	22±3
Menthol:hexanoic acid (1:1)	4.4	11±1	26±3
Menthol:octanol (1:1)	3.3	15±1; 13.1 [16][d]	14±2

[a] T. M.Aminabhavi, B. Gopalkrishna, Densities, Viscosities, Refractive Indices, and Speeds of Sound of the Binary Mixtures of Bis-(2-methoxyethyl) Ether with Nonane, Decane, Dodecane, Tetradecane, and Hexadecane at 298.15, 308.15, and 318.15 K. *J.Chem.Eng.Data* **1994**, *39*, 529-534

[b] Water content 2580 ppm

[c] Unknow water content

[d] Unknown temperature

3.2.3.2 Tribological tests with the tribopair SS/Si

Preliminary experiments were performed for the tribopair SS sphere/Si substrate for a load of 1N in order to evaluate the lubrication capacity of the prepared DESs. A low load and short duration were chosen to avoid wear, which complicates the interpretation of the friction results. The Stribeck curves (CoF *vs.* speed, v/ mm·s^{-1}) for the two sets of DESs (ionic and non-ionic) are presented in Figure 3.2.2. Stribeck curves are usually presented as a function of Z, the Sommerfeld parameter but, since the viscosities of the liquids are very different, the lubrication regimes are not the same, making the representation as a function of Z difficult to understand.

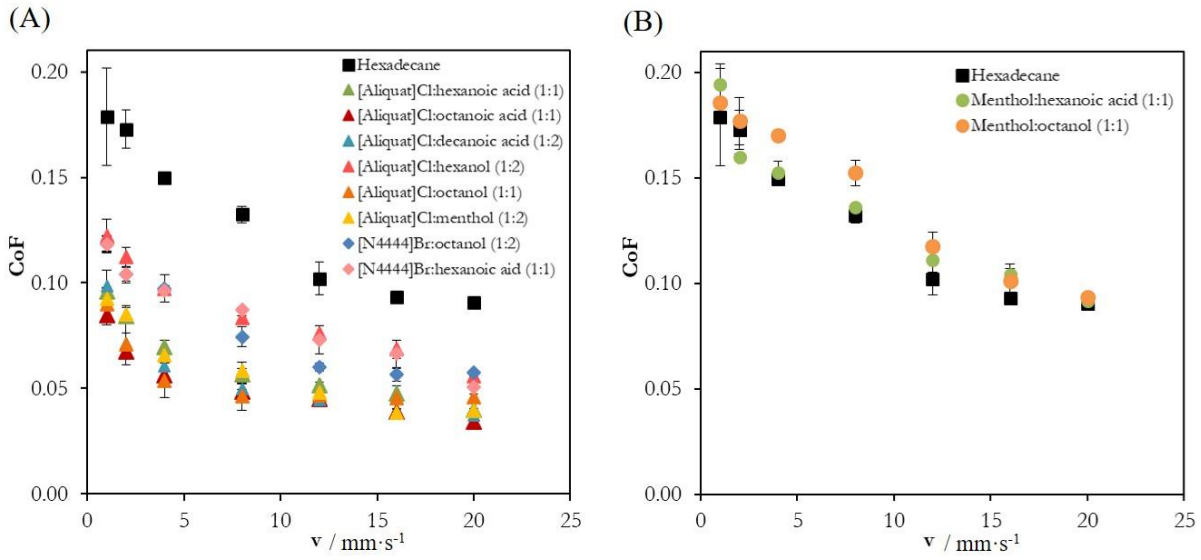

Figure 3.2.2. CoF *vs.* speed, *v*/ mm·s^{-1}, for the pair SS sphere/Si substrate using: (A) ionic and (B) non-ionic DESs. Hexadecane was added for comparison purposes. The errors are ± standard deviation (n ≥ 3).

All the prepared ionic DESs led to a decrease in the CoF when compared to hexadecane. On the contrary, the non-ionic ones did not lead to improvement of the CoF values. The most plausible reason for this behavior is the very low viscosity of these mixtures that hampers their lubrication capacity. It is possible to see that the ionic DES containing [Aliquat]Cl yielded the lowest CoF, except for [Aliquat]Cl:hexanol (1:2), which behaved similarly to the DESs containing [N_{4444}]Br. Once again, the lowest viscosity of [Aliquat]Cl:hexanol (1:2) when compared to the other [Aliquat]Cl-based DES may justify the poorer tribological performance. All liquids wet the Si surface, and no correlation can be found between CoFs and the contact angle values.

3.2.3.3 Tribological tests with the tribopair Si/Si

Among the best DESs tested with the tribopair SS/Si for the short tests at the load of 1N, [Aliquat]Cl:octanol (1:1) and [Aliquat]Cl:menthol (1:2) were chosen for further studies using the tribological pair Si sphere/Si substrate., which mimics the MEMS/NEMS operation. Figure 3.2.3 shows CoF *vs.* *v*/ mm·s^{-1} for the best performing DESs and hexadecane, added for comparison purposes. Comparing these results with the previous ones obtained with SS/Si, a CoF reduction is observed for all the liquids as Si spheres have a much smaller roughness (15 nm) than SS spheres (1 μm). The better performance of the DESs with respect to hexadecane is more significant in the boundary lubrication regime (low sliding velocities).

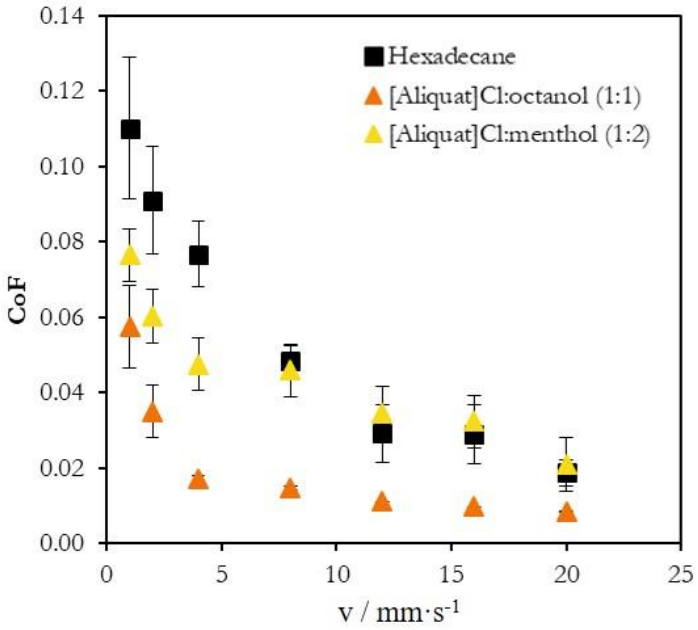

Figure 3.2.3. CoF *vs*. speed, *v*/ mm·s^{-1}, for the pair Si sphere/Si substrate using the best performing DESs in short tests under load of 1N. Hexadecane was added for comparison purposes. The errors are ± standard deviation (n ≥ 3).

With the aim of studying wear, longer tests (3738 s) were performed with higher loads of 2, 4, 8, 10 and 12N at a sliding velocity of 8 mm·s^{-1}. The choice of this value was based on the analysis of the Stribeck curves (Figure 3.2.2), which shows that for this intermediate speed the lubrication regime may be considered boundary/mixed, with the load being carried mainly by the surface asperities or partially by the asperities and the lubricant film. The obtained CoF values for the longer tests are presented in Figure 3.2.4 and may be grouped in two sets: lower loads (2, 4 and 8N), and higher loads (10 and 12N). At lower loads, both DES led to CoF values significantly lower than hexadecane, being the smaller values obtained with [Aliquat]Cl:octanol (1:1). However, for higher loads, the lubrication capacity of [Aliquat]Cl:octanol (1:1) dropped remarkably and the CoF value obtained under 10N is similar to the value of hexadecane. At 12 N, the substrates lubricated with both [Aliquat]Cl:octanol (1:1) and hexadecane broke after a few minutes of contact between the sliding surfaces. In contrast, [Aliquat]Cl:menthol (1:2) kept its excellent performance under these high loads. The time evolution of CoF measured in the experiments performed under the maximum load supported by the three tested liquids (10N) is presented in Figure A.4.2 (Annex A.4). The CoF values remain constant over time for all liquids, with the exception of hexadecane where a running-in period is visible and some sporadic peaks in the CoF values appear, giving evidence to the existence of third-body wear. This type of wear occurs due to the low

toughness of silicon which promotes adhesive wear, followed by the formation of the first debris which cause abrasion.[26,27]

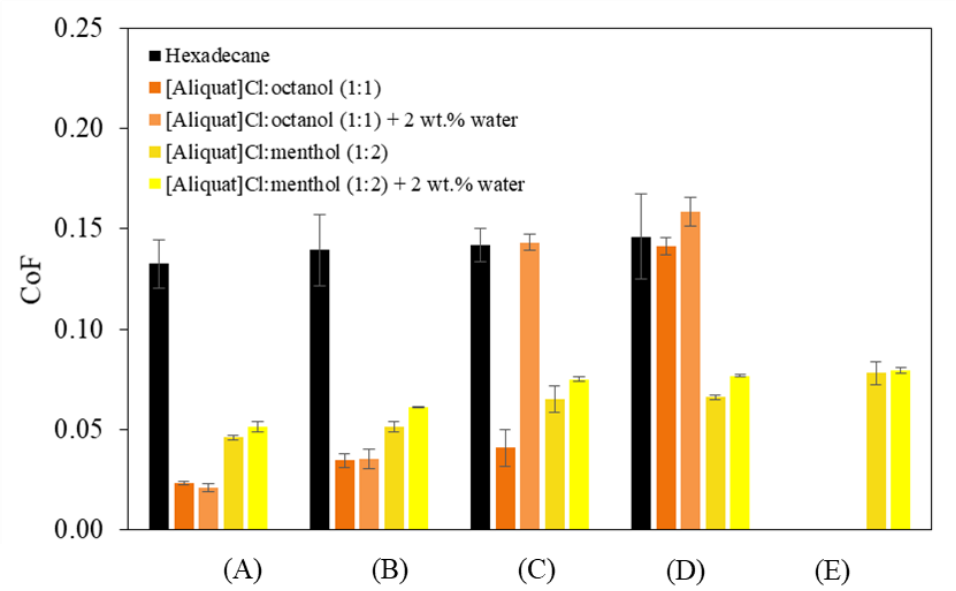

Figure 3.2.4. Average CoF values obtained for the longer tests with the pair Si sphere/Si substrate using hexadecane and the best performing DESs under the loads of 2N (A), 4N (B), 8N (C), 10N (D) and 12N (E). The errors are ± standard deviation (n ≥ 3). The results obtained with the DES with higher water content (2 wt.% of added water) are included for testing the effect of the presence of water in Section 3.2.3.4.

The surfaces of the Si substrates were imaged with a profilometer after the long tribological tests and the calculated wear volumes are given in Table 3.2.2.

Table 3.2.2. Wear volumes, in mm^3, obtained after long tribological tests for the load of 10N and the sliding speed of 8 $mm \cdot s^{-1}$. The errors are ± standard deviation (n ≥ 3).

Load/ N	Wear volume/ mm^3		
	Hexadecane	[Aliquat]Cl:octanol (1:1)	[Aliquat]Cl:menthol (1:2)
2	$2\times10^{-5}\pm9\times10^{-6}$	-	-
4	$3\times10^{-5}\pm6\times10^{-6}$	-	-
8	$8\times10^{-4}\pm8\times10^{-5}$	-	-
10	$1.4\times10^{-3}\pm6\times10^{-5}$	$13\times10^{-3}\pm3\times10^{-3}$	-

As an example, the images of the Si substrates after long tests with hexadecane, [Aliquat]Cl:octanol (1:1), and [Aliquat]Cl:menthol (1:2), under the load of 10N, are presented

in Figure 3.2.5. No wear was detected at the five studied loads for [Aliquat]Cl:menthol (1:2). In the case of hexadecane and [Aliquat]Cl:octanol (1:1), the wear could not be measured at 12 N because of the referred breakage of the substrates. Wear was detected at all loads for hexadecane and, only at 10 N, for [Aliquat]Cl:octanol (1:1). The wear volumes obtained with hexadecane increase steadily with the applied load. On the contrary, [Aliquat]Cl:octanol (1:1) exhibited a discontinuous behavior: the wear volume changed from zero to 1.3×10^{-2} mm^3 when the load increased from 8N to 10 N. A similar effect may be seen in the CoF values, which suffered a 4-fold increase. Comparison of the tribological performance of this DES with model lubricant hexadecane at 10 N shows that, although both liquids led to similar values of CoF, the wear volume obtained with [Aliquat]Cl:octanol (1:1) is nine times higher, which is in agreement with the much deeper and wider wear profile on the Si substrate. This shows that the DES [Aliquat]Cl:octanol (1:1) above a threshold value of pressure loses the lubrication capacity.

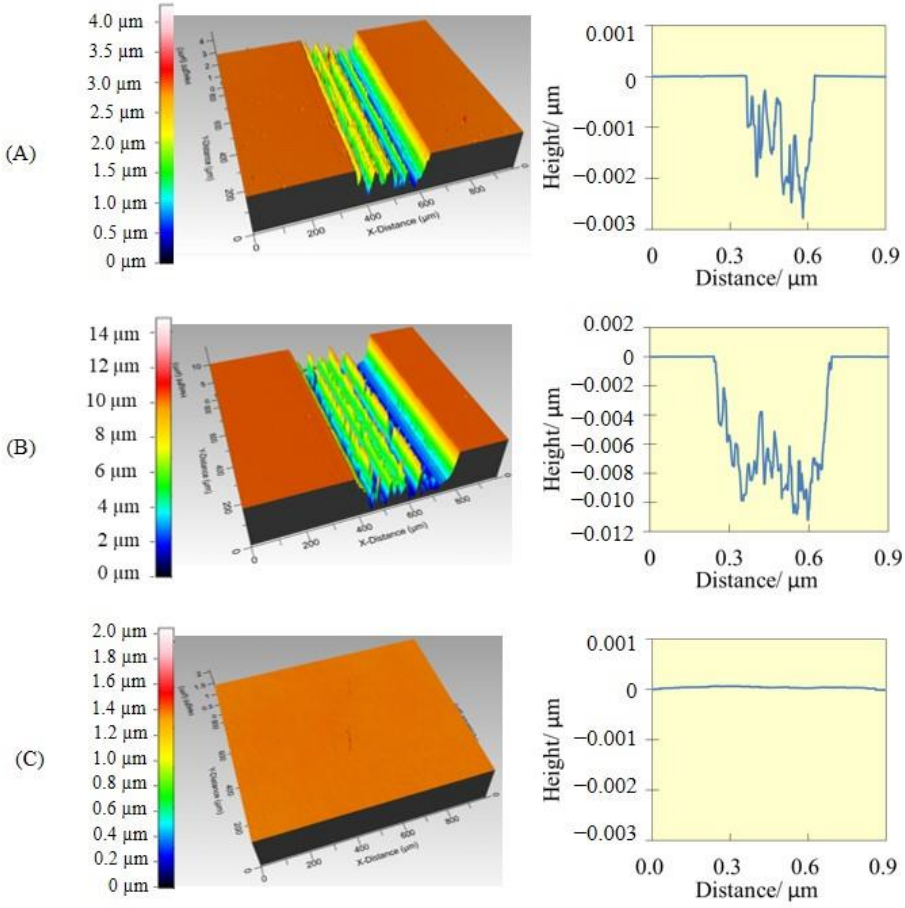

Figure 3.2.5. Profilometer images of the Si substrates (20× magnification) after long tribological tests under the load of 10N using as lubricants: (A) hexadecane, (B) [Aliquat]Cl:octanol (1:1) and (C) [Aliquat]Cl:menthol (1:2).

SEM images of the Si spheres and the Si substrates after long tests with hexadecane, [Aliquat]Cl:octanol (1:1) and [Aliquat]Cl:menthol (1:2), under the load of 10N, are shown in Figure 3.2.6. For the tests with hexadecane (Figure 3.2.6A), the worn surfaces of both spheres and substrates display signs of three body abrasive wear, where some debris and indentations on the surface can be clearly observed. The debris are small irregular-shaped Si fragments that are released from the surface during the tribological experiments. Some are black, resulting from the oxidation generated by heat and pressure. In addition to the abrasive scratches, the surface of the worn sphere shows darker areas, that may result from stress induced phase transformations, as previously observed by Arcifa *et al*.,[28] which are not visible on the surface of the substrate. The reason for the more intense wear of the sphere can be attributed to its permanent contact with the underlying substrate, while the substrate moves and contacts the sphere intermittently. In the case of [Aliquat]Cl:octanol (1:1), the SEM images show that the worn surfaces of the sphere and the substrate are practically free of debris (Figure 3.2.6B). Instead, plastic flow due to phase transformation of Si is visible on both worn surfaces, as well as abrasive scratches parallel to the direction of the sliding. As expected, the surfaces lubricated with [Aliquat]Cl:menthol (1:2) do not show any wear signs (Figure 3.2.6C).

In order to further understand the features of [Aliquat]Cl:octanol (1:1) and [Aliquat]Cl:menthol (1:2), which may justify the difference in the tribological behavior, thermal analysis by DSC of the mixtures was performed. The thermograms are presented in Figure 3.2.7A for [Aliquat]Cl:octanol (1:1) and in Figure 3.2.7B for [Aliquat]Cl:menthol (1:2). In Figure 3.2.7A the exothermic peaks correspond to crystallizations and the endothermic signature is associated with the eutectic melting. In contrast, for [Aliquat]Cl:menthol (1:2) no crystallization was found and only a glass transition can be detected in both cooling and heating ramps. This difference in the thermal behavior shows that the interaction of [Aliquat]Cl with menthol is stronger than with octanol, preventing the organization of the molecules of [Aliquat]Cl:menthol (1:2) in crystals.

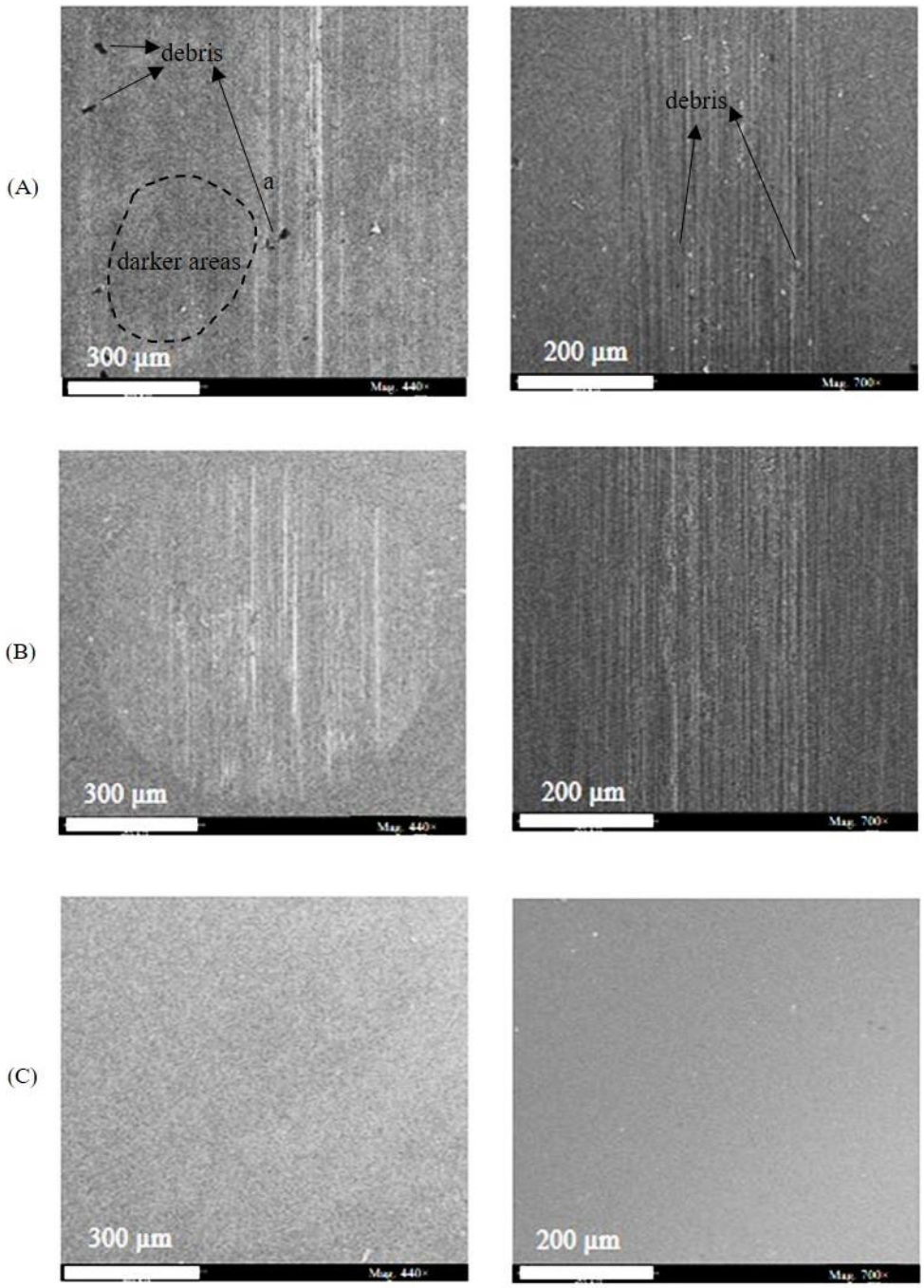

Figure 3.2.6. SEM images of the Si balls (440× magnification, left) and the Si substrates (700× magnification, right) after long tribological tests under the load of 10N using as lubricants: (A) hexadecane, (B) [Aliquat]Cl:octanol (1:1) and (C) [Aliquat]Cl:menthol (1:2). The arrows in Figure 3.2.6A indicate the debris as well as debris indentation (arrow (a)).

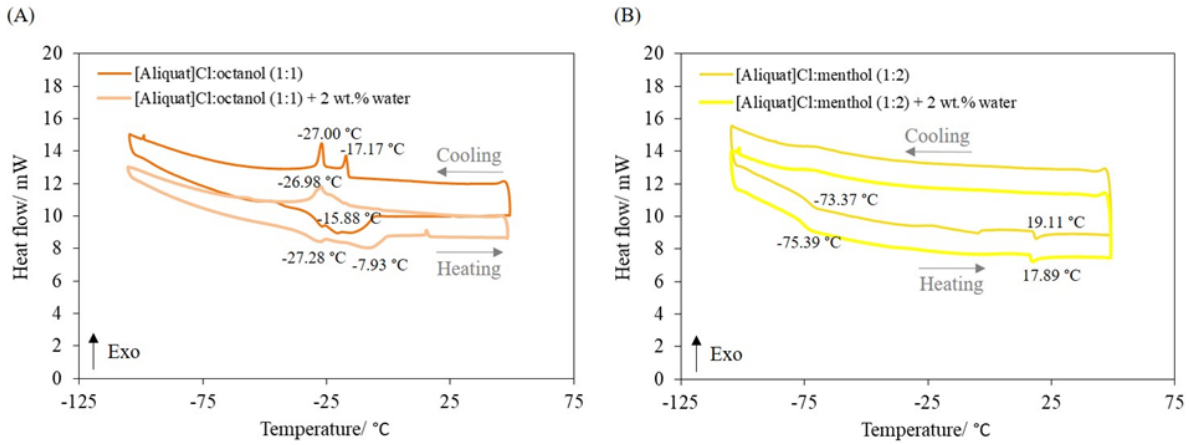

Figure 3.2.7. Thermograms of the DES [Aliquat]Cl:octanol (1:1) (A) and [Aliquat]Cl:menthol (1:2) (B). The figures include thermograms obtained with wet samples for testing the effect of the presence of water in Section 3.2.3.4.

HSPM of [Aliquat]Cl:octanol (1:1) was done to visualize the changes in the structure, which occur during the cooling/heating cycle between -40 °C and 120 °C. The sample of [Aliquat]Cl:menthol (1:2) was not analysed because it did not crystalize. The images obtained at different temperatures, presented in Figure 3.2.8, illustrate that some crystals (isolated with needle shape and agglomerated) can be observed in the liquid sample, at room temperature, which crystallized (on cooling) around -27 °C, began to melt (on heating) around -14 °C, and were still present at 120 °C. The thermogram of [Aliquat]Cl:octanol (1:1) showed two crystallization peaks but only one crystallization can be detected in the HSPM. This is not surprising because the thermogram was obtained with a bulk liquid, while the imaged sample was a liquid film between two glass slides.

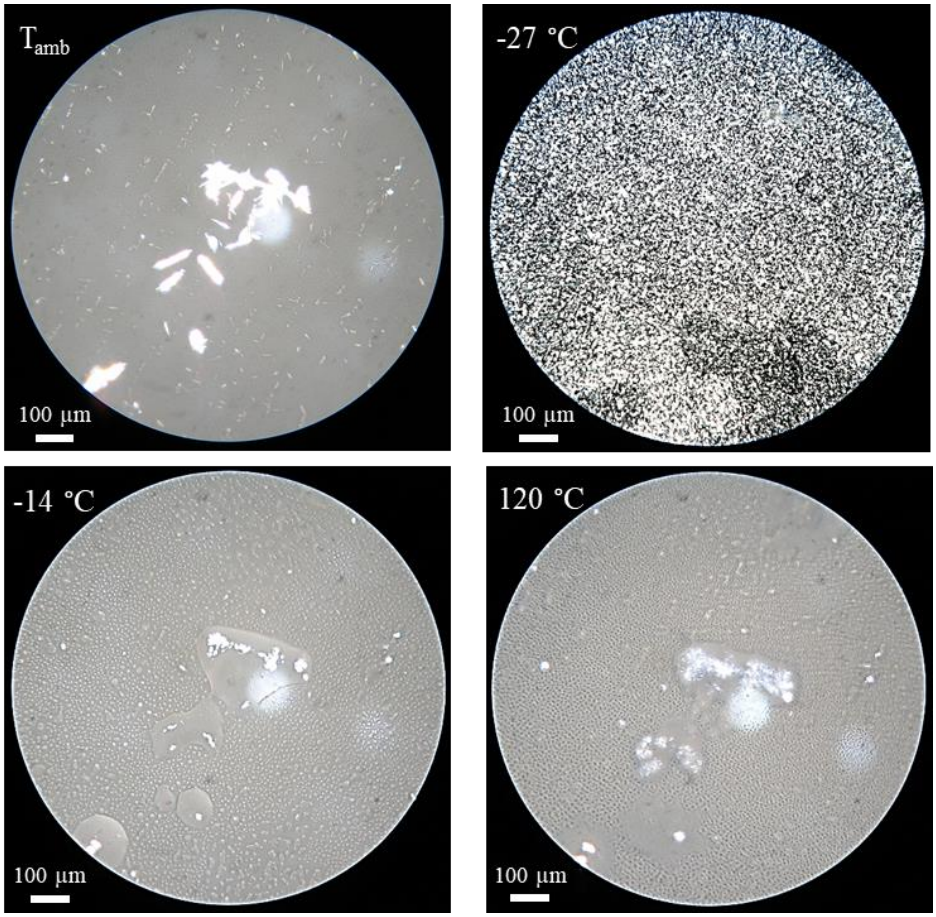

Figure 3.2.8. HSPM images of [Aliquat]Cl:octanol (1:1) obtained at different temperatures beginning at room temperature, cooling till -40 °C, and heating up to 120 °C.

The presence of crystals in [Aliquat]Cl:octanol (1:1) helps to explain the strong dependence of the lubrication capacity of this DES on the applied load. For the tribological tests using loads up to 8 N, the average distance between the two sliding surfaces is large enough to accommodate the crystals and the load is carried mainly by the lubricant film. In contrast, under 10 N the crystals may became squeezed between the surfaces leading to more severe two-body and three-body abrasive wear (the later in the case of rolling of the crystals during the movement). This hypothesis seems to be confirmed by the SEM images (Figure 3.2.6B) of the worn surfaces the Si sphere and substrate exhibiting significant abrasive scratches. To assess eventual modifications produced in the structure of [Aliquat]Cl:octanol (1:1) by the tribological tests under high load (10N), HSPM images of one sample taken after the test were obtained (Figure A.4.3). Comparison with Figure 3.2.8 clearly shows that the size of the crystalline agglomerates decreased significantly after the tribological experiment and, in contrast with the initial sample, two crystallizations could be identified at the same temperature of the crystallization peaks in the thermogram (-27 °C and -17 °C). This confirms that [Aliquat]Cl:octanol (1:1) suffered irreversible structural changes induced by pressure and

local heating (resulting from friction), which leads to crystal melting and a signification reduction in the size of the crystals initially present in the mixture at room temperature. Furthermore, the crystals became roundish instead of needle-shaped.

Altogether, these results show that the wear modes of silicon may be related to different processes of surface damage depending on the characteristics of the lubricants. It is known that being a brittle material, silicon is expected to undergo microfracture and/ or plastic flow during tribological tests. Microfracture occurs mainly under dry conditions or when the lubricant is a grease, while plastic flow leading to phase transformations (metallization) of silicon is detected in oil lubrication.[29]

When the viscosity of the lubricant was low, as in the case of hexadecane, contact between the asperities of the sliding surfaces occurred, even at low loads, and the debris formed due to microfracture of those asperities acted as abrasive agents leading to scratching of the surfaces. The CoF was high, although its value did not change much for increasing loads, in contrast with wear, which increased significantly until complete fracture of the surface of the substrate, leading to severe wear at 12 N. At 10 N, it is possible to detect plastic deformation of the worn Si ball and debris indentation (e.g. arrow (a) in Figure 3.2.6A). When the lubricants were [Aliquat]Cl:octanol (1:1) and [Aliquat]Cl:menthol (1:2) the situation was completely different. The viscosities of these DES are much higher and the surfaces were kept separated during sliding at low loads. However, the tendency for the mixture to adsorb on the sliding surfaces forming a protective layer, able to protect them from contact, is a more important factor than the lubricant viscosity.[11] In fact, the viscosities of [Aliquat]Cl:octanol (1:1) and [Aliquat]Cl:menthol (1:2) lie within the same range of other DES based on ionic quaternary ammonium salts (see Table 3.2.1), but their lubrication capacity is much higher, as demonstrated in the preliminary tests (Figure 3.2.2).

Both DES were able to avoid contact between surface asperities during tribological tests under loads < 10N and no wear was detected. However, [Aliquat]Cl:octanol (1:1), in contrast with [Aliquat]Cl:menthol (1:2), became abrasive under the load of 10N due to the presence of a significant number of crystals at room temperature. In this case, the dominant wear mode is the abrasion by the crystals contained inside the lubricant film, and the wear volume was much higher than the value obtained with hexadecane (see Table 3.2.2).

XPS analysis of the Si substrates after the tribological tests at 10 N, reveals that the chemical composition inside and outside the contact areas (Table 3.2.3) is similar in the case of [Aliquat]Cl:menthol (1:2), where no wear occurred, while for [Aliquat]Cl:octanol (1:1) the amounts of Si 2p, O 1s and C 1s are different, indicating the formation of a new surface due to wear. The amounts of N 1s and Cl 2p, resulting from the adsorption of [Aliquat]Cl, are very small and the differences between the values found inside and outside the contact areas are not significant. The main difference between the substrates lubricated with [Aliquat]Cl:menthol (1:2) and [Aliquat]Cl:octanol (1:1) resides on the amounts of Si 2p, C 1s and O 1s found on the contact areas: Si 2p and O 1s are more abundant in the former case and

C 1s, in the latter. These results are consistent with the increased surface roughness, which lowers the emission angle (the angle between the analyzer and the surface), causing a decrease in information depth. This enhances the contribution of surface species, most prominently carbon. The XPS spectra of the main components of the Si substrates inside and outside the wear tracks observed after long tribological tests under the load of 10N using hexadecane, [Aliquat]Cl:octanol (1:1) and [Aliquat]Cl:menthol (1:2) are compared in Figure 3.2.9. For the Si 2p emission, doublets with a fixed separation of 0.6 eV were used for each component. The corresponding XPS spectra of N 1s and Cl 2p are given in Figure A.4.7 in Annexx A.4.

Table 3.2.3. Chemical composition of the Si substrates, inside and outside the contact areas, after long tribological tests under the load of 10N.

Lubricant	Relative Atomic Percentages									
	Si 2p		O 1s		C 1s		N 1s		Cl sp	
	Contact	Non Contact	Contact	Non Contact	Contact	Non Contact	Contact	Non Contact	Contact	Non Contact
Hexadecane	11.32	24.09	23.12	24.85	65.55	51.05	-	-	-	-
[Aliquat]Cl: menthol (1:2)	45.56	45.73	37.64	38.10	15.73	15.12	0.23	0.32	0.84	0.74
[Aliquat]Cl: octanol (1:1)	38.42	41.38	26.71	35.70	33.91	21.89	0.35	0.27	0.61	0.77

No charge neutralization method was used during the measurement. Judging from the C 1s binding energy between 285.5 eV and 286.7 eV, slight differential charging may have occurred in part of the samples. However, the Si $2p_{3/2}$ binding energy of elemental silicon of all samples outside the wear tracks was consistently found at 99.85 ±0.03 eV, only 0.5 eV above the value reported in the literature.[30] For this reason, a rigid shift of -0.5 eV was applied to all spectra to correct for the differential charging.

Outside the wear tracks, O 1s is found at 532.9-533 eV. Besides elemental silicon, the Si 2p emission includes the Si^{4+} component of the native surface oxide at 103.6 eV (103.3 eV if considering only Si $2p_{3/2}$). C 1s shows the typical spectrum of adventitious carbon. After applying the load of 10N, the surface changes depended significantly on the type of lubricant.

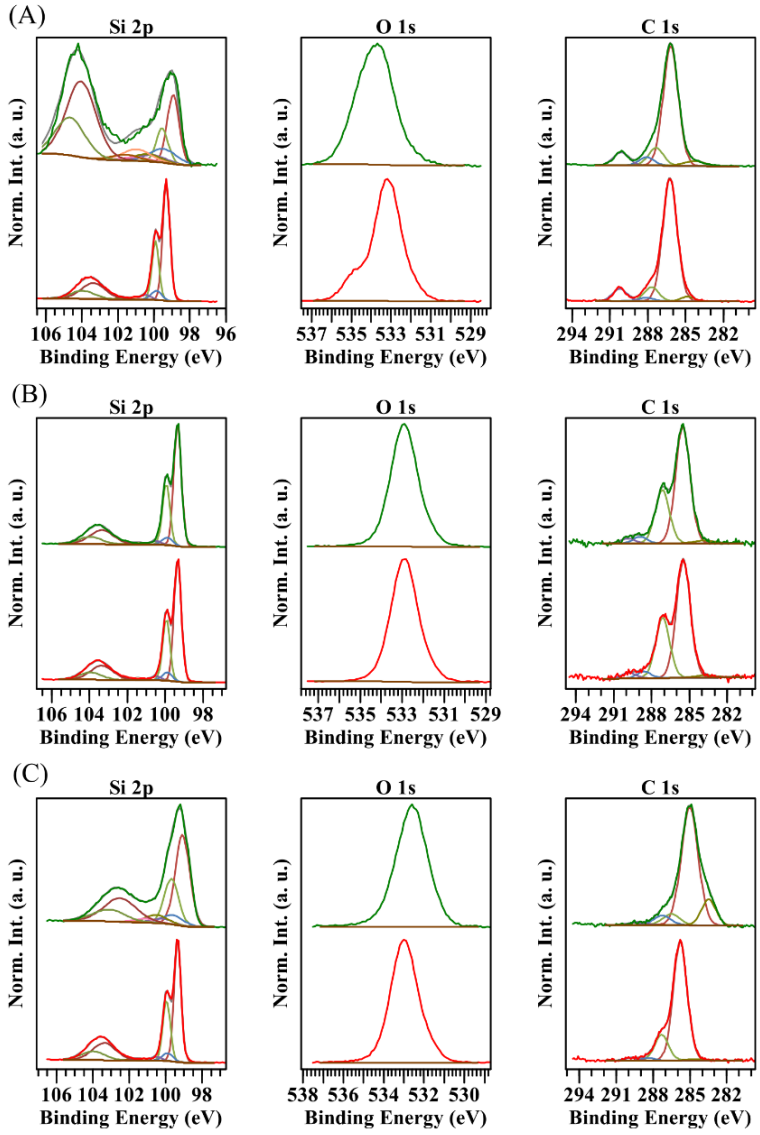

Figure 3.2.9. Comparison between XPS spectra for (A) hexadecane, (B) [Aliquat]Cl:menthol (1:2) and (C) [Aliquat]Cl:octanol (1:1) after tribological tests at 10N, inside (top spectra) and outside (bottom spectra) the wear tracks.

Hexadecane (Figure 3.2.9A) induced the additional sub-oxide components Si^{1+}, Si^{2+} and Si^{3+} (fitted according to Arcifa *et al.*[28]) and more Si^{4+}. Besides that, the elemental silicon components shifted to lower binding energy, whereas the Si^{4+} components shifted to higher binding energy. Furthermore, all components are broadened. Also, the O 1s components appeared broader and shifted to higher binding energy. Note that significant changes in the differential charging (from the unloaded to the loaded samples) are not suspected to be related to these observations, because the main C 1s component did not change more than 0.05 eV.
Using [Aliquat]Cl:menthol (1:2), shown in Figure 3.2.9B, did not introduce any measurable change in the Si 2p, O 1s and C 1s spectra. This was not the case for [Aliquat]Cl:octanol (1:1),

shown in Figure 3.2.9C. Comparing the loaded with the unloaded case, all Si 2p components became wider and the contributions of the Si^{1+}, Si^{2+}, Si^{3+} and Si^{4+} increased (however, less than in the case of hexadecane). The elemental silicon component was shifted by -0.25 eV to lower binding energies. Contrarily to hexadecane, the Si^{4+} component was shifted to lower binding energies, almost for -0.9 eV. O 1s also shifted to lower binding energies (532.6 eV), as well as C 1s (285.0 eV). The latter could indicate a different degree of differential charging in the loaded [Aliquat]Cl:octanol (1:1) sample, so these peak shifts should be considered with caution. However, a definite sign for the interaction with the ionic liquid under load is the additional C 1s component at 283.5 eV.[28]

3.2.3.4 Effect of the presence of water on the best lubricants

As previously referred, other authors found that the structural, transport and chemical properties of hydrophobic DESs are affected by the presence of small amounts of water resulting from contact with humid environments.[23] We chose [Aliquat]Cl:octanol (1:1) and [Aliquat]Cl:menthol (1:2), to assess those effects through the addition of a fixed amount of 2% (w/w) of water. For simplicity, the mixtures with added water are designated by "wet DES".

3.2.3.4.1 Wet DES characterization

The water content, the viscosity and the contact angle of the wet DES are given in Table 3.2.4.

Table 3.2.4. Water content, viscosity, η, at 25 °C and equilibrium contact angle on Si substrates of the wet DESs. The standard deviations correspond to n = 3 for viscosity and n ≥ 4 for contact angle.

Wet DES	Water content/ %	η/ mPa·s	Contact angle/ °
[Aliquat]Cl:octanol (1:1)	4.0	173±4	18±1
[Aliquat]Cl:menthol (1:2)	4.7	220±5	22±3

Addition of water affects the structure and dynamics of the hydrophobic DESs due to the hydration of the chloride ion and the OH groups in the HBA molecule, which become less available to form hydrogen bonds. Moreover, this effect favours the electrostatic interaction between the $[Aliquat]^+$ and Cl^- ions. The water-induced structural changes enhanced molecular mobility, which led to a significant decrease in viscosity: 38% for [Aliquat]Cl:octanol (1:1) and 45% for [Aliquat]Cl:menthol (1:2). As expected, the wettability of the Si substrate by the wet DES improved: 18% for [Aliquat]Cl:octanol (1:1) and 21% for [Aliquat]Cl:menthol (1:2).

Thermal analysis by DSC of the mixtures with added water is presented in Figure 3.2.7A for [Aliquat]Cl:octanol (1:1) and in Figure 3.2.7B for [Aliquat]Cl:menthol (1:2), where the

thermograms obtained with the DES without water are also shown. Addition of water practically does not affect the thermal behavior of [Aliquat]Cl:menthol (1:2). The situation is different for [Aliquat]Cl:octanol (1:1), where the presence of water led to the coalescence of the two crystallization peaks, and the separation of the endothermic broad peak in two smaller peaks, which eventually correspond to the melting of two phases with different water content. HSPM images of wet [Aliquat]Cl:octanol (1:1) obtained at different temperatures beginning at room temperature, cooling till -40 °C, and heating up to 120 °C are compared in Figure A.4.4. At room temperature, many small needle-shape crystals can be observed in the liquid sample, which crystallized (on cooling) at -28 °C, began to melt (on heating) around -20 °C, and were still present at 120 °C, although in smaller number at room temperature. The main difference between the samples with and without water, at room temperature, is the absence of crystalline agglomerates observed in wet [Aliquat]Cl:octanol (1:1), confirming that the presence of water disturbs the structure of this DES.

3.2.3.4.2 Corrosion of the Si surfaces

The effect of the amount of water present in the DES sample on the eventual corrosion of the Si surface was evaluated through the comparison of the surface of Si substrates before and after contact with DES and wet DES for two weeks. No signs of corrosion of the surfaces by both DES, independently of their water content, were detected by naked eye observation. This was confirmed by the SEM images shown in Figure A.4.5.

3.2.3.4.3 Tribological tests with wet DES

The effect of the presence of water in the lubrication capacity of DES has not been investigated, to our knowledge. However, several authors addressed this question with respect to ILs and the results are contradictory. Arcifa *et al*.[28,31] found that the lubrication performance of silica/silicon pairs using both hydrophobic and hydrophilic ILs depended on the relative humidity and the lubrication regime. Hydrophobic imidazolium-based ILs, at a small applied load (0.5 N), showed an increase of wear and friction when the tests were done in humid air,[31] while the opposite effect was found with [emim][$EtSO_4$] at high load (4.5 N).[28] In the former case, the worst lubrication was attributed to the disruption of the lubricant film; in the latter, the decrease in friction and wear was attributed to the smoothing of the silica surface due to the formation of a ductile layer of hydrated silica. Yet other results were obtained by our group when studying the lubrication of steel/silicon pairs by imidazolium [32] and picolinium-based hydrophobic ionic liquids [33] added to PEG200. No effect of the water content of the lubricants on friction was found at low loads, 15 and 30 mN, respectively for imidazolium and picolinium-based additives.

Comparison of the average CoF values obtained with [Aliquat]Cl:octanol (1:1) and [Aliquat]Cl:menthol (1:2), with different water contents, for the pair Si sphere/Si substrate, at constant sliding speed (8 $mm \cdot s^{-1}$) and under different loads, is presented in Figure 3.2.4. The

tests under 12 N, led to the breakage of the Si substrates except in the case of [Aliquat]Cl:menthol (1:2).

Analysis of the figure shows that the effect of addition of water upon the CoF obtained with [Aliquat]Cl:menthol (1:2) is slight or even null at all applied loads. In contrast, when [Aliquat]Cl:octanol (1:1) was used, the presence of water did not affect the CoF at low loads but, at 8N, the wet DES was no longer able to protect the sliding surfaces and CoF increased remarkably to 0.14. At 10 N, neither of the two samples of [Aliquat]Cl:octanol (1:1) were good lubricants and the obtained CoF values are similar to the CoF obtained with hexadecane.

No wear was detected on the surfaces of the Si balls and substrates after long tests under 8N, 10N and 12N with wet [Aliquat]Cl:menthol (1:2) (images not shown). In contrast, deep and wide wear tracks were found on the profilometer images of Si substrates after the long tests under 8N and 10N, with wet [Aliquat]Cl:octanol (1:1), as shown, respectively, in Figure 3.2.10A and Figure 3.2.10B. The calculated wear volumes are 10×10^{-3} mm^3 and 16×10^{-3} mm^3, which compare with zero and 12×10^{-3} mm^3 for [Aliquat]Cl:octanol (1:1) (see Table 3.2.2).

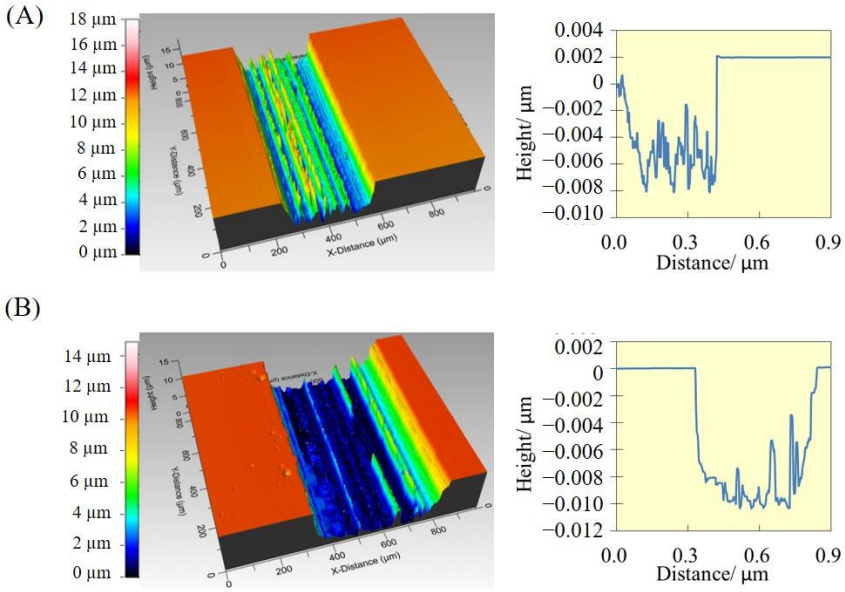

Figure 3.2.10. Worn surface of the Si substrate (profilometer images with 20× magnification) after long tribological tests using wet [Aliquat]Cl:octanol (1:1) as lubricant: (A) under 8N and (B) under 10N.

SEM images of the worn surfaces of the Si balls and the Si substrates after long tests under 8N and 10N using wet [Aliquat]Cl:octanol (1:1) as lubricant are shown in Figure 3.2.11. The equivalent SEM images obtained with wet [Aliquat]Cl:menthol (1:2) are not shown because no wear could be detected. After the tribological tests under 8N, abrasive scratches appear on both surfaces, and large debris are visible on the rim of the wear track on the substrate (Figure 10A). Besides, the surface of the ball presents signs of indentation, as a result of continuous

rubbing against the substrate. The signs of abrasive wear are more intense on the surfaces tested under 10N, where a higher number of debris can be identified on the edges of the wear track on the substrate and some debris appear on the surface of the ball.

The effect of the water is clearly seen by comparison of the results obtained using wet [Aliquat]Cl:octanol (1:1) and [Aliquat]Cl:octanol (1:1). The most striking difference is observed under 8N, where no wear was detected on the substrates lubricated by [Aliquat]Cl:octanol (1:1) in the absence of added water. Under 10N, wet [Aliquat]Cl:octanol (1:1) led to more severe wear than [Aliquat]Cl:octanol (1:1) without water (Figure 3.2.6B) which should result mainly from the abrasive action of the debris present in high amount and not from the presence of crystals in the DES. These observations seem to confirm that, during the test under high loads, the presence of water promotes the formation and oxidation of the Si fragments, which accumulate outside the track.

Furthermore, comparison of the HSPM images of wet [Aliquat]Cl:octanol (1:1) before (Figure A.4.4) and after being submitted to tribological tests (8N) (Figure A.4.6) demonstrates a reduction in the number of crystals after the tribological experiment. In addition, the DSC thermogram (Figure 3.2.7) shows a broad peak at -27 °C, which has an equivalent effect in the HSPM images in Figure A.4.4. This means that the addition of water and the pressure have synergistic effects inducing the disruption of the crystals previously existing in [Aliquat]Cl:octanol (1:1). It is interesting to notice that the reduction in the number of crystalline agglomerates present in wet [Aliquat]Cl:octanol (1:1) did not improve the lubrication capacity at high loads. These apparently contradictory results might be explained by the complexity of the wear mechanisms. The lack of aggressive crystals in the wet DES did not compensate the probable disruption of the lubricant film caused by the presence of water.

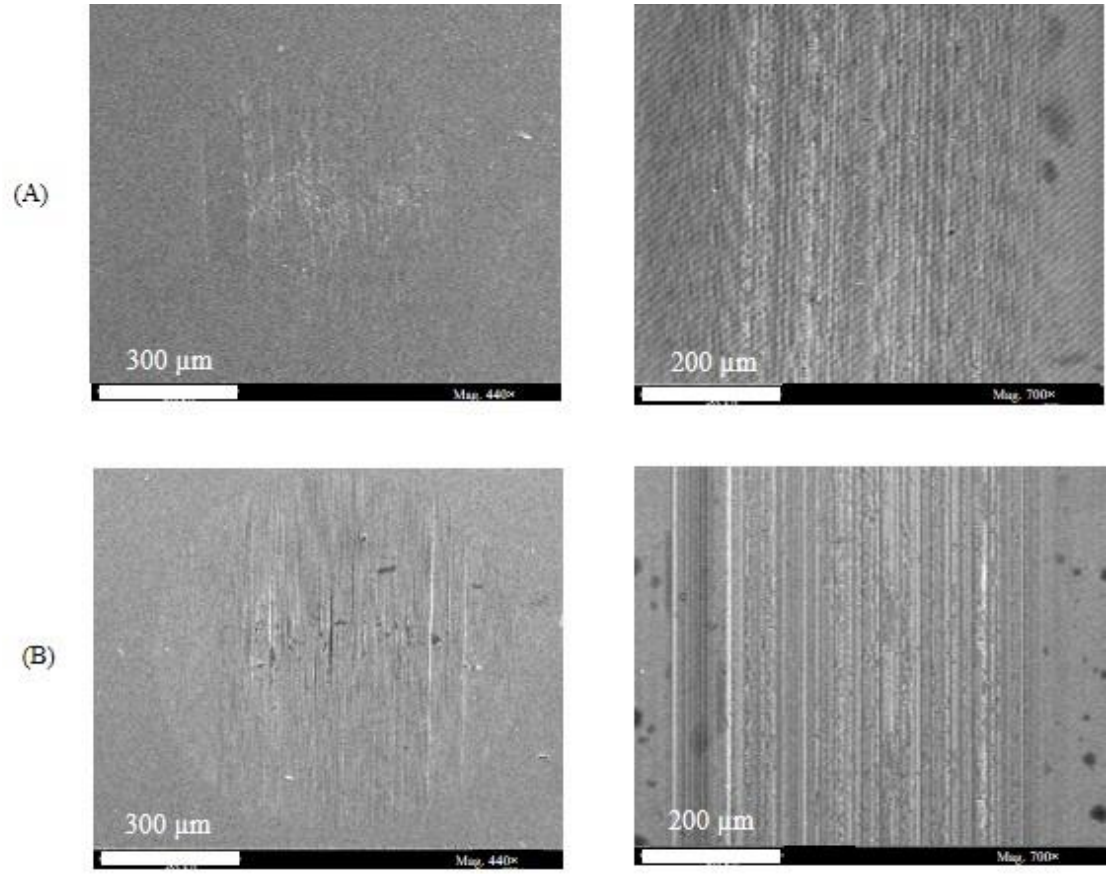

Figure 3.2.11. SEM images of worn surfaces of the Si balls (440× magnification, left) and Si substrates (700× magnification, right) after long tribological tests using wet [Aliquat]Cl:octanol (1:1): (A) under 8N and (B) under 10N.

These results suggest that [Aliquat]Cl:octanol (1:1) has lower stability towards water than [Aliquat]Cl:menthol (1:2), *i.e.* hydrogen bonding network in the former DES is more susceptible to breaking by the added water. The interaction of water with the OH group of octanol is stronger than with the same group of menthol (octanol is more water soluble than menthol), which means that Cl···H-O, the most important structural factor in these DESs, is more weakened in wet [Aliquat]Cl:octanol (1:1). This change in structure, which was apparent in the HSPM images, might imply a decrease in the adsorption capacity of wet [Aliquat]Cl:octanol (1:1) on the Si surfaces opening the way to the contact between them when the applied load is high and the film becomes unable to protect the surfaces against wear.
To understand better the role played by water in the decrease of the lubrication performance of wet [Aliquat]Cl:octanol (1:1), the surfaces of the Si substrates inside and outside the contact areas after long tribological testes under the load of 8N, were analyzed by XPS. We should remember that the presence of water led to the most significant effect under this load: CoF increased from 0.04 to 0.14 (see Figure 3.2.4) and wear volume changed from zero to 1.0×10^{-2} mm^3. The main difference between the substrates lubricated with [Aliquat]Cl:octanol (1:1) and

wet [Aliquat]Cl:octanol (1:1) (Table 3.2.5) lies on the amounts of Si 2p, O 1s and C 1s inside and outside the contact area. In contrast with [Aliquat]Cl:octanol (1:1) where those amounts do not vary much, for wet [Aliquat]Cl:octanol (1:1), the atomic percentages of Si 2p and O 1s found on the contact area are much smaller than those on the non-contact area, while the atomic percentage of C 1s is much higher, which is consistent with the fact that wear of the SiO_2 layer on top of the silicon wafer occurred only in the presence of water. The increase of the C 1s signal on the wear track most likely related to the increased surface roughness, which lowers the emission angle (the angle between analyzer and surface), causing a decrease in information depth. The atomic percentages of N 1s and Cl 2p, which indicate the presence of adsorbed [Aliquat]Cl are very small and do not allow any conclusion about the effect of water on the adsorption strength of [Aliquat]Cl:octanol (1:1).

Table 3.2.5. Chemical composition of the Si substrates, inside and outside the contact areas after long tribological tests under the load of 8 N using [Aliquat]Cl:octanol (1:1) with and without added water.

Lubricant	Relative Atomic Percentages									
	Si 2p		O 1s		C 1s		N 1s		Cl sp	
	Contact	Non Contact	Contact	Non Contact	Contact	Non Contact	Contact	Non Contact	Contact	Non Contact
[Aliquat]Cl: octanol (1:1)	28.87	32.79	26.55	28.03	43.42	38.11	0.60	0.51	0.57	0.56
Wet [Aliquat]Cl: octanol (1:1)	20.57	39.85	24.90	33.16	53.51	25.43	0.68	0.67	0.35	0.89

The XPS spectra of the Si substrates inside the wear tracks are compared with the ones outside the wear tracks, after long tribological tests under the load of 8 N using [Aliquat]Cl:octanol (1:1) with and without added water in Figure 3.2.12. The XPS spectra of N 1s and Cl 2p are given in Figure A.4.8 in Annexx A.4.

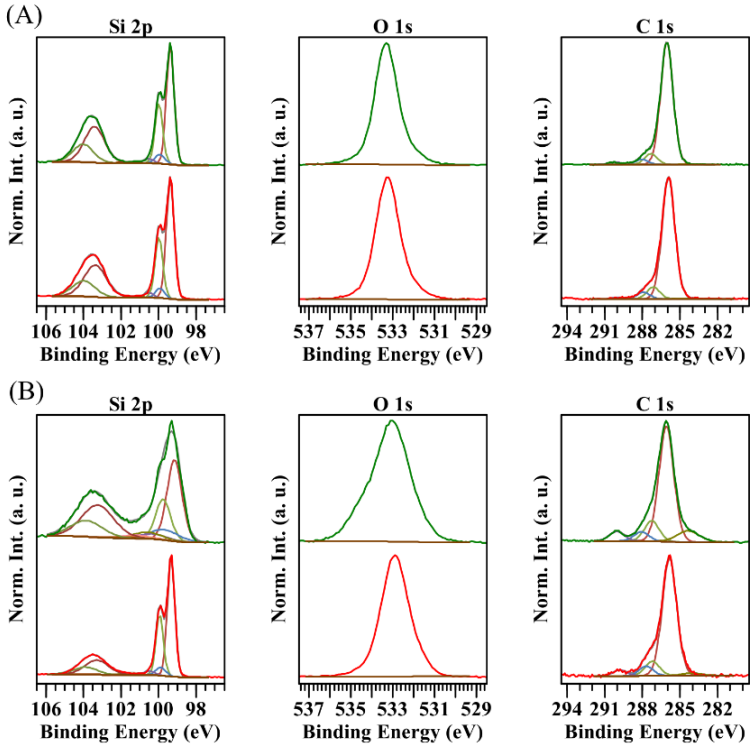

Figure 3.2.12. Comparison between XPS spectra for (A) [Aliquat]Cl:octanol (1:1) and (B) wet [Aliquat]Cl:octanol (1:1) after tribological tests at 8N, inside (top spectra) and outside (bottom spectra) the wear tracks.

In terms of peak shape and binding energies, the Si 2p, O 1s and C 1s emissions remain unchanged after the wear test with dry [Aliquat]Cl:octanol (1:1), as seen in Figure 3.2.12A. However, when using wet [Aliquat]Cl:octanol (1:1), shown in Figure 3.2.12B, the wear causes a broadening of the Si 2p components (as well as O 1s), the appearance of the suboxides and peak shifts of the Si^{0} and Si^{4+} components to lower binding energies. In addition, the characteristic low binding energy component of C 1s appears, indicating the interaction with the ionic liquid.

Finally, it is worthwhile to compare the results presented in this work with others recently obtained by our group concerning the lubrication of the same tribological pair.[34] Several protic ILs based on the sulfur-containing hydrogen sulfate ([HSO_4]) and mesylate ([$MeSO_3$]) anions were tested as additives to the base oil PEG200. The best IL was 4-picolinium hydrogenosulfate ([4-picH][HSO_4]), which led to CoF ~0.2 and 2×10^{-4} mm^3 of wear volume, 15 times smaller than the wear value obtained with PEG200 under 4N of load and after 2375 cycles. In the same testing conditions, [Aliquat]Cl:menthol (1:2) and [Aliquat]Cl:octanol (1:1) led, respectively, to CoF values of 0.03 and 0.06 and no wear. Thus, these eutectic mixtures appear to significantly better lubricants for Si surfaces.

3.2.4 Conclusions

The tribological properties of two families of hydrophobic DES, one based on nonionic menthol and the other based on ionic quaternary ammonium salts, were compared to the model lubricant hexadecane in steel/Si contacts. Then, [Aliquat]Cl:octanol (1:1) and [Aliquat]Cl:menthol (1:2) were chosen for further studies with Si/Si pairs that mimic MEMS/NEMS. At low loads (2, 4 and 8 N), both DES led to CoF values significantly lower than hexadecane and no wear, but for higher loads (10 and 12N), [Aliquat]Cl:octanol (1:1) lost its lubrication capacity, while [Aliquat]Cl:menthol (1:2) kept its excellent performance. XPS analysis of the Si surfaces after the tribological tests show the presence of adsorbed DES which protect the surfaces from contact under low loads. However, at high loads, the crystals present in the film of [Aliquat]Cl:octanol (1:1), which were detected on the HSPM images, led to abrasion of the Si surface. Finally, the effect of the addition of a fixed amount of 2% (w/w) of water on the physicochemical properties of [Aliquat]Cl:octanol (1:1) and [Aliquat]Cl:menthol (1:2) and on their tribological behavior was assessed. The viscosity of both wet DES decreased and the wettability of the Si surface improved. No corrosion of the Si substrates was observed. The lubrication capacity of wet [Aliquat]Cl:menthol (1:2) was not affected by the presence of water. In contrast, wet [Aliquat]Cl:octanol (1:1) became similar to hexadecane at the load of 8N leading to abrasive wear and the formation of large debris. In this case, the presence of water changed the structure of the DES leading to a reduction in the number of crystals, and wear might be mainly attributed to the formation of Si fragments, which act as abrasives of the sliding surfaces. In conclusion, when compared to other DES and ILs previously studied by our group, [Aliquat]Cl:menthol (1:2) stands out as an extremely promising lubricant for Si-based MEMS/NEMS, in view of its low price, efficient performance under high loads and resistance to the ambient humidity.

3.2.5 References

[1] H. Passos, D. J. P Tavares, A. M. Ferreira, M. G. Freire, J. A. P. Coutinho, Are Aqueous Biphasic Systems Composed of Deep Eutectic Solvents Ternary or Quaternary Systems? *ACS Sustainable Chem. Eng.* **2016**, *4*, 2881-2886. https://doi.org/10.1021/acssuschemeng.6b00485

[2] D. J. G. P. Van Osch, L. F. Zubeir, A. van den Bruinhorst, M. A. A. Rocha, M. C. Kroon, Hydrophobic Deep Eutectic Solvents as Water-Immiscible Extractants. *Green Chem*. **2015**, *17*, 4518-4521. https://doi.org/10.1039/C5GC01451D

[3] B. D. Ribeiro, C. L. Florindo, C. Iff, M. A. Z. Coelho, I. M. Marrucho, Menthol-Based Eutectic Mixtures: Hydrophobic Low Viscosity Solvents. *ACS Sustainable Chem. Eng*. **2015**, *3*, 2469-2477. https://doi.org/10.1021/acssuschemeng.5b00532

[4] C. Florindo, L. C. Branco, I. M. Marrucho, Quest for Green-Solvent Design: From Hydrophilic to Hydrophobic (Deep) Eutectic Solvents. *ChemSusChem* **2019**, *12*, 1549-1559. https://doi.org/10.1002/cssc.201900147

[5] D. J. G. P. Van Osch, C. H. J. T. Dietz, S. E. E. Warrag, M. C. Kroon, The Curious Case of Hydrophobic Deep Eutectic Solvents: A Story on the Discovery, Design, and Applications. *ACS Sustainable Chem. Eng*. **2020**, *8*, 10591-10612. https://doi.org/10.1021/acssuschemeng.0c00559

[6] M. H. Zainal-Abidin, M. Hayyan, W. F. Wong, Hydrophobic Deep Dutectic Dolvents: Current Progress and Future Directions. *J. Ind. Eng. Chem*. **2021**, *97*, 142-162. https://doi.org/10.1016/j.jiec.2021.03.011

[7] P. Makoś, E. Słupek, J. Gębicki, Hydrophobic Deep Eutectic Solvents in Microextraction Techniques - A Review. *J. Microchem.* **2020**, *152*, 104384. https://doi.org/10.1016/j.microc.2019.104384

[8] D. D. A. Lawes, S. V. Hainworth, P. Blake, K. S. Ryder, A. P. Abbot, Lubrication of Steel-Steel Contacts by Choline Chloride Ionic Liquids. *Tribol. Letters* **2010**, *37*, 103-110. https://doi.org/10.1007/s11249-009-9495-6

[9] A. P. Abbott, E. I. Ahmed, R. C. Harris, K. S. Ryder, Evaluating Water Miscible Deep Eutectic Solvents (DESs) and Ionic Liquids as Potential Lubricants. *Green Chemistry* **2014**, *16*, 4156-4161. https://doi.org/10.1039/C4GC00952E

[10] E. I. Ahmed, A. P. Abbott, K. S. Ryder, Lubrication Studies of Some Type III Deep Eutectic Solvents (DESs). *AIP Conference Proceedings* **2017**, *1888*, 020006. https://doi.org/10.1063/1.5004283

[11] M. Antunes, A. S. Campinhas, M. S. Freire, F. Caetano, H. P. Diogo, R. Colaço, L. C. Branco, B. Saramago, Deep Eutectic Solvents (DES) Based on Sulfur as Alternative Lubricants for Silicon Surfaces. *J. Mol. Liq*. **2019**, *295*, 111728. https://doi.org/10.1016/j.molliq.2019.111728

[12] M. T. Donato, L. Santos, H. P. Diogo, R. Colaço, L. C. Branco, B. Saramago, Eutectic Systems Containing an Ionic Liquid and PEG200 as Lubricants for Silicon Surfaces: Effect of the Mixture's Molar Ratio. *J. Mol. Liq*. **2022**, *350*, 118572. https://doi.org/10.1016/j.molliq.2022.118572

[13] Z. Rymuza, Control Tribological and Mechanical Properties of MEMS Surfaces. Part 1: Critical Review, *Microsyst. Technol*. **1999**, *5*, 173-180. https://doi.org/10.1007/s005420050160

[14] I. S. Y. Ku, T. Reddyhoff, A. S. Holmes, H. A. Spikes, Wear of Silicon Surfaces in MEMS. *Wear* **2011**, *271*,1050-1058. https://doi.org/10.1016/j.wear.2011.04.005

[15] T. Krízek, M. Bursova, R. Horsley, M. Kuchar, P. Tuma, R. Cabala, T. Hlozek, Menthol-Based Hydrophobic Deep Eutectic Solvents: Towards Greener and Efficient Extraction of Phytocannabinoids. *J. Cleaner Prod*. **2018**,*193*, 391-396. https://doi.org/10.1016/j.jclepro.2018.05.080

[16] X. H. Fan, L. T. Wang, Y. H. Chang, J. Y. An, Y. W. Zhu, Q. Yang, D. Meng, Y. J. Fu, Application of Green and Recyclable Menthol-Based Hydrophobic Deep Eutectic Solvents Aqueous for the Extraction of Main Taxanes from Taxus Chinensis Needles. *J. Mol. Liq*. **2021**, *326*, 114970. https://doi.org/10.1016/j.molliq.2020.114970

[17] W. Tang, Y. Dai, K. H. Row, Evaluation of Fatty Acid/Alcohol-Based Hydrophobic Deep Eutectic Solvents as Media for Extracting Antibiotics from Environmental Water. *Anal. Bioanal. Chem*. **2018**, *410*, 7325-7336. https://doi.org/10.1007/s00216-018-1346-6

[18] Z. Triaux, H. Petitjean, E. Marchioni, M. Boltoeva, C. Marcic, Deep Eutectic Solvent–Based Headspace Single-Drop Microextraction for the Quantification of Terpenes in Spices. *Anal. Bioanal. Chem*. **2020**, *412*, 933–948. https://doi.org/10.1007/s00216-019-02317-9

[19] J. Cao, M. Yang, F. Cao, J. Wang, E. Su, Well-Designed Hydrophobic Deep Eutectic Solvents as Green and Efficient Media for the Extraction of Artemisinin from Artemisia Annua Leaves. *ACS Sustainable Chem. Eng*. **2017**, *5*, 3270–3278. https://doi.org/10.1021/acssuschemeng.6b03092

[20] N. A. Milevskii, I. V. Zinoveva, A Yu Zakhodyaeva, A. A. Voshkin, Separation of Li(I), Co(II), Ni(II), Mn(II), and Fe(III) from Hydrochloric Acid Solution Using a Menthol-Based Hydrophobic Deep Eutectic Solvent. *Hydrometallurgy* **2022**, 207, 105777. https://doi.org/10.1016/j.hydromet.2021.105777

[21] C. Ma, A. Laaksonen, C. Liu, X. Lu, X. Ji, The Peculiar Effect of Water on Ionic Liquids and Deep Eutectic Solvents. *Chem. Soc. Rev*. **2018**, *47*, 8685-8720. https://doi.org/10.1039/c8cs00325d

[22] T. El Achkar, S. Fourmentin, H. Greige-Gerges, Deep Eutectic Solvents: An Overview on Their Interactions With Water and Biochemical Compounds. *J. Mol. Liq*. **2019**, *288*, 111028. https://doi.org/10.1016/j.molliq.2019.111028

[23] Y. Chen, D. Yu, W. Chen, L. Fua, T. Mu, Water Absorption by Deep Eutectic Solvents. *Phys. Chem. Chem. Phys*. **2019**, *21*, 2601-2610. https://doi.org/10.1039/C8CP07383J

[24] H. Kivelä, M. Salomäki, P. Vainikka, E. Mäkilä, F. Poletti, S. Ruggeri, F. Terzi, J. Lukkari, Effect of Water on a Hydrophobic Deep Eutectic Solvent. *J. Phys. Chem. B* **2022**, *126*, 513-527. https://doi.org/10.1021/acs.jpcb.1c08170

[25] J. Restolho, J. L. Mata, B. Saramago, On the Interfacial Behavior of Ionic Liquids: Surface Tensions and Contact Angles. *J. Colloid Interface Sci*. **2009**, *340*, 82-86. https://doi.org/10.1016/j.jcis.2009.08.013

[26] G. Subhash, A. D. Corwin, M. P. Boer, Evolution of Wear Characteristics and Frictional Behavior in MEMS Devices, *Tribol. Lett.* **2011**, *41*, 177–189. https://doi.org/10.1007/s11249-010-9696-z

[27] D. H. Alsem, M. T. Dugger, E. A. Stach, R. O. Ritchie, Micron-Scale Friction and Sliding Wear of Polycrystalline Silicon Thin Structural Films in Ambient Air, *J. Microelectrom. Sys*. **2008**, *17*, 1144-1154. https://doi.org/10.1109/JMEMS.2008.927751

[28] A. Arcifa, A. A. Rossi, R. M. Espinosa-Marzal, N. D. Spencer, Influence of Environmental Humidity on the Wear and Friction of a Silica/Silicon Tribopair Lubricated with a Hydrophilic Ionic Liquid. *ACS Appl. Mater. Interfaces* **2016**, *8*, 2961-2973. https://doi.org/10.1021/acsami.5b09370

[29] A. Kovalchenko, Y. Gogotsi, V. Domnich, A. Erdemir, Phase Transformations in Silicon Under Dry and Lubricated Sliding, *Tribol. Trans*. **2002**, *45*, 372-380. https://doi.org/10.1080/10402000208982562

[30] J. F. Moulder, W. F. Stickle, P. E. Sobol, K. D. Bomben, Handbook of X-ray Photoelectron Spectroscopy, Physical Electronics, Inc., Minnesota, USA, **1995**.

[31] A. Arcifa, A. Rossi, R. M. Espinosa-Marzal, N. D. Spencer, Environmental Influence on the Surface Chemistry of Ionic-Liquid-Mediated Lubrication in a Silica/Silicon Tribopair. *J. Phys. Chem. C* **2014**, *118*, 29389-29400. https://doi.org/10.1021/jp505998k

[32] P. M. Amorim, A. M. Ferraria, R. Colaço, L. C. Branco, B. Saramago, Imidazolium-Based Ionic Liquids Used as Additives in Nanolubrication of Silicon Surfaces. *Beilstein J. Nanotechnol*. **2017**, *8*, 1961-1971. https://doi.org/10.3762/bjnano.8.197

[33] M. T. Donato, F. Caetano, R. Colaço, L. C. Branco, B. Saramago, Picolinium-Based Hydrophobic Ionic Liquids as Additives to PEG200 to Lubricate Steel-Silicon Contacts. *Chemistry Select* **2020**, *5*, 5864-5872. https://doi.org/10.1002/slct.202000613

[34] M. T. Donato, J. Deuermeier, R. Colaço, L. C. Branco, B. Saramago, New Protic Ionic Liquids as Potential Additives to Lubricate Si-Based MEMS/NEMS. *Molecules* **2023**, *28* (6), 2678. https://doi.org/10.3390/molecules28062678

4

IONIC LIQUIDS AND DEEP EUTECTIC SOLVENTS AS LUBRICANTS OF STEEL BEARINGS

This chapter presents the results obtained using some of the most promising Ionic Liquids and Deep Eutectic Solvents as lubricants for steel/steel contacts in a more realistic system. The work presented here was performed at the University of Pennsylvania, Philadelphia, USA. It is based on the article in preparation **M. T. Donato**, P. Nautiyal, R. Colaço, L. C. Branco, B. Saramago, R. W. Carpick, Ionic Liquids as extreme pressure additives for bearing steel applications.

4.1 Introduction

Steel is widely used in bearings of vehicle parts, turbines, engines and varied manufacturing equipment as it is a hard and resistant material.[1] Steel-on-steel contact caused by lack of efficient lubrication leads to energy losses and increased energy consumption, which represents an issue for several industries.[2,3] Commercial lubricants are usually composed by grease or oil containing several types of additives designed for protecting the contacting surfaces from wear. However, those additives will often lower the viscosity of the lubricants and increase surface contact by shifting the lubrication regime to mixed/boundary conditions. In this context, Ionic Liquids (ILs) have emerged as potential anti-wear lubricants and/or additives to counteract wear under harsh conditions. ILs are organic salts with a melting point below 100 °C, composed by cation/anion combinations that can be tuned according to the desired final application. They have several interesting properties such as high chemical and thermal stability, almost negligible vapor pressure, – hence ILs are considered environmentally friendly compounds – non-flammability, ease in dissolving organic, inorganic and polymeric materials and high ionic conductivity.[4] Besides that, being highly polar compounds, contrarily to most additives used in synthetic or mineral oils that are non-polar, ILs are highly surface active, presenting a high tendency to adsorb on metal surfaces.[5] One drawback of ILs, however, is their high cost, which is why they have recently been used as additives to commonly used base oils.[6-9]

ILs, in general, and protic ILs (PILs), in particular, have shown great performance as anti-friction and anti-wear additives for several types of contacts, including steel.[9-13] The group of Khatri *et al*.[14] focused on fatty acids-derived trioctylphosphonium cation-based PILs with various alkyl chain lengths, as additives to polyethylene glycol 200 (PEG 200) to lubricate steel-steel contacts. The studied ILs allowed for a friction reduction between 28% and 41% and wear decrease of 15-32% under boundary lubrication regime when comparing to neat base oil. The improvement in tribological properties was due to phosphorous-containing tribofilms formed on the steel surfaces. Horng *et al*.[15] reported tert-octylamine oleate and diethanolamine oleate PILs as additives to water, showing increased tribological performance in terms of friction and wear reduction. Friction was reduced up to 80% and wear up to 85% when comparing to water, which was attributed to the formation of an adsorption layer on the surfaces. Iglesias *et al*.[16] studied three PILs, 2-hydroxyethylammonium 2-ethylhexanoate, 2-hydroxymethylammonium 2-ethylhexanoate and 2-hydroxydimethylammonium 2-ethylhexanoate, as neat lubricants and as additives to a mineral oil for steel–steel pairs. All PILs showed reduced friction and wear up to 19.5% and 48%, respectively. The same group also studied ammonium-based ILs as additives to a mineral oil at room temperature and 100 °C.[17] Friction was reduced after adding the ILs, for both temperatures, in 29% and 35.5%, respectively, due to the formation of an oxygen-enriched tribofilm. More recently, Hu *et al*.[18] studied the lubricating performance of two trialkylammonium carboxylate ILs with different

alkyl chain size, as additives to polyalphaolefin (PAO) applied to steel contacts at room temperature and low temperatures. At room temperature, the shorter alkyl chain IL showed the best performance while at low temperature (-20 °C) both ILs revealed excellent wear reduction due to the formation of ordered adsorbed films, although their friction reduction was not evident.

Deep Eutectic Solvents (DESs), which are considered by some authors as IL analogues,[19] might be another way of overcoming the high cost involved in the use of ILs as lubricants. DESs are mixtures which show a melting point lower than that of an ideal liquid mixture (see Figure 4.1) and are cheaper, less toxic and easier to prepare than ILs. They are composed of two or three components capable of self-association through hydrogen bond interactions (hydrogen bond donors, HBDs, and hydrogen bond acceptors, HBAs). The term DES was first proposed by Abbott *et al.*[20] to describe the mixture of choline chloride and urea (1:1 or 1:2). Since then, many articles have been published,[21,22] including a few studies on the use of DESs as lubricants for several types of contacts.[8,9,23]

A relevant number of publications reporting the use of ILs as lubricants and lubricant additives are available, in contrast with the reduced number of studies focusing the application of DES in lubrication. However, the understanding of tribofilm formation, which is responsible for the protection of the sliding surfaces, is not yet very clear.

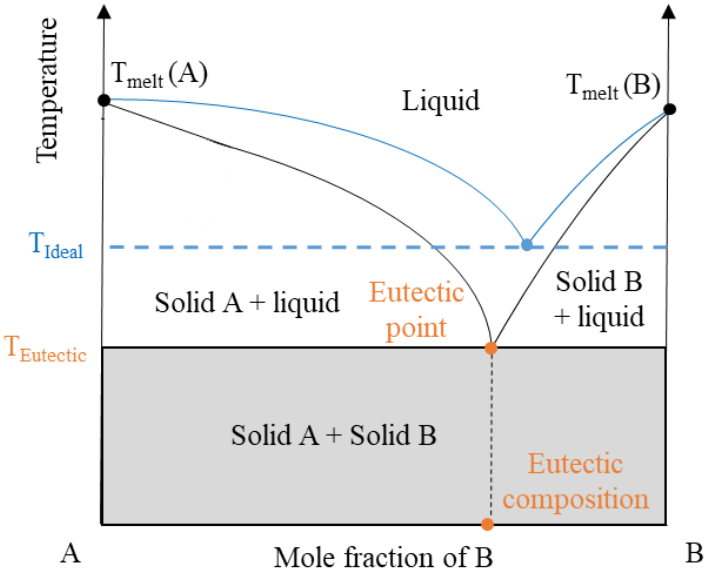

Figure 4.1. Phase diagram of a Deep Eutectic Solvent (DES), adapted from references [24,25].

With the aim of studying the performance of additives or neat lubricants under mixed sliding/rolling conditions, which are representative of gears and bearings, three ILs and two DES, which demonstrated very good lubrication capacity for stainless steel/silicon and silicon/silicon contacts in previous studies [7,8,26] were chosen to be tested as lubricants for ASTM 52,100 bearing steel. The ILs based on sulfur-containing anions, 1-hexyl-

methylimidazolium trifluoromethanesulfonate ([C6mim][TfO]), 1-hexyl-4-picolinium trifluoromethanesulfonate ([C6-4-pic][TfO]) and 4-picolinium hydrogen sulfate ([4-picH][HSO4]), were used as 2 wt.% additives in base oil polyethylene glycol MW 200 (PEG 200). The chosen DESs were the following: [C6-4-pic][TfO]:PEG 200:water (1:2:10%) and [Aliquat]Cl:octanol (1:1), where [Aliquat]Cl stands for methyltrioctylammonium chloride. For the first eutectic solvent, dissolution during scale-up was an issue, so water was added to help in the process. The structures of the studied liquids are presented in Figure 4.2. Previous to the tribolgical studies, the corrosive behavior of the liquids was determined since ASTM 52,100 steel with low chromium level has poor resistance to corrosion.[27] In view of the obtained results, addition of corrosion inhibitors was needed. The tribological properties were assessed, namely friction and wear, and the worn surfaces of both balls and discs were imaged and chemically analyzed in order to gain insight on the wear mechanism, whenever possible.

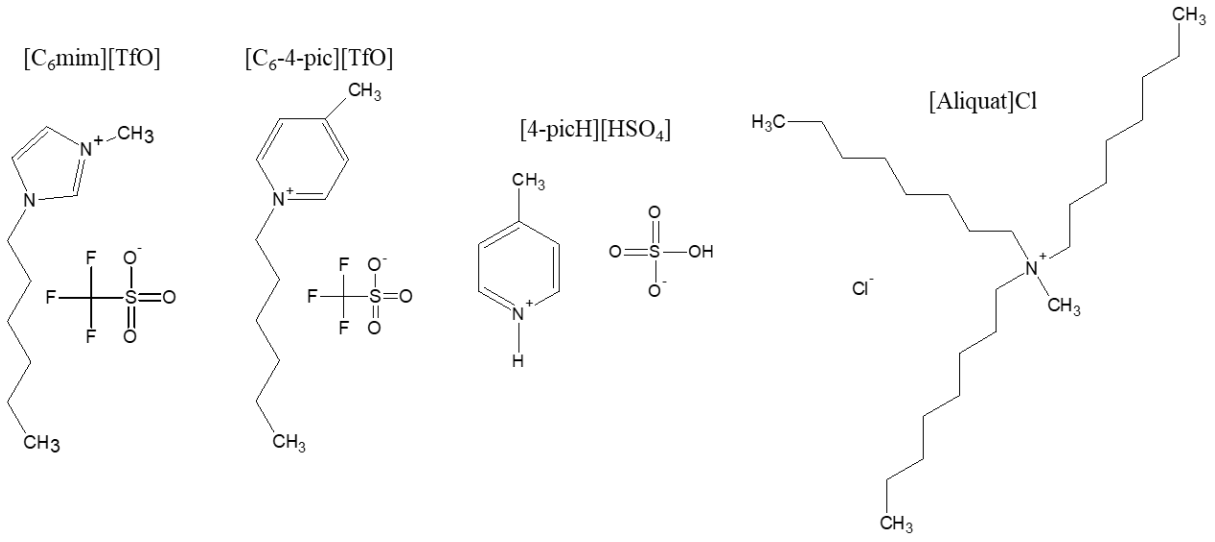

Figure 4.2. Chemical structures of the studied ILs and DES.

4.2 Experimental

4.2.1 Materials

All reagents for the synthesis of ILs and preparation of DES were purchased and used without additional purification. The list of reagents is the following: 4-methylpyridine 98% from Alfa Aesar (Tewksbury, MA, USA), methylimidazole 99% from Alfa Aesar (Tewksbury, MA, USA), sulfuric acid 95-97% from Merck (Rahway, NJ, USA), trioctylmethylammonium chloride [Aliquat]Cl from Alfa Aesar (Tewksbury, MA, USA) and 1-octanol 99% from Alfa Aesar (Tewksbury, MA, USA).

The solvents were acetonitrile 99.8% from Merck (Darmstadt, Germany) and deuterated water 99.9% from Eurisotop (Gif sur Yvette, France). Polyethylene glycol (MW 200) – PEG200 was from Sigma-Aldrich (Rahway, NJ, USA), with water content <0.5 %. Corrosion inhibitor Additin® RC 4801 was from Lanxess (Pittsburgh, PA, USA). Distilled and deionized water (DD) was obtained with a Millipore system.

4.2.2 Methods

The syntheses of ILs [C_6mim][TfO], [C_6-4-pic][TfO] and [4-picH][HSO_4] were described in previous works.[7,24] The preparation of DES [C_6-4-pic][TfO]:PEG 200:water (1:2:10%) was done in an analogous way to the described in a previous work,[8] apart from the addition of water due to solubility issues during scale-up. DES [Aliquat]Cl:octanol (1:1) was prepared by mixing the components in a 1:1 proportion under vigorous stirring for 24h. This eutectic was characterized by ^{1}H-NMR in order to check the chemical structure and purity (see Figure A.4.1 in Annex 4.1).

Corrosion tests were done by deposition of two to three drops of the ILs and DES, with and without corrosion inhibitor RC 4801, on steel discs for 48 h. Afterwards, the steel samples were carefully washed with toluene and isopropanol, each for 10 minutes, in an ultrasound bath.

The viscosity of the liquids was measured using a rheometer MCR 92 (Anton Paar, Graz, Austria). The results are average values obtained from three measurements.

The tribological tests were conducted in a Mini-Traction Machine (MTM, PCS Instruments, London, UK) that was used to measure traction coefficients under specified conditions. MTM is a ball-on-disc tribometer presented in Figure 4.3 in which the rotation of the ball is independent to the rotation of the disc, enabling access to a range of slide-to-roll ratios (SRR). 52,100 steel highly polished balls (19.05 mm diameter, RMS = 0.5±0.2 nm) and discs (46 mm diameter, RMS = 0.5±0.2 nm) from PCS Instruments (London, UK) were used for the tribological tests. The balls and discs were AISI/ASTM 52,100 bearing steel which is a high carbon, chromium containing low alloy steel.

Stribeck curve measurements were performed at 60 °C, over a wide range of speeds (from 2000 to 10 mm·s^{-1} entrainment speed), SRR of 50% and an applied load of 50 N, yielding a Hertzian maximum contact pressure of 1.12 GPa. All other MTM measurements were carried out at an entrainment speed of 10 mm·s^{-1}. Prior to testing, the specimen (balls and discs) and the removable MTM components were cleaned by sonication for 10 minutes in each of toluene and 2-propanol. All parts were wiped with Kimwipe after the cleaning process and residual fibers were removed with compressed nitrogen gas. The MTM pot was rinsed in toluene followed by 2-propanol and dried with compressed nitrogen gas. This rinsing and drying procedure was performed three times or until the lubricants were removed completely.

After the tribological tests, the tracks were imaged with White Light Interferometry using a Zygo NewView 6300 Interferometer with a 20× objective and 0.5× internal multiplier, yielding

a magnifcation level of 10× and a 530 μm×700 μm field of view. The images were analyzed using software program Gwyddion.[28] The MTM balls were imaged with a vertical scan range of 150 μm and the images were leveled through a spherical subtraction in Gwyddion.

A BX51 Optical Microscope (Olympus, Florida, USA) was used to assess the tribofilm formation on the wear tracks after the tribological tests. The images were analyzed using ImageJ software.[29]

The elemental composition of the wear tracks on the 52,100 steel discs was studied by X-ray photoelectron spectroscopy (XPS), using an Axis Supra spectrometer (Kratos Analytical Ltd., Manchester, UK). A monochromatic Al Kα source was run at 225W. The detailed spectra were acquired at a pass energy of 20 eV through an aperture of 110 μm. Data analysis was done with CasaXPS. Atomic percentages were calculated assuming a homogenous distribution of elements, using the Kratos relative sensitivity factors.

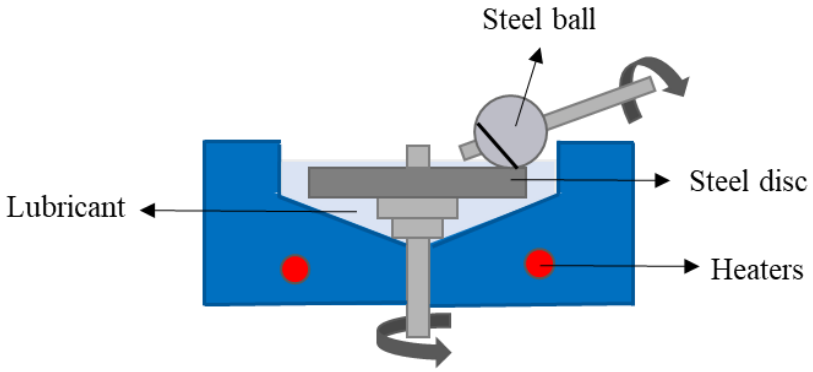

Figure 4.3. Schematic representation of the Mini-Traction Machine (MTM) used for the tribological experiments.

4.3 Results and Discussion

4.3.1 Corrosion experiments

ILs are known to be corrosive of steel [30,31] so all fluids were tested and corrosion of the steel surfaces was observed. A semi-ester of succinic acid derivative corrosion inhibitor, RC 4801 (acid value: 160 mg KOH/g, and is cut in 30% mineral oil) was added to the liquids at a 1 wt.% concentration and the corrosion inhibition capability was evaluated.

The mixtures of PEG 200 with 2% [C_6mim][TfO] and 2% [C_6-4-pic][TfO], the two less chemically aggressive liquids, corroded the steel when no corrosion inhibitor was used, but adding a small amount of corrosion inhibitor was enough to prevent corrosion. Optical microscopy images of the steel surfaces after contacting the two tested ILs, with and without corrosion inhibitor, are presented in Figure 4.4.

In contrast, the addition of corrosion inhibitor was not sufficient to prevent corrosion for the mixture PEG200+2%[4-picH][HSO_4] and the DESs [Aliquat]Cl:octanol (1:1) and [C_6-4-pic][TfO]:PEG 200:water (1:2:10%), even when a higher concentration (5 wt.%) of corrosion inhibitor was used. The optical microscopy images showing signs of corrosion for these fluids are presented in Figure A.5.1 in the Supporting Information. Considering these results, further tests were only carried out with PEG 200 + 2% [C_6mim][TfO] + 1%RC 4801 and PEG 200 + 2% [C_6-4-pic][TfO] + 1%RC 4801.

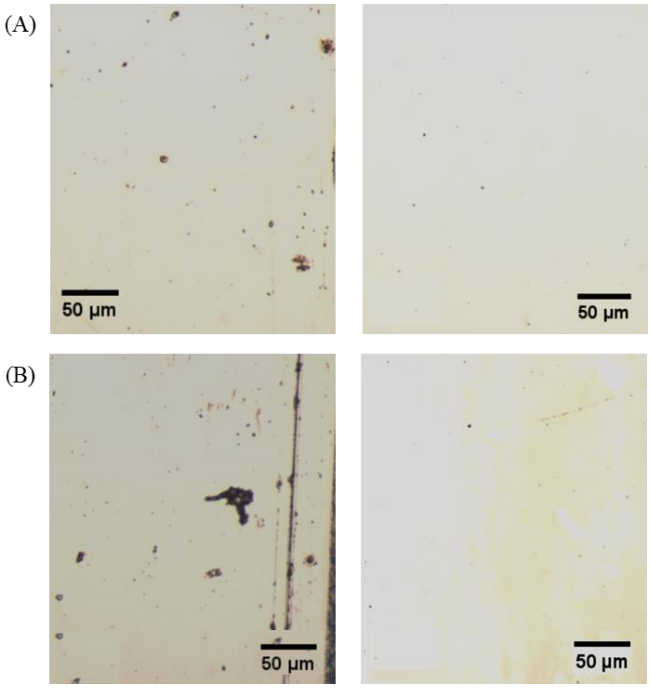

Figure 4.4. Optical microscopy images (10× magnification) of 52,100 steel discs after contacting (A) PEG 200 + 2%[C_6-4-pic][TfO] and (B) PEG 200 + 2%[C_6mim][TfO], without (left) and with (right) corrosion inhibitor.

4.3.2 Traction coefficient measurements

The viscosities of PEG 200 + 1% RC 4801, PEG200 + 2% [C_6-4-pic][TfO] + 1% RC 4801 and PEG200 + 2% [C_6mim][TfO] + 1% RC 4801 were measured as a function of temperature from 25 °C to 60 °C, prior to the tribological tests. The results are presented in Figure 4.5 which shows that the three mixture have similar, low viscosities in the whole temperature range.
Stribeck curves (traction coefficient *vs*. rolling speed) obtained for the mixtures of ILs + PEG 200 at 60 °C from 2000 to 10 mm·s^{-1} entrainment speed are shown in Figure 4.6. The measurements were performed under mixed sliding/rolling contact conditions through the application of a slide-to-roll ratio (SRR) of 50%, which is given by the following equation:

$$SRR = \frac{|u_D - u_B|}{U} \qquad \text{Eq. 4.1}$$

where u_B is the ball speed, u_D is the disc speed and U is the entrainment speed, defined as $(u_B + u_D)/2$.

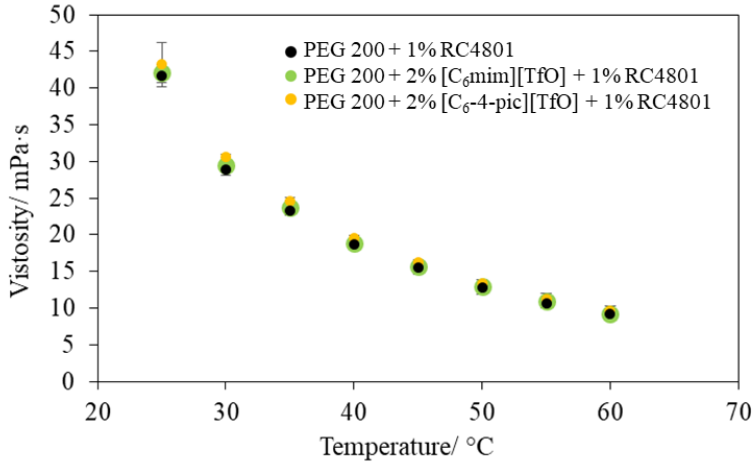

Figure 4.5. Viscosity *vs*. temperature for the studied mixtures. The values correspond to the average of three measurements for each sample.

Although the differences on the Stribeck curves are small, it is possible to observe that, at low and intermediate speeds, the mixture with [C6mim][TfO] led to a decrease in friction relative to the value obtained without the IL (neat PEG), while [C6-4-pic][TfO] increased the friction. The minimum film thickness, h_0, was calculated according to the elastohydrodynamic theory and the Hamrock-Dowson model [32] for an entrainment speed of 10 mm·s^{-1}. The obtained value was 2.25 nm, which compared with the composite surface roughness yields a specific film thickness λ of 0.45 (λ<1), indicating boundary contact conditions. The details of these calculations are given in Annex A.5. In order to assess wear performance of the ILs under aggressive boundary contact, subsequent tests were performed at the speed of 10 mm·s^{-1}.

A mixing of sliding and rolling was applied through the application of a slide-to-roll ratio (SRR) of 50%. Traction curves were obtained at the determined conditions and each 4h test was performed with new and washed 52,100 ball/disc pairs. The results are presented in Figure 4.7 where it is possible to see a slight improvement (up to 12%) on the traction coefficient of PEG 200 + 2% [C6mim][TfO] + 1%RC 4801 when compared to neat PEG 200+1%RC 4801. These results indicate that [C6mim][TfO] can be used as an anti-friction modifier. In order to assess the potential effect of the IL concentration on friction reduction, a higher concentration of 5 wt.% was used. The results are presented in Figure A.5.2 (Supporting Information), where it is possible to see that this ILimproved significantly the traction coefficient for the first hour,

indicating that [C6mim][TfO] 5% PEG+1% RC 4801 could be used as a friction modifier for short periods of time. After the running-in period, this mixture reaches high traction coefficients but stabilizes to values close to PEG 200+1% RC4801 after three hours.

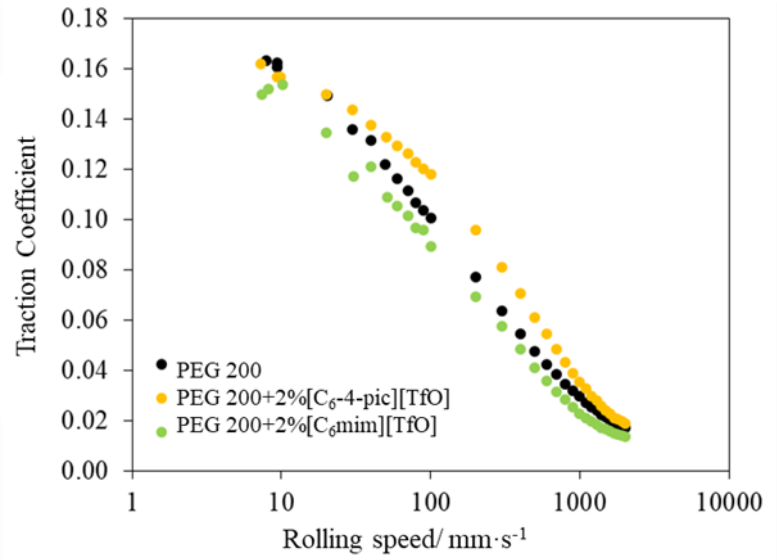

Figure 4.6. Stribeck curves obtained at 50 N and 60 °C, from 2000 to 10 mm·s^{-1} entrainment speed, for PEG 200 + 1% RC 4801, PEG 200 + 2% [C6-4-pic][TfO] + 1% RC 4801 and PEG 200 + 2% [C6mim][TfO] +1% RC 4801. These results correspond to averages of at least two runs.

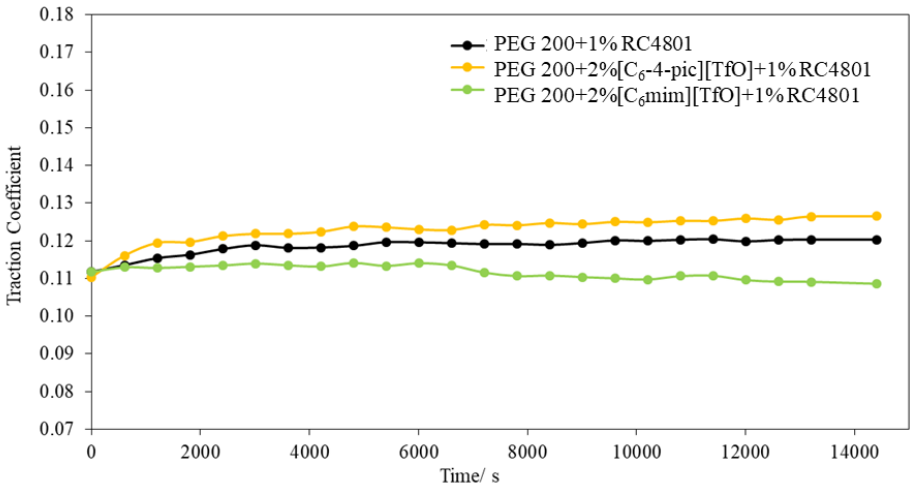

Figure 4.7. Traction coefficient *vs*. time for 52,100 steel/steel tribopairs at an entrainment speed of 10 mm·s^{-1} and under the load of 50N for the studied liquids. These results correspond to averages of at least two runs.

4.3.3 Surface characterization

After the wear experiments, the ball and disc surfaces were imaged by White Light Interferometry (WLI) and the wear profiles were obtained. The wear volumes obtained for the balls and discs are shown in Figure 4.8. These values were calculated based on the mean of at least four cross-section profiles for each sample.

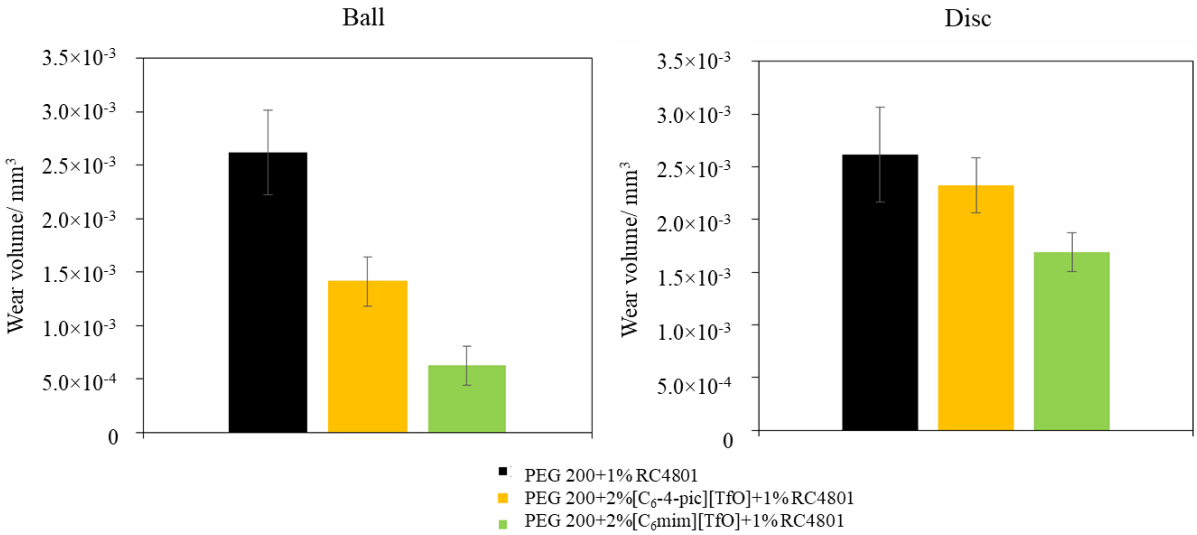

Figure 4.8. Average wear volumes obtained for steel balls (left image) and discs (right image) after long tribological tests (4h) at an entrainment speed of 10 mm·s^{-1} and under the load of 50N. The errors are ± standard deviation (n ≥ 4).

Regarding the steel balls, PEG 200 + 2% [C$_6$-4-pic][TfO] + 1%RC 4801 allowed an improvement on the wear protection of ~46% when compared to neat PEG 200+1%RC 4801, while the equivalent improvement for PEG 200 + 2% [C$_6$mim][TfO] + 1%RC 4801 was of ~76%. In the case of the discs, when comparing to PEG+1%RC 4801, [C$_6$-4-pic][TfO] allowed for a wear reduction of ~11% while [C$_6$mim][TfO] reduced wear in ~35%, showing the best wear performance overall.

In Figure 4.9 and Figure 4.10 the WLI images and wear profiles of the balls and discs are shown. The mixtures containing ILs presented narrower and less deep profiles for both ball and disc when compared to neat PEG 200+1%RC 4801, specially the one containing [C$_6$mim][TfO].

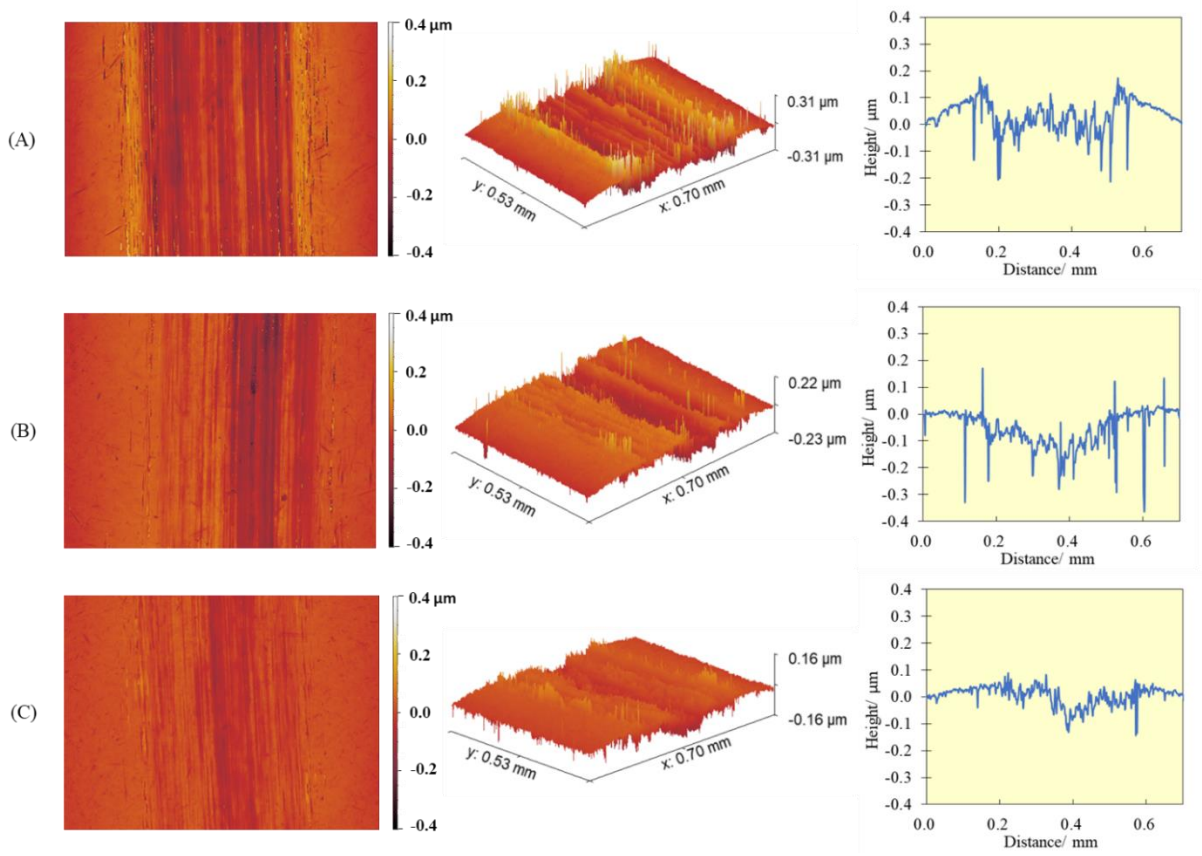

Figure 4.9. Wear profiles of the steel balls (WLI images with 20× magnification) after long tribological tests (4h) at an entrainment speed of 10 mm·s^{-1}, under the load of 50N using as lubricants: (A) PEG200 + 1%RC 4801, (B) PEG 200 + 2%[C_6-4-pic][TfO] + 1%RC 4801 and (C) PEG 200 + 2% [C_6mim][TfO] + 1%RC 4801. Z scale is 1000× magnified compared to lateral scale.

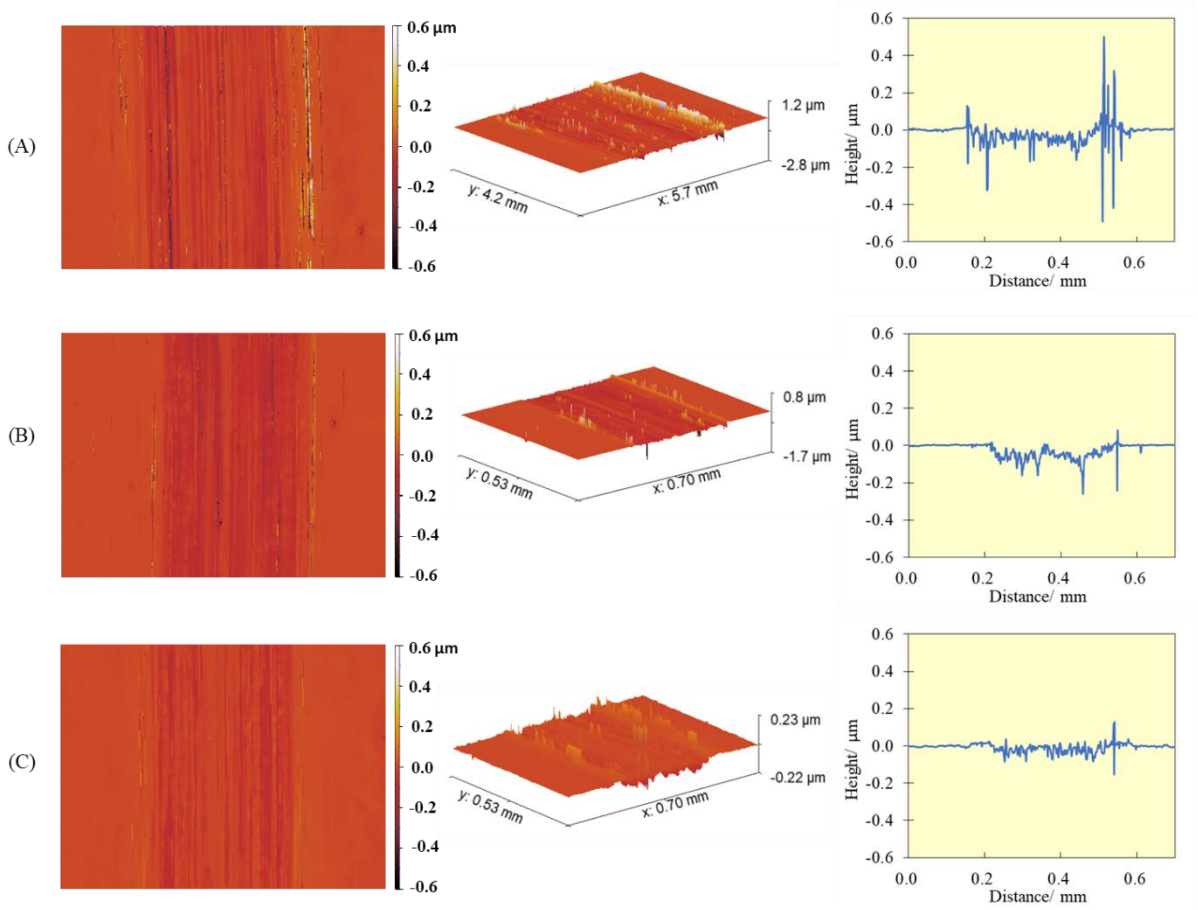

Figure 4.10. Wear profiles of the steel discs (WLI images with 20× magnification) after long tribological tests (4h) at an entrainment speed of 10 mm·s^{-1}, under the load of 50N using as lubricants: (A) PEG200 + 1%RC 4801, (B) PEG 200 + 2% [C$_6$-4-pic][TfO] + 1%RC 4801 and (C) PEG 200 + 2% [C$_6$mim][TfO] + 1%RC 4801. Z scale is 1000× magnified compared to lateral scale.

The wear tracks of the discs were also analyzed by optical microscopy in order to check for indication of tribofilm formation (see Figure 4.11). As can be seen from the images, when the tests were carried out with PEG 200+1%RC 4801, no evidence of tribofilm formation was seen. However, a bluish color can be seen on the wear tracks of the tests carried out with both ILs added to PEG 200+1%RC 4801, indicating the formation of a tribofilm, as reported by other authors in zinc dialkyldithiophosphate (ZDDP) tribofilms.[33-35] This blue color is due to interference of light reflecting off the underlying substrate and the light reflecting off the top surface of the tribofilm.

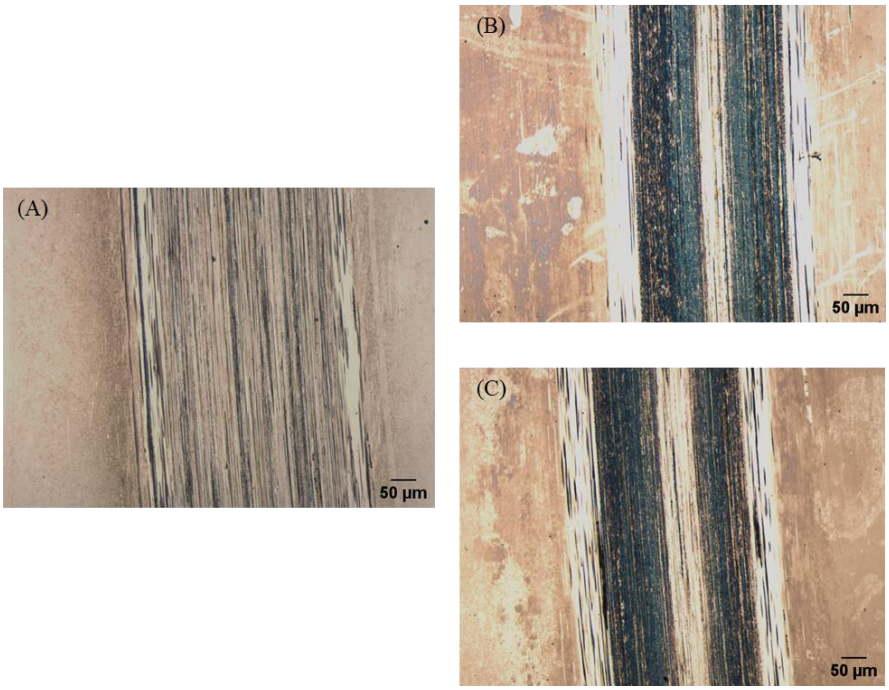

Figure 4.11. Optical microscopy images (10× magnification) of the wear tracks after the tribological tests for (A) PEG 200 + 1%RC 480, (B) PEG 200 + 2% [C_6-4-pic][TfO] + 1%RC 4801 and (C) PEG 200 + 2% [C_6mim][TfO] + 1%RC 4801.

XPS analysis of the 52,100 steel discs inside the wear tracks was performed, providing insight on the chemical composition of the tribofilms (see Table 4.1). It is possible to see the presence of N and S inside the wear tracks in both the discs with ILs. However, the atomic percentages of N 1s and S 2p are considerably higher for the best performing mixture PEG 200 + 2% [C_6mim][TfO] + 1% RC 4801, confirming that this IL has more tendency to adsorb to the surface. Comparison between the N 1s and S 2p signs suggests that the IL interacts preferentially with the steel surface through the N-containing cation, although the S-containing anion takes some part in the adsorption as well. Regarding Fe 1s, O 1s and C 1s signs, the data are in agreement with the presence of an IL adsorbed layer, which partially hides the underlying iron oxides, leading to the reduction of the relative amounts of Fe 2p and O1s and the increase of the relative amount of C 1s.

Table 4.1. Relative surface atomic concentrations inside the wear tracks.

Lubricant	Relative Atomic Percentages				
	Fe 2p	O 1s	C 1s	N 1s	S 2p
PEG200 + 1% RC 4801	5.32	34.53	60.14	-	-
PEG200+2% [C_6-4-pic][TfO] + 1%RC 4801	0.88	27.87	70.94	0.21	0.09
PEG200 + 2% [C_6mim][TfO] + 1%RC 4801	2.17	30.21	66.51	0.96	0.14

4.4 Conclusions

The tribological performance of several ILs and DES was studied for 52,100 steel contacts. Some of the studied liquids were corrosive of steel, even when a corrosion inhibitor was added, and were disregarded. Two ILs, [C_6mim][TfO] and [C_6-4-pic][TfO], were tested with 1 wt.% corrosion inhibitor as anti-wear additives in base oil PEG 200 and revealed very interesting lubricating properties. PEG 200 + 2% [C_6mim][TfO] + 1% RC4801 allowed for a decrease in wear up to ~76%, acting as an anti-wear additive and reduced friction, acting as a friction modifier. On the other hand, PEG 200 + 2% [C_6-4-pic][TfO] + 1% RC4801 did not have an evident effect on friction reduction but reduced wear up to ~46% when comparing to neat PEG 200 + 1% RC4801, acting as an anti-wear additive. XPS analysis allowed to conclude that [C_6mim][TfO] has a higher tendency to adsorb to the steel surface, leading to a significant protection of the sliding surfaces. Regarding the other studied ILs and DES, further studies need to be done, particularly focusing on preventing the corrosion of 52,100 steel.

The results obtained with the two ILs open the way to the use of these environmentally friendly compounds as potential lubricants for steel bearings. These ILs were able to reduce wear of the steel surfaces under extreme pressure conditions (1.12 GPa), which is of great importance for several industries due to the lowering costs in replacing bearing steel parts.

4.5 References

[1] A. Panda, A. K. Sahoo, R. Kumar, R. K. Das, A Review on Machinability Aspects for AISI 52100 Bearing Steel. *Mater. Today Proc.* **2020**, *23*, 617–621. https://doi.org/10.1016/j.matpr.2019.05.422

[2] R. Ferreira, Ó. Carvalho, J. Pires, L. Sobral, S. Carvalho, F. Silva, A New Tribometer for the Automotive Industry: Development and Experimental Validation. *Exp. Mech.* **2022**, *62* (3), 483–492. https://doi.org/10.1007/s11340-021-00805-7

[3] S. C. Tung, M. L. McMillan, Automotive Tribology Overview of Current Advances and Challenges for the Future. *Tribol. Int.* **2004**, *37* (7), 517–536. https://doi.org/10.1016/j.triboint.2004.01.013

[4] Y. Zhou, J. Qu, Ionic Liquids as Lubricant Additives: A Review. *ACS Appl. Mater. Interfaces* **2017**, *9* (4), 3209–3222. https://doi.org/10.1021/acsami.6b12489

[5] W. Wijanarko, H. Khanmohammadi, N. Espallargas, Ionic Liquid Additives in Water-Based Lubricants for Bearing Steel – Effect of Electrical Conductivity and PH on Surface Chemistry, Friction and Wear. *Front. Mech. Eng.* **2022**, *7*, 756929. https://doi.org/10.3389/fmech.2021.756929

[6] M. Antunes, M. T. Donato, V. Paz, F. Caetano, L. Santos, R. Colaço, L. C. Branco, B. Saramago, Improving the Lubrication of Silicon Surfaces Using Ionic Liquids as Oil Additives: The Effect of Sulfur-Based Functional Groups. *Tribol. Lett.* **2020**, *68* (2), 70. https://doi.org/10.1007/s11249-020-01308-7

[7] M. T. Donato, F. Caetano, R. Colaço, L. C. Branco, B. Saramago, Picolinium-Based Hydrophobic Ionic Liquids as Additives to PEG200 to Lubricate Steel-Silicon Contacts. *ChemistrySelect* **2020**, *5* (20), 5864–5872. https://doi.org/10.1002/slct.202000613

[8] M. T. Donato, L. Santos, H. P. Diogo, R. Colaço, L. C. Branco, B. Saramago, Eutectic Systems Containing an Ionic Liquid and PEG200 as Lubricants for Silicon Surfaces: Effect of the Mixture's Molar Ratio. *J. Mol. Liq.* **2022**, *350*, 118572. https://doi.org/10.1016/j.molliq.2022.118572

[9] M. T. Donato, R. Colaço, L. C. Branco, B. Saramago, A Review on Alternative Lubricants: Ionic Liquids as Additives and Deep Eutectic Solvents. *J. Mol. Liq.* **2021**, *333*, 116004. https://doi.org/10.1016/j.molliq.2021.116004

[10] S. D. A. Lawes, S. V. Hainsworth, P. Blake, K. S. Ryder, A. P. Abbott, Lubrication of Steel/Steel Contacts by Choline Chloride Ionic Liquids. *Tribol. Lett.* **2010**, *37* (2), 103–110. https://doi.org/10.1007/s11249-009-9495-6

[11] A. Sierra, M. G. Coleman, P. Iglesias, Tribological Properties of Borate-Based Protic Ionic Liquids as Neat Lubricants and Biolubricant Additives for Steel-Steel Contact. *Lubricants* **2022**, *10* (10), 269. https://doi.org/10.3390/lubricants10100269

[12] M. Yao, Y. Liang, Y. Xia, F. Zhou, Bisimidazolium Ionic Liquids as the High-Performance Antiwear Additives in Poly(Ethylene Glycol) for Steel–Steel Contacts. *ACS Appl. Mater. Interfaces* **2009**, *1* (2), 467–471. https://doi.org/10.1021/am800132z

[13] L. Weng, X. Liu, Y. Liang, Q. Xue, Effect of Tetraalkylphosphonium Based Ionic Liquids as Lubricants on the Tribological Performance of a Steel-on-Steel System. *Tribol. Lett.* **2007**, *26* (1), 11–17. https://doi.org/10.1007/s11249-006-9175-8

[14] A. Khan, R. Gusain, M. Sahai, O. P. Khatri, Fatty Acids-Derived Protic Ionic Liquids as Lubricant Additive to Synthetic Lube Base Oil for Enhancement of Tribological Properties. *J. Mol. Liq.* **2019**, *293*, 111444. https://doi.org/10.1016/j.molliq.2019.111444

[15] R. Kreivaitis, M. Gumbytė, A. Kupčinskas, K. Kazancev, T. N. Ta, J. H. Horng, Investigation of Tribological Properties of Two Protic Ionic Liquids as Additives in Water for Steel–Steel and Alumina–Steel Contacts. *Wear* **2020**, *456–457*, 203390. https://doi.org/10.1016/j.wear.2020.203390

[16] H. Guo, J. Pang, A. R. Adukure, P. Iglesias, Influence of Hydrogen Bonding and Ionicity of Protic Ionic Liquids on Lubricating Steel–Steel and Steel–Aluminum Contacts: Potential Ecofriendly Lubricants and Additives. *Tribol. Lett.* **2020**, *68* (4), 114. https://doi.org/10.1007/s11249-020-01354-1

[17] H. Guo, P. Iglesias, Tribological Behavior of Ammonium-Based Protic Ionic Liquid as Lubricant Additive. *Friction* **2021**, *9* (1), 169–178. https://doi.org/10.1007/s40544-020-0378-z

[18] H. Fang, Y. Li, S. Zhang, Q. Ding, L. Hu, Lubricating Performances of Oil-Miscible Trialkylanmmonium Carboxylate Ionic Liquids as Additives in PAO at Room and Low Temperatures. *Appl. Surf. Sci.* **2021**, *568*, 150922. https://doi.org/10.1016/j.apsusc.2021.150922

[19] E. L. Smith, A. P. Abbott, K. S. Ryder, Deep Eutectic Solvents (DESs) and Their Applications. *Chem. Rev.* **2014**, *114* (21), 11060–11082. https://doi.org/10.1021/cr300162p

[20] A. P. Abbott, G. Capper, D. L. Davies, R. K. Rasheed, V. Tambyrajah, Novel Solvent Properties of Choline Chloride/Urea Mixtures. *J. Chem. Commun.* **2003**, No. 1, 70–71. https://doi.org/10.1039/b210714g

[21] E. L. Smith, A. P. Abbott, K. S. Ryder, Deep Eutectic Solvents (DESs) and Their Applications. *Chem. Rev.* **2014**, *114* (21), 11060–11082. https://doi.org/10.1021/cr300162p

[22] B. Gurkan, H. Squire, E. Pentzer, Metal-Free Deep Eutectic Solvents: Preparation, Physical Properties, and Significance. *J. Phys. Chem. Lett.* **2019**, *10* (24), 7956–7964. https://doi.org/10.1021/acs.jpclett.9b01980

[23] M. Antunes, A. S. Campinhas, M. de Sá Freire, F. Caetano, H. P. Diogo, R. Colaço, L. C. Branco, B. Saramago, Deep Eutectic Solvents (DES) Based on Sulfur as Alternative Lubricants for Silicon Surfaces. *J. Mol. Liq.* **2019**, *295*, 111728. https://doi.org/10.1016/j.molliq.2019.111728

[24] M. T. Donato, J. Deuermeier, R. Colaço, L. C. Branco, B. Saramago, New Protic Ionic Liquids as Potential Additives to Lubricate Si-Based MEMS/NEMS. *Molecules* **2023**, *28* (6), 2678. https://doi.org/10.3390/molecules28062678

[25] E. L. Smith, A. P. Abbott, K. S. Ryder, Deep Eutectic Solvents (DESs) and Their Applications. *Chem. Rev.* **2014**, *114* (21), 11060–11082. https://doi.org/10.1021/cr300162p

[26] M. A. R. Martins, S. P. Pinho, J. A. P. Coutinho, Insights into the Nature of Eutectic and Deep Eutectic Mixtures. *J. Solut. Chem.* **2019**, *48* (7), 962–982. https://doi.org/10.1007/s10953-018-0793-1

[27] E. V. Zaretsky, Rolling Bearing Steels – a Technical and Historical Perspective. *Mater. Sci. Technol.* **2012**, *28* (1), 58–69. https://doi.org/10.1179/1743284711Y.0000000043

[28] D. Nečas, P. Klapetek, Gwyddion: An Open-Source Software for SPM Data Analysis. *Open Phys.* **2012**, *10* (1). https://doi.org/10.2478/s11534-011-0096-2

[29] C. A. Schneider, W. S. Rasband, K. W. Eliceiri, NIH Image to ImageJ: 25 Years of Image Analysis. *Nat. Methods* **2012**, *9* (7), 671–675. https://doi.org/10.1038/nmeth.2089

[30] M. Uerdingen, C. Treber, M. Balser, G. Schmitt, C. Werner, Corrosion Behavior of Ionic Liquids. *Green Chem.* **2005**, *7* (5), 321. https://doi.org/10.1039/b419320m

[31] M. F. Arenas, R. G. Reddy, Corrosion of Steel in Ionic Liquids. *J. Min. Metall. Sect. B Metall.* **2003**, *39* (1–2), 81–91. https://doi.org/10.2298/JMMB0302081A

[32] B. J. Hamrock, D. Dowson, Isothermal Elastohydrodynamic Lubrication of Point Contacts: Part III—Fully Flooded Results. *J. Lubr. Technol.* **1977**, *99*, 264–275. https://doi.org/10.1115/1.3453074

[33] C. J. Hsu, A. Stratmann, A. Rosenkranz, C. Gachot, Enhanced Growth of ZDDP-Based Tribofilms on Laser-Interference Patterned Cylinder Roller Bearings. *Lubricants* **2017**, *5* (4), 39. https://doi.org/10.3390/lubricants5040039

[34] M. Lorenz, A. A. Pawlicki, H. E. Hysmith, K. Cogen, H. Thaker, O. S. Ovchinnikova, Direct Multimodal Nanoscale Visualization of Early Phosphorus-Based Antiwear Tribofilm Formation. *ACS Appl. Mater. Interfaces* **2022**, *14* (30), 35157–35166. https://doi.org/10.1021/acsami.1c16761

[35] K. J. Kubiak, T. G. Mathia, M. Bigerelle, Influence of Roughness on ZDDP Tribofilm Formation in Boundary Lubricated Fretting. *Tribol. - Mater. Surf. Interfaces* **2012**, *6* (4), 182–188. https://doi.org/10.1179/1751584X12Y.0000000020

5

CONCLUSIONS AND FUTURE PERSPECTIVES

One of the 12 Principles of Green Chemistry relies on the Design for Energy Efficiency, so reactions that use environmentally friendly solvents or that do not require any solvent are extremely important. Aiming to reduce the use of toxic and volatile organic solvents, Ionic Liquids have emerged as greener alternatives, showing improved properties in several fields, such as in the lubrication of different types of contacts.

Tribological contacts are responsible for around 23% of the world's total energy consumption, mostly due to friction and wear created between moving parts. Efficient lubrication could eventually decrease the energy losses caused by friction and wear by 40% in the long term and by 18% in the short term. This would correspond to savings of 1.4% of the gross domestic product in the USA and 8.7% of the worldwide energy consumption in the long term. With that in mind and moving towards a more sustainable world, it is of extreme importance to have good lubrication between moving parts, aiming to improve global energy efficiency.

Ionic Liquids as environmentaly friendly and sustainable functional materials have shown very interesting lubricanting properties. However, they are very expensive to be applied as neat lubricants; the use of Ionic Liquids as additives to commonly used base oils or the use of Deep Eutectic Solvents might be a good way to overcome this drawback.

This thesis focuses on the search of efficient lubricants for silicon surfaces, as silicon is one of the main components of MEMS and NEMS, which are miniturized devices with great impact in our day-to-day lives. Although studies in silicon are the main focus of this thesis, some studies and applications in steel surfaces are also addressed, as steel is yet one of the most used materials due to its hardness and resistance. In the scope of this work, several Ionic Liquids and Deep Eutectic Solvents have been synthesized or prepared: aprotic and protic ILs as additives and hydrophilic or hydrophobic DESs based on ionic liquids and/or natural compounds. Ionic Liquids were used at a 2 wt.% concentration in base oil PEG 200, which is a very small amount, making this approach more economically viable.

The first series of results were obtained with aprotic ILs based on imidazolium and pyridinium cations in combination with an anion containing sulfur (triflate, [TfO]), as previous studies already showed that S-containing ILs lead to improved lubrication. The ILs were synthesized using the microwave process, which is a much more sustainable approach, allowing to obtain the desired ILs with higher purities and prepared in considerably less time (35 minutes *vs*. 24-48 hours using conventional heating). The tribological results obtained with these ILs as additives were very promising, particularly in the case of [C_6-4-pic][TfO], which demonstrated good friction reduction for low loads (in the order of magnitude of mN) comparing to base oil PEG 200. This behavior was attributed to the symmetry of the cation leading to an ordered adsorbed layer.

Regarding protic Ionic Liquids (PILs), five different cations were chosen in combination with two different S-containing anions, methylsulfate [$MeSO_3$] and hydrogensulfate [HSO_4]. The results obtained with these liquids were very promising, particularly [4-picH][HSO_4], which revealed excellent lubrication capacity and minimized third-body abrasive wear up to 15 times

when comparing to base oil PEG 200. Analysis of the wear tracks allowed to conclude that the symmetric cation [4-picH] and the anion [HSO_4] adsorbed strongly to the Si surface, leading to the formation of a protective film.

In parallel, eutectic mixtures, without the requirement of being deep eutectic solvents, that were designated by eutectic systems (ES), containing the previouly synthesized ionic liquid [C_6-4-pic][TfO] in combination with PEG 200 in different molar ratios (1:2, 1:4, 1:8 and 1:16) were studied. ES (1:2) revealed to be in the eutectic composition, having the stronger interactions between the mixture's components. This ES (1:2) packs in order to maximize the hydrogen bonds and leads to the formation of a stable tribofilm, which ensures the lowest values of CoF and wear of the Si surface for the highest applied load.

Moreover, hydrophobic DESs based on ILs, such as [Aliquat]Cl, showed very interesting properties, particularly in combination with natural components such as menthol and octanol. The results obtained with this set of compounds were very promising in terms of friction and wear reduction when comparing to hexadecane, which was proven by XPS to be related with the adsorption of [Aliquat]Cl on the surface. Although [Aliquat]Cl:octanol (1:1) was slightly better than [Aliquat]Cl:menthol (1:2) for low load (1N), the latter revealed to be much more effective for higher loads, presenting no wear on the Si surface for loads up to 12 N, which corresponds to a maximium contact pressure of 1.34 GPa.

In general, the best performing IL was [4-picH][HSO_4] and the best DES was [Aliquat]Cl:menthol (1:2), reaching CoF values of ~0.06 and ~0.03, respectively, for low loads. The mentioned DES, in particular, stands out as a very promising lubricant for Si-based MEMS/NEMS as it is composed of low cost and commercial components. Besides that, it exhibited very good tribological performance under high contact stresses, being resistant to ambient humidy.

Some of the best Ionic Liquids and Deep Eutectic Solvents were applied in more realistic conditions to lubricate steel contacts. Although some of the mixtures corroded the steel surfaces, such as the ones containing [4-picH][HSO_4] and [Aliquat]Cl, [C_6mim][TfO] as 2 wt.% additive to PEG 200 showed very interesting lubricating properties. This IL allowed for a decrease in wear up to ~76% comparing to base oil PEG 200, acting as an anti-wear additive, and reduced friction, acting as a friction modifier. Regarding the other studied ILs and DESs, further studies need to be done, particularly in regard to preventing corrosion of 52,100 steel.

Most studied ILs and DESs reduced the friction between moving parts when comparing to the neat base oils (PEG 200 or hexadecane) and effectively protected the steel and/or silicon surfaces from wear, sometimes under extreme pressure conditions (1.12 GPa or higher). This translates into lower costs in replacing parts which is of extreme importance on the lubrication of MEMS/NEMS and for several industries that use steel (in vehicle parts, turbines, engines and varied manufacturing equipment) such as the automotive industry and others.

With the experience acquired from this thesis, it is possible to conclude that both Ionic Liquids and Deep Eutectic Solvents are very promising lubricant alternatives. Using a small amount

of 2 wt.% of ILs as additives to commonly used base oils is a very inexpensive and efficient way to modulate properties such as viscosity, which is very important in lubrication. ILs can be easily tuned according to the final desired application, through the choice of an adequate cation/ anion combination, which is a great advantage regarding the design of efficient materials. In terms of cations, choosing aromatic ones may enhance the interaction with other components, such as the contacting surface, through π-π interactions. The labile proton of protic ILs is also more available to interact with the surface, when comparing to aprotic ILs.

In the case of Deep Eutectic Solvents, studies with hydrophilic and hydrophobic DESs were performed, with the aim of trying to control the water adsorption. Although hydrogen bond donors and acceptors already interact with each other to form hydrogen bonding, making DESs, in principle, less predisposed to interact with the surface, one of the best results was obtained using a hydrophobic DES. This may be explained by the fact that DESs have higher cohesive forces than ILs in solution. Further analysis could be performed in order to understand these results, namely through *in situ* analysis of the formed tribofilms.

Both studied approaches can be interesting from an industrial point of view. ILs are more adaptable in terms of applications because they can be used as additives to already existing and commercialized base oils, enhancing the tribological properties without increasing the price too much. However, depending on the final application, problems such as corrosion may need to be taken into account. DESs are very promising lubricant alternatives as well, mainly due to their easy preparation and low cost, which are very interesting points for their application in industry.

Molecular Dynamic simulations are currently undergoing in collaboration with Karina Shimizu from CQE of Instituto Superior Técnico in order to give insight on the adsorption mechanism of some of the studied liquids, which will allow a better understanding of the role of the molecular structure on the lubrication capacity. MD simulations are a very effective way to avoid the trial and error approach and can save a lot of time on the design of efficient ILs and DESs as lubricants.

Overall, the results presented in this thesis represent a contribution for the design and development of new ILs and DESs to be used as neat lubricants or lubricant additives, providing significant friction and wear reduction in machines with moving parts. Further work can be done in regard to exploring other types of contacts, using the results obtained in this thesis and in the MD simulations to better design ILs and DESs for different types of applications. For industrial application of these types of materials, challenges such as solubility, scale-up and potential corrosion need to be taken into account.

A

APPENDIX

This section presents the Supporting Information of each chapter. For **Chapter 2.1** the details of the synthesis are presented, including the analysis of the NMR spectra and the physico-chemical characterization of the prepared ionic liquids (^{1}H-NMR, ^{13}C-NMR, ^{19}F-NMR and FTIR data and viscosities and contact angles on Si surface for ILs with different water contents). An explanation for the calculation of the theoretical minimum film thickness is given and the variation of CoF with time is presented. For **Chapter 2.2** the detailed synthesis and characterization (^{1}H-NMR, ^{13}C-NMR, FTIR and elemental analysis) of the PILs is given. A comparison between the Stribeck curves of the different PILs according to the anion is presented. The film thickness is given, obtained both experimentally (AFM) and theoretically. The variation of CoF with time is presented. For **Chapter 3.1** the DSC thermograms of the eutectic mixtures in different molar ratios are presented. The chemical characterization (FTIR and ^{1}H-NMR) and properties such as viscosity and contact angle are given. CoF variations with time for longer tribological tests, as well as CoF values and wear volumes obtained for the mixtures are presented. For **Chapter 3.2** the ^{1}H-NMR spectra of the prepared hydrophobic DES are presented and analyzed. The CoF variation with time for the best performing DES is given. HSPM images of [Aliquat]Cl:octanol (1:1) under different conditions are presented. SEM images obtained after the corrosion tests are given. For **Chapter 4** the images of the corrosion experiments are presented, as well as the traction coefficient variation with time for IL [C_6mim][TfO] as 2 and 5 wt.% in PEG 200 + corrosion inhibitor.

A.1 Supporting Information of Chapter 2.1

Synthesis of ILs

Three new ionic liquids were synthesized: [C_6-3-pic][TfO], [C_6-2-pic][TfO] and [C_6-4-pic][TfO]. For [C_6-3-pic][TfO] two synthetic approaches were followed: the conventional reflux method and the microwave-assisted synthesis. Two previously studied ionic liquids were also synthesized: [C_6mim][TfO] and [C_6pyr][TfO]. All the synthesized ionic liquids were characterized by NMR (Bruker 400MHz, model Avance III, USA) and FTIR-ATR, 4 cm^{-1} resolution and 128 scans, (Nicolet 5700 FTIR spectrometer, Thermo Electron Corporation, USA). The spectra of the final compounds are given in Figure A.1.1.

Conventional synthesis of cationic scaffolds

1-hexyl-methyl imidazolium bromide: [C_6mim][Br]

2 mL of methyl imidazolium (0.02512 mol) and 4.1 mL of bromohexane (0.02906 mol) were added to a 25 mL round-bottom flask. The alkylating agent was added in excess to assure that the reaction was complete. 7 mL of acetonitrile were also added and the mixture was stirred and heated at 80 °C under reflux for 27h. The solvent was evaporated and the final product was obtained as a viscous light yellow liquid and dried in vacuum (5.88 g; 86 % yield).
^{1}H-NMR (δ, $CDCl_3$-d, 400 MHz): 10.46 (s, 1H), 7.50 (s, 1H), 7.36 (s, 1H), 4.30 (t, 2H, ^{3}J=8 Hz), 4.12 (s, 3H), 1.92-1.86 (m, 2H), 1.30 (s, 6H), 0.85 (m, 3H) ppm

1-hexyl-3-methylpyridinium bromide: [C_6-3-pic][Br]

1.9 mL of 3-methylpyridine (0.01950 mol) and 3.3 mL of bromohexane (0.02339 mol) were added to a 25 mL round-bottom flask. The alkylating agent was added in excess to assure that the reaction was complete. 8 mL of acetonitrile were also added and the mixture was stirred and heated at 80 °C under reflux for 116h. The solvent was evaporated and the final product was obtained as a viscous dark orange liquid and dried in vacuum (1.6 g; 88% yield).
^{1}H-NMR (δ, $CDCl_3$-d, 400 MHz): 9.38 (s, 1H), 9.20 (d, 1H, ^{3}J=4 Hz), 8.24 (d, 1H, ^{3}J=8 Hz), 7.99 (t, 1H, ^{3}J=8 Hz), 4.82 (t, 2H, ^{3}J=8 Hz), 3.23-3.16 (m, 1H), 2.56 (s, 3H), 1.95 (t, 2H, ^{3}J=8 Hz), 1.29-1.20 (m, 6H), 0.75 (t, 3H, ^{3}J=8 Hz) ppm

Microwave synthesis of cationic scaffolds

1-hexyl-methyl imidazolinium bromide: [C_6mim][Br]

To a quartz vessel, 1 mL of methyl imidazolium (0.01256 mol) and 1.95 mL of bromohexane (0.01382 mol) were added and mixed together with 5 mL of acetonitrile. The mixture was

heated at 120 °C for 30 minutes under microwave irradiation. The solvent was evaporated and the final product was obtained as a viscous light yellow liquid and dried in vacuum (3.14 g; 95% yield).
^{1}H-NMR (δ, $CDCl_3$-d, 400 MHz): 10.35 (s, 1H), 7.51 (s, 1H), 7.37 (s, 1H), 4.30 (t, 2H, ^{3}J=8 Hz), 4.11 (s, 3H), 1.92-1.85 (m, 2H), 1.29 (s, 6H), 0.85 (m, 3H) ppm

1-hexyl-3-methylpyridinium bromide: [C_6-3-pic][Br]
To a quartz vessel, 1 mL of 3-methylpyridine (0.01028 mol) and 1.5 mL of bromohexane (0.01063 mol) were added and mixed together with 5 mL of acetonitrile. The mixture was stirred at 600 rpm and heated to 130 °C for 35 minutes. The solvent was evaporated and the final product was obtained as a viscous dark orange liquid and dried in vacuum (2.7 g; 99% yield).
^{1}H-NMR (δ, $CDCl_3$-d, 400 MHz): 9.44 (s, 1H), 9.270 (d, 1H, ^{3}J=8 Hz), 8.25 (d, 1H, ^{3}J=8 Hz), 8.00 (t, 1H, ^{3}J=8 Hz), 4.91 (t, 2H, ^{3}J=8 Hz), 2.62 (s, 3H), 1.98 (m, 2H), 1.35-1.27 (m, 6H), 0.82 (t, 3H, ^{3}J=8 Hz) ppm

1-hexyl-2-methylpyridinium bromide: [C_6-2-pic][Br]
To a quartz vessel, 1 mL of 2-methylpyridine (0.01028 mol) and 2 mL of bromohexane (0.01417 mol) were added and mixed together with 5 mL of acetonitrile. The mixture was stirred at 600 rpm and heated to 130 °C for 30 minutes. The solvent was evaporated and the final product was obtained as a light brown solid and dried in vacuum (2.44 g; 74% yield).
^{1}H-NMR (δ, $CDCl_3$-d, 400 MHz): 9.54 (d, 1H, ^{3}J=4 Hz), 8.39 (t, 1H, ^{3}J=8 Hz), 8.04 (d, 1H, ^{3}J=8 Hz), 7.91 (t, 1H, ^{3}J=8 Hz), 4.78 (t, 2H, ^{3}J=8 Hz), 2.92 (s, 3H), 1.81-1.72 (m, 2H), 1.40-1.16 (m, 6H), 0.77 (t, 3H, ^{3}J=8 Hz) ppm

1-hexyl-4-methylpyridinium bromide: [C_6-4-pic][Br]
To a quartz vessel, 2 mL of 4-methylpyridine (0.02055 mol) and 3 mL of bromohexane (0.02126 mol) were added and mixed together with 5 mL of acetonitrile. The mixture was stirred at 600 rpm and heated to 130 °C for 35 minutes. The solvent was evaporated and the final product was obtained as a light brown solid and dried in vacuum (5.12 g; 94% yield).
^{1}H-NMR (δ, $CDCl_3$-d, 400 MHz): 9.33 (d, 1H, ^{3}J=8 Hz), 7.89 (d, 1H, ^{3}J=8 Hz), 4.84 (t, 2H, ^{3}J=8 Hz), 2.63 (s, 3H), 2.01-1.94 (m, 2H), 1.33-1.21 (m, 6H), 0.81 (t, 3H, ^{3}J=8 Hz) ppm

1-hexyl-pyridinium bromide: [C_6pyr][Br]
To a quartz vessel, 2 mL of pyridine (0.02483 mol) and 4.2 mL of bromohexane (0.02497 mol) were added and mixed. The mixture was stirred at 600 rpm and heated to 120 °C for 30 minutes. The solvent was evaporated and the final product was obtained as a viscous brown liquid and dried in vacuum (6.87 g; 99% yield).

^{1}H-NMR (δ, $CDCl_3$-d, 400 MHz): 9.53 (d, 2H, ^{3}J=4 Hz), 8.52 (t, 1H, ^{3}J=8 Hz), 8.15 (t, 2H, ^{3}J=8 Hz), 4.99 (t, 2H, ^{3}J=8 Hz), 2.07-1.96 (m, 2H), 1.40-1.21 (m, 6H), 0.83 (t, 3H, ^{3}J=8 Hz) ppm

Preparation of triflate-based ILs by exchange reactions

The ionic liquid was first dissolved in a mixture of acetone and methanol. 1.1 equivalents of a triflate salt (sodium or potassium triflate) were added to the mixture, which was kept in vigorous stirring for 48h at room temperature. At the end of the reaction the solution was filtered, the solvent was evaporated and the mixture was re-dissolved in dichloromethane. The solution was filtrated one more time and the solvent evaporated. The final product was dried in vacuum with stirring at 50 ºC for the time required to achieve a water content smaller than 1000 ppm.

1-hexyl-methyl imidazolium triflate: [C_6mim][TfO]

This IL was prepared according to a previous experimental procedure (adapted from [1]).

^{1}H-NMR (δ, $CDCl_3$-d, 400 MHz): 9.12 (s, 1H), 7.42 (s, 1H), 7.36 (s, 1H), 4.15 (t, 2H, ^{3}J=8 Hz), 3.94 (s, 3H), 1.83 (m, 2H), 1.26 (s, 6H), 0.83 (m, 3H) ppm

^{19}F-NMR (δ, $CDCl_3$-d, 282MHz): -78.66 ppm

1-hexyl-3-methylpyridinium triflate: [C_6-3-pic][TfO]

The desired product was obtained as an orange solid (7.1 g; 83% yield).

^{1}H-NMR (δ, $CDCl_3$-d, 400MHz): 9.10 (s, 1H), 8.86 - 8.77 (m, 1H), 8.23 - 7.88 (m, 1H), 7.41 (s, 1H), 7.36 (s, 1H), 4.59 (t, 1H, ^{3}J=8 Hz), 4.13 (t, 2H, ^{3}J=4 Hz), 2.54 (s, 2H), 1.98 (m, 2H), 1.23-1.18 (m, 6H), 0.79 (s, 3H) ppm

^{13}C-NMR (δ, $CDCl_3$-d, 100MHz): 145.69, 144.31, 141.91, 140.04, 127.84, 122.29, 119.11, 62.14, 31.66, 31.01, 25.64, 22.29, 18.53, 13.85 ppm

^{19}F-NMR (δ, $CDCl_3$-d, 282MHz): -78.64 ppm

FTIR-ATR: $\bar{\nu}$ = 3076; 2937; 2857; 1743; 1632; 1506; 1263; 1159; 1026; 812; 758; 694; 638; 572; 515 cm^{-1}.

Elemental analysis: expected C 45.21%, H 6.43%, N 4.06%; found C 45.76%, H 6.33%, N 3.86%.

1-hexyl-2-picolinium triflate: [C_6-2-pic][TfO]

The desired product was obtained as a brown solid (3.94 g; 95% yield).

^{1}H-NMR (δ, $CDCl_3$-d, 400MHz): 8.88 (d, 1H, ^{3}J=8 Hz), 8.32 (t, 1H, ^{3}J=8 Hz), 7.89-7.83 (m, 2H), 4.55 (t, 2H, ^{3}J=8 Hz), 2.85 (s, 3H), 1.90-1.83 (m, 2H), 1.39-1.29 (m, 6H), 0.84 (m, 3H) ppm

^{13}C-NMR (δ, $CDCl_3$-d, 100MHz): 154.52, 145.72, 145.19, 130.38, 126.28, 122.23, 119.24, 58.52, 31.07, 30.43, 25.86, 22.32, 20.21, 13.84 ppm

^{19}F-NMR (δ, $CDCl_3$-d, 282MHz): -78.42 pm

FTIR-ATR: $\bar{\nu}$ = 2927; 2861; 1746; 1634; 1508; 1251; 1164; 1023; 787; 711; 633; 574; 517 cm^{-1}

Elemental analysis: expected C 47.69%, H 6.17%, N 4.28%; found C 47.24%, H 6.05%, N 4.07%.

1-hexyl-4-picolinium triflate: [C6-4-pic][TfO]

The desired product was obtained as a viscous brown liquid (2.47 g; 97% yield).

^{1}H-NMR (δ, $CDCl_3$-d, 400MHz): 8.83 (d, 2H, ^{3}J=8 Hz), 7.82 (d, 2H, ^{3}J=4 Hz), 4.58 (t, 2H, ^{3}J=8 Hz), 2.64 (s, 3H), 1.99-1.91 (m, 2H), 1.28 (m, 6H), 0.85 (m, 3H) ppm

^{13}C-NMR (δ, $CDCl_3$-d, 100MHz): 159.19, 143.69, 128.95, 125.42, 122.24, 119.06, 115.88, 61.33, 31.34, 30.92, 25.48, 22.21, 21.99, 13.77 ppm

^{19}F-NMR (δ, $CDCl_3$-d, 282MHz): -78.44 ppm

FTIR-ATR: $\bar{\nu}$ = 3070; 2940; 2857; 1641; 1475; 1258; 1156; 1029; 824; 754; 636; 571; 518 cm^{-1}

Elemental analysis: expected C 47.69%, H 6.17%, N 4.28%; found C 47.60%, H 6.30%, N 4.11%.

1-hexyl-pyridinium triflate: [C6pyr][TfO]

This IL was prepared according to a previous experimental procedure (adapted from [2]).

^{1}H-NMR (δ, $CDCl_3$-d, 400MHz): 8.90 (d, 2H, ^{3}J=4 Hz), 8.48 (t, 1H, ^{3}J=8 Hz), 8.06 (t, 2H, ^{3}J=8 Hz), 4.66 (t, 2H, ^{3}J=8 Hz), 2.03-1.95 (m, 2H), 1.37-1.25 (m, 6H), 0.86 (t, 3H, ^{3}J=8 Hz) ppm

^{19}F-NMR (δ, $CDCl_3$-d, 282MHz): -78.49 ppm

[C6-2-pic][TfO]

^{1}H-NMR

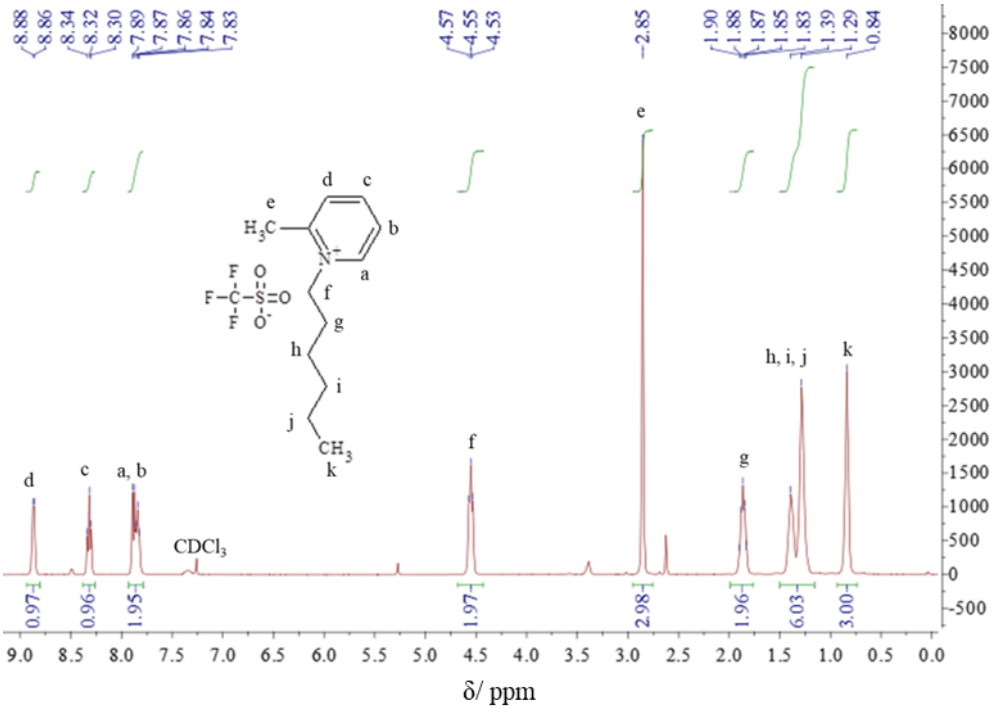

^{13}C-NMR

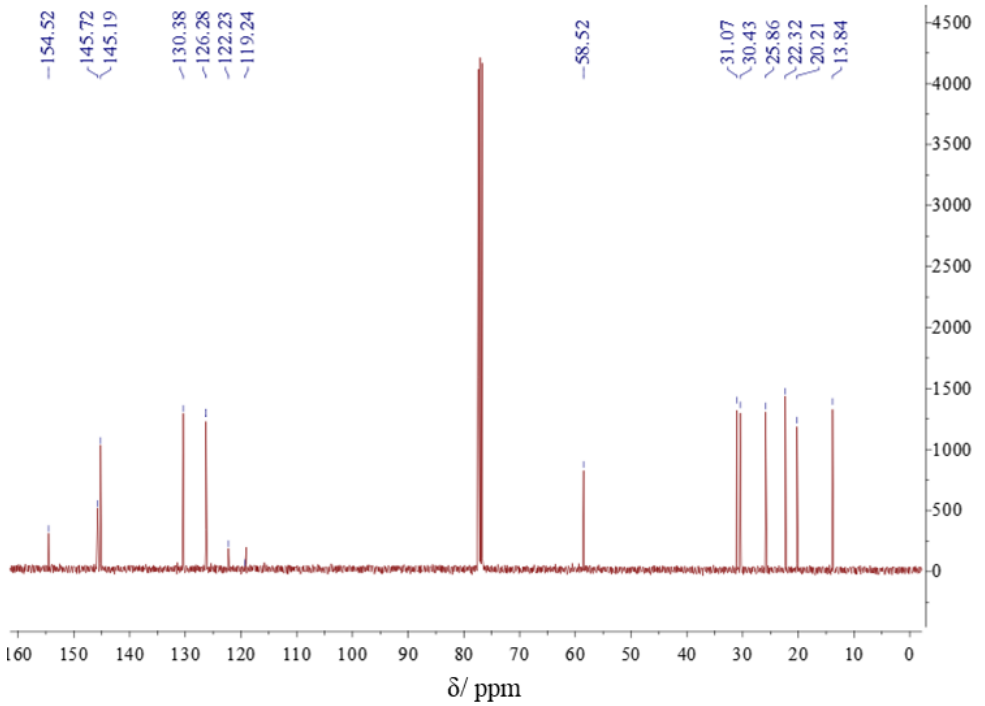

^{19}F-NMR

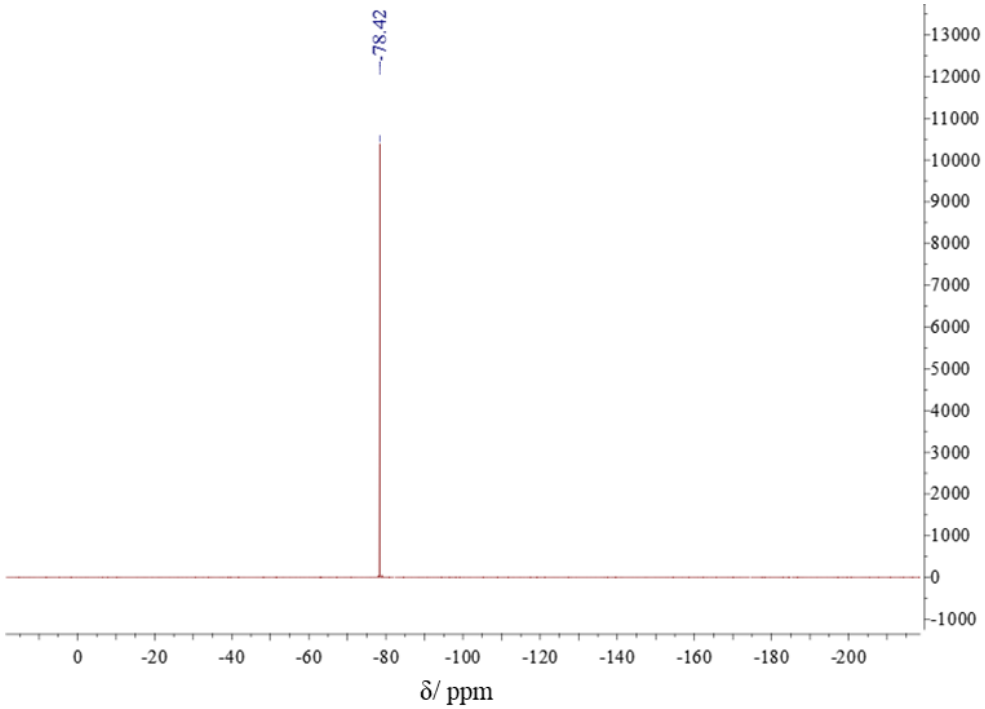

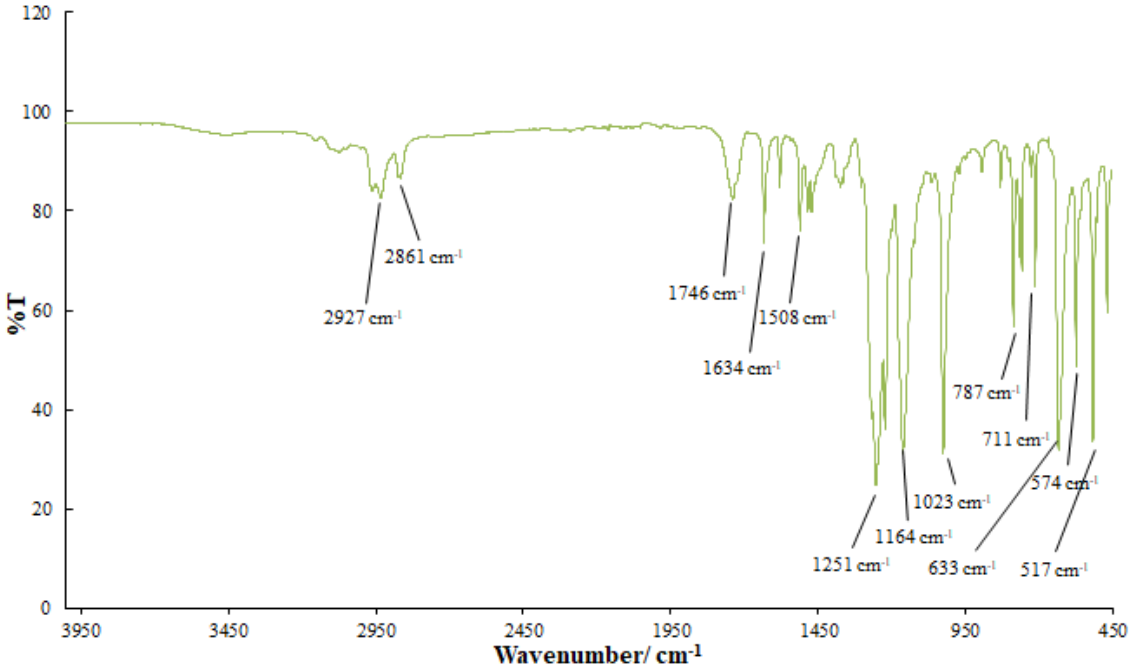

[C6-3-pic][TfO]

^{1}H-NMR

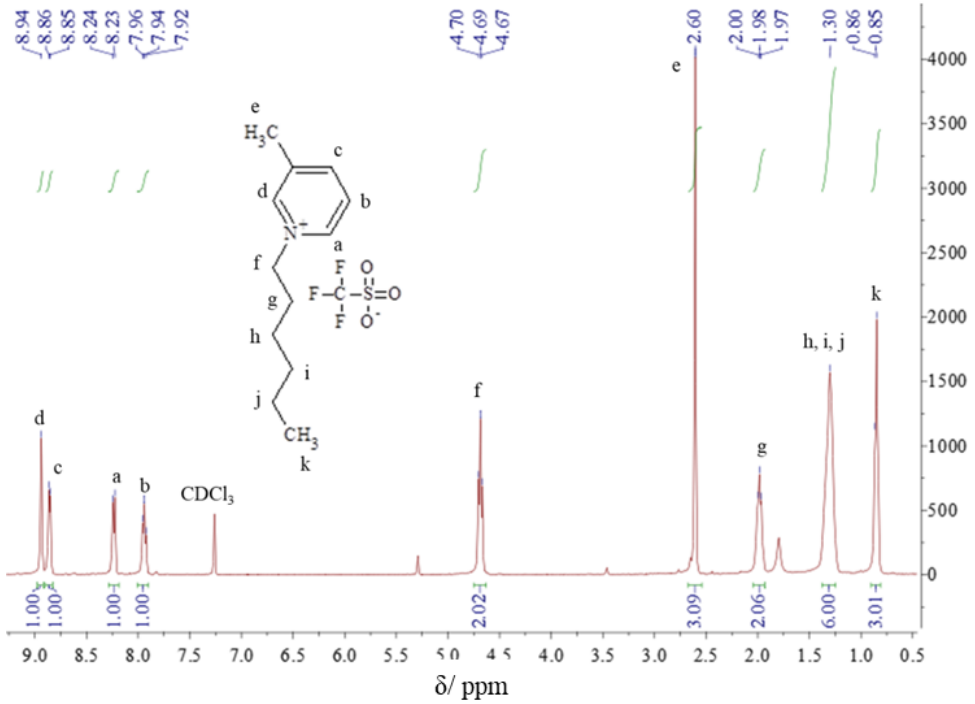

^{13}C-NMR

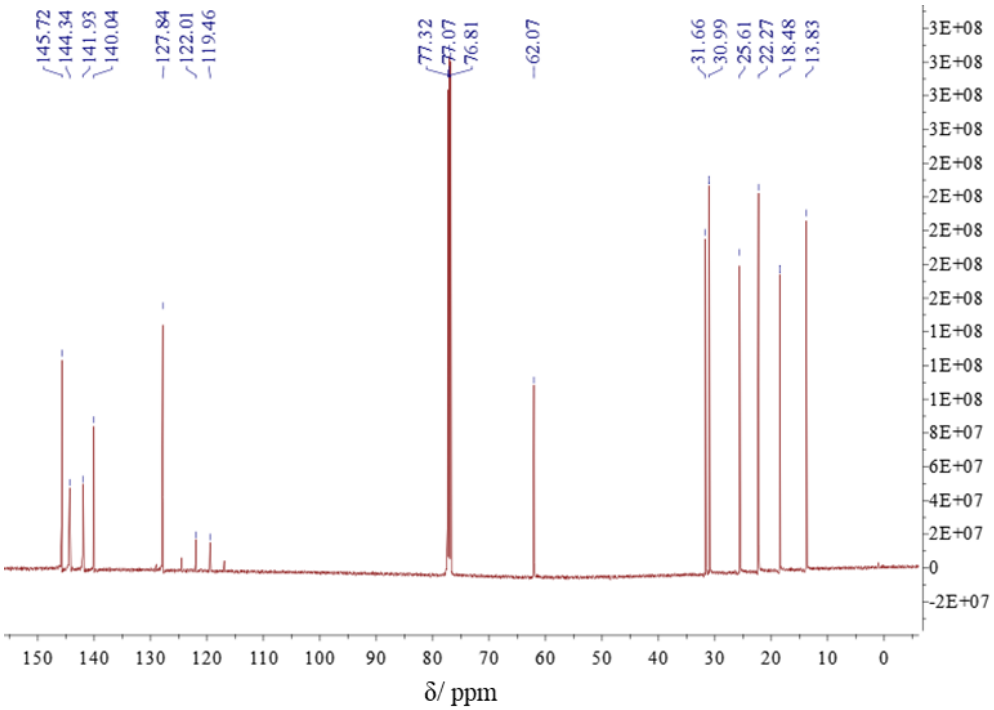

^{19}F-NMR

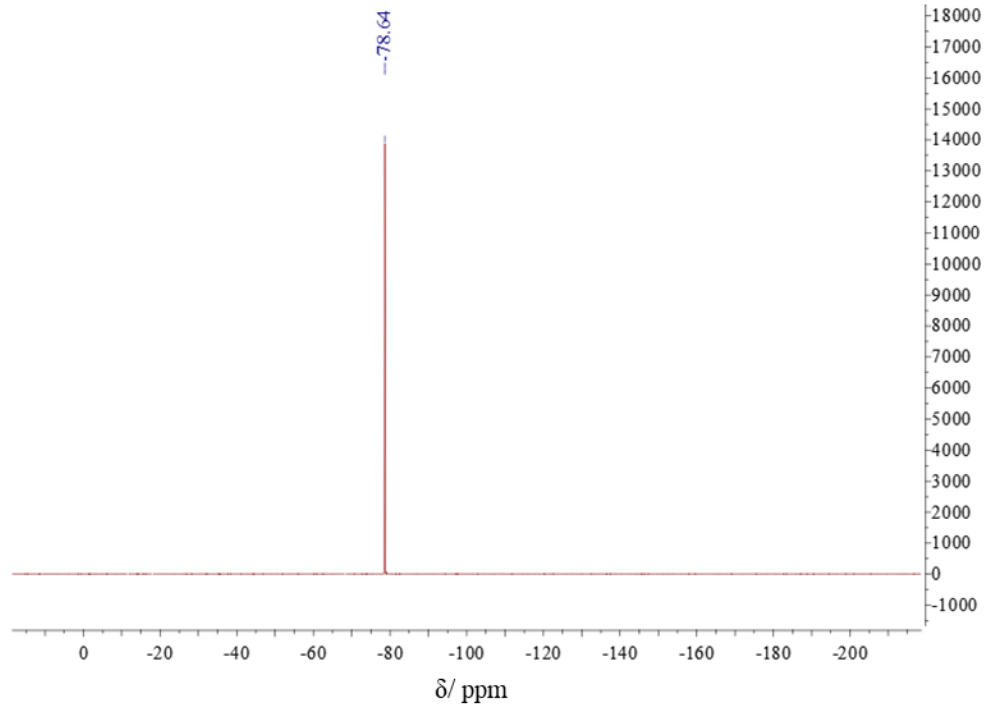

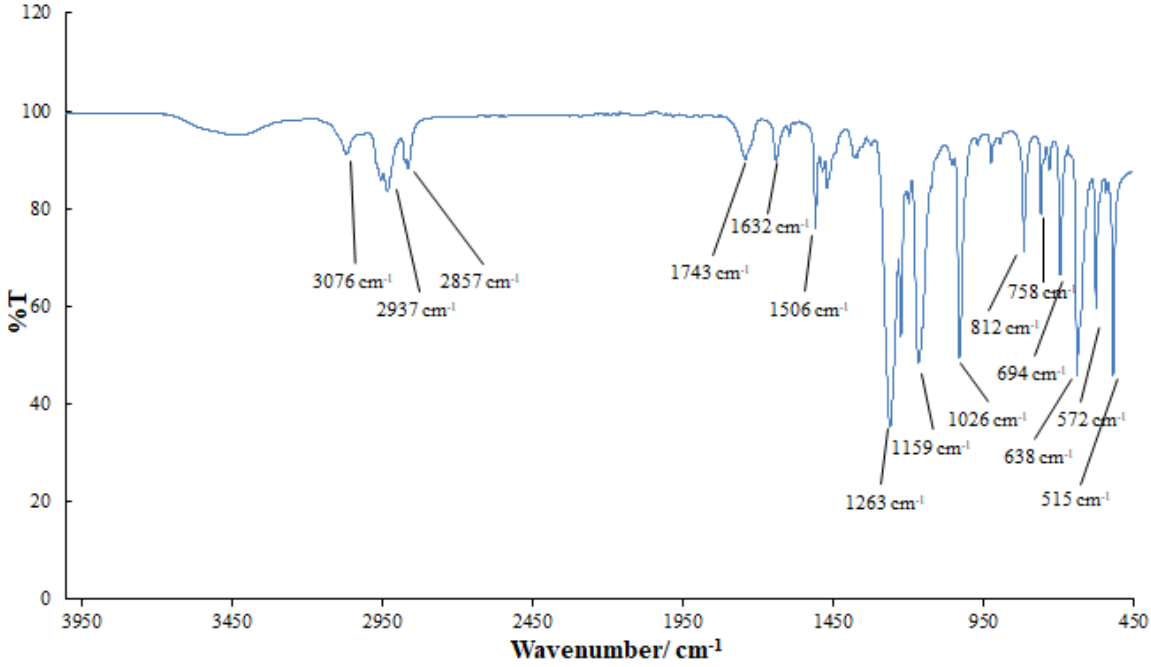

[C6-4-pic][TfO]

^{1}H-NMR

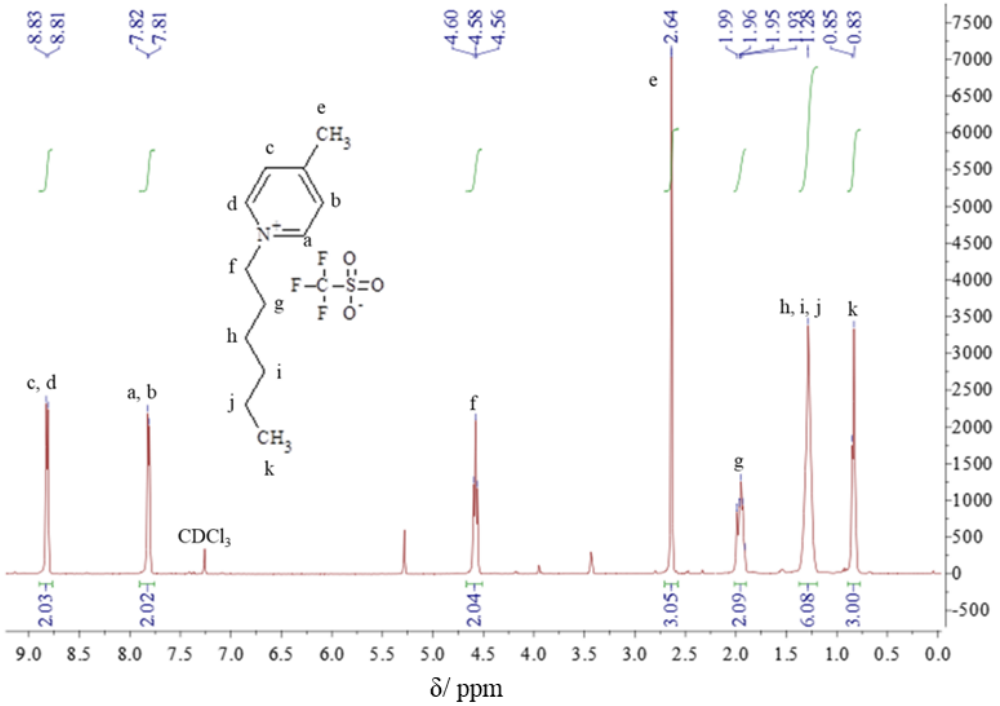

^{13}C-NMR

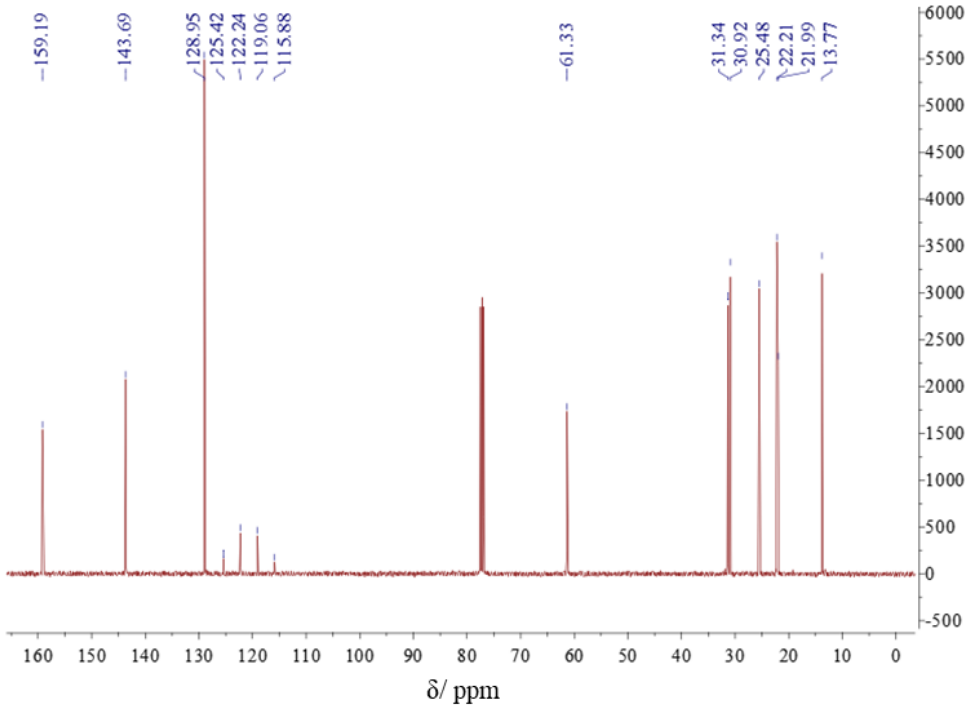

^{19}F-NMR

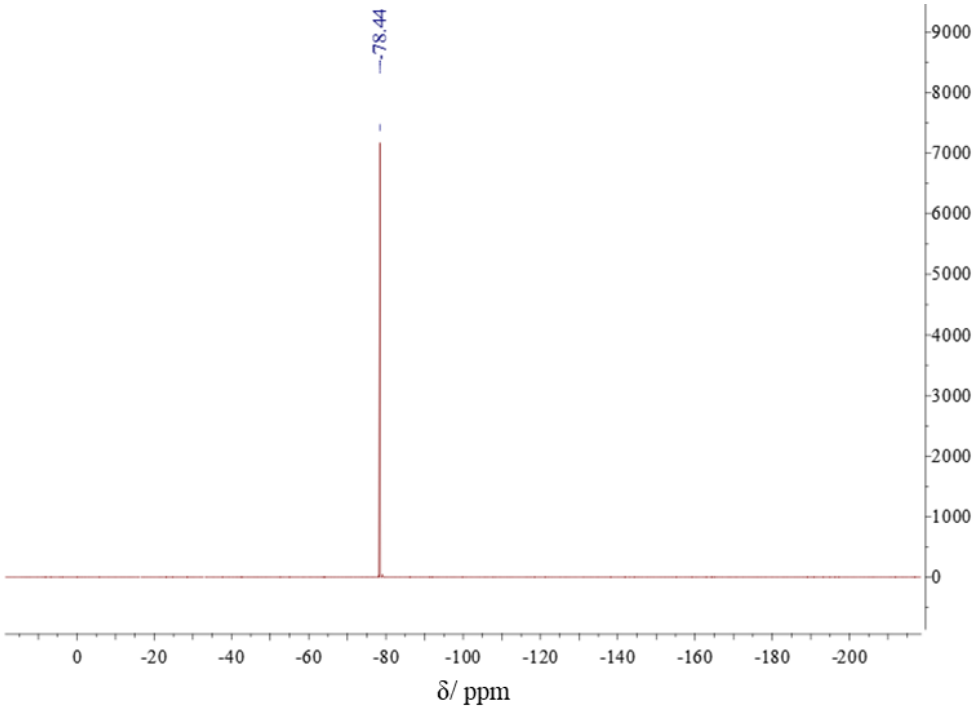

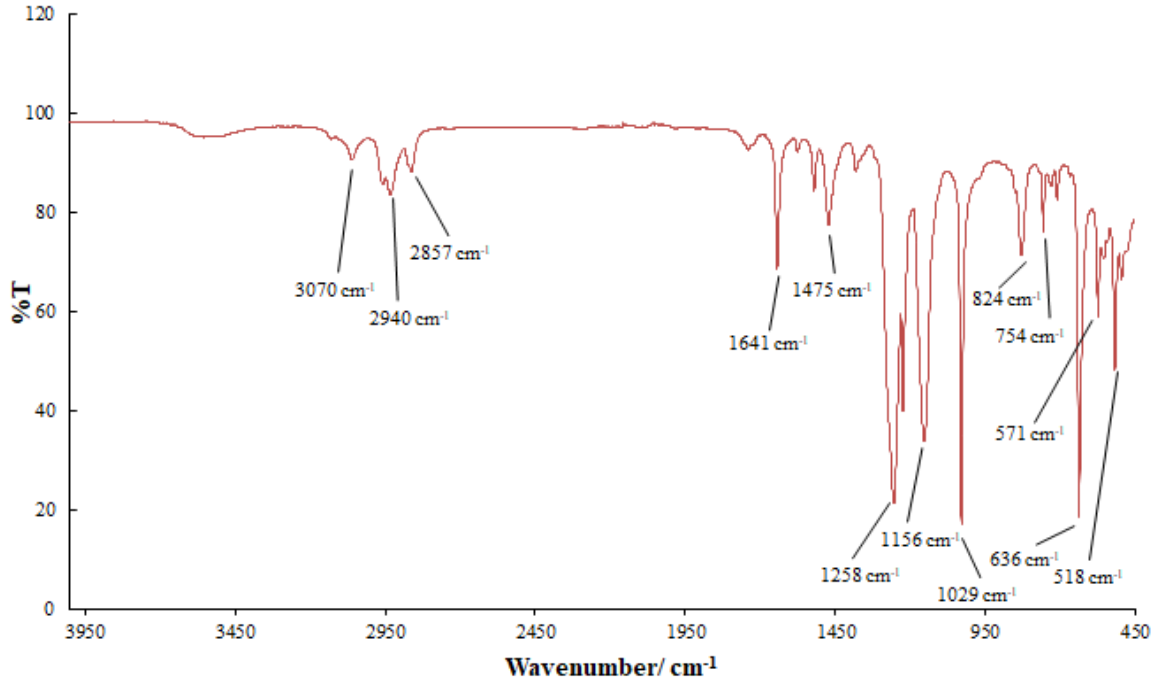

Figure A.1.1. ^{1}H-NMR, ^{13}C-NMR, ^{19}F-NMR and FTIR spectra of [C$_6$-2-pic][TfO], [C$_6$-3-pic][TfO] and [C$_6$-4-pic][TfO].

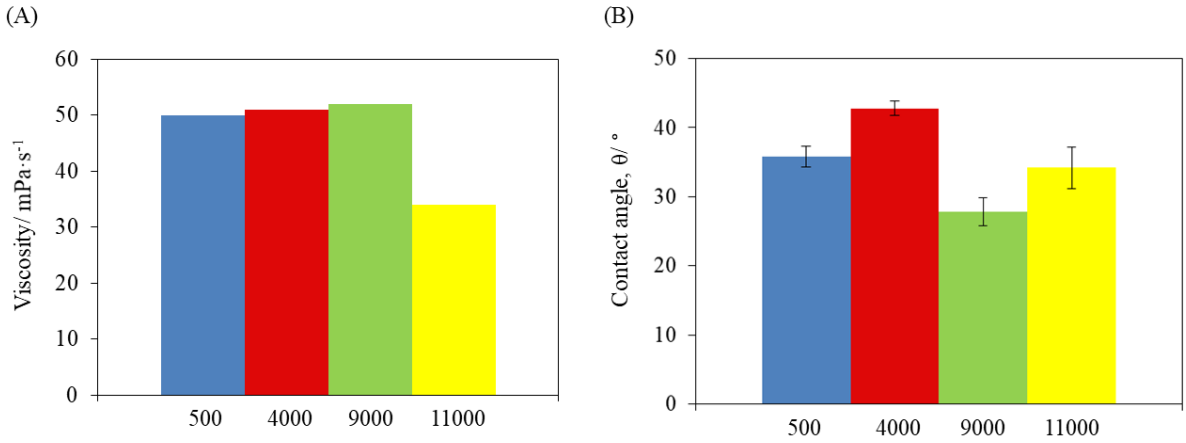

Figure A.1.2. Effect of water content (in ppm) of PEG 200 + 2% [C$_6$-4-pic][TfO] on (A) viscosity and (B) contact angle on the Si surface.

Calculation of the theoretical minimum film thickness using elastohydrodynamic theory of lubrication

The theoretical minimum film thickness, h, may be calculated using an approach of elastohydrodynamic theory of lubrication (EHL) applied to nonconformal geometry of ball-on-disc contact. Thus, the film thickness depends on the flow properties of the lubricant (viscosity at atmospheric pressure, η_{atm}, and pressure-viscosity coefficient, α) and the reduced modulus of the contact between the surfaces, E_r. According to the Hamrock model,[3] the equation for the minimum film thickness is the following:

$$h = 3.63R\left(\frac{U\eta_{atm}}{E_rR}\right)^{0.68}(\alpha E_r)^{0.49}\left(\frac{W}{E_rR^2}\right)^{-0.073}\left(1-e^{-0.68k}\right) \qquad \text{Eq. A.1}$$

where R is half of the radius of the ball, U is half of the sliding speed (in the present case, since we have used reciprocal movement, we took as a close approximation in equation 1 the average sliding speed of the test), W is the load and k is ellipticity parameter, taken as 1 for point contact. The values of α and E_r used in the calculations are given in Table A.1.1.

Table A.1.1. Mechanical properties of the pair stainless steel sphere/ Si surface.

	Young modulus (E)/ GPa	**Poisson ratio (ν)**
Stainless steel	190-205	0.265-0.275
Si	165	0.22

E_r=191 GPa from $\frac{1}{E_r} = \frac{1}{2}\left[\left(\frac{1-\vartheta_{disc}^2}{E_{disc}}\right)+\left(\frac{1-\vartheta_{ball}^2}{E_{ball}}\right)\right]$

The pressure-viscosity parameter, $\alpha = \frac{1}{\eta}\left(\frac{\partial\eta}{\partial P}\right)_T$, was calculated as 17 GPa^{-1} for tetraethylene glycol from data in the literature at 25 °C.[4] The same value was used, as an approximation, for PEG200 and for the PEG200+IL mixtures, since the molecular weights of PEG200 and tetraethylene glycol are very similar.

Table A.1.2 (Annex A.1) presents the values of the thickness obtained for [C_6-4-pic][TfO]+PEG200 in the range of loads where the lubrication regime may be considered as elastohydrodynamic (45 mN, 60 mN and 75 mN) with smooth and rough spheres. The comparison was made at constant sliding velocity (8 mm·s^{-1}) to avoid the drag effect in the lubricant with varies with the velocity.

Table A.1.2. Theoretical minimum film thickness of PEG 200 + 2% [C_6-4-pic][TfO] in elastohydrodynamic conditions.

	Theoretical minimum film thickness (*h*)/ nm		
	45 mN	60 mN	75 mN
Smooth spheres	2.1	2.1	2.0
Rough spheres	1.8	1.7	1.7

(A)

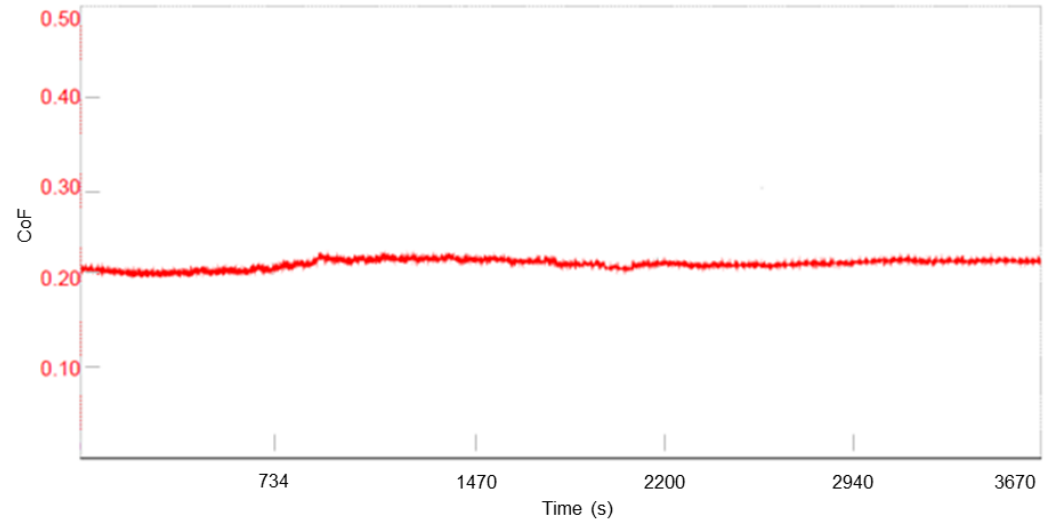

(B)

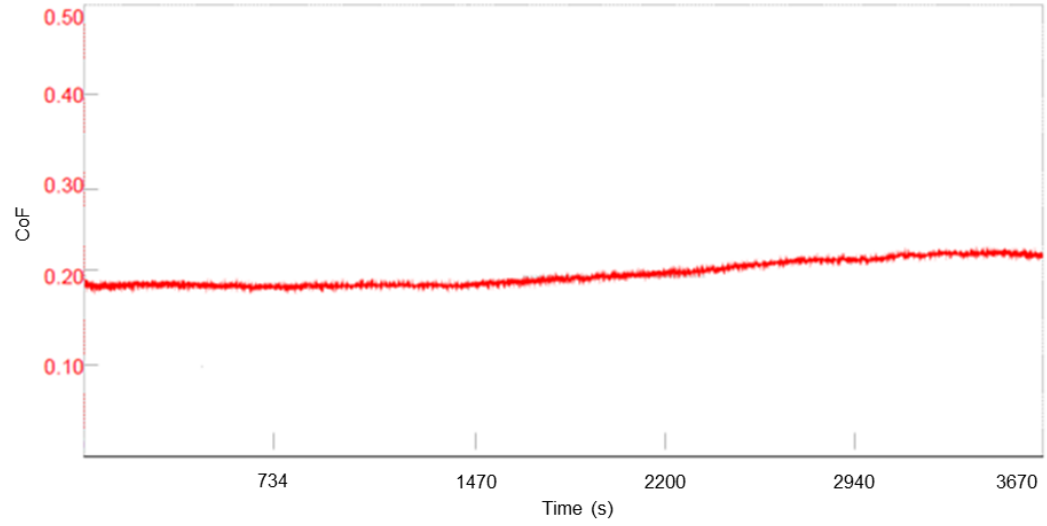

Figure A.1.3. CoF as a function of time (11000 cycles, v=8 mm·s^{-1}) obtained with PEG using (A) rough steel spheres and (B) smooth steel spheres sliding on silicon substrates. These results correspond to one specific run for each liquid.

(A)

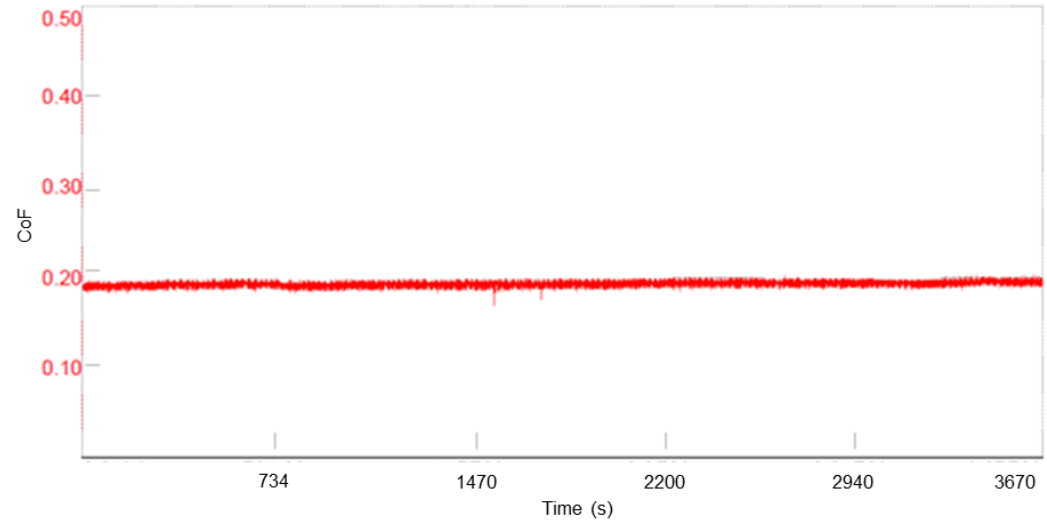

(B)

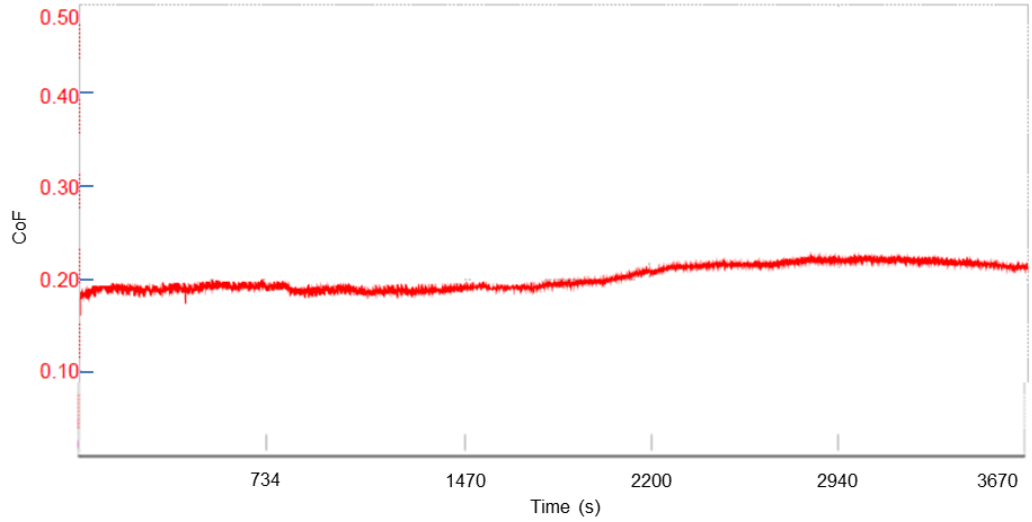

Figure A.1.4. CoF as a function of time (11000 cycles, v=8 mm·s^{-1}) obtained with PEG 200 + 2% [C$_6$-4-pic][TfO] using (A) rough steel spheres and (B) smooth steel spheres sliding on silicon substrates. These results correspond to one specific run for each liquid.

References

[1] P. S. Kulkarni, L. C. Branco, J. G. Crespo, M. C. Nunes, A. Raymundo, C. A. M. Afonso, *Chem. Eur. J.* **2007**, *13*, 8478–8488. 10.1002/chem.200700965

[2] A. Aupoix, B. Pégot, G. Vo-Thanh, *Tetrahedron* **2010**, *66*, 1352–1356. 10.1016/j.tet.2009.11.110

[3] B. J. Hamrock, D. Dowson, *J. Lubr. Technol.* **1977**, *99*, 264–275. 10.1115/1.3453074

[4] M. F. V. Pereira, H. M. N. T. Avelino, F. J. P. Caetano, J. M. N. A. Fareleira, *Fluid Phase Equilib.* **2018**, *480*, 87–97. 10.1016/j.fluid.2018.09.026

A.2 Supporting Information of Chapter 2.2

Synthesis

4-picolinium mesylate: [4-picH][$MeSO_3$]

2.1 mL of 4-picoline (0.02147 mol) and 1 equivalent of methanesulfonic acid (1.4 mL) were added to a 50 mL round-bottom flask. A total of 30 mL of acetonitrile was added and the mixture was stirred for 24h at room temperature. The solvent was evaporated and the final product was dried in vacuum and obtained as a white solid (quantitative yield).

^{1}H-NMR (δ, D_2O, 400 MHz): 8.61 (d, 2H, J=4.0 Hz), 7.91 (d, 2H, J= 4.0 Hz), 2.81 (s, 3H), 2.68 (s, 3H) ppm.

^{13}C-NMR (δ, D_2O, 100 MHz): 161.70, 139.93, 127.84, 38.42, 21.69 ppm.

FTIR-ATR: $\bar{\nu}$ = 3411 (NH), 1641 (C=N), 1508 (CC aromatic), 1162 (C-SO_2), 1040 (C-O), 775 (CH aromatic), 517 (CH aromatic) cm^{-1}.

Elemental analysis $C_7H_{11}NO_3S{\cdot}1.4H_2O$: expected C 39.20%, H 6.12%, N 6.53%; found C 39.26%, H 6.16%, N 6.49%.

4-picolinium hydrogen sulfate: [4-picH][HSO_4]

2.1 mL of 4-picolinium (0.02147 mol) and 1 equivalent of sulfuric acid (1.15 mL) were added to a 50 mL round-bottom flask. 25 mL of acetonitrile were added and the mixture was stirred for 24h at room temperature. The solvent was evaporated and the final product was dried in vacuum and obtained as a white solid (quantitative yield).

^{1}H-NMR (δ, $CDCl_3$, 400 MHz): 14.37 (s, 1H), 8.47 (m, 2H), 7.66 (m, 2H), 2.31 (s, 3H) ppm.

^{13}C-NMR (δ, D_2O, 100 MHz): 161.64, 139.93, 127.81, 21.67 ppm.

FTIR-ATR: $\bar{\nu}$ = 3416 (NH), 3081 (OH), 1640 (C=N), 1507 (CC aromatic), 1156 (C-O), 1029 (C-O), 855 (CH aromatic), 794 (CH aromatic), 571 (CH aromatic), 476 (CC aliphatic) cm^{-1}.

Elemental analysis $C_6H_9NO_4S{\cdot}1.2H_2O$: expected C 33.86%, H 5.22%, N 6.58%; found C 33.85%, H .15%, N 6.53%.

Pyridinium mesylate: [PyrH][$MeSO_3$]

2 mL of pyridine (0.02528 mol) and 1 equivalent of methanesulfonic acid (1.64 mL) were added to a 100 mL round-bottom flask. A total of 50 mL of acetonitrile was added and the mixture was stirred for 24h at room temperature. The solvent was evaporated and the final product was dried in vacuum and obtained as a white solid (quantitative yield).

^{1}H-NMR (δ, D_2O, 400 MHz): 8.80 (d, 2H, J=4.0 Hz), 8.64 (t, 1H, J= 8.0 Hz), 8.09 (t, 2H, J= 8.0 Hz), 2.79 (s, 3H) ppm.

^{13}C-NMR (δ, D_2O, 100 MHz): 147.19, 141.14, 127.42, 38.43 ppm.

FTIR-ATR: $\bar{\nu}$ = 3674 (OH), 2972 (CH), 2902 (CH), 1621 (C=N), 1548 (CC aromatic), 1491 (C=C-C aromatic), 1145 (C-SO_2), 1021 (C-O), 748 (CH aromatic), 678 (CH aromatic), 608 (CH aromatic), 526 (CH aromatic) cm^{-1}.
Elemental analysis $C_6H_9NO_3S$: expected C 41.13%, H 5.18%, N 7.99%; found C 41.13%, H 5.39%, N 8.03%.

Pyridinium hydrogen sulfate: [PyrH][HSO_4]
2 mL of pyridine (0.02528 mol) and 1 equivalent of sulfuric acid (1.36 mL) were added to a 50 mL round-bottom flask. A total of 30 mL of acetonitrile was added and the mixture was stirred for 24h at room temperature. The solvent was evaporated and the final product was dried in vacuum and obtained as an off-white solid (quantitative yield).
^{1}H-NMR (δ, D_2O, 400 MHz): 8.77 (m, 2H), 8.62 (m, 1H), 8.07 (m, 2H) ppm.
^{13}C-NMR (δ, D_2O, 100 MHz): 147.20, 141.07, 127.41 ppm.
FTIR-ATR: $\bar{\nu}$ = 3661 (OH), 2972 (CH), 2900 (CH), 1618 (CC aromatic), 1545 (NH), 1488 (C=C-C aromatic), 1151 (C-O), 1032 (C-O), 842 (CH aromatic), 748 (CH aromatic), 678 (CH aromatic), 526 (CH aromatic) cm^{-1}.
Elemental analysis $C_5H_7NO_4S{\cdot}0.7H_2O$: expected C 31.64%, H 4.79%, N 7.38%; found C 31.74%, H 4.24%, N 7.47%.

Methylimidazolium mesylate: [MIMH][$MeSO_3$]
The synthesis of this PIL was performed according to a previously reported method.[14]

Methylimidazolium hydrogen sulfate: [MIMH][HSO_4]
2 mL of methylimidazole (0.02436 mol) and 1 equivalent of sulfuric acid (1.33 mL) were added to a 50 mL round-bottom flask. A total of 35 mL of acetonitrile was added and the mixture was stirred for 24h at room temperature. The solvent was evaporated and the final product was dried in vacuum and obtained as a pale yellow viscous liquid (quantitative yield).
^{1}H-NMR (δ, DMSO, 400 MHz): 9.05 (s, 1H), 7.69 (m, 2H), 6.89 (s, 1H), 3.87 (s, 3H) ppm.
^{13}C-NMR (δ, D_2O, 100 MHz): 134.96, 122.93, 119.43, 35.41 ppm.
FTIR-ATR: $\bar{\nu}$ = 3661 (OH), 3149 (OH), 2972 (CH), 2882 (CH), 1587 (CC aromatic), 1553 (NH), 1160 (C-O), 1038 (C-O), 843 (CH aromatic), 756 (CH aromatic), 591 (CH aromatic), 572 (CH aromatic), 436 (CC aliphatic) cm^{-1}.
Elemental analysis $C_4H_8N_2O_4S{\cdot}1H_2O$: expected C 24.24%, H 5.09%, N 14.13%; found C 24.18%, H 4.92%, N 13.39%.

Tetramethylguanidinium mesylate: [TMGH][$MeSO_3$]
The synthesis of this PIL was performed according to a previously reported method.[14]

Tetramethylguanidinium hydrogen sulfate: [TMGH][HSO_4]

2.1 mL of tetramethylguanidine (0.01736 mol) and 1 equivalent of sulfuric acid (0.9 mL) were added to a 50 mL round-bottom flask. A total of 25 mL of acetonitrile was added and the mixture was stirred for 24h at room temperature. The solvent was evaporated and the final product was dried in vacuum and obtained as a white solid (quantitative yield).
^{1}H-NMR (δ, $CDCl_3$, 400 MHz): 2.81 (s, 1H), 1.61 (s, 12H), 0.91 (s, 2H) ppm.
^{13}C-NMR (δ, D_2O, 100 MHz): 161.38, 38.83 ppm.
FTIR-ATR: $\bar{\nu}$ = 3661 (OH), 2972 (CH), 2902 (CH), 1618 (C=C-C aromatic), 1549 (NH), 1491 (C=C-C aromatic), 1147 (C-O), 1020 (C-O), 748 (CH aromatic), 678 (CH aromatic), 626 (CH aromatic) cm^{-1}.
Elemental analysis $C_5H_{15}N_3O_4S{\cdot}0.7H_2O$: expected C 26.59%, H 7.60%, N 18.61%; found C 26.56%, H 7.16%, N 19.09%.

1,8-diazabicyclo(5.4.0)undec-7-enium mesylate: [DBUH][$MeSO_3$]
1.96 mL of 1,8-diazabicyclo(5.4.0)undec-7-ene (0.01314 mol) and 1 equivalent of methanesulfonic acid (0.85 mL) were added to a 50 mL round-bottom flask. 20 mL of acetonitrile were added and the mixture was stirred for 24h at room temperature. The solvent was evaporated and the final product was dried in vacuum and obtained as a pale yellow viscous liquid (quantitative yield).
^{1}H-NMR (δ, D_2O, 400 MHz): 3.56-3.49 (m, 4H), 3.31-3.28 (m, 2H), 2.78 (s, 3H), 2.61-2.59 (m, 2H), 2.02-1.96 (m, 2H), 1.71-1.66 (m, 6H) ppm.
^{13}C-NMR (δ, D_2O, 100 MHz): 165.95, 54.13, 48.20, 38.46, 37.96, 32.79, 28.42, 25.85, 23.30, 18.90 ppm.
FTIR-ATR: $\bar{\nu}$ = 3248 (OH), 3131 (OH), 2931 (CH), 1647 (CC aromatic), 1325 (C-N aromatic), 1156 (C-SO_2), 1038 (C-O), 771 (CH aromatic), 551 (CH aromatic), 522 (CH aromatic) cm^{-1}.
Elemental analysis $C_{10}H_{20}N_2O_3S$: expected C 48.36%, H 8.12%, N 11.28%; found C 47.98%, H 8.88%, N 11.19%.

1,8-diazabicyclo(5.4.0)undec-7-enium hydrogen sulfate: [DBUH][HSO_4]
The synthesis of this PIL was performed according to a previously reported method.[27]

[4-picH][MeSO$_3$]

^{1}H-NMR

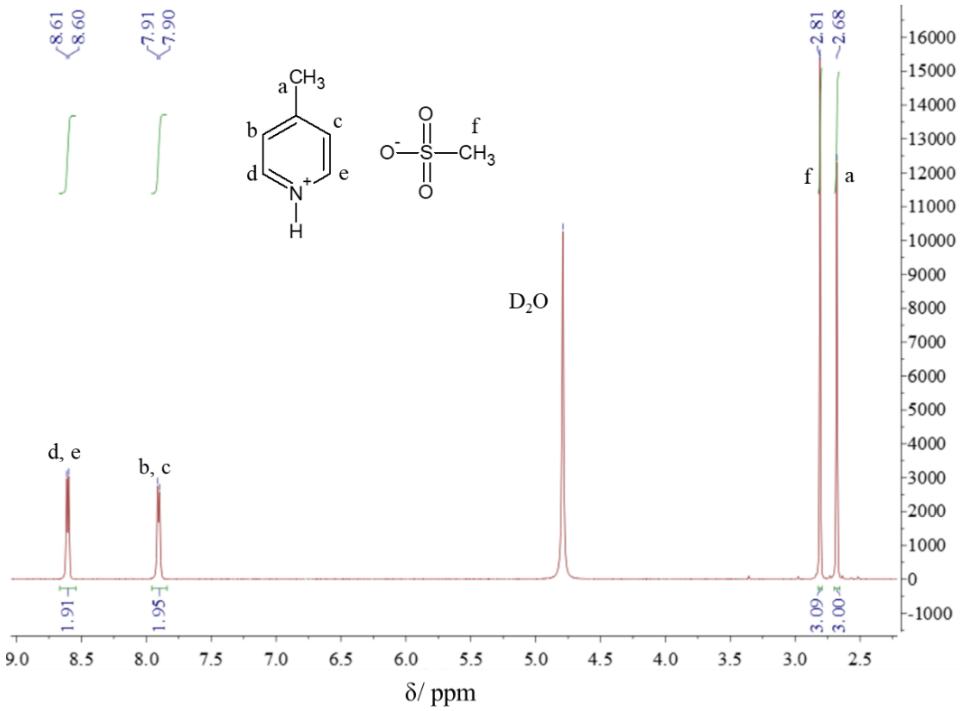

^{13}C-NMR

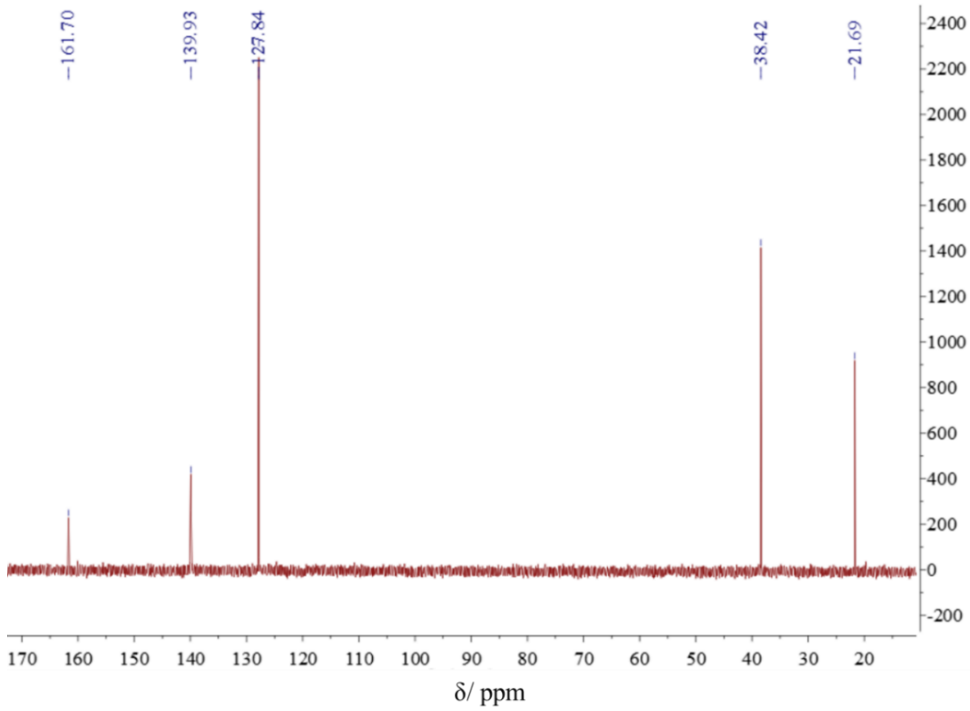

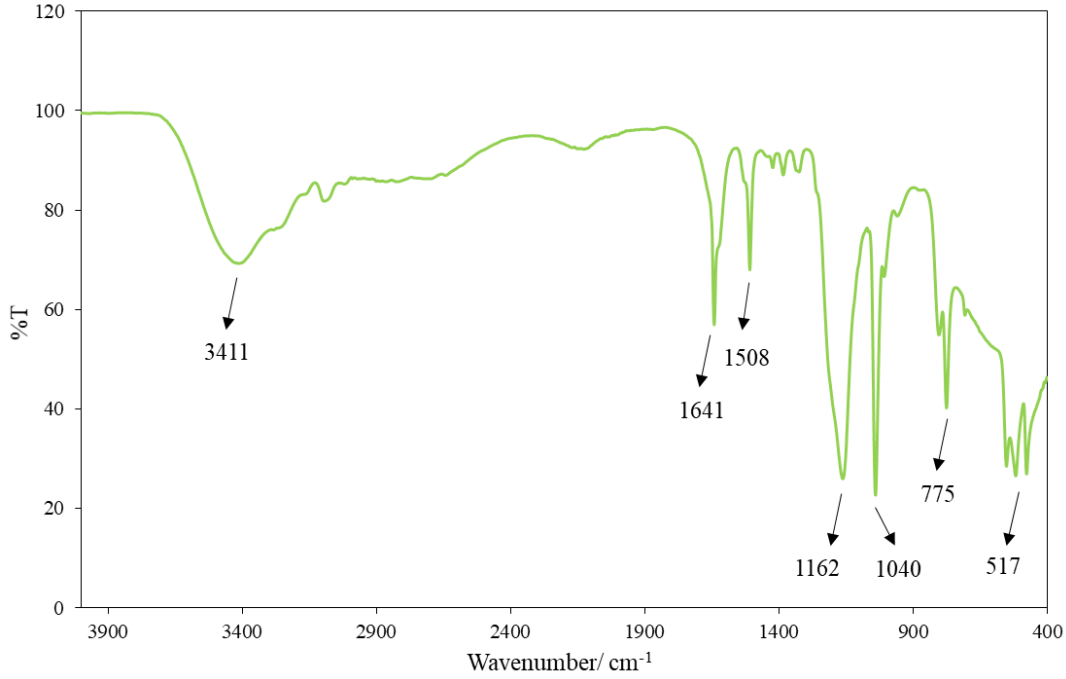

[4-picH][HSO4]

^{1}H-NMR

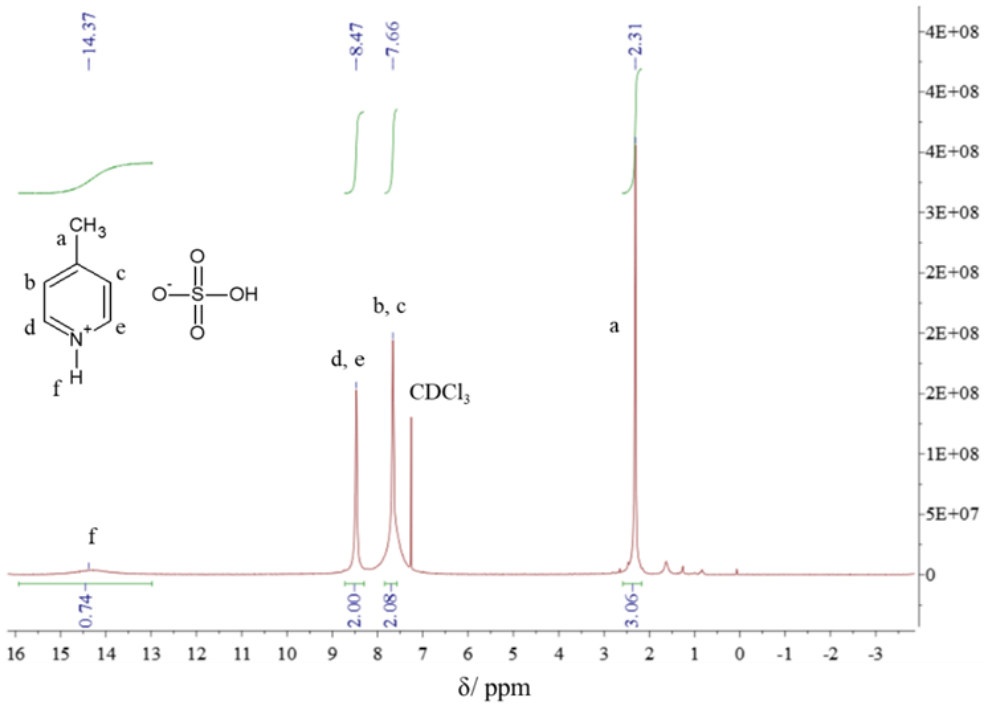

^{13}C-NMR

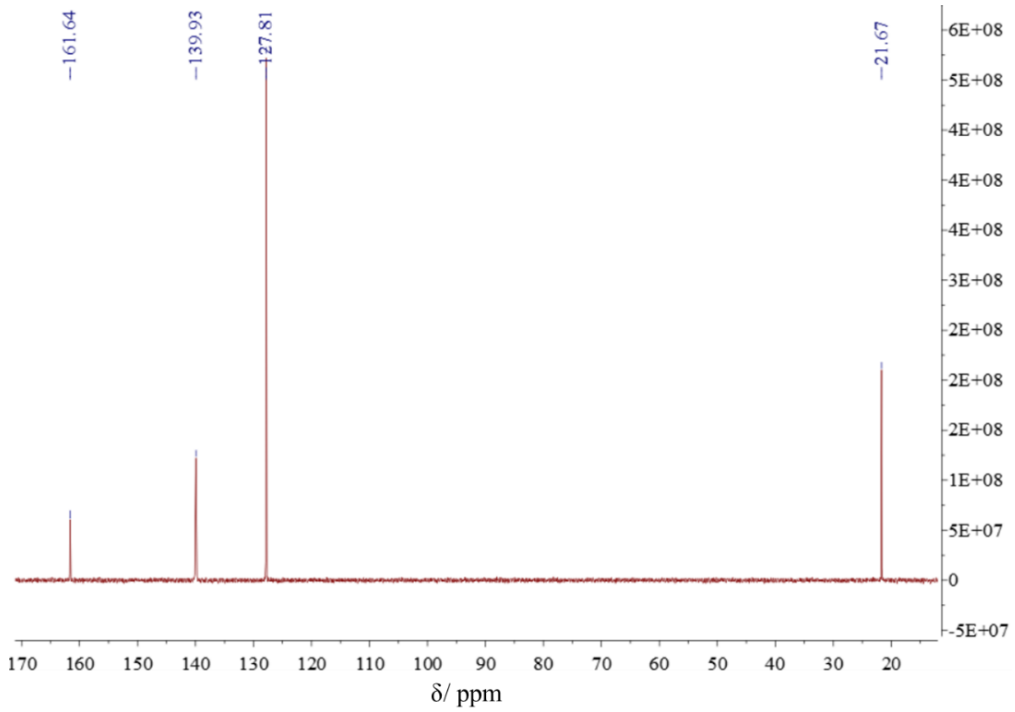
161.64
139.93
127.81
21.67
6E+08
5E+08
4E+08
4E+08
4E+08
3E+08
2E+08
2E+08
2E+08
1E+08
5E+07
0
-5E+07
170 160 150 140 130 120 110 100 90 80 70 60 50 40 30 20
δ/ ppm

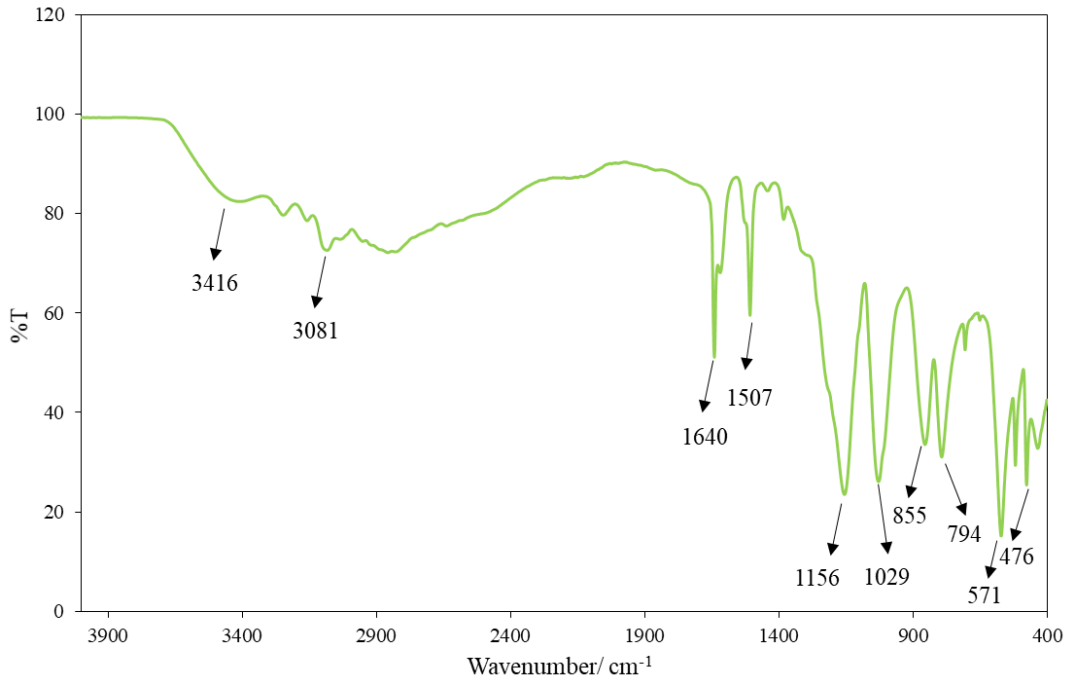
%T
120
100
80
60
40
20
0
3416
3081
1640
1507
1156
1029
855
794
571
476
3900 3400 2900 2400 1900 1400 900 400
Wavenumber/ cm-1

[PyrH][MeSO$_3$]

^{1}H-NMR

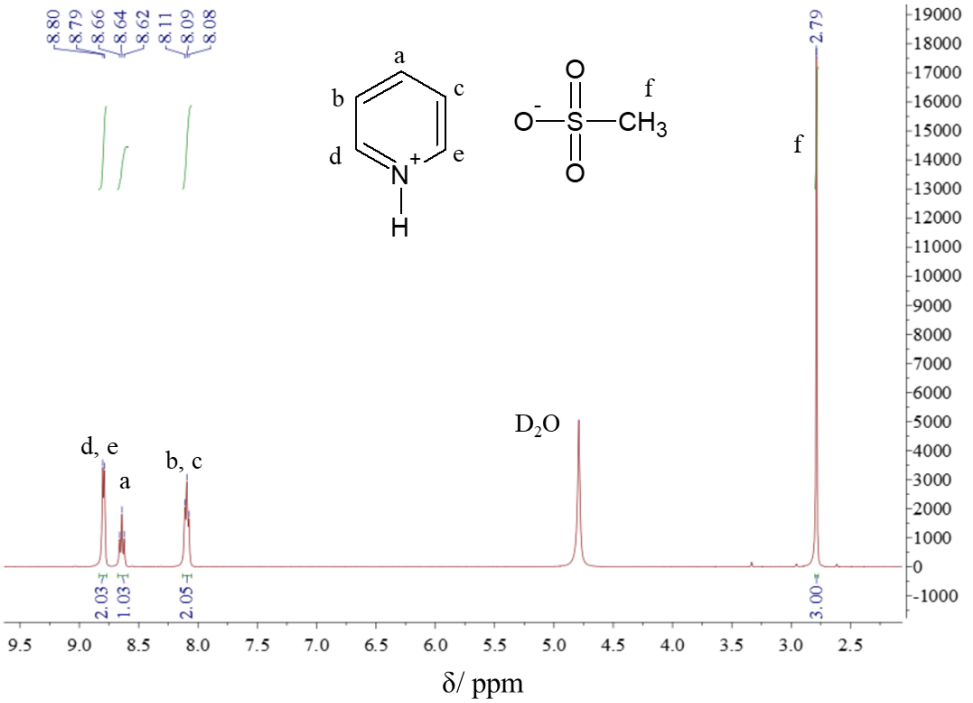

^{13}C-NMR

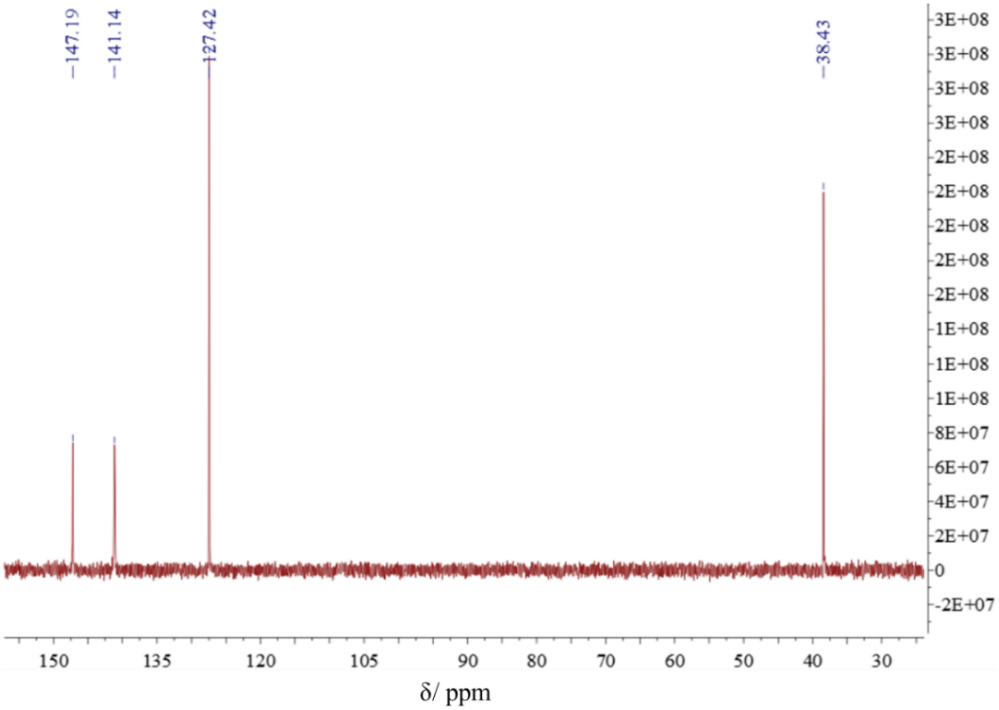

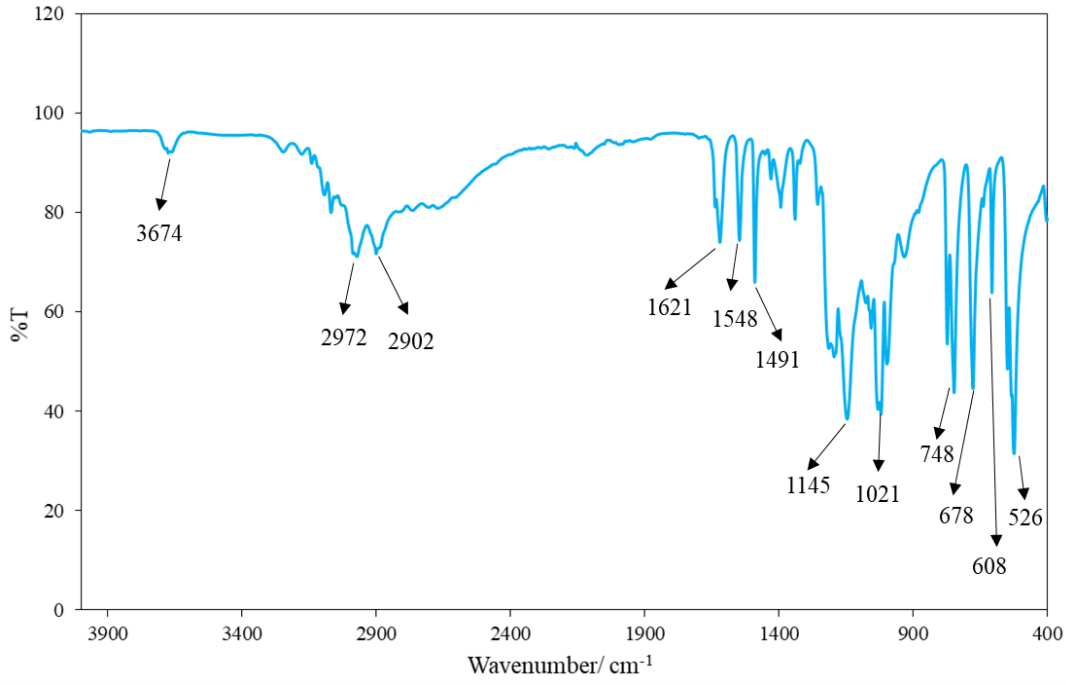

[PyrH][HSO$_4$]

^{1}H-NMR

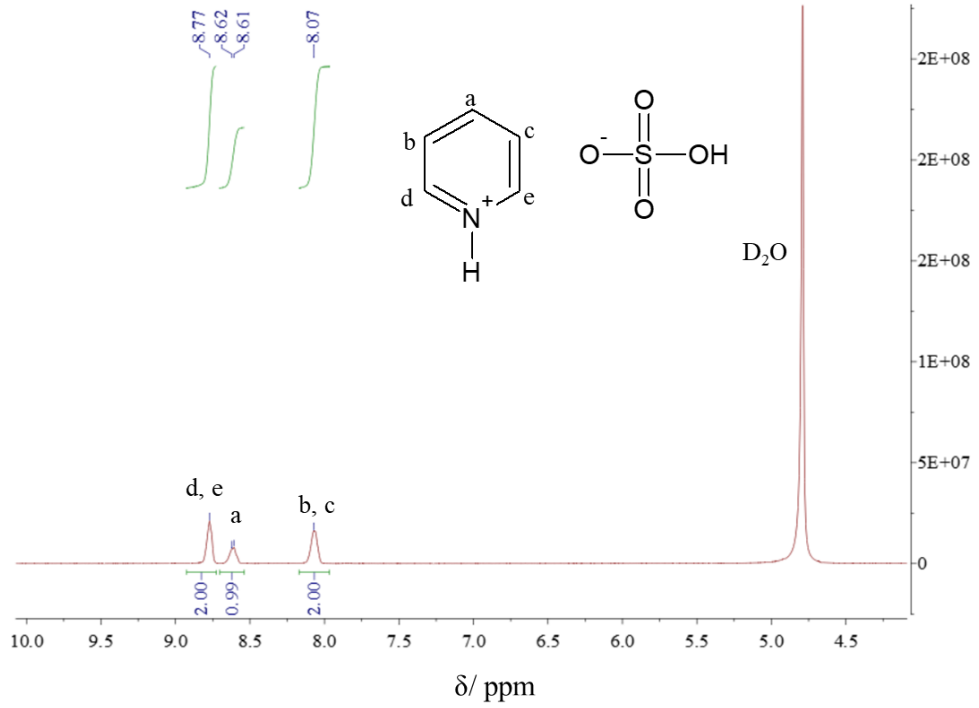

^{13}C-NMR

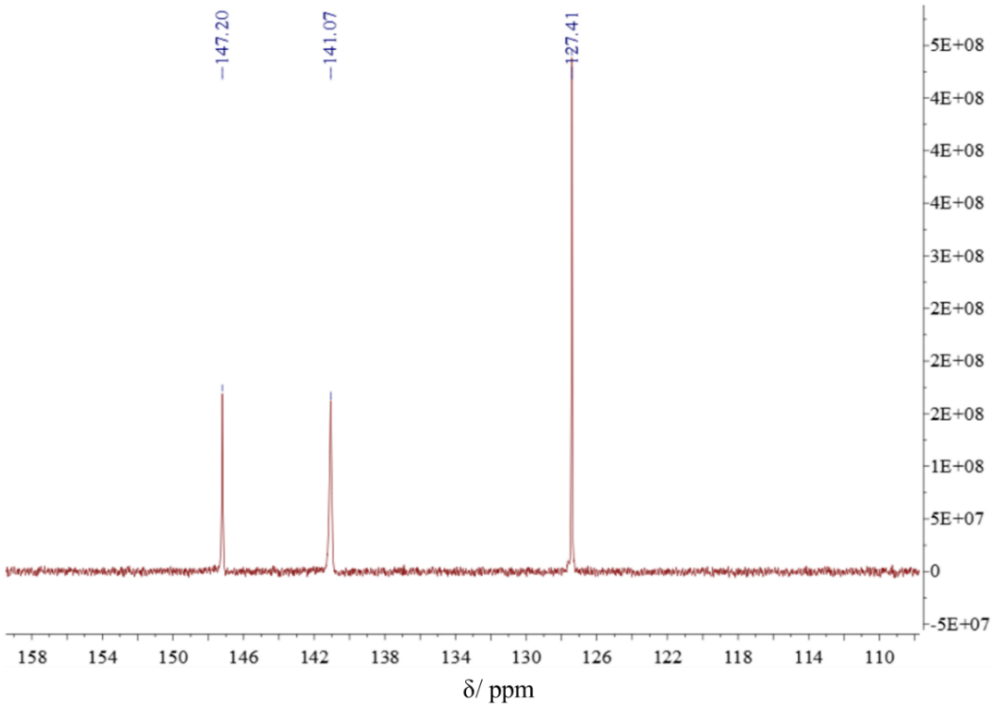
147.20
141.07
127.41
5E+08
4E+08
4E+08
4E+08
3E+08
2E+08
2E+08
2E+08
1E+08
5E+07
0
-5E+07
158
154
150
146
142
138
134
130
126
122
118
114
110
δ/ ppm

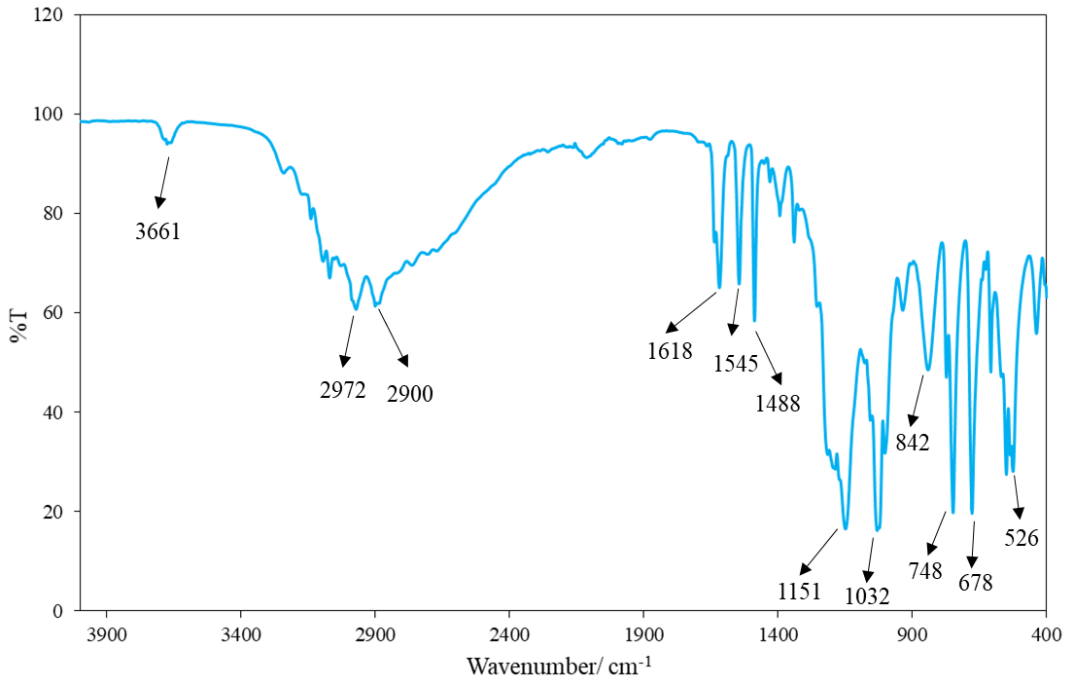
120
100
80
60
40
20
0
%T
3661
2972
2900
1618
1545
1488
842
1151
1032
748
678
526
3900
3400
2900
2400
1900
1400
900
400
Wavenumber/ cm-1

[MIMH][HSO$_4$]

^{1}H-NMR

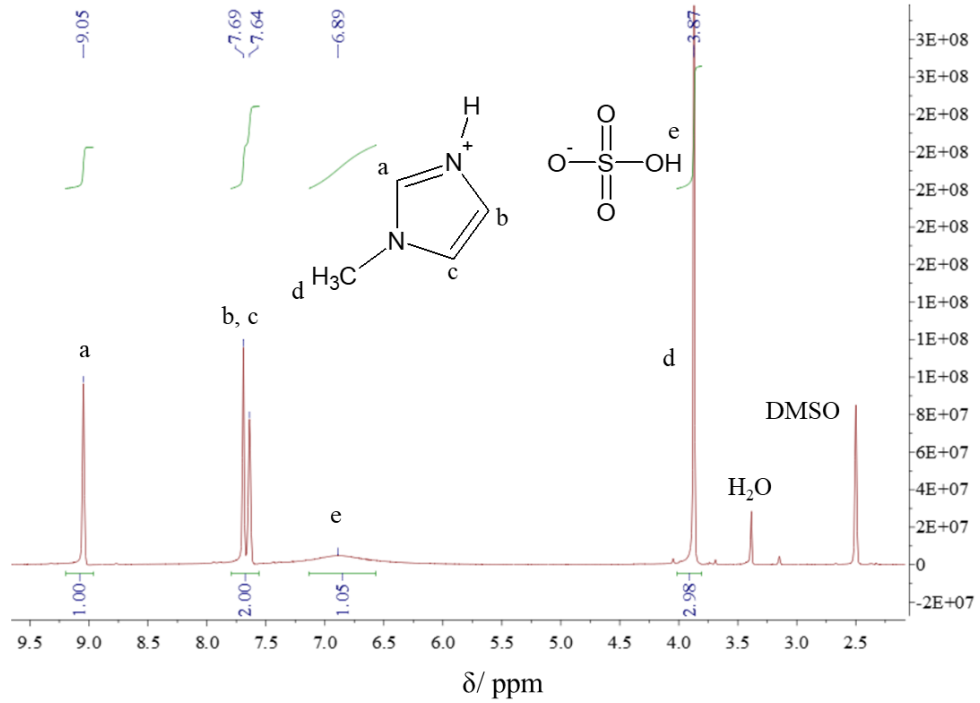

^{13}C-NMR

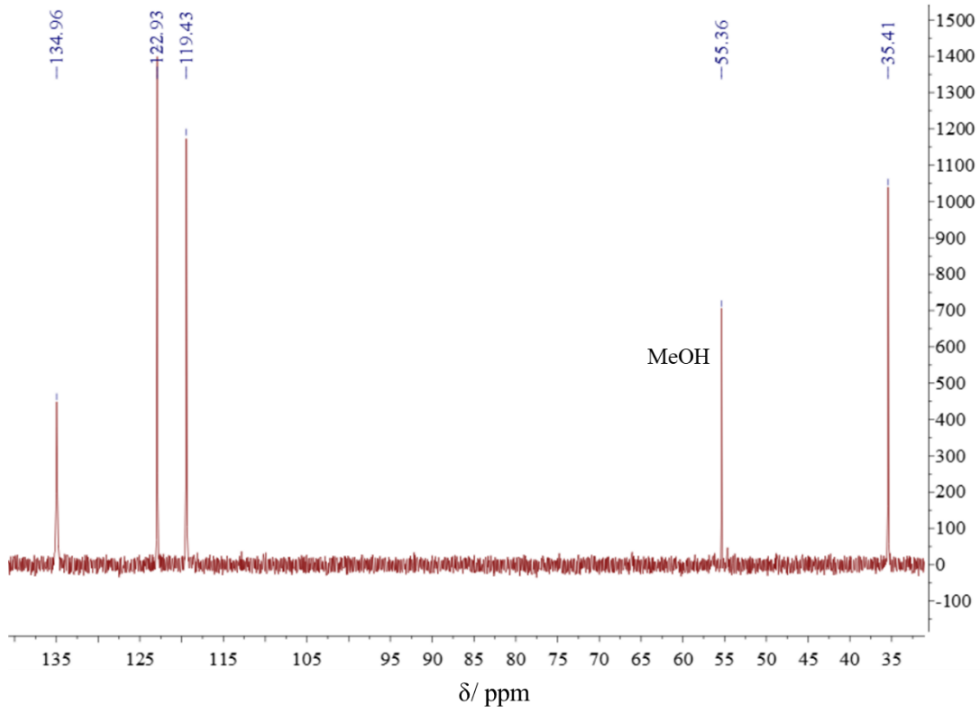

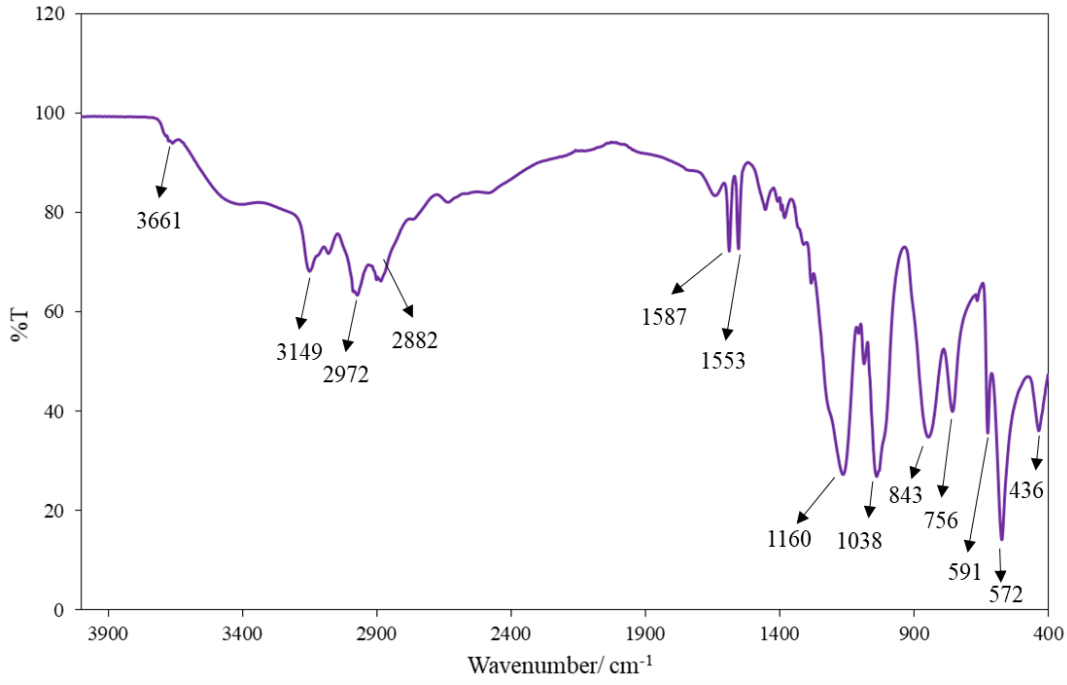

[TMGH][HSO4]

^{1}H-NMR

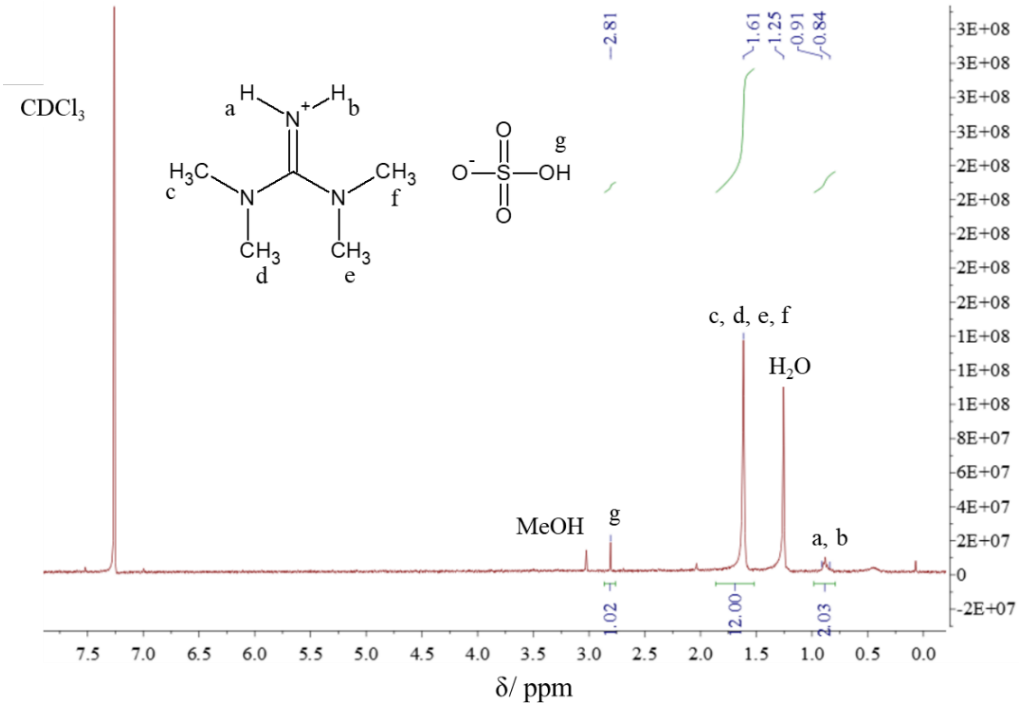

^{13}C-NMR

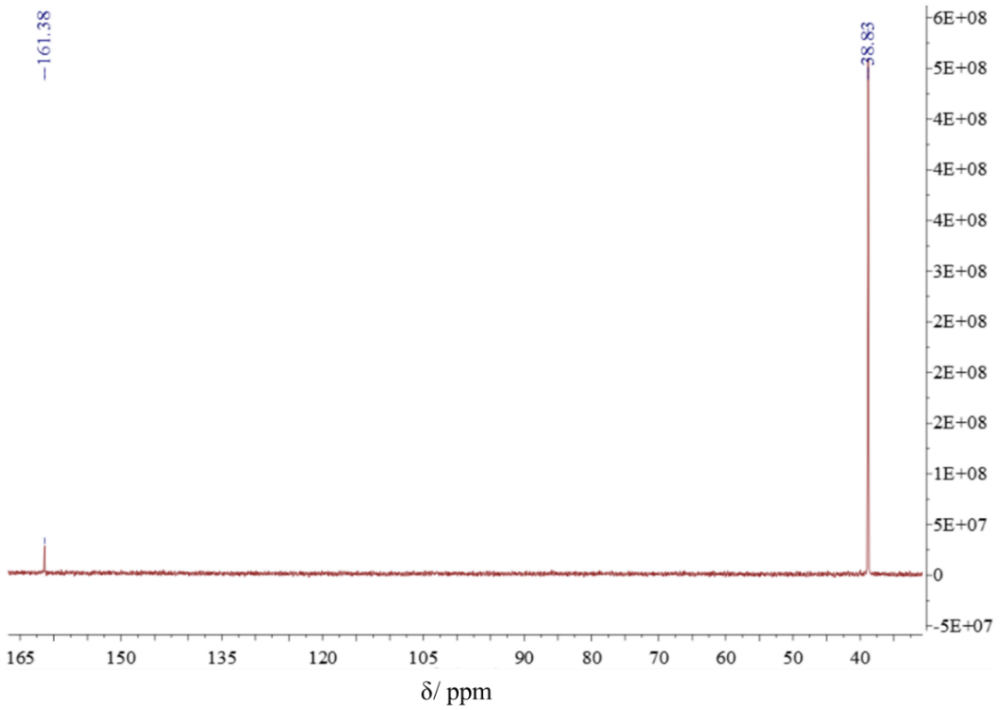
161.38
38.83
6E+08
5E+08
4E+08
4E+08
4E+08
3E+08
2E+08
2E+08
2E+08
1E+08
5E+07
0
-5E+07
165
150
135
120
105
90
80
70
60
50
40
δ/ ppm

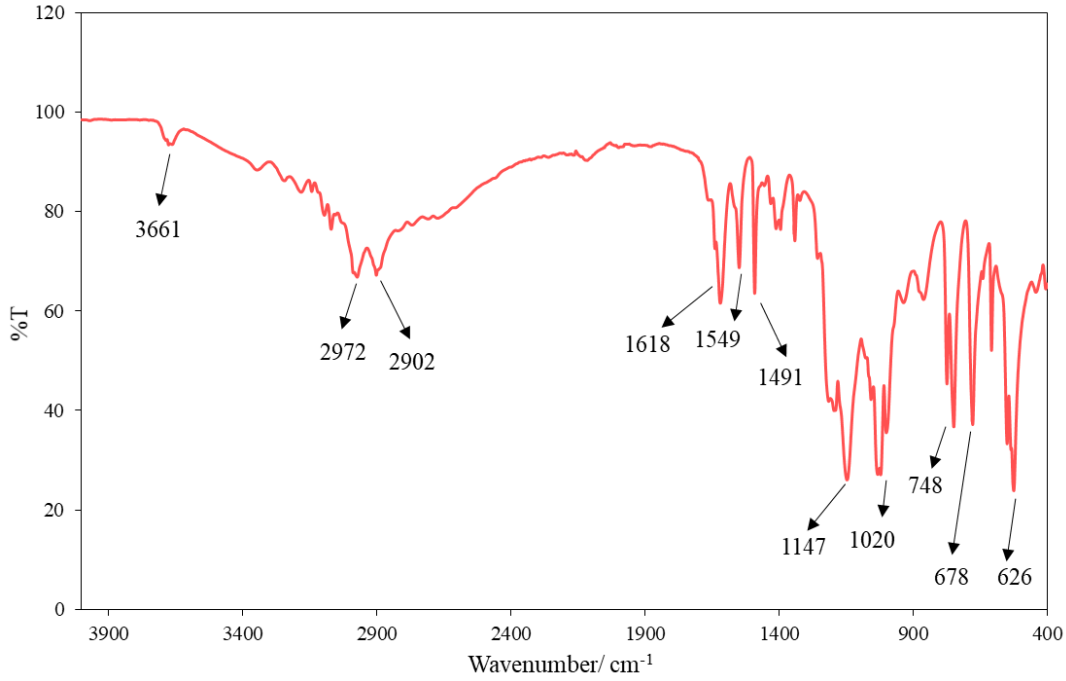
120
100
80
60
40
20
0
%T
3661
2972
2902
1618
1549
1491
1147
1020
748
678
626
3900
3400
2900
2400
1900
1400
900
400
Wavenumber/ cm-1

[DBUH][MeSO$_3$]

^{1}H-NMR

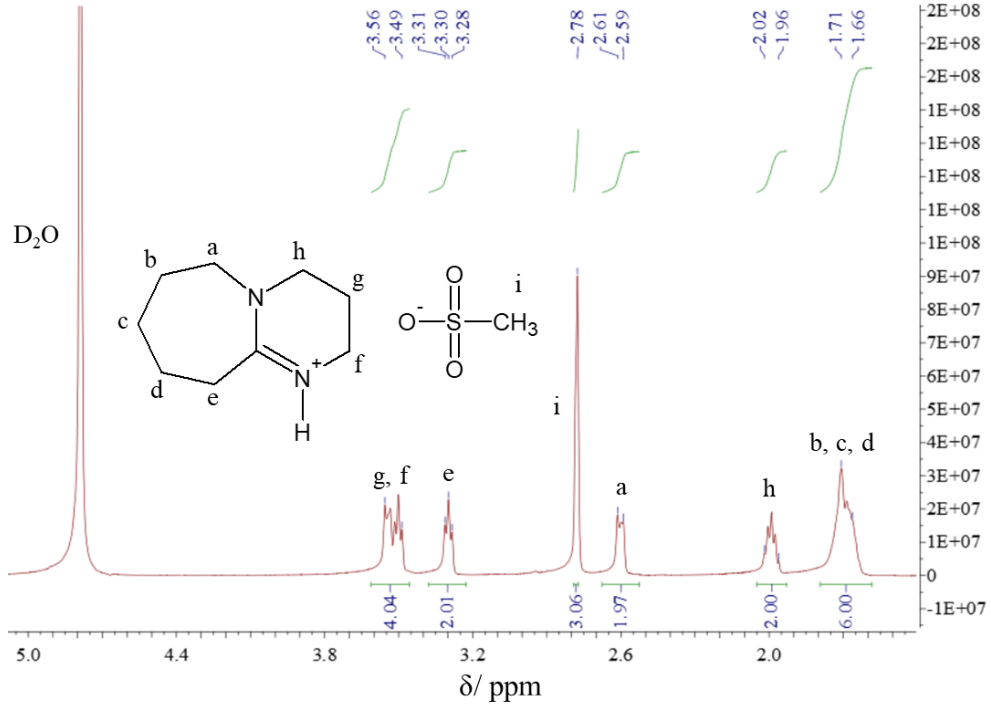

^{13}C-NMR

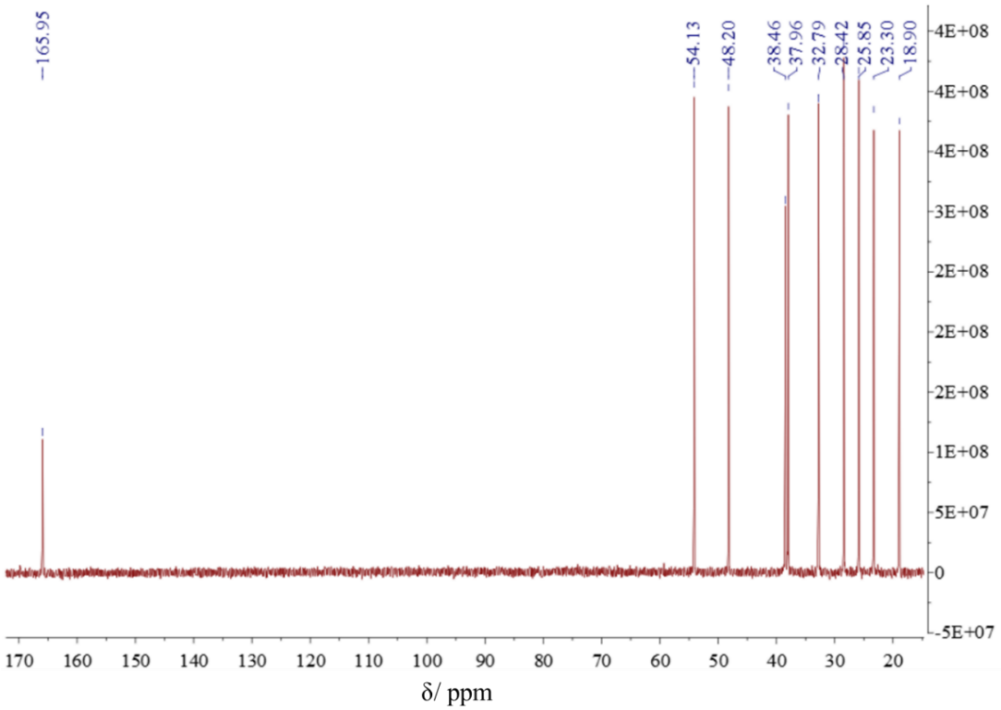

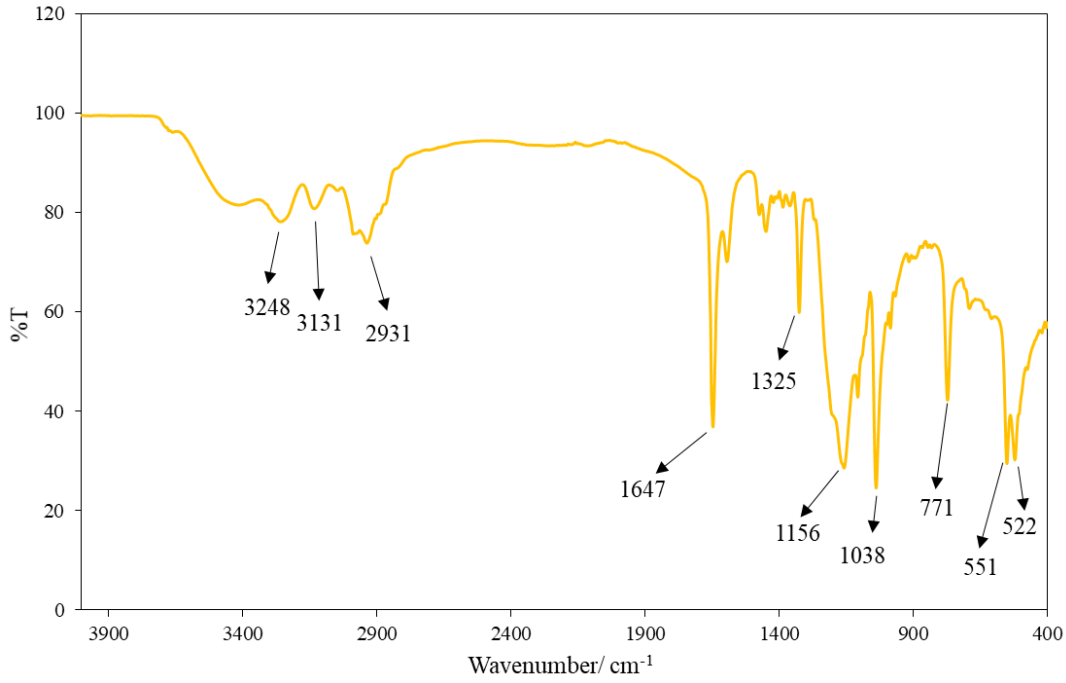

Figure A.2.1. ^{1}H-NMR, ^{13}C-NMR and FTIR spectra of the synthesized PILs.

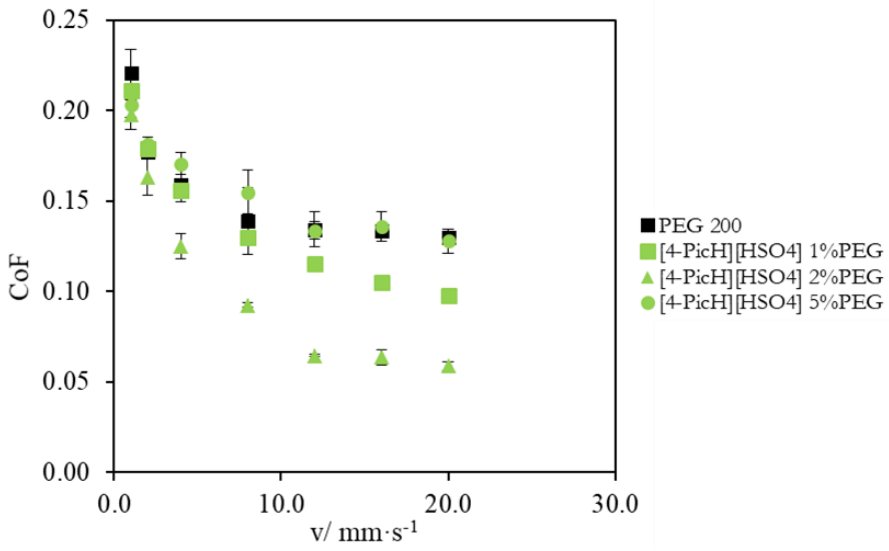

Figure A.2.2. CoF *vs.* sliding velocity obtained with three concentrations of [4-PicH][HSO_4] in PEG200: 0% (■), 1% (■), 2% (▲) and 5% (●).The errors are ± standard deviation (n ≥ 3).

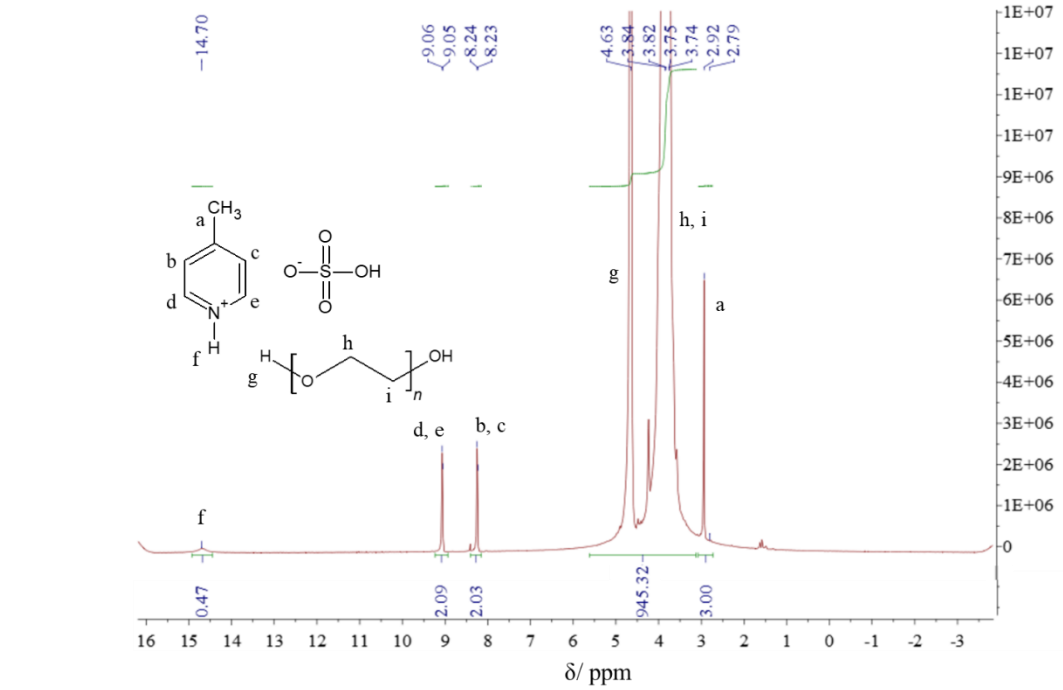

Figure A.2.3. ^{1}H-NMR spectrum of the mixture PEG200 + 2% [4-picH][HSO_4].

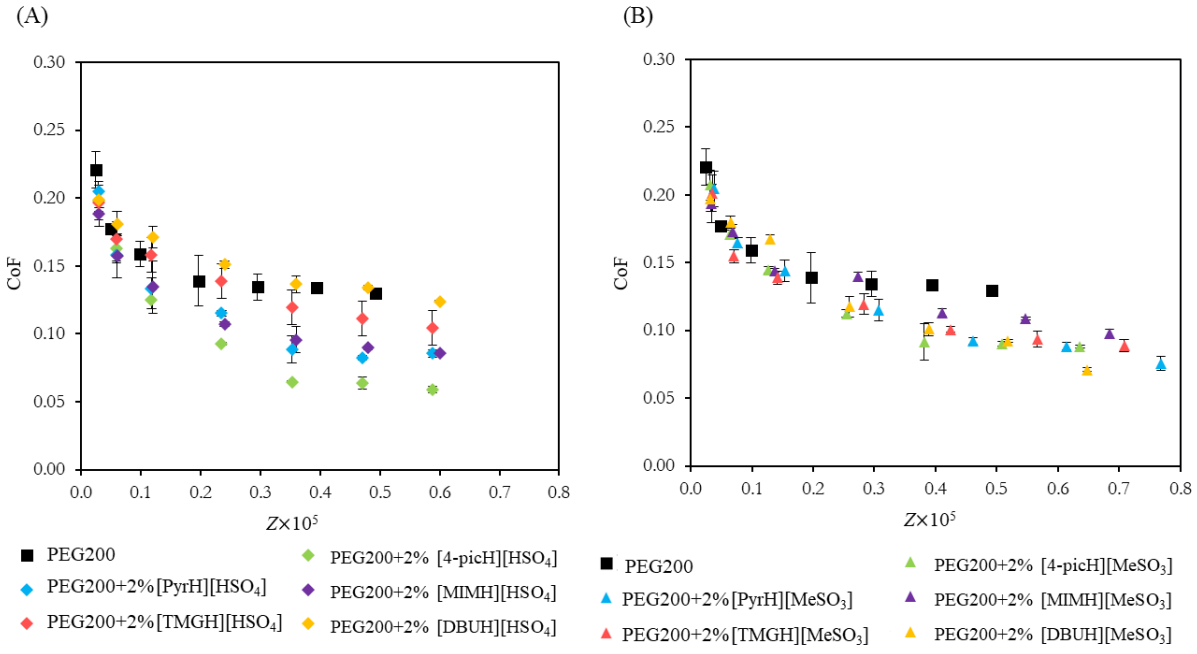

Figure A.2.4. CoF *vs*. Sommerfeld parameter, *Z*, for neat PEG200 and the mixtures PEG200 + 2% PIL: (A) PILs based on the anion [HSO_4]$^-$ and (B) PILs based on the anion [$MeSO_3$]$^-$. The errors are ± standard deviation (n ≥ 3).

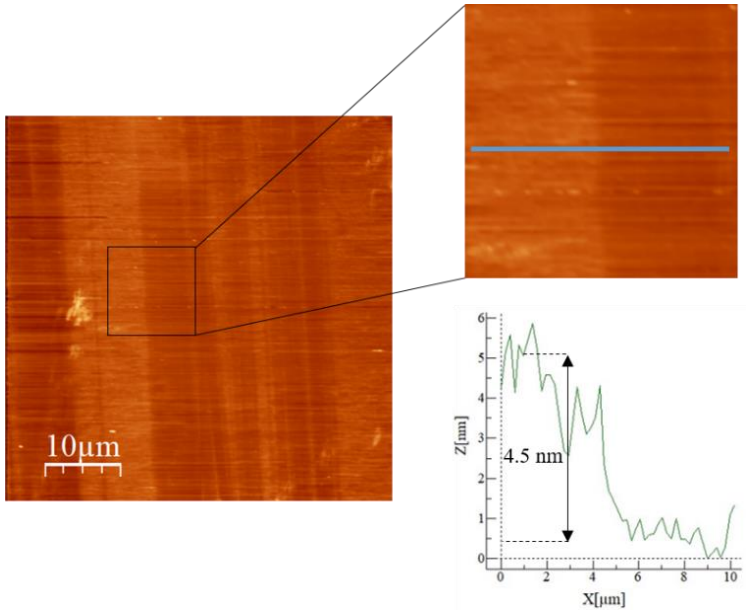

Figure A.2.5. AFM image of the film remaining on the Si substrate after the tribological test with PEG200 + 2% [4-picH][HSO_4] (2375 cycles, 1N). The insert represents the magnification of marked area on the track and adsorbed layer.

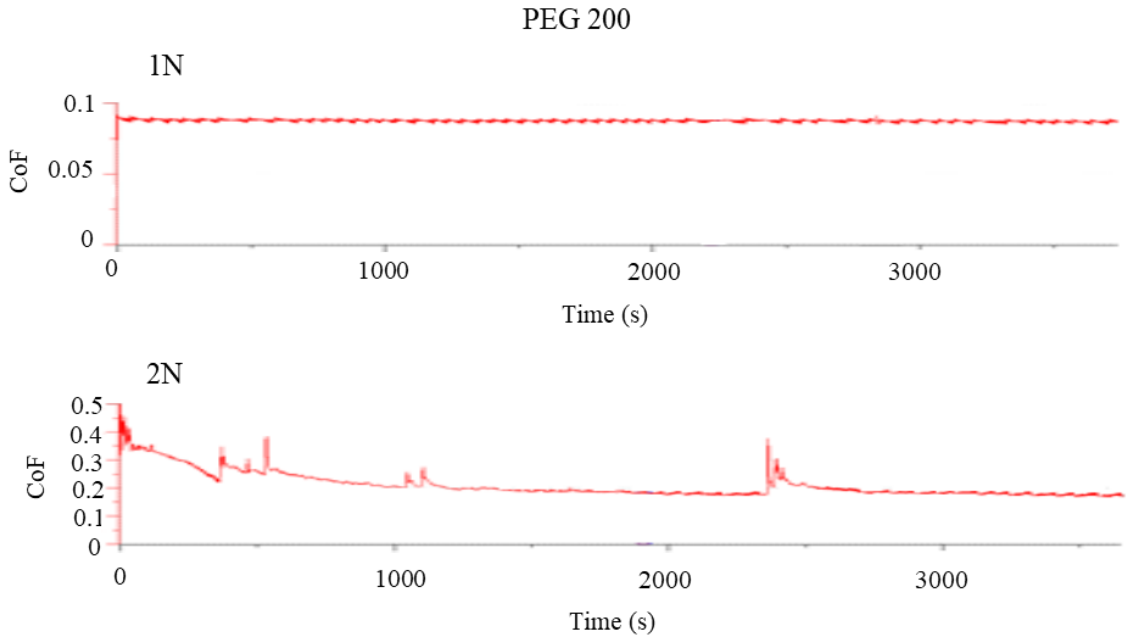

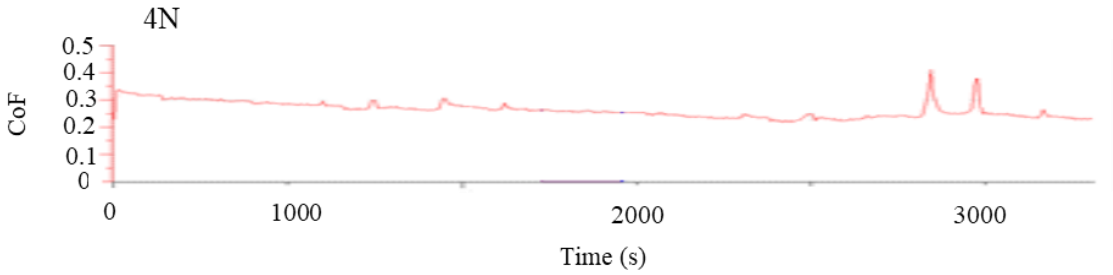

PEG200+2% [4-picH][$MeSO_3$]

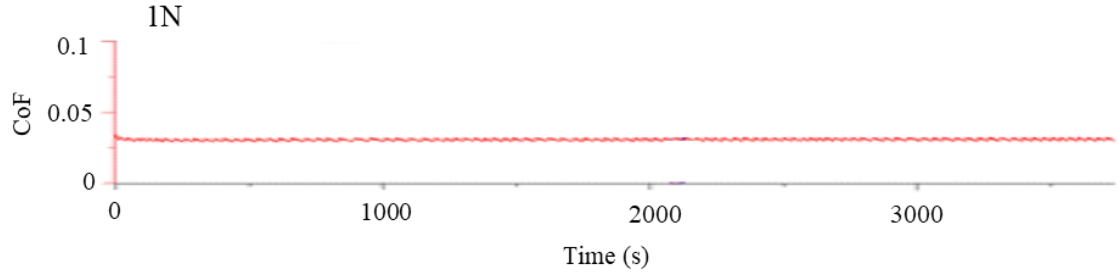

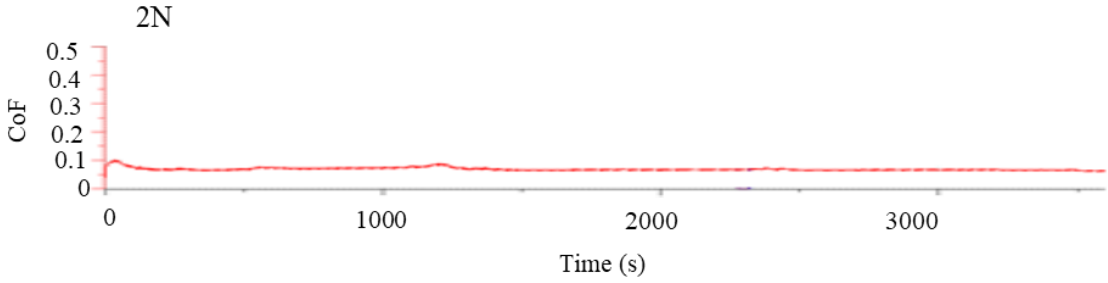

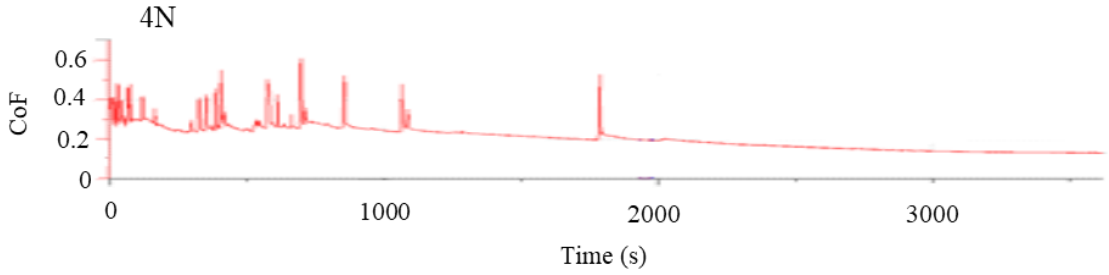

PEG200+2% [4-picH][HSO_4]

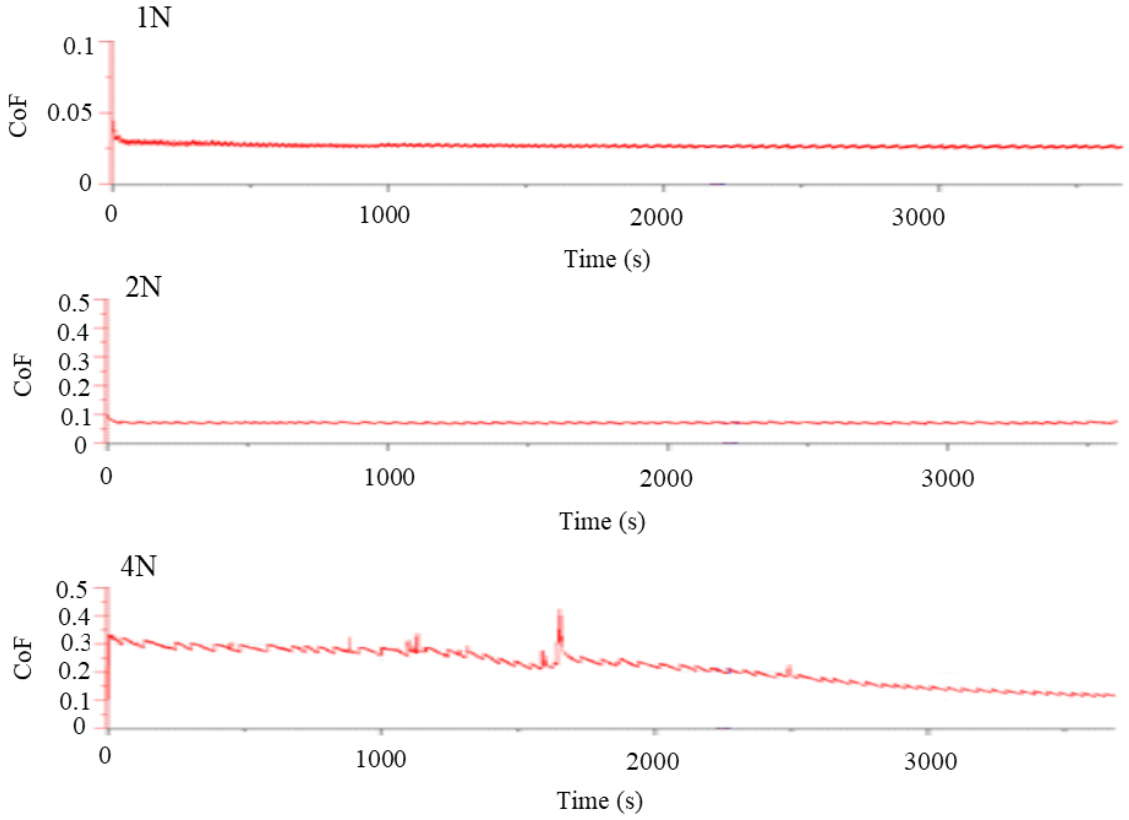

PEG200+2% [DBUH][$MeSO_3$]

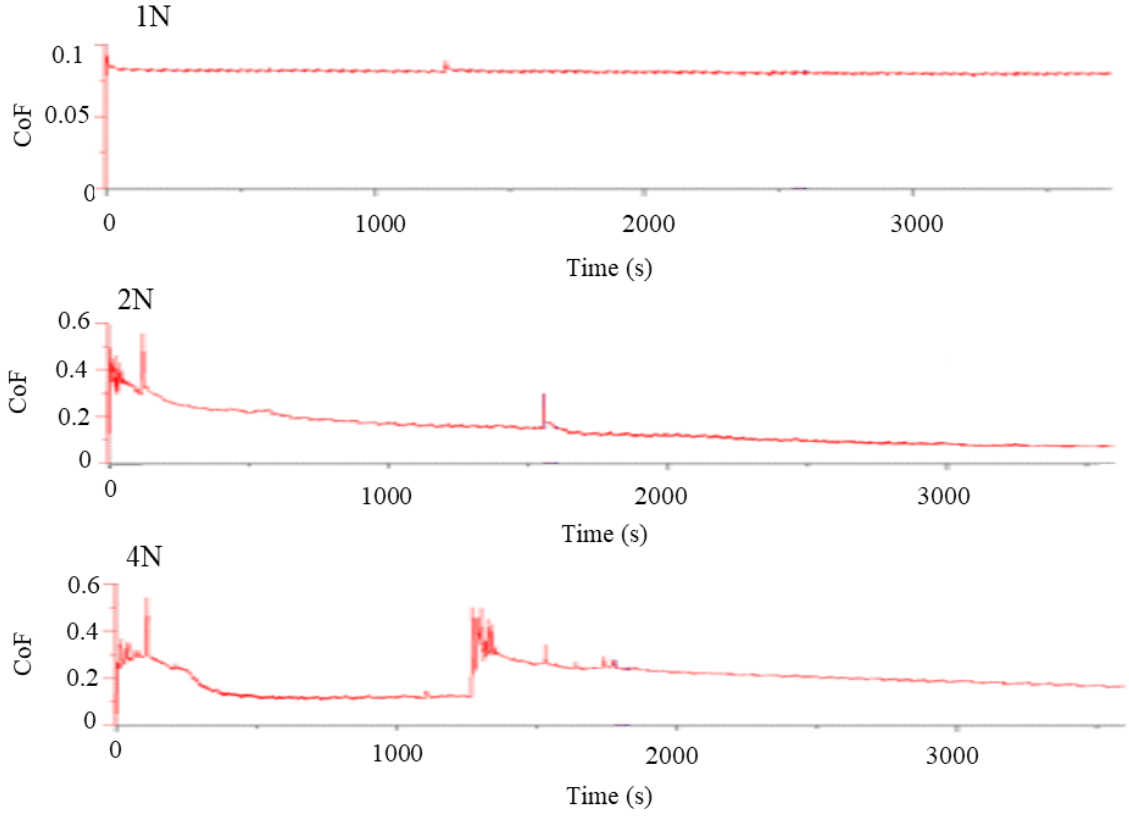

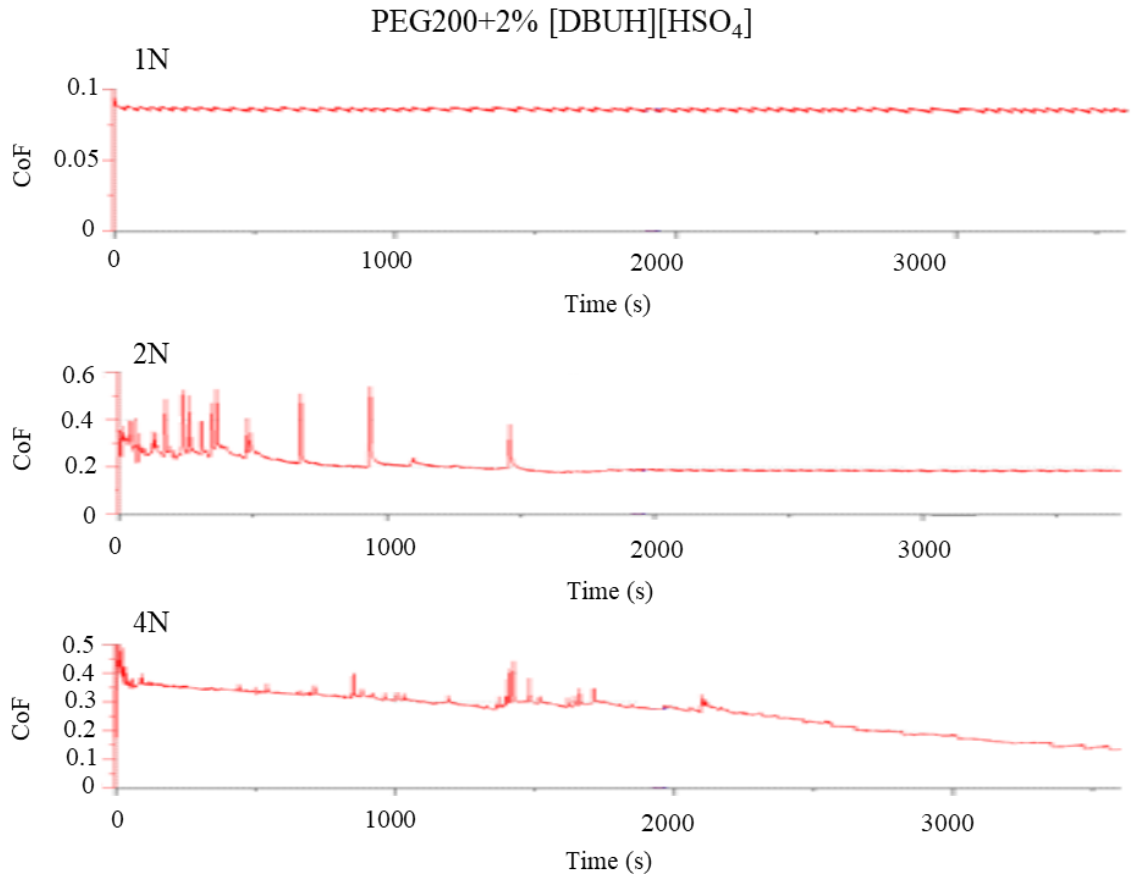

Figure A.2.6. CoF as a function of time obtained in long tests with the pair Si/Si, under 1N, 2N and 4N, and v=8mm·s^{-1} using PEG200 and the mixtures of PEG200 with [4-picH][$MeSO_3$], [4-picH][HSO_4], [DBUH][$MeSO_3$] and [DBUH][HSO_4] as lubricants. These results correspond to one specific run for each liquid.

Calculation of the theoretical minimum film thickness using elastohydrodynamic theory of lubrication (EHL)

According to the elastohydrodynamic theory of lubrication (EHL) applied to non-conformal geometry of ball-on-disc contact, the theoretical minimum film thickness, h, depends on the viscosity at atmospheric pressure (η_{atm}), and pressure-viscosity coefficient (α) of the lubricant and reduced modulus of the contact between the surfaces (E_r). The value of E_r was calculated using equation 1:

$$\frac{1}{E_r} = \frac{1}{2}\left[\left(\frac{1-\vartheta_{disc}^2}{E_{disc}}\right) + \left(\frac{1-\vartheta_{ball}^2}{E_{ball}}\right)\right] \qquad \text{Eq. A.2}$$

where the values of Poisson's ratio and Young's modulus for Si, taken from reference [1], are 0.27-0.22 and 130-165 GPa, respectively.

The theoretical minimum film thickness, h, can be calculated using the Hamrock model [2], through the following equation:

$$h = 3.63R\left(\frac{U\eta_{atm}}{E_r R}\right)^{0.68}(\alpha E_r)^{0.49}\left(\frac{W}{E_r R^2}\right)^{-0.073}\left(1 - e^{-0.68k}\right) \qquad \text{Eq. A.3}$$

where R is half of the radius of the ball, U is half of the sliding speed (as an approximation, in reciprocating movement, can be taken as the average sliding speed of the test), W is the load and k is ellipticity parameter (taken as 1 for point contact). The pressure-viscosity coefficient, $\alpha = \frac{1}{\eta}\left(\frac{\partial \eta}{\partial P}\right)_T$, was calculated as 17 GPa^{-1} for tetraethylene glycol, from data reported in the literature at 25 °C.[3] The same value was used, as an approximation, for the PEG200+ 2% [4-picH][HSO_4] mixture, since PEG200 and tetraethylene glycol have very similar molecular weights and the solution of IL in PEG200 is very diluted.

References

[1] M. A. Hopcroft, W. D. Nix, T. W. Kenny, What Is the Young's Modulus of Silicon? *J. Microelectromechanical Syst.* 2010, *19* (2), 229–238. https://doi.org/10.1109/JMEMS.2009.2039697

[2] B. J. Hamrock, D. Dowson, Isothermal Elastohydrodynamic Lubrication of Point Contacts: Part III—Fully Flooded Results. *J. Lubr. Technol.*, 1977, 99, 264-275. https://doi.org/10.1115/1.3453074

[3] M. F. V. Pereira, H. M. N. T. Avelino, F. J. P. Caetano, J. M. N. A. Fareleira, Viscosity of Liquid Diethylene, Triethylene and Tetraethylene Glycols at Moderately High Pressures Using a Vibrating Wire Instrument. *Fluid Phase Equilibria* 2019, *480*, 87–97. https://doi.org/10.1016/j.fluid.2018.09.026

A.3 Supporting Information of Chapter 3.1

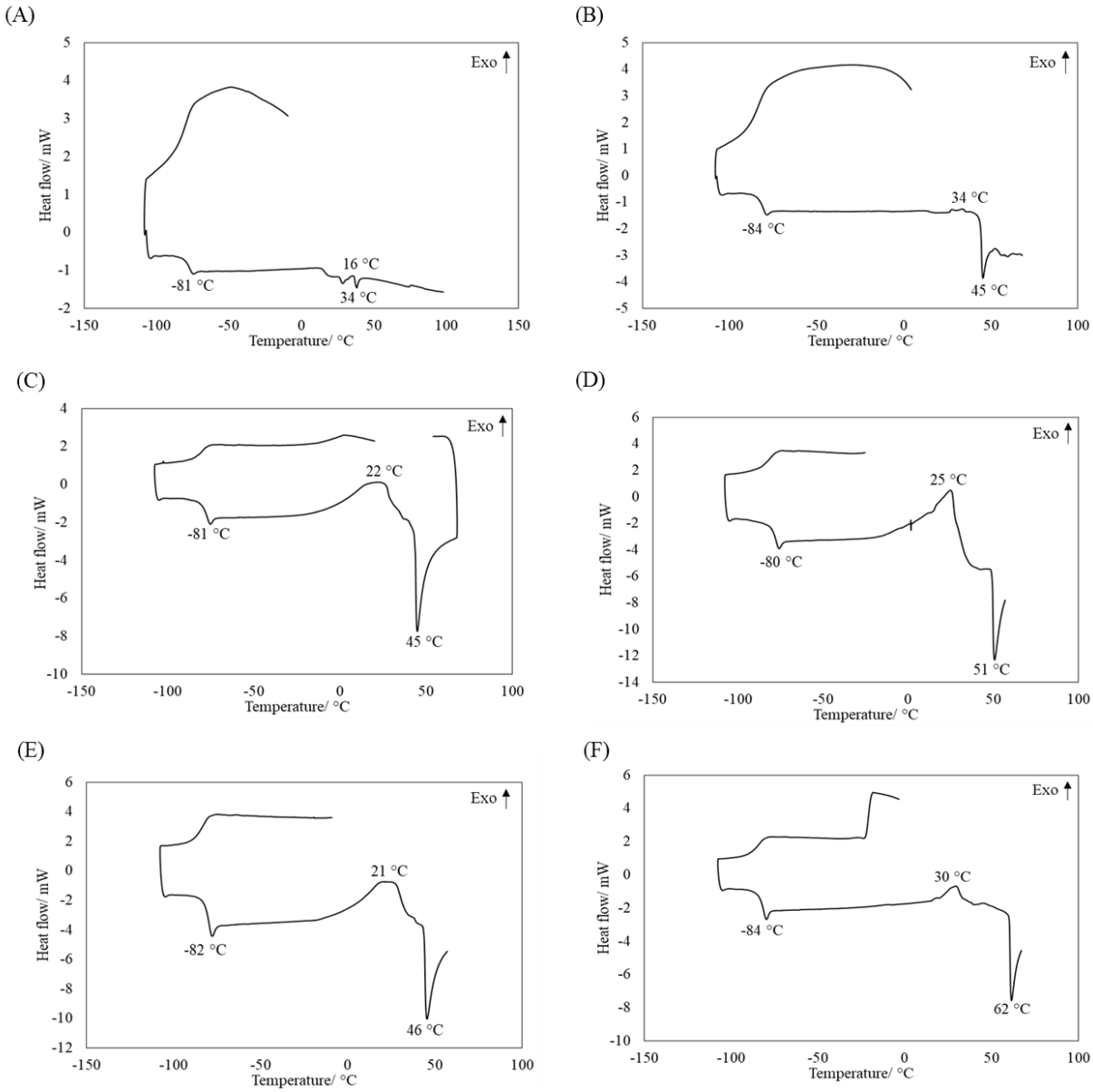

Figure A.3.1. (A) DSC thermograms of the IL; DSC thermograms of the ESs in different HBA:HBD ratios: (B) 1:2, (C) 1:4, (D) 1:8 and (E) 1:16; (F) DSC thermogram of PEG200.

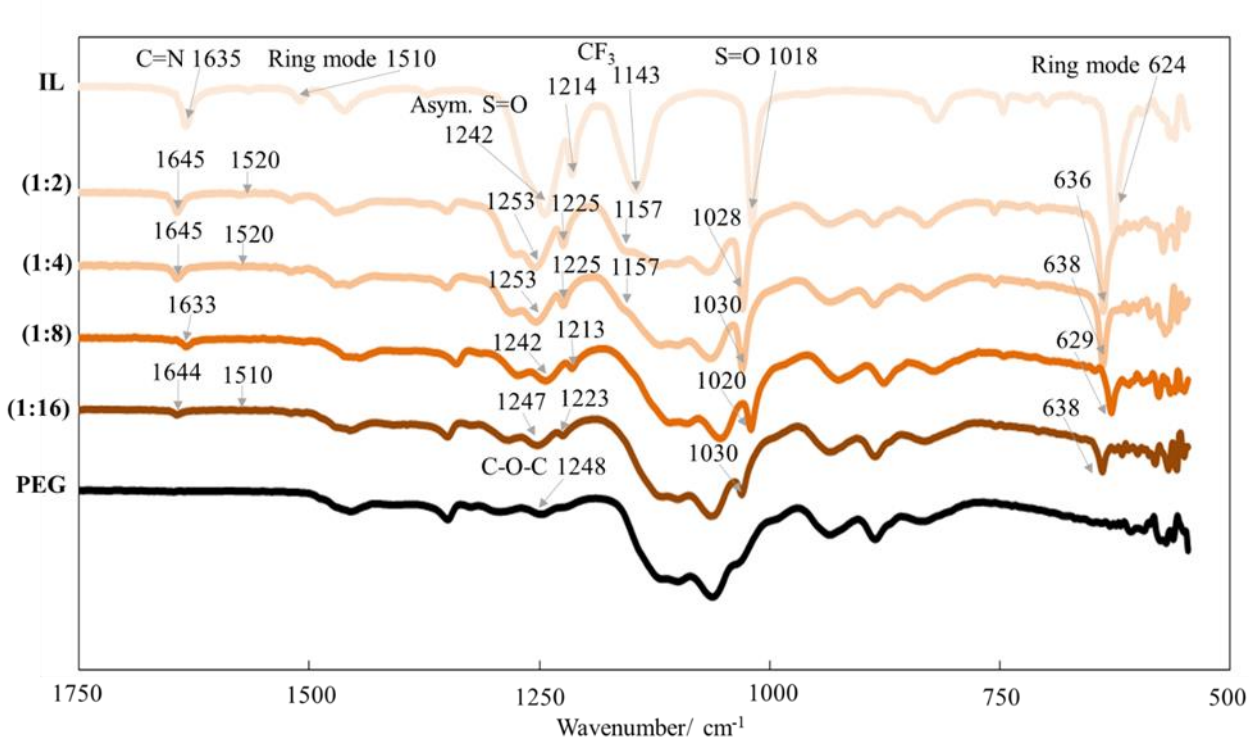

Figure A.3.2. FTIR spectra of the IL, the ESs (1:2, 1:4, 1:8 and 1:16) and PEG200.

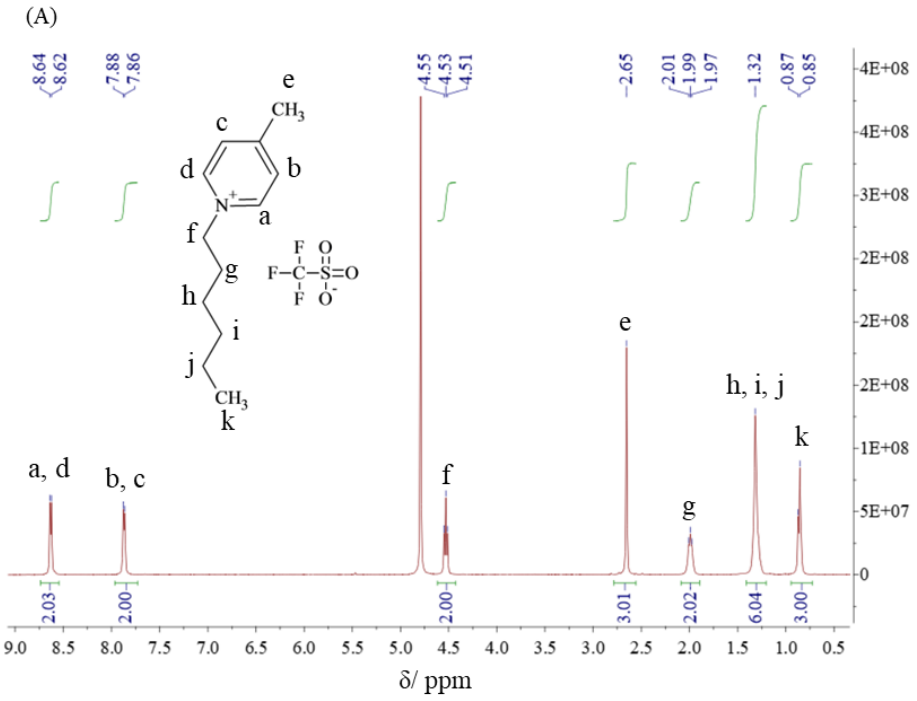

(B)

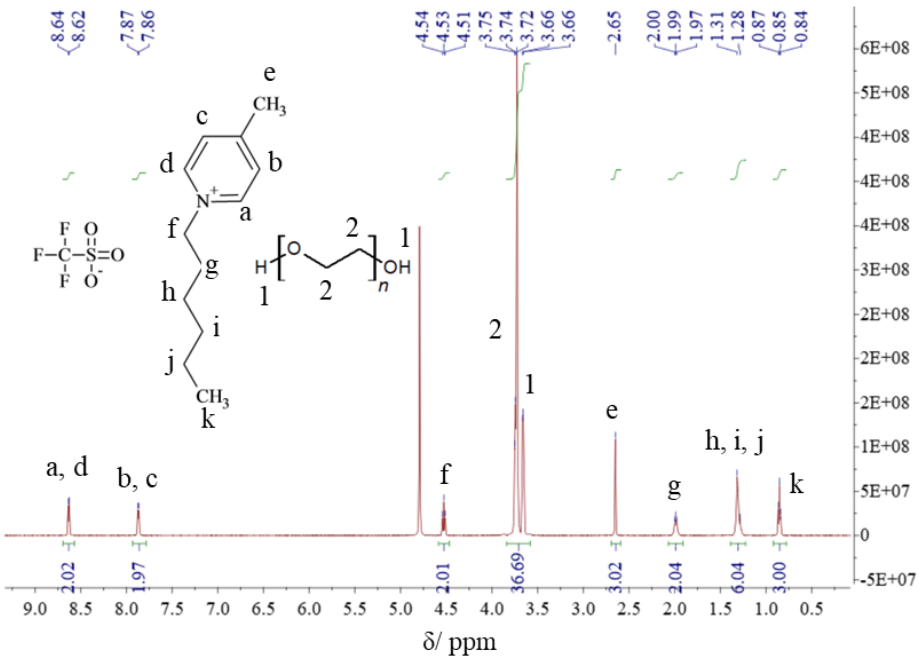

(C)

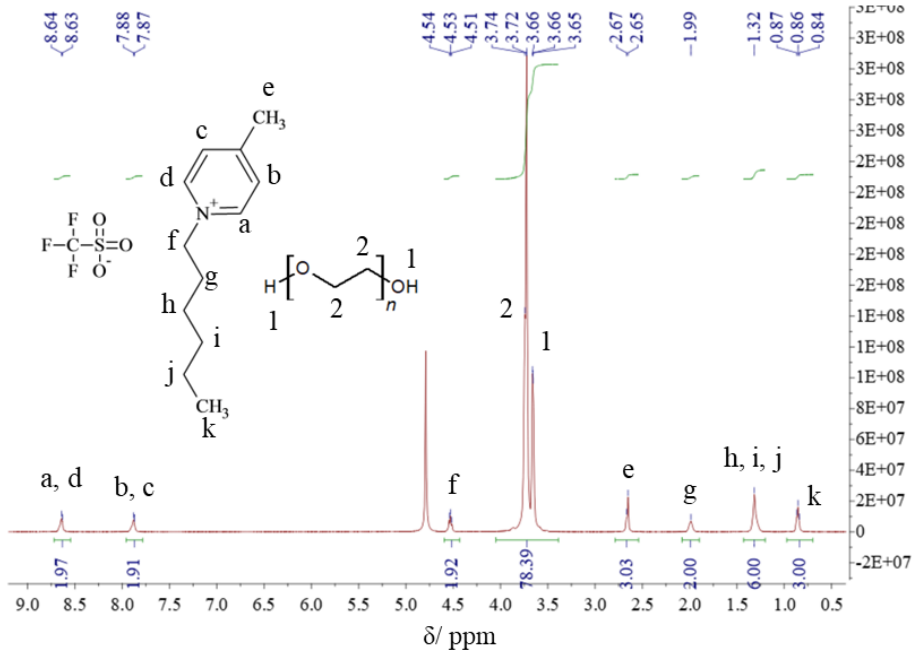

(D)

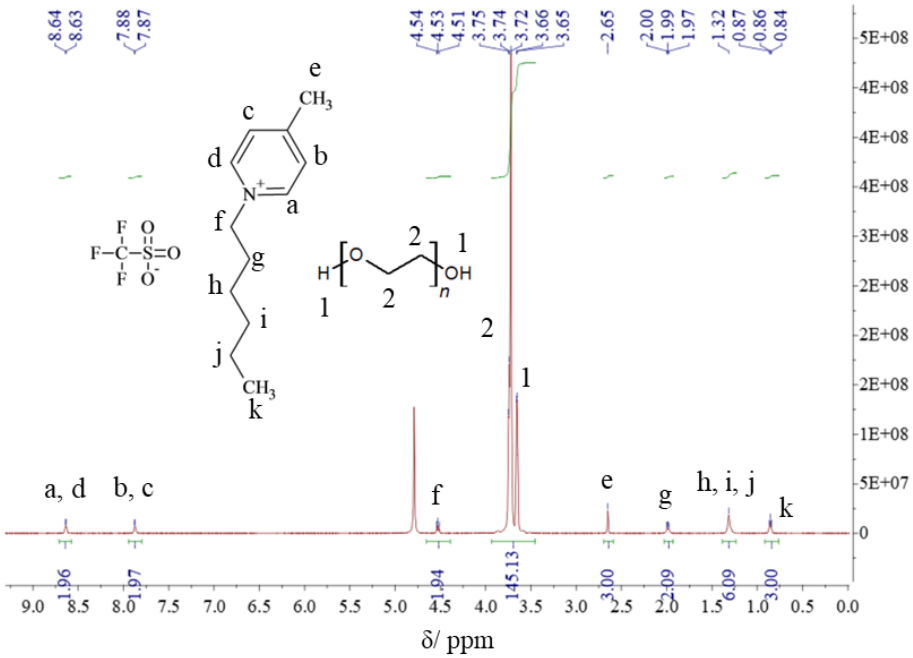
8.64
8.63
7.88
7.87
4.54
4.53
4.51
3.75
3.74
3.72
3.66
3.65
2.65
2.00
1.99
1.97
1.32
0.87
0.86
0.84
a, d
b, c
f
e
g
h, i, j
k
δ/ ppm

(E)

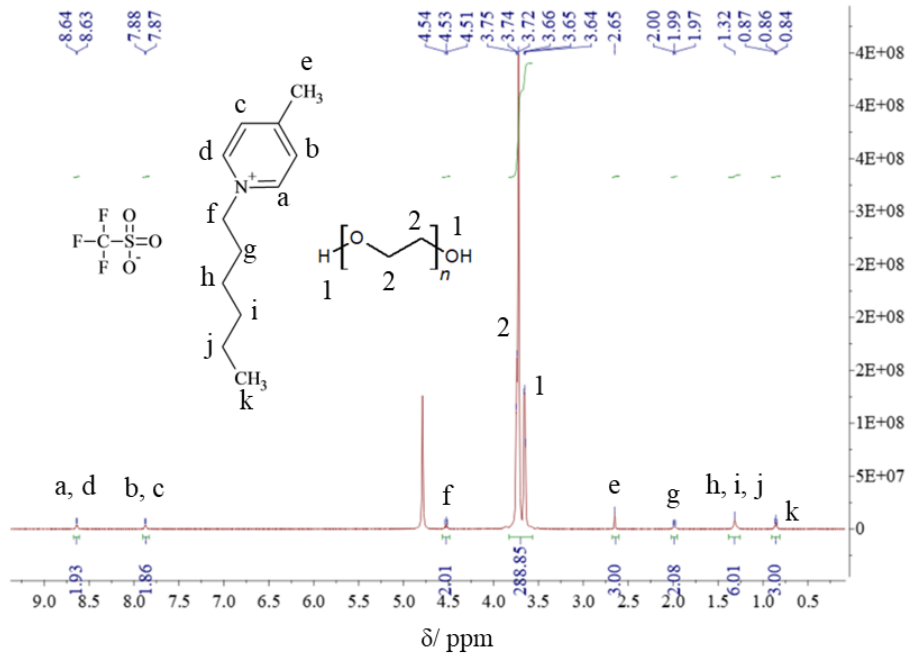
8.64
8.63
7.88
7.87
4.54
4.53
4.51
3.75
3.74
3.72
3.66
3.65
3.64
2.65
2.00
1.99
1.97
1.32
0.87
0.86
0.84
a, d
b, c
f
e
g
h, i, j
k
δ/ ppm

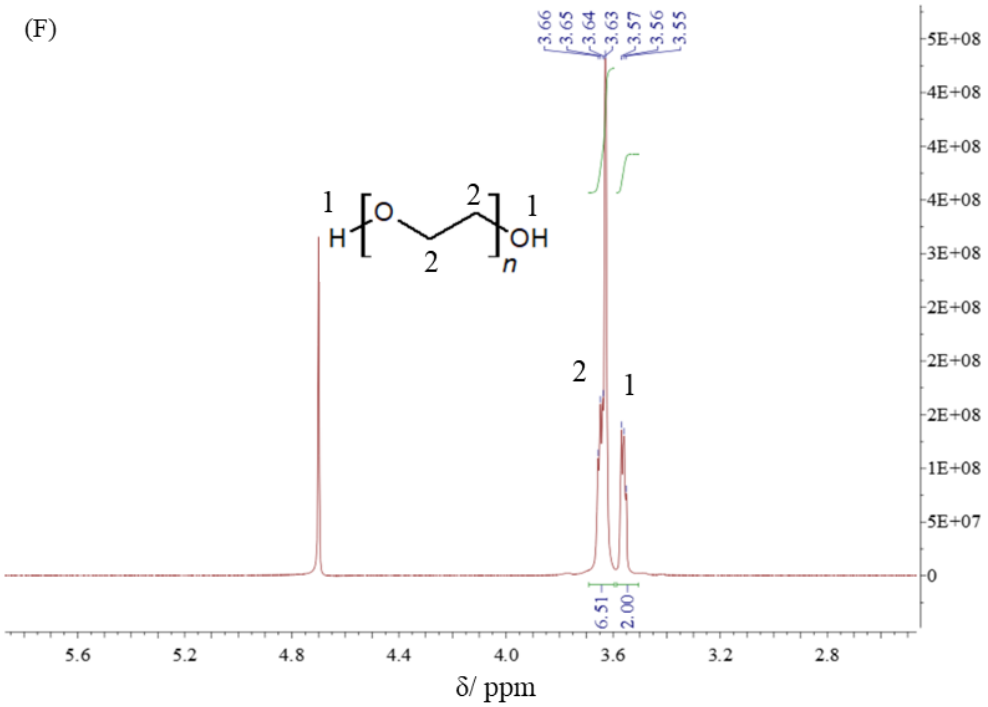

Figure A.3.3. (A) ^{1}H-NMR of the IL [C_6-4-pic][TfO]; ^{1}H-NMR of the ESs [C_6-4-pic][TfO]:PEG200 (HBA:HBD) in different ratios: (B) 1:2 [comparing the signals a, d (expected 2H) *vs*. 1, 2 (expected 36H; ratio = 2.02:36.69]; (C) 1:4 [comparing the signals a, d (expected 2H) *vs*. 1, 2 (expected 78H; ratio = 1.97:78.39)]; (D) 1:8 [comparing the signals a, d (expected 2H) *vs*. 1, 2 (expected 144H; ratio = 1.96:145.13] and (E) 1:16 (comparing the signals a, d (expected 2H) *vs*. 1, 2 (expected 288H; ratio = 1.93:288.85]; (F) ^{1}H-NMR of PEG200.

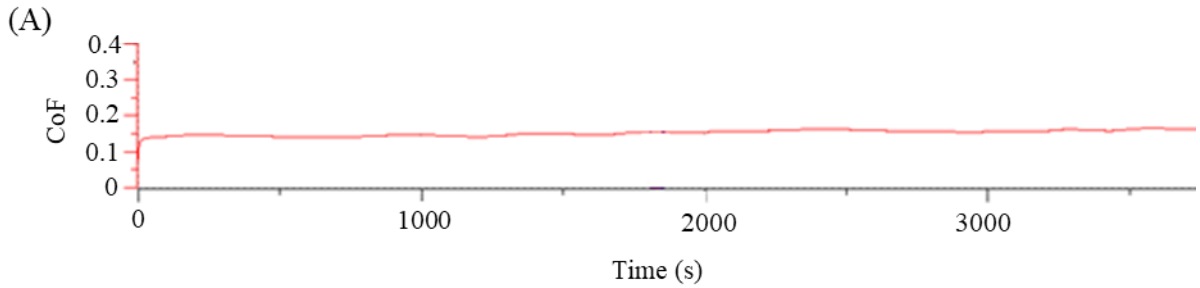

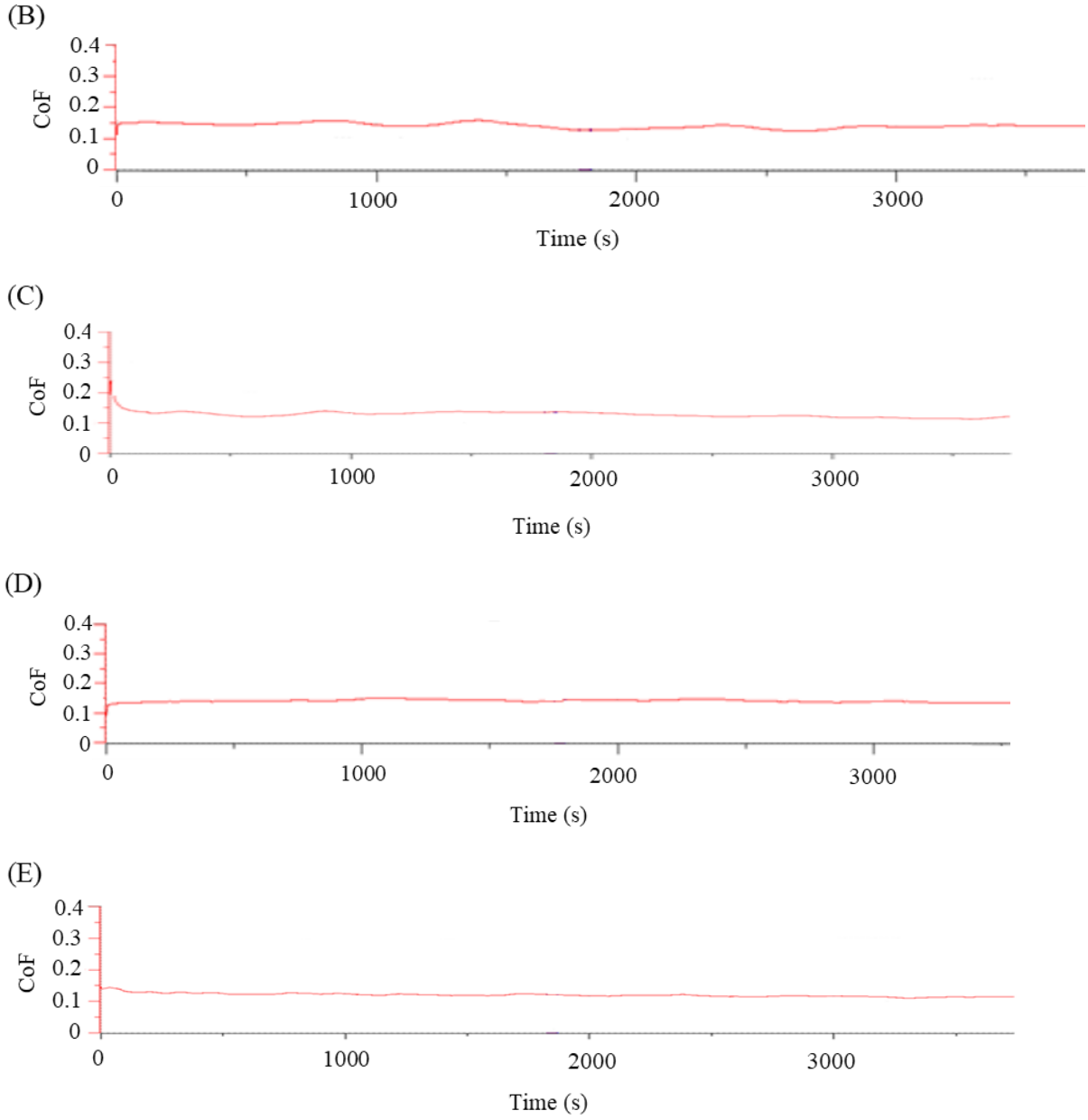

Figure A.3.4. CoF as a function of time (2375 cycles) obtained for the tribological pair steel/Si with v=8 mm·s^{-1} for 8N, using as lubricants: (A) PEG 200, (B) ES 1:16, (C) ES 1:8, (D) ES 1:4 and (E) ES 1:2. These results correspond to one specific run for each liquid.

Table A.3.1. Viscosity at 25 °C and contact angles of the tested liquids.

Liquid	Viscosity/ mPa·s	Contact angle/ °
[C_6-4-pic][TfO]	128±2	33±1
[C_6-4-pic][TfO]:PEG200 (1:2)	64±1	30±3
[C_6-4-pic][TfO]:PEG200 (1:4)	46±0	28±5
[C_6-4-pic][TfO]:PEG200 (1:8)	45±0	30±4
[C_6-4-pic][TfO]:PEG200 (1:16)	47.0±0.6	28±2
PEG200	41.0±0.6	28±2

Table A.3.2. Average CoF values ± standard deviation (n ≥ 3) and average wear volumes ± standard deviation (n ≥ 5) obtained with the ESs and PEG200 in tribological tests with the pair steel/Si under normal forces of 2N, 4N and 8N and 2375 cycles.

Liquids	CoF			Wear volume/ 10^5 mm^3		
	2N	4N	8N	2N	4N	8N
[C_6-4-pic][TfO]: PEG200 (1:2)	0.101±0.008	0.12±0.01	0.120±0.002	0.2±0.1	2.4±0.8	3.5±0.6
[C_6-4-pic][TfO]: PEG200 (1:4)	0.123±0.007	0.13±0.01	0.143±0.004	0.19±0.06	2.8±0.8	5.7±0.3
[C_6-4-pic][TfO]: PEG200 (1:8)	0.133±0.004	0.13±0.01	0.128±0.004	1.0±0.3	3±1	4.8±0.4
[C_6-4-pic][TfO]: PEG200 (1:16)	0.14±0.01	0.135±0.008	0.15±0.01	0.6±0.2	2.8±0.6	5±1
PEG200	0.13±0.02	0.145±0.009	0.18±0.01	0.8±0.1	3.5±0.9	7±1

A.4 Supporting Information of Chapter 3.2

^{1}H-NMR [Aliquat]Cl:hexanoic acid (1:1) (δ, $CDCl_3$, 400 MHz): 4.93 (m, 1H), 3.44-3.27 (m, 9H), 2.32 (t, 2H, J = 7.6 Hz), 1.64 (m, 8H), 1.33-1.20 (m, 34H), 0.86 (t, 12H, J = 5.8 Hz) ppm.
^{1}H-NMR [Aliquat]Cl:octanoic acid (1:1) (δ, $CDCl_3$, 400 MHz): 3.44-3.40 (m, 6H), 3.31-3.27 (m, 3H), 2.12 (m, 1H), 1.64 (m, 6H), 1.34-1.24 (m, 42H), 0.86-0.84 (m, 12H) ppm.
^{1}H-NMR [Aliquat]Cl:decanoic acid (1:2) (δ, $CDCl_3$, 400 MHz): 4.03-3.98 (m, 1H), 3.32-3.20 (m, 9H), 2.30-2.26 (m, 4H), 1.60-1.56 (m, 10H), 1.22 (m, 54H), 0.82 (m, 15H) ppm.
^{1}H-NMR [Aliquat]Cl:hexanol (1:2) (δ, DMSO-d_6, 400 MHz): 4.41 (m, 2H), 3.45-3.38 (m, 4H),

3.20-3.19 (m, 6H), 2.93 (m, 3H), 1.59 (m, 6H), 1.24 (m, 42H), 0.85 (m, 15H) ppm.

^{1}H-NMR [Aliquat]Cl:octanol (1:1) (δ, $CDCl_3$, 400 MHz): 3.61-3.59 (m, 3H), 3.39 (m, 6H), 3.29 (m, 3H), 2.41-2.17 (m, 3H), 1.63-1.52 (m, 6H), 1.33-1.23 (m, 42H), 0.85-0.83 (m, 12H) ppm.

^{1}H-NMR [Aliquat]Cl:menthol (1:2) (δ, $CDCl_3$, 400 MHz): 3.32-3.18 (m, 11H), 2.10-2.09 (m, 2H), 1.88-0.68 (m, 79H) ppm.

^{1}H-NMR [N_{4444}]Br:octanol (1:2) (δ, $CDCl_3$, 400 MHz): 3.58-3.56 (m, 4H), 3.32-3.30 (m, 8H), 1.49-1.22 (m, 40H), 0.97-0.94 (m, 12H), 0.83-0.82 (d, 6H, J = 1.8 Hz) ppm.

^{1}H-NMR [N_{4444}]Br:hexanoic acid (1:1) (δ, $CDCl_3$, 400 MHz): 3.35-3.31 (m, 8H), 2.32-2.30 (m, 2H), 1.69-1.58 (m, 6H), 1.47-1.38 (m, 8H), 1.30-1.28 (m, 8H), 0.99-0.96 (m, 12H), 0.88-0.84 (m, 3H) ppm.

^{1}H-NMR menthol:hexanoic acid (1:1) (δ, $CDCl_3$, 400 MHz): 3.44-3.38 (m, 1H), 2.33-2.29 (m, 2H), 2.19-2.12 (m, 1H), 1.97-1.94 (m, 1H), 1.65-1.58 (m, 4H), 1.42-1.31 (m, 8H), 1.13-1.08 (m, 1H), 1.00-0.78 (m, 14H) ppm.

^{1}H-NMR menthol:octanol (1:1) (δ, $CDCl_3$, 400 MHz): 3.32-3.18 (m, 3H), 2.10-2.09 (m, 1H), 1.88-1.58 (m, 4H), 1.48-1.26 (m, 16H), 1.19-0.68 (m, 12H) ppm.

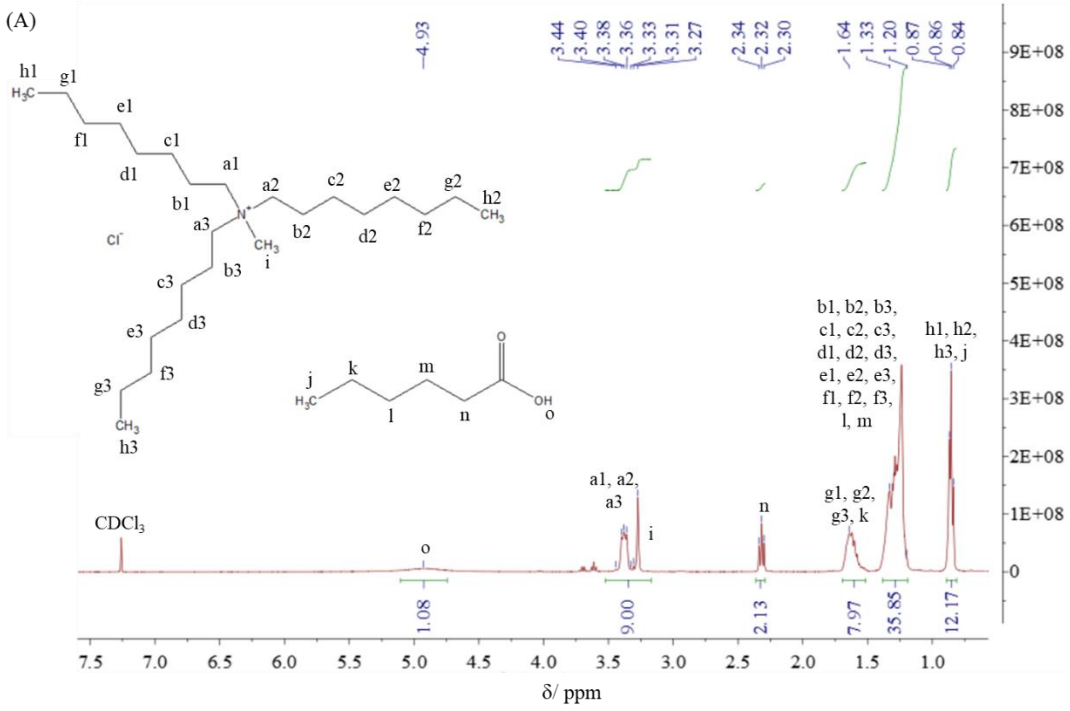

(B)

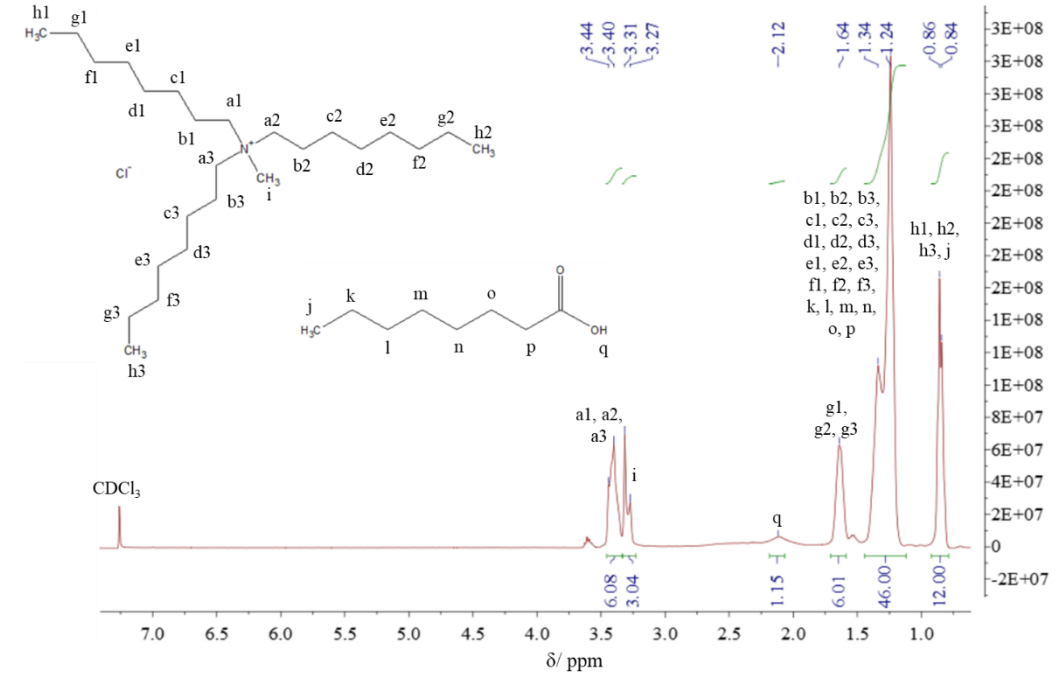
3.44
3.40
3.31
3.27
2.12
1.64
1.34
1.24
0.86
0.84
b1, b2, b3, c1, c2, c3, d1, d2, d3, e1, e2, e3, f1, f2, f3, k, l, m, n, o, p
h1, h2, h3, j
g1, g2, g3
a1, a2, a3
i
q
CDCl3
6.08
3.04
1.15
6.01
46.00
12.00
δ/ ppm

(C)

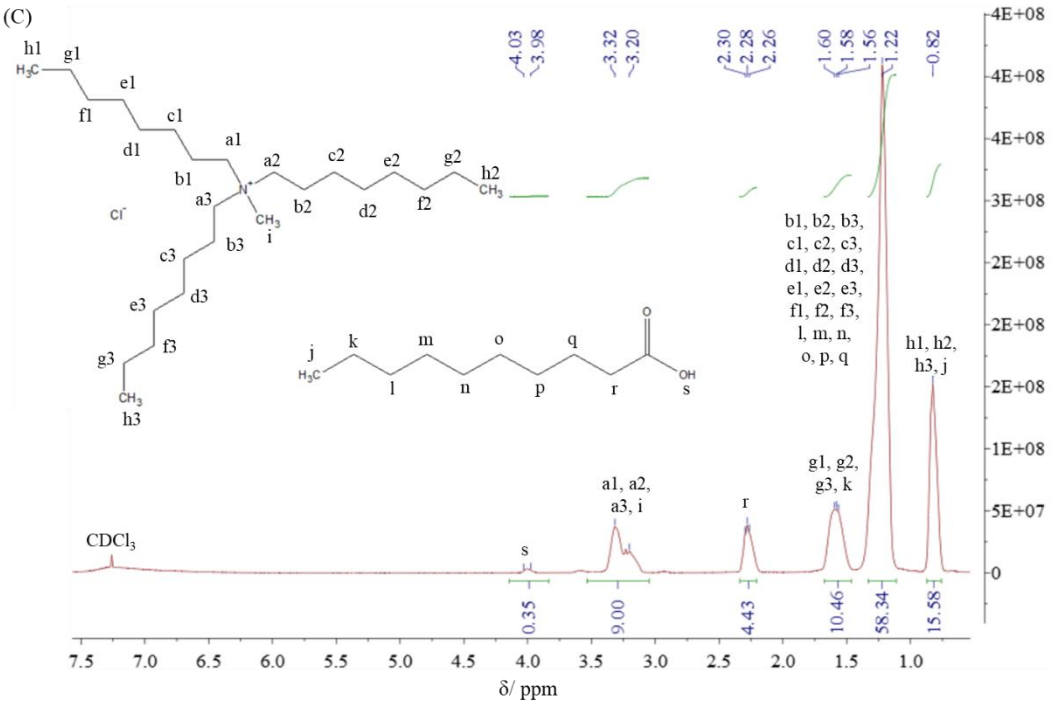
4.03
3.98
3.32
3.20
2.30
2.28
2.26
1.60
1.58
1.56
1.22
0.82
b1, b2, b3, c1, c2, c3, d1, d2, d3, e1, e2, e3, f1, f2, f3, l, m, n, o, p, q
h1, h2, h3, j
g1, g2, g3, k
a1, a2, a3, i
r
s
CDCl3
0.35
9.00
4.43
10.46
58.34
15.58
δ/ ppm

(D)

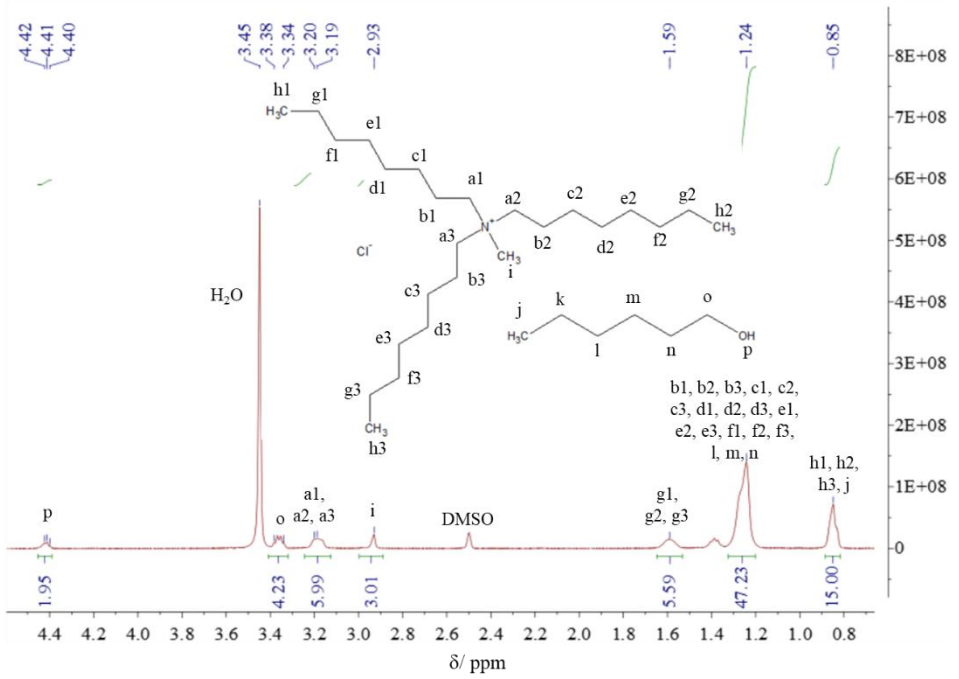
4.42
4.41
4.40
3.45
3.38
3.34
3.20
3.19
2.93
1.59
1.24
0.85
h1 g1
e1
f1
c1
d1
a1
a2 c2 e2 g2 h2
b1
a3
b2 d2 f2
i
b3
c3
d3
e3
f3
g3
h3
j k m o
l n p
OH
H2O
DMSO
p
o
a1, a2, a3
i
g1, g2, g3
b1, b2, b3, c1, c2, c3, d1, d2, d3, e1, e2, e3, f1, f2, f3, l, m, n
h1, h2, h3, j
1.95
4.23
5.99
3.01
5.59
47.23
15.00
δ/ ppm

(E)

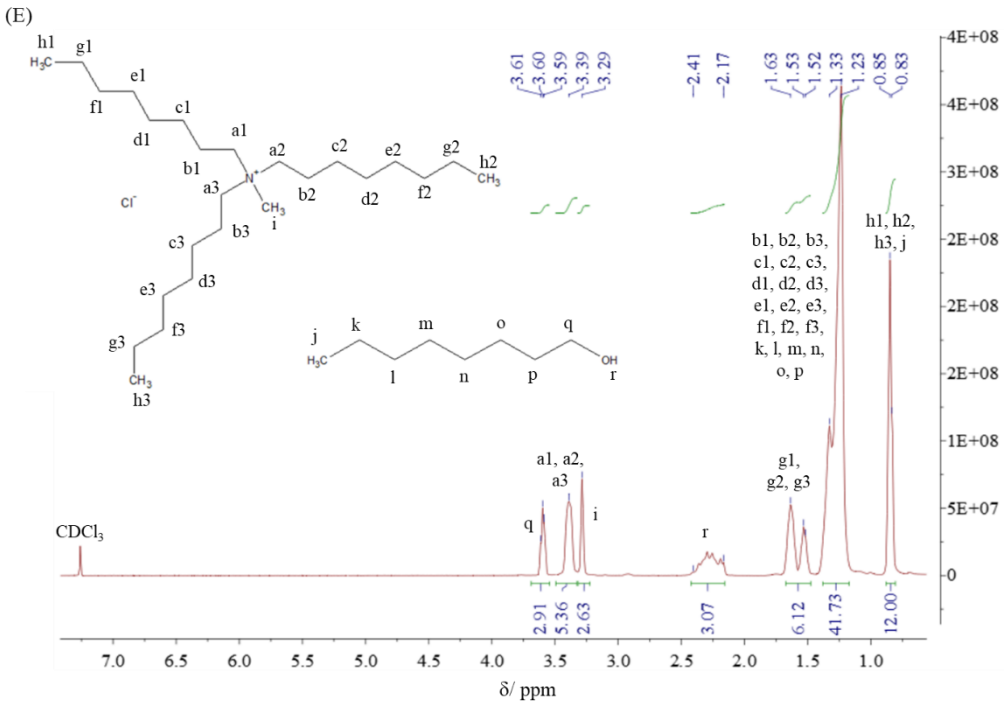
3.61
3.60
3.59
3.39
3.29
2.41
2.17
1.63
1.53
1.52
1.33
1.23
0.85
0.83
h1 g1
e1
f1
c1
d1
a1
a2 c2 e2 g2 h2
b1
a3
b2 d2 f2
i
b3
c3
d3
e3
f3
g3
h3
j k m o q
l n p r
OH
b1, b2, b3, c1, c2, c3, d1, d2, d3, e1, e2, e3, f1, f2, f3, k, l, m, n, o, p
h1, h2, h3, j
CDCl3
q
a1, a2, a3
i
r
g1, g2, g3
2.91
5.36
2.63
3.07
6.12
41.73
12.00
δ/ ppm

(F)

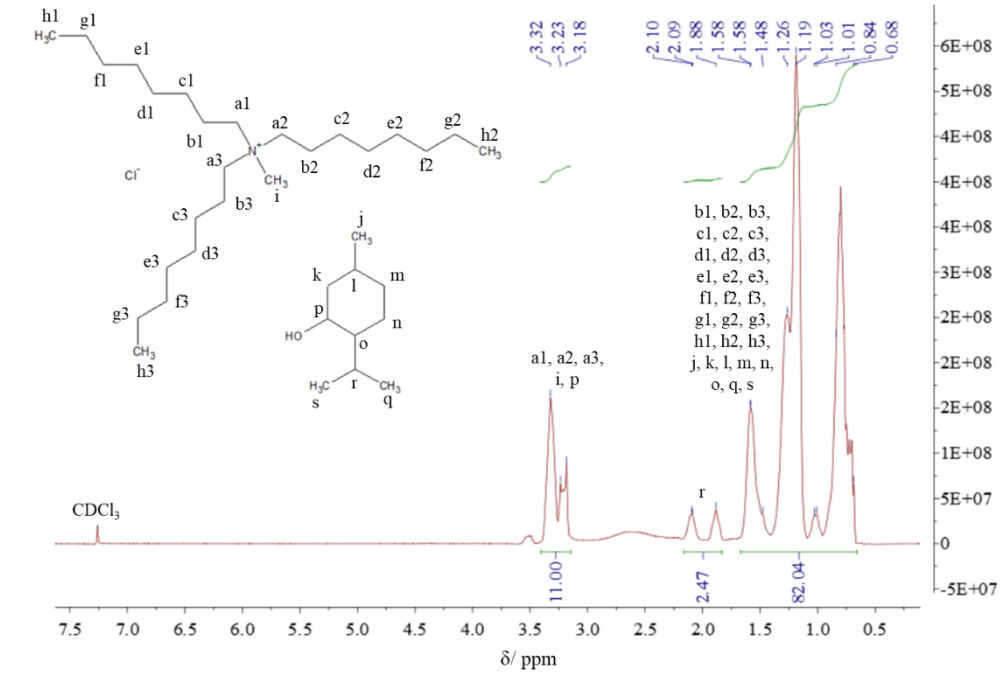
3.32
3.23
3.18
2.10
2.09
1.88
1.58
1.58
1.48
1.26
1.19
1.03
1.01
0.84
0.68
a1, a2, a3, i, p
b1, b2, b3, c1, c2, c3, d1, d2, d3, e1, e2, e3, f1, f2, f3, g1, g2, g3, h1, h2, h3, j, k, l, m, n, o, q, s
r
CDCl3
11.00
2.47
82.04
δ/ ppm

(G)

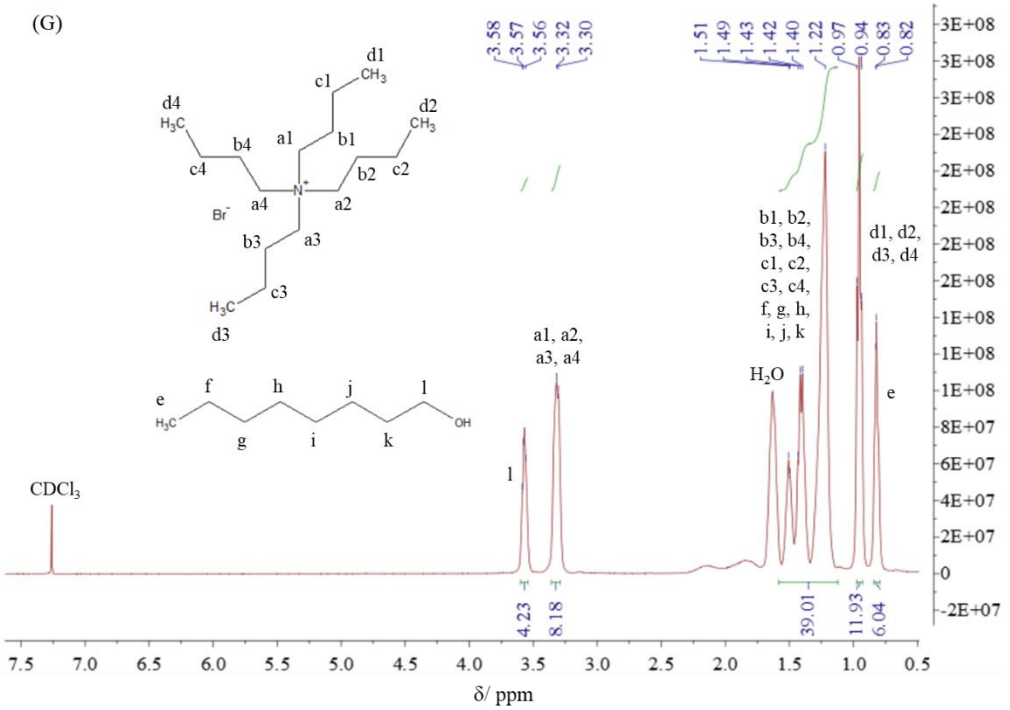
3.58
3.57
3.56
3.32
3.30
1.51
1.49
1.43
1.42
1.40
1.22
0.97
0.94
0.83
0.82
a1, a2, a3, a4
b1, b2, b3, b4, c1, c2, c3, c4, f, g, h, i, j, k
d1, d2, d3, d4
H2O
e
l
CDCl3
4.23
8.18
39.01
11.93
6.04
δ/ ppm

(H)

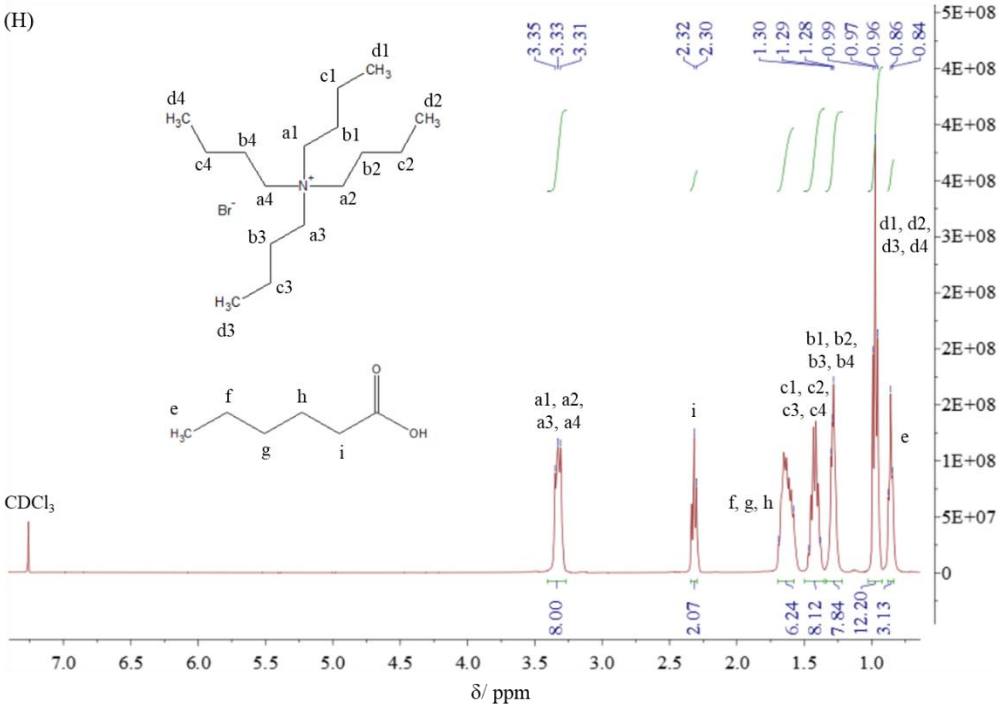
3.35
3.33
3.31
2.32
2.30
1.30
1.29
1.28
0.99
0.97
0.96
0.86
0.84
d1
c1
CH3
d4
H3C
d2
CH3
b4
a1
b1
c4
b2
c2
N+
Br-
a4
a2
b3
a3
H3C
c3
d3
e
f
h
O
H3C
OH
g
i
a1, a2,
a3, a4
i
b1, b2,
b3, b4
c1, c2,
c3, c4
d1, d2,
d3, d4
e
f, g, h
CDCl3
8.00
2.07
6.24
8.12
7.84
12.20
3.13
5E+08
4E+08
4E+08
4E+08
3E+08
2E+08
2E+08
2E+08
1E+08
5E+07
0
7.0
6.5
6.0
5.5
5.0
4.5
4.0
3.5
3.0
2.5
2.0
1.5
1.0
δ/ ppm

(I)

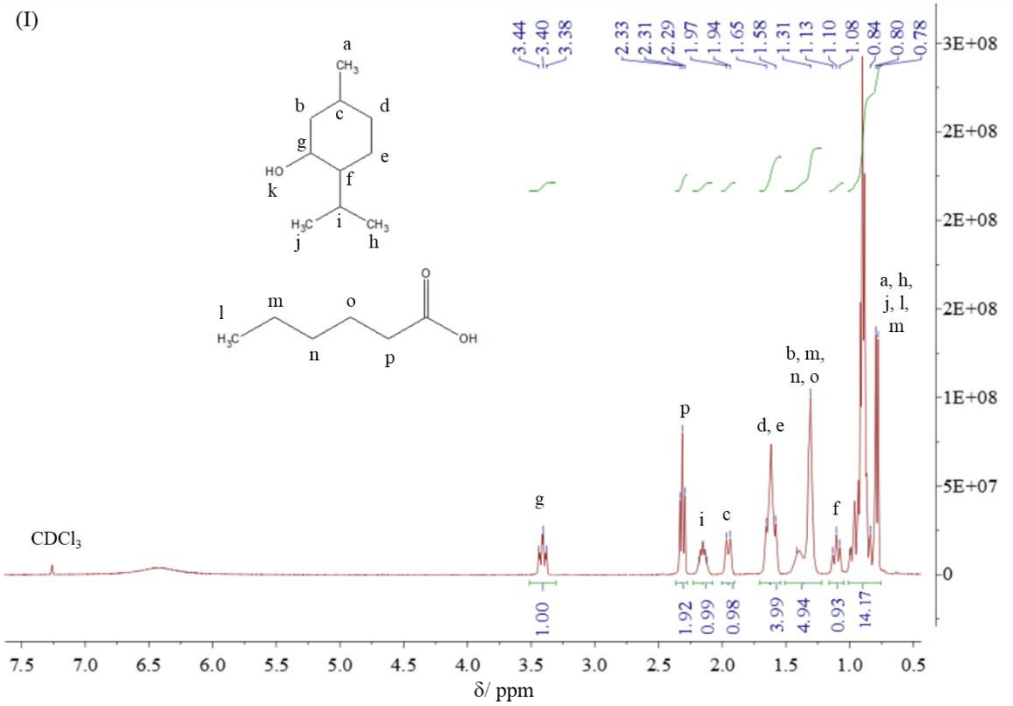
3.44
3.40
3.38
2.33
2.31
2.29
1.97
1.94
1.65
1.58
1.31
1.13
1.10
1.08
0.84
0.80
0.78
a
CH3
b
c
d
g
e
HO
k
f
H3C
i
CH3
j
h
l
m
o
O
H3C
OH
n
p
a, h,
j, l,
m
b, m,
n, o
p
d, e
g
i
c
f
CDCl3
1.00
1.92
0.99
0.98
3.99
4.94
0.93
14.17
3E+08
2E+08
2E+08
2E+08
1E+08
5E+07
0
7.5
7.0
6.5
6.0
5.5
5.0
4.5
4.0
3.5
3.0
2.5
2.0
1.5
1.0
0.5
δ/ ppm

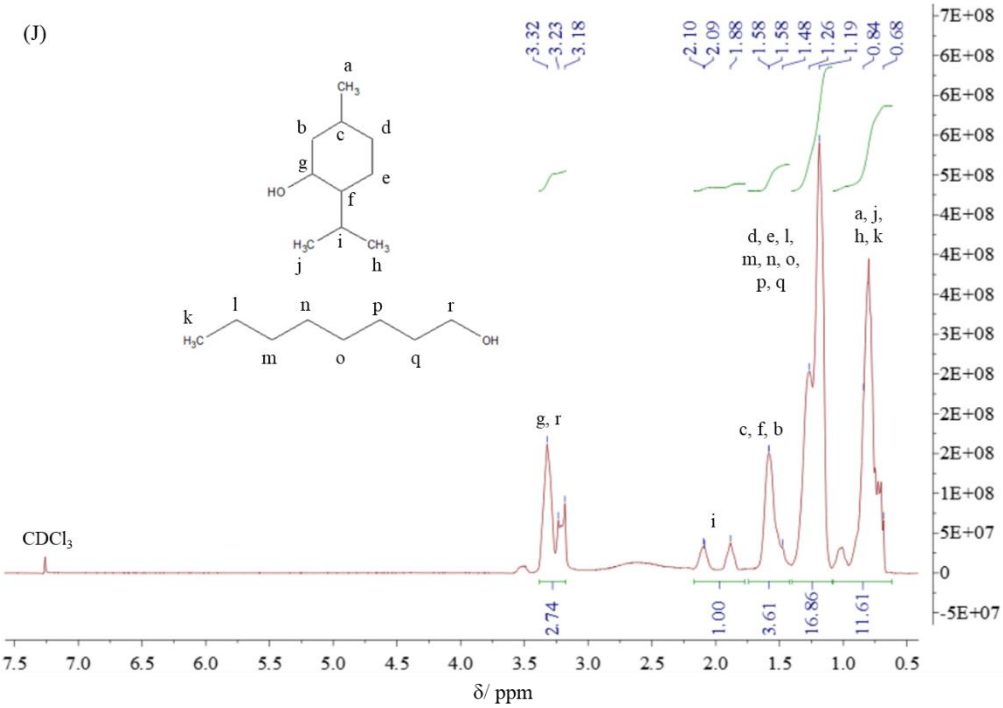

Figure A.4.1. ^{1}H-NMR spectra of (A) [Aliquat]Cl:hexanoic acid (1:1), (B) [Aliquat]Cl:octanoic acid (1:1), (C) [Aliquat]Cl:decanoic acid (1:2), (D) [Aliquat]Cl:hexanol (1:2), (E) [Aliquat]Cl:octanol (1:1), (F) [Aliquat]Cl:menthol (1:2), (G) [N_{4444}]Br:octanol (1:2), (H) [N_{4444}]Br:hexanoic acid (1:1), (I) menthol:hexanoic acid (1:1) and (J) menthol:octanol (1:1).

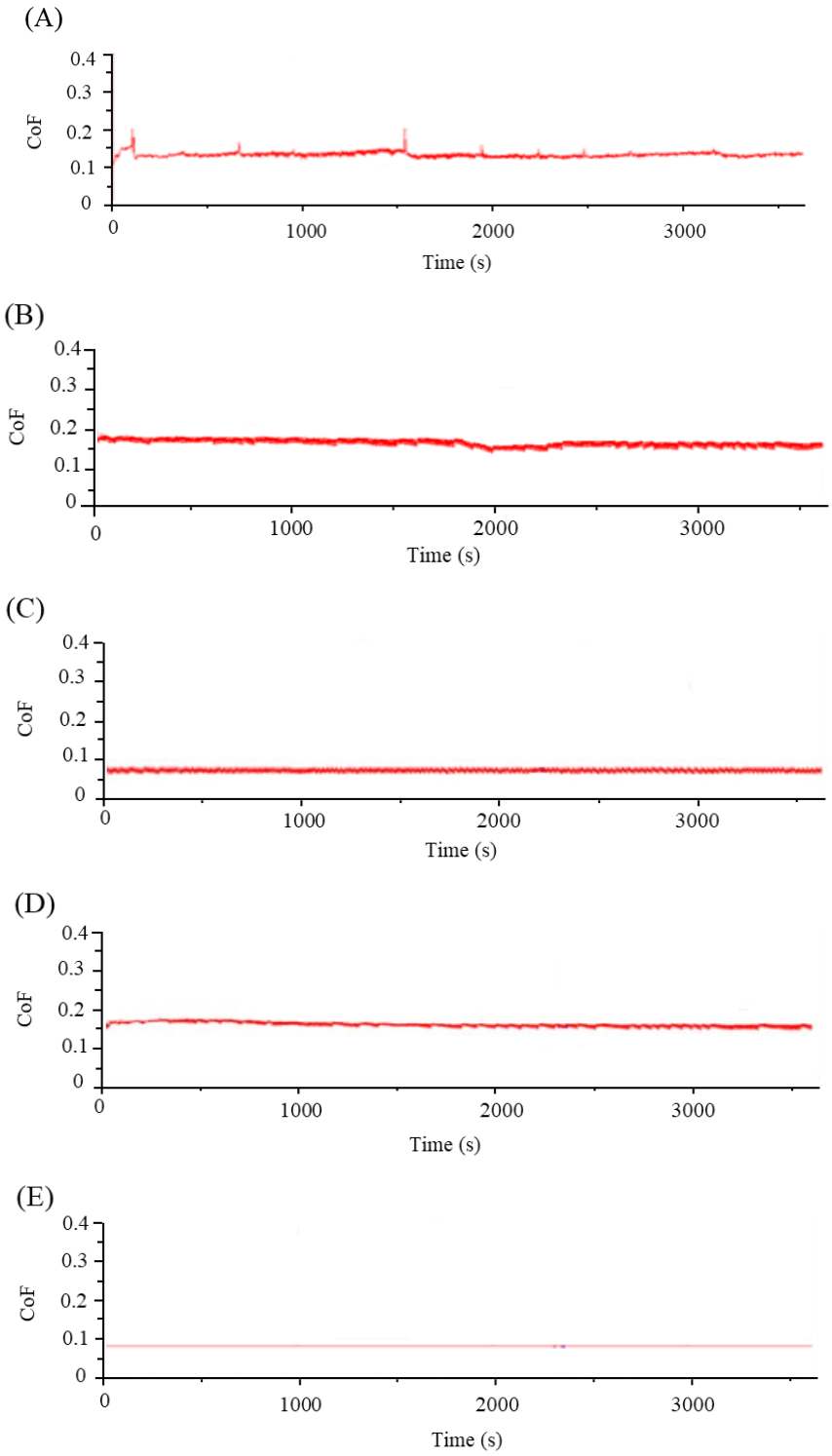

Figure A.4.2. CoF *vs*. time (2375 cycles) with v=8 mm·s^{-1} for 10N, using as lubricants: (A) hexadecane, (B) [Aliquat]Cl:octanol (1:1), (C) [Aliquat]Cl:menthol (1:2), (D) wet [Aliquat]Cl:octanol (1:1) and (E) wet [Aliquat]Cl:menthol (1:2). These results correspond to one specific run for each liquid.

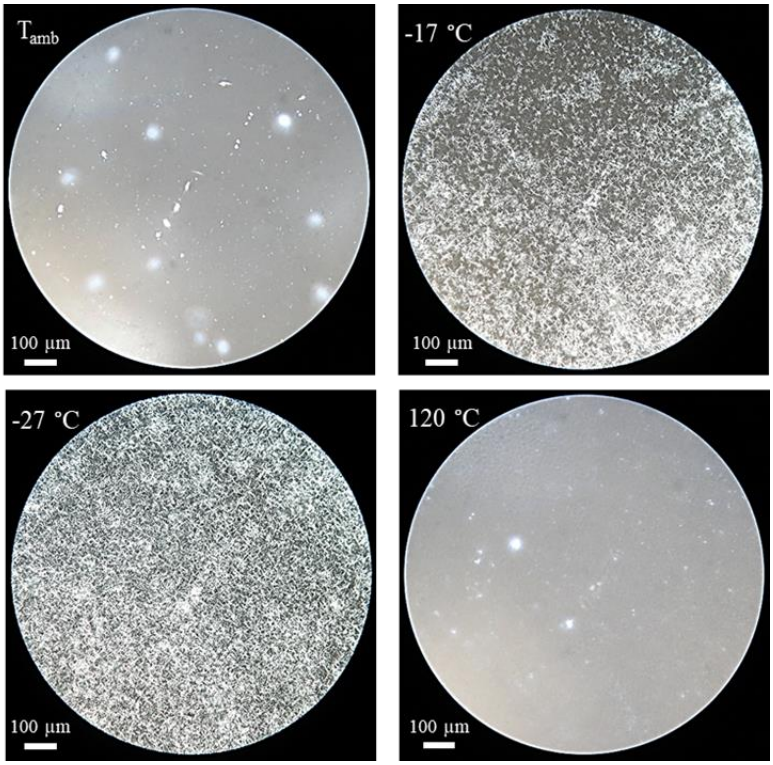

Figure A.4.3. HSPM images of one sample of [Aliquat]Cl:octanol (1:1) taken after the tribological test under 10N, beginning at room temperature, cooling till -40 °C, and heating up to 120 °C.

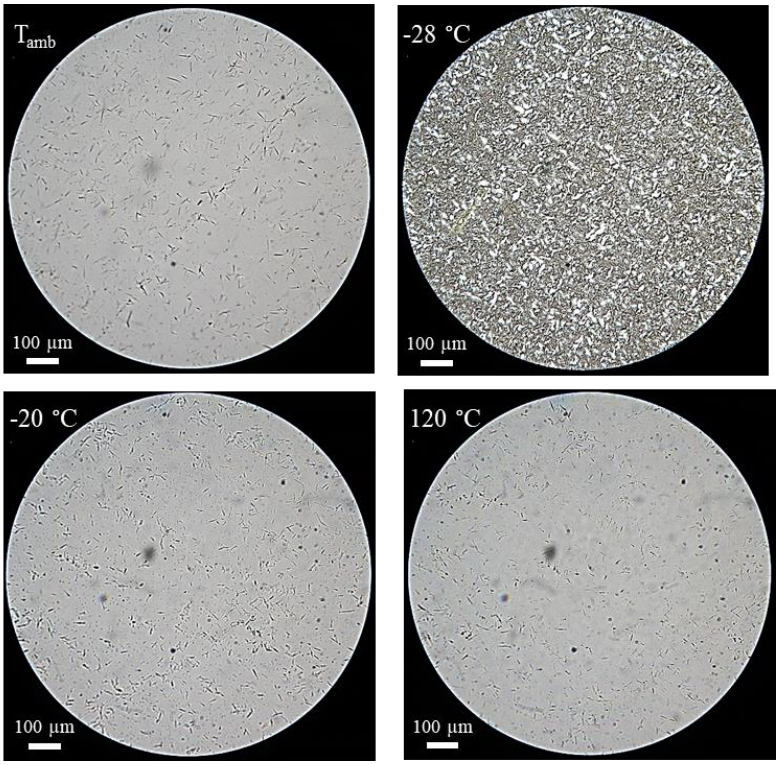

Figure A.4.4. HSPM images of wet [Aliquat]Cl:octanol (1:1) obtained at different temperatures beginning at room temperature, cooling till -40 °C, and heating up to 120 °C.

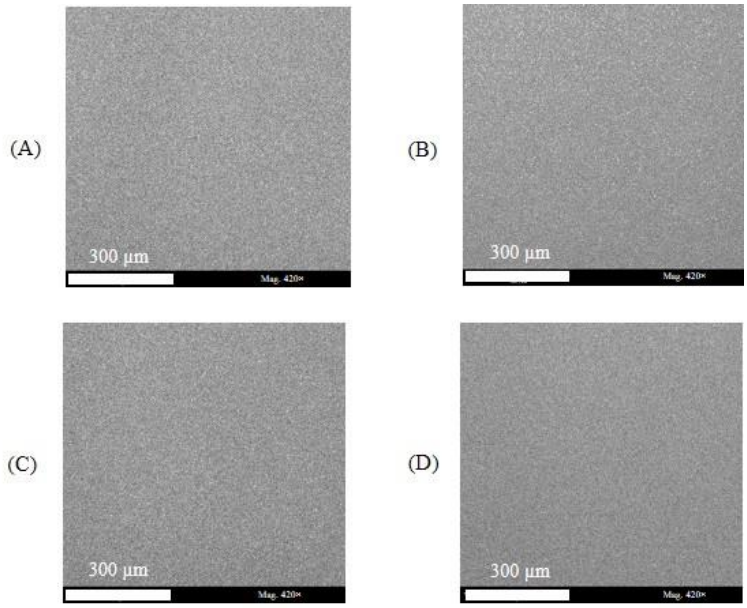

Figure A.4.5. SEM images of the Si substrates after contact with (A) [Aliquat]Cl:octanol (1:1), (B) [Aliquat]Cl:menthol (1:2), (C) wet [Aliquat]Cl:octanol (1:1) and (D) wet [Aliquat]Cl:menthol (1:2) for two weeks.

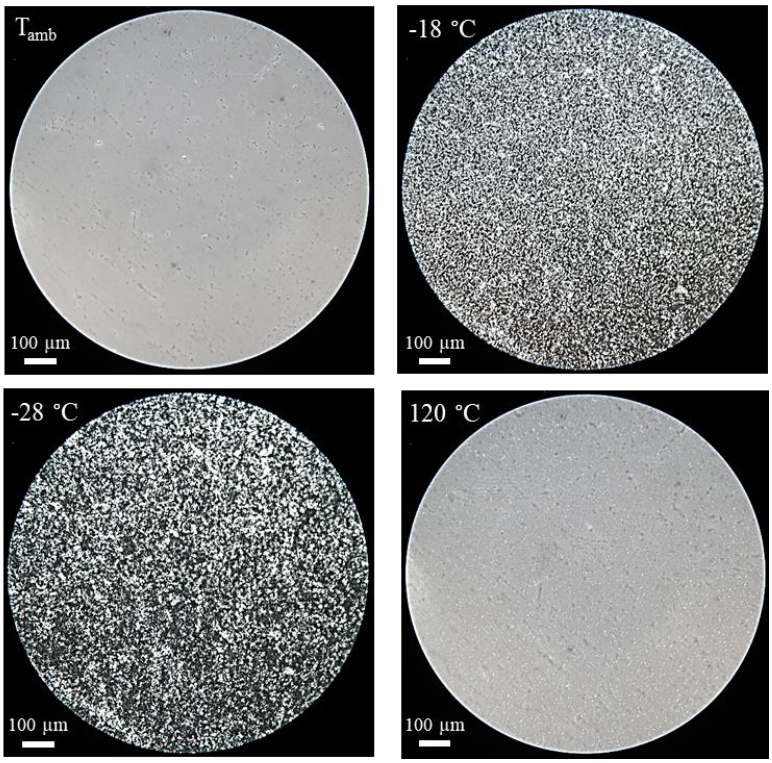

Figure A.4.6. HSPM images of one sample of wet [Aliquat]Cl:octanol (1:1) taken after the tribological test under 8N, beginning at room temperature, cooling till -40 °C, and heating up to 120 °C.

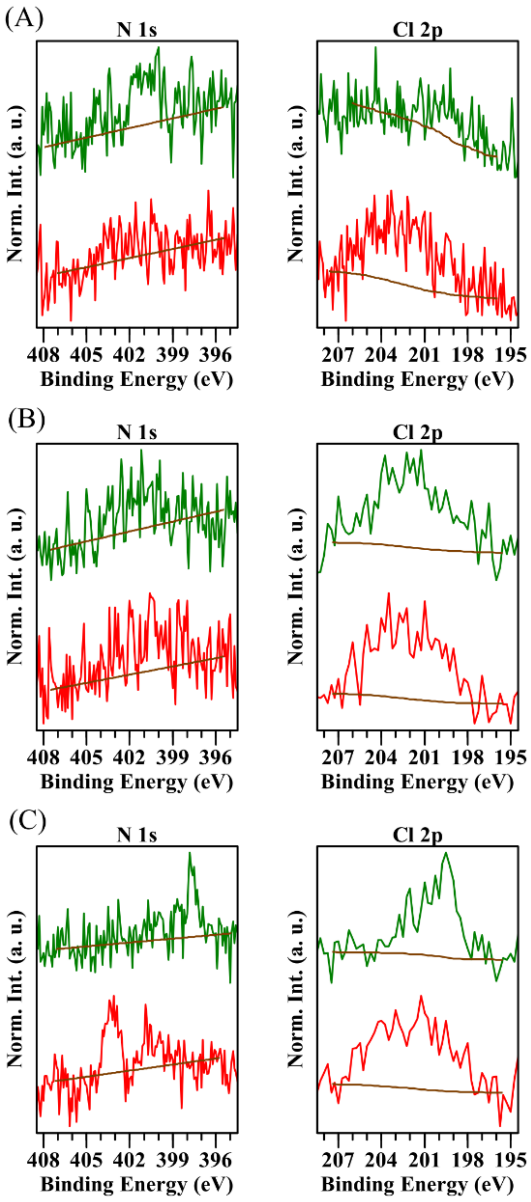

Figure A.4.7. Comparison between N 1s and Cl 2p XPS spectra for (A) hexadecane, (B) [Aliquat]Cl:menthol (1:2) and (C) [Aliquat]Cl:octanol (1:1) after tribological tests at 10N, inside (green lines) and outside (red lines) the wear tracks.

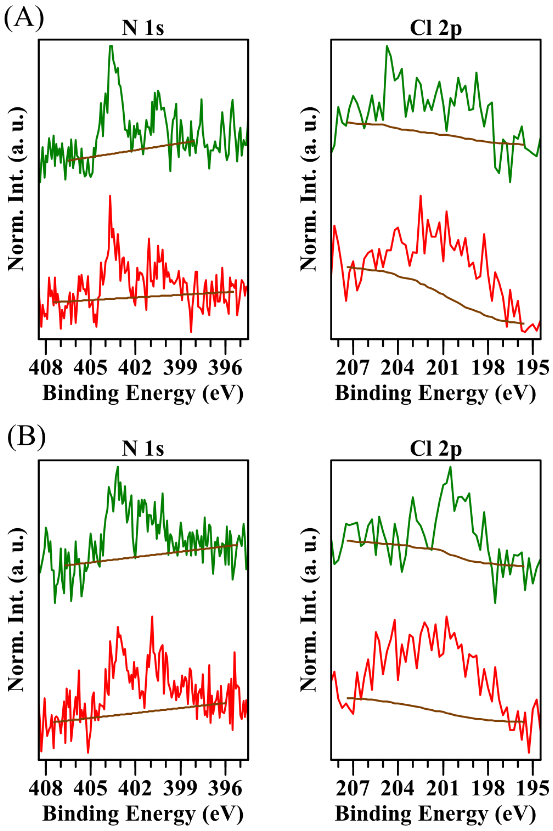

Figure A.4.8. Comparison between N 1s and Cl 2p XPS spectra for (A) [Aliquat]Cl:octanol (1:1) and (B) wet [Aliquat]Cl:octanol (1:1) after tribological tests at 8N, inside (green lines) and outside (red lines) the wear tracks.

A.5 Supporting Information of Chapter 4

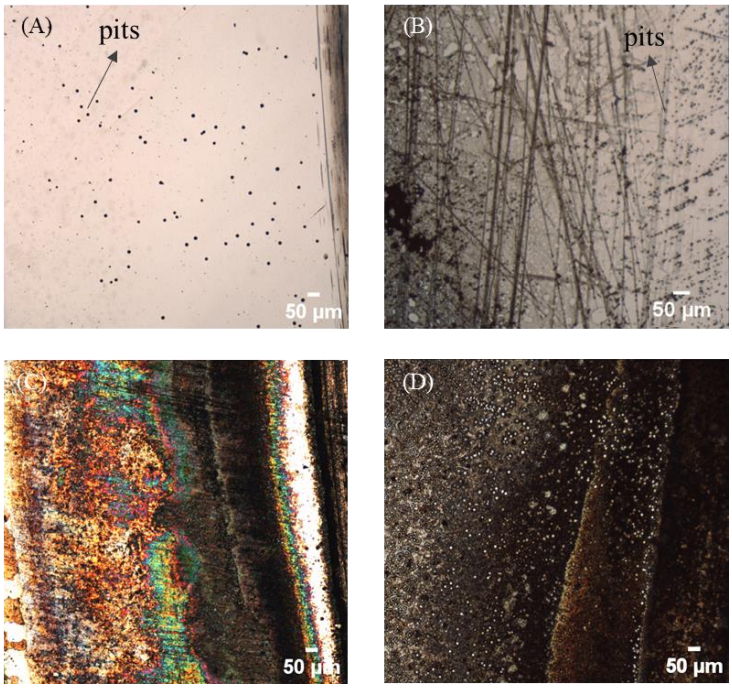

Figure A.5.1. Optical microscopy images (5× magnification) after corrosion tests with corrosion inhibitor for liquids (A) [Aliquat]Cl:octanol (1:1) + 1% RC 4801, (B) [C_6-4-pic][TfO]:PEG 200:water (1:2:10%) + 1% RC 4801, (C) PEG 200 + 2% [4-picH][HSO_4] + 1% RC 4801 and (D) PEG 200 + 2 % [4-picH][HSO_4] + 5% RC 4801.

Calculation of the theoretical minimum film thickness using elastohydrodynamic theory of lubrication (EHL)

According to the elastohydrodynamic theory of lubrication (EHL) applied to non-conformal geometry of ball-on-disc contact, the theoretical minimum film thickness, h_0, depends on the viscosity at atmospheric pressure (η_{atm}), and pressure-viscosity coefficient (α) of the lubricant and reduced modulus of the contact between the surfaces (E_r). The value of E_r. was calculated using the following equation:

$$\frac{1}{E_r} = \frac{1}{2}\left[\left(\frac{1-\vartheta_{disk}^2}{E_{disk}}\right) + \left(\frac{1-\vartheta_{ball}^2}{E_{ball}}\right)\right] \qquad \text{Eq. A.5.1}$$

where the values of Poisson's ratio and Young's modulus for 52,100 steel are 0.3 and 210 GPa, respectively.

The theoretical minimum film thickness, h_0, can be calculated using the Hamrock model,[1] through the following equation:

$$h_0 = 3.63R\left(\frac{U\eta_{atm}}{E_r R}\right)^{0.68}(\alpha E_r)^{0.49}\left(\frac{W}{E_r R^2}\right)^{-0.073}(1 - e^{-0.68k}) \qquad \text{Eq. A.5.2}$$

where R is half of the radius of the ball, U is half of the sliding speed, W is the load and k is the ellipticity parameter (taken as 1 for point contact). The pressure-viscosity coefficient, $\alpha = \frac{1}{\eta}\left(\frac{\partial \eta}{\partial P}\right)_T$, was calculated as 8.75 GPa^{-1} for PEG 200, from data reported in the literature at 60 °C.[2] The same value was used, as an approximation, for the mixtures of IL + 2% PEG + 1% RC 4801, since the solutions of IL in PEG 200 are very diluted.

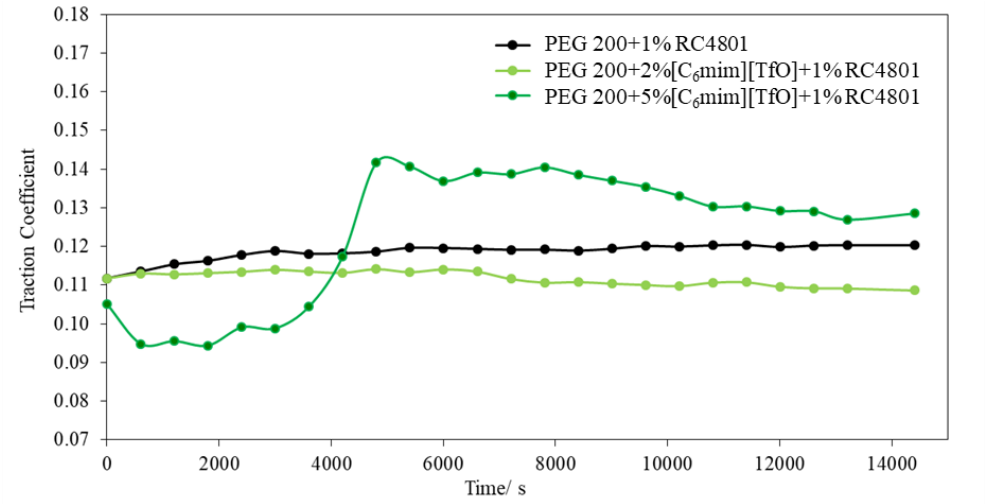

Figure A.5.2. Comparison between traction coefficient *vs*. time for PEG 200 + 2% [C6mim][TfO] + 1%RC 4801 and PEG 200 + 5% [C6mim][TfO] + 1%RC 4801, with PEG 200 + 1% RC4801 as reference. These results correspond to averages of at least two runs.

References

[1] B. J. Hamrock, D. Dowson, Isothermal Elastohydrodynamic Lubrication of Point Contacts: Part III—Fully Flooded Results. *J. Lubr. Technol.* **1977**, *99* (2), 264–275. https://doi.org/10.1115/1.3453074

[2] R. Majumdar, K. S. Alexander, A. T. Riga, Physical Characterization of Polyethylene Glycols by Thermal Analytical Technique and the Effect of Humidity and Molecular Weight. *Pharmazie* **2010**, 5, 343–347. https://doi.org/10.1691/ph.2010.9280

2023

MARIANA DONATO

TASK-SPECIFIC IONIC LIQUIDS AND DEEP EUTECTIC SOLVENTS FOR LUBRICATION TECHNOLOGY

2023

MARIANA TRINDADE DE DONATO

TASK-SPECIFIC IONIC LIQUIDS AND DEEP EUTECTIC SOLVENTS FOR LUBRICATION TECHNOLOGY